Dynamic behaviour of a high speed valve train system in a four-stroke engine

José Miguel Oliveira Sarilho

"Leave this world a little better than you found it"

Baden-Powell's Last Message (1945)

U.PORTO
FEUP FACULDADE DE ENGENHARIA
UNIVERSIDADE DO PORTO
Departamento de Engenharia Mecânica

Dynamic behaviour of a high speed valve train system in a four-stroke engine

José Miguel Oliveira Sarilho

Master thesis presented to
Faculdade de Engenharia da Universidade do Porto

Thesis supervised by:
Dr. José Fernando Dias Rodrigues
Associated Professor at FEUP

Dr. Jorge Humberto Oliveira Seabra
Professor at FEUP

Eng. César Luciano Mendes Ferreira
Development Engineer at AJP Motos

Porto, July of 2015

Acknowledgements

Firstly, I would like to express my sincere gratitude to my supervisors Prof. José Dias Rodrigues and Prof. Jorge Seabra and Eng. César Ferreira for the challenge they gave me and all the support confidence and guidance given to achieve this work I am presenting.

I would like to thank to my colleagues and friends with whom I shared moments of friendship and fellowship during this course at FEUP, without saying names they will know who they are. I also thank to my colleagues who were making their master thesis project at CETRIB (André Falcão, António Coimbra, Claudio Pinho, David Costa, Diogo Santos and Pedro Aires), for all the shared knowledge, fellowship and support during this last months working together.

I thank to the remarkable people working at CETRIB, for the companion and great welcoming into the group.

At last, I would like to express my gratitude for my parents and brothers for making me who I am today, as they have been my most important guides during my life, and I owe them the achievements and successes which allowed me to get to this final step of my degree in Mechanical Engineering.

Abstract

The Enduro and Cross Motorcycle's market is very competitive in concern to innovation technologies and products, since every year the most important manufacturers launch new improvements to its models, increasing power, handling and performance. For the last years, AJP Motos, Lda., have been tried to play a role in this market with singular solutions in their products. They are building an image about producing high performance enduro and cross motorcycles for everyday usage.

To understand the philosophy of AJP^{TM}, we can take a look at the model PR5^{TM}. We can easily distinguish this motorcycle from other competitors by its frame, made from aluminium, with an exclusive design. It was made with the goal of lowering the centre of gravity, by placing the fuel tank under the driver's seat. Despite representing a market niche, AJP^{TM} products are now riding in 4 continents, receiving positive reviews from pilots and magazines. In order to increase the satisfaction from clients, AJP^{TM}'s collaborators keep pushing the models to a higher level of performance, what requires more powerful engines.

For this company, it is not easy to produce their own engine or even go to the market and search for a high performance engine, so that its still possible to keep their model's competitive price. Nevertheless, AJP^{TM} knew that the performance of an engine is highly influenced by the quality of the combustion inside the cylinder, which in its turn depend on the admission of the air and fuel, as the exhaust of the combustion gases, as well as its timing. Therefore, the idea was to increase the power of the engine by improving its Valve Train System.

For many decades, motorcycle producers have been trying to increase the performance of valve train systems in 4-stroke engines, because its response affects the performance of the motorcycle. Some companies have invented their own solutions (for example: Ducati^{TM} with the Desmodromic^{TM} or Honda^{TM} with the Unicam^{TM}), while others use the standard ones (Single or Double Over Head Camshaft).

The AJP Motos, Lda. solution, Innercam^{TM}, is not yet ready for market because of its short life working time. As so, the goal of this thesis is to create a model that is able to describe the Dynamic behaviour of the mechanism in order to predict vibration responses of specific degrees of freedom. The results obtained in previous works were given, some weaknesses and strengths analysed in order to produce knowledge and development in this Engineering subject.

Resumo

O mercado das motos de Enduro e de Cross é muito competitivo no que toca a inovação e desenvolvimento, uma vez que todos os anos as principais marcas lançam novos melhoramentos aos seus modelos, aumentando a potência e manobrabilidade. Nos ultimos anos a AJP Motos Lda., tem tentado marcar posição neste mercado através de inovações e opções singulares. Estão assim a construir uma imagem de marca fabricando modelos de Enduro e Cross para o dia-a-dia, sem perder competitividade em pista.

Para perceber melhor a filosofia da AJP^{TM}, analisemos o modelo PR5^{TM}. Podemos distinguir facilmente a marca através do design exclusivo do quadro, feito em alumínio, que permite alocar o depósito de combustível por baixo do assento, baixando o centro de gravidade do conjunto. Apesar de representar um nicho de mercado, as motos AJP^{TM} estão atualmante a rodar em 4 continentes, somando boas críticas de pilotos ou algumas revistas especializadas. De modo a aumentar a satisfação dos clientes, os colaboradores da AJP^{TM} continuam a desenvolver a performance dos seus modelos, obrigando ao recurso a melhores motores e mais potência.

Dado o pequeno volume de negócios da empresa, é muito difícil o desenvolvimento de um motor próprio, mas também não é fácil encontrar no mercado motores performantes a um preço competitivo. Contudo, a AJP percebe que a resposta de um motor depende, consideravelmente, da qualidade da combustão dentro do cilindro, que por sua vez depende da qualidade do ar/combustível admitido e da eficiente limpeza do cilindro. Deste modo, a solução encontrada foi de aumentar a potência do motor, melhorando o sistema de abertura de válvulas (em português frequentemente denominado de árvore de cames).

Durante as últimas décadas, os fabricantes de motos têm tentado melhorar a performance das árvores de cames nos motores a 4 tempos, uma vez que a sua resposta influencia a performance do veículo. Algumas grandes construtoras inventaram os seus próprios sistemas (por exemplo: a Ducati^{TM} tem a *Desmodromic*^{TM} e a Honda^{TM} usa a *Unicam*^{TM}), enquanto que outras continuam a usar versões mais standardizadas (árvore de 1 ou 2 veios à cabeça).

A solução da AJP Motos, Lda., *Innercam*^{TM}, ainda não está pronta a ser produzida devido ao seu curto tempo de vida útil (provocado por elevado desgaste). Ao passo que, o objetivo desta dissertação é criar um modelo capaz de descrever o comportamento dinâmico do mecanismo, de modo a prever as respostas, nomeadamente a nível de vibrações, em determinados graus de liberdade. Os resultados obtidos em trabalhos anteriores foram fornecidos e os seus pontos fortes e menos fortes analisados, de modo a produzir algum conhecimento e desenvolver este ramo da Engenharia.

Keywords

Enduro Motorcycles
AJP Motos, Lda
Four-stroke engines
Valve Train Systems
Innercam^{TM}
Dynamic Analysis
Jerk (3rd derivative of position)
MSC ADAMS^{TM}

Palavras chave

Motos Enduro
AJP Motos, Lda
Motores 4-tempos
Árvore de Cames
Innercam^{TM}
Análise Dinâmica
Jerk (3^{a} derivada da posição)
MSC ADAMS^{TM}

Nomenclature

Symbol	Units	Description
sub i or e	-	Indication for Intake or Exhaust sub-system
a	mm	Length for vector $\overline{AC}$
b	mm	Length for vector $\overline{AB}$
$r_{-}(t)$	mm	Length for vector $\overline{OC_{-}}$
s	mm	Exterior radius of the roller
$lift$	mm	Positive displacement of a valve
β_{-}	$^{\circ}$	Angle between rocker's local referential and global
ϕ_{-}	$^{\circ}$	Angle between $\overrightarrow{AB}$ and global referential
ρ	$^{\circ}$	Angle between valve's local referential and global
α_{-}	$^{\circ}$	Angle between $\overrightarrow{OC}$ and global referential
α_{jk}	-	FRF of type receptance of DoF j in relation to DoF k
λ_{-}	$^{\circ}$	Angle between $\overrightarrow{CI_{-}}$ and global referential
O	-	Origin of the global referencial
C	-	Centre point of the roller
A	-	Centre of rotation for the rocker arms
B	-	Contact point on the tappet
I	-	Contact point between roller and the camshaft
G_{-}	-	Centre of gravity
ω_{ij}	$rad \cdot s^{-}1$	Speed of rotation of the referential i relatively to j
$jerk_{-}$	$- \cdot s^{-}3$	Third derivative of a variable
m_{-}	kg	Mass for a specified body
$[I_{-}]$	$kg \cdot mm^2$	Inertia matrix for a specified body
τ_{-}^{QA}	-	Torsor of quantity of acceleration in a specified point
$\dot{\overrightarrow{Q_{-}}}$	N	Rate change of momentum for a specified body
$\dot{\overrightarrow{K_{-}}}$	$N \cdot m$	Rate change of angular momentum for a specified body
Ω_{ij}	$rad \cdot s^{-}2$	Acceleration of rotation of the referential i relatively to j
$\overrightarrow{R_O}$	N	Reaction force at the origin
$\overrightarrow{R_A}$	N	Reaction force at point A
$\overrightarrow{F_c}$	N	Contact normal force at I
$\overrightarrow{F_t}$	N	Contact tangential force at I
$\overrightarrow{g}$	N	Gravity
$\overrightarrow{M_m}$	$N \cdot m$	Given torque at the camshaft

Symbol	Units	Description
μ	rate	Coefficient of friction
$\overrightarrow{F_k}$	$N \cdot m$	Spring force
μ_s	rate	Static coefficient of friction
μ_d	rate	Dynamic coefficient of friction
v_s	$m \cdot s^-1$	Stiction transition velocity
v_d	$m \cdot s^-1$	Friction transition velocity
R_z or R_x	mm	Geometry radius of bodies in contact
A_H or A_H	mm^{-1}	Geometrical parameters of contact in Hertz Theory
k, C_a C_δ	-	Dimensionless parameters of contact
E	Mpa	Young Modulus
ν	-	Poison rate
E_{eq}	Mpa	Equivalent Young Modulus
a_H	mm	Hertz contact half-width
δ	mm	Hertz contact penetration
k_c	$N \cdot mm^{-1}$	Contact stiffness
c_{eq}	$N \cdot s \cdot mm^{-1}$	Equivalent damping coefficient
ξ	-	Rate of damping
ω_n	$rad \cdot s^{-1}$	Natural frequency of vibration
ω_d	$rad \cdot s^{-1}$	Natural damped frequency of vibration
Phi	rad	Phase angle
Amp	mm or rad	Amplitude of vibration in a DoF response
$\alpha(\omega)$	$m \cdot N^{-1}$	FRF receptance for a 1 DoF system
$\{u\}$	-	Eigenvector
$\{\Phi\}$	-	Normalized Eigenvector
$\alpha_{ij}(\omega)$	$m \cdot N^{-1}$	FRF receptance in DoF i, for a solicitation in DoF j

List of Acronyms

Acronym	Meaning
OHC	Over Head Camshaft
DOHC	Double Over Head Camshaft
OHV	Over Head Valves
DoF	Degree of Freedom
FFT	Fast Fourier Transformation
FRF	Frequency response function
FEA	Finite Element Analysis

Contents

List of Figures

List of Tables

1. Introduction

This thesis was proposed to be a continuity of the work done in last two years, during other thesis projects. It is a part of my curricular program in the Integrated Master degree in Mechanical Engineering, at Faculty of Engineering from University of Porto (FEUP).

Firstly, a new concept for a Valve Train System was proposed by AJP Motos S.A., the InnerCam, in order to increase the performance of its engines. A preliminary Dynamic Analysis was done, as well as some experimental tests and benchmarking tests. Three different sets of the InnerCam were produced, tested and the results were analysed. Some failure diagnosis were done, revealing that problems of lubrication, high wear, and temperature caused the undoing of those sets. Also some power loss was identified at high speeds, like it happened in the standard OHC. [11]

For that reasons a more deep dynamic analysis was proposed, including a multibody vibrational study to understand in which way the high speed affects the behaviour of the each part, and if that behaviour can generate vibrational important forces in the contacts that generate the identified wear.

In a second work, an analytical dynamic model was developed in order to obtain new curves for the dynamic parameters (like accelerations and forces). Maximum values were identified and the influence of speed and acceleration of the engine was characterized in graphical results. [8]

The third work I am presenting is meant to be a vibrational study on the behaviour of the InnerCam^{TM}. Some previous results will be confirmed using the software MatLab^{TM} and SolidWorks^{TM} and thereafter a new model will be presented in MSC Adams^{TM}, multi-body dynamic's software. The results of that model are to be confirmed with analytical vibrational models with multiple degrees of freedom.

1.1. Thesis outline

On chapter 2, a theoretical contextualization will allow the reader to understand the importance of the valve train system in the engine and get to know different concepts used in motorcycle industry.

On chapter 3, the InnerCam^{TM} system will be presented as the AJP^{TM}'s solution.

On chapter 4, a Kinematic model will be presented and its parameters characterized in equations and graphical results for position, velocity, acceleration and Jerk.

On chapter 5, a Dynamic model will be studied, detailing each body and presenting some results.

On chapter 6, the model built in MSC Adams^{TM} will be explained to detail and every options taken to introduce the parameters, as well as some considerations for its weaknesses and approximations.

On chapter 7, the results obtained in the 1st MSC Adams^{TM} model will be presented and discussed.

On chapter 8, some analytical vibrational models are studied and its free natural modes characterized.

At last, on chapter 9, an improvement to MSC Adams^{TM} model is discussed, considering the results obtained from the vibrational models and a new set of results is presented.

1.2. Thesis Aim

The main goal it was expected to reach was to understand the reasons for the failure of the InnerCam^{TM} valve train system, through the vibrational analysis.

It is sought to evaluate the potential of this system, and if possible to propose solutions to improve its dynamic behaviour.

A secondary aim is to explore the software MSC Adams^{TM} in treating multibody dynamic systems, by the usage of different embed resources in both modelling and Post/Processor interfaces. For instance, is intended to identify its user-friendliness and quality of results.

2. Theoretical contextualization

In the last years motorcycle producers have been replacing the compact two stroke engines for new small four stroke engines. There are many different economical, marketing, environmental or engineering reasons for that, between which is that 4-stroke engines became easier and cheaper to produce, but also much more powerful than before. They are used to be more fuel efficient (less emissions and taxes) and reliable. Besides they are more complex than 2-stroke ones, have more components, then heavier, slower speeding up, but also cannot handle so well the high regimes.

While in a 2-stroke engine the intake and exhaust system interact with the combustion chamber through lateral windows, which are opened and closed by the piston, in a 4-stroke engine we have a set of valves, which require a proper system to open and close them, allowing the admission of air/fuel mixture in the cylinder, and the exhausting of combustion leftover gases.

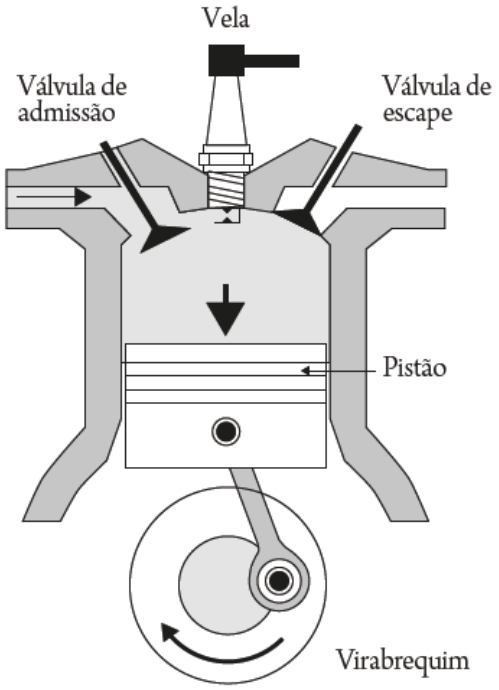

Figure 2.1.: Scheme of a single-cylinder Otto engine [1]

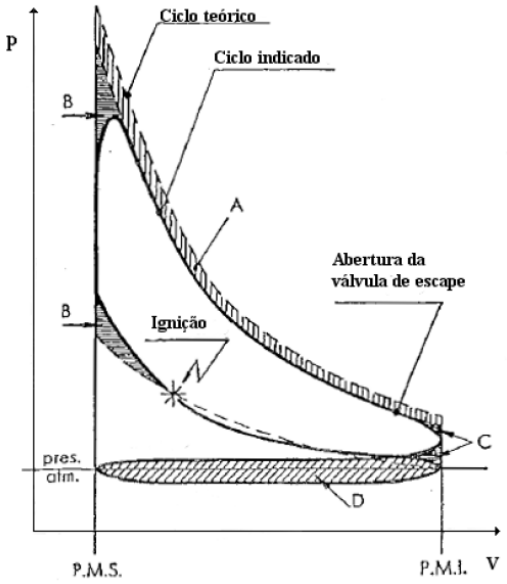

Figure 2.2.: p-v diagram for a 4-stroke Otto cycle [2]

As the name says the 4-stroke petrol engine cycle can be divided in 4 main steps:

- **intake** -> in the first stroke the piston begin in the top dead centre and the intake valve(s) opens, then as the piston goes down, the air/fuel mixture fills the free volume;
- **compression** -> with all the valves closed, the piston goes up, compressing the fluid inside and giving it energy;
- **combustion** -> the piston is again in the dead top centre position and a spark plug ignites the compressed mixture, causing its combustion and pushing the piston down. This is called the motor stroke, because it's the only that provides energy to the crankshaft;
- **exhaust** -> all the volume of the cylinder is full with the leftover gases from the combustion, with no usable chemical energy. So the exhaust valve(s) opens, and as the piston goes up, the exhaust gases leaves the cylinder;
- the cycle goes on and on.

Important also to state that there is a crucial very short moment when both exhaust and intake valves are partially opened at the same time, between exhaust and intake strokes. This moment can be called 'the cleaning', because the intake flow is used to push the left exhaust gas out of the chamber. An economical, low power engine may not need this to work properly, but in high performance engines this really makes the difference. In 2-stroke engines this step is responsible for the high consumption. [2]

The timing of the valves is one of the most important variables to the engine's power, so that an accurate and fast valve train system makes the difference in a high performance engine. For that reason is not difficult to find in motorcycle magazines some highlights on the cylinder head, when comparing different models.

The AJP Motos S.A. produces leisure off-road motorcycles with a brand standard of being easy to ride for a beginner. However, even a beginner will soon or latter demand for more power and AJP^{TM}needed a good performance engine for its top motorcycle. So, instead of install a new bigger engine, they decided to produce some changes in the existing one.

2.1. Valve Train System

A valve train system is a mechanism that provides the correct opening of the valves of the engine. There are different types of concepts, using different components, but

usually the following body-parts can be found:

- **camshaft:** the rotational speed from the crankshaft is transmitted to the camshaft through gears, belts or chains, in a reason of $\frac{1}{2}$ (in each cycle the crankshaft makes two revolutions). The camshaft has lobes and its profile defines the impulse transmitted to the valves;
- **rocker-arm:** this body-part may, or not, exist and is responsible for transmitting the impulse from the camshaft to the valve;
- **valves:** component that opens and closes the windows between the intake or exhaust canals and the cylinder;
- **springs:** each valve has one. Are commonly used to store mechanical energy, provided by the camshaft to open the valve(s), and recover it back to close them.

A perfect assembly of all the components is crucial to provide the well functioning of the engine. For instance, if the camshaft is not precisely aligned with the crankshaft, it may result in a serious damage to the connecting rod or piston (due to the combustion wrong timing), failure on the valves, or the undoing of the hole engine.

The main kinds of valve train systems used nowadays in the motorcycle industry are presented in the following sub-sections.

2.1.1. Over-Head Camshaft (OHC)

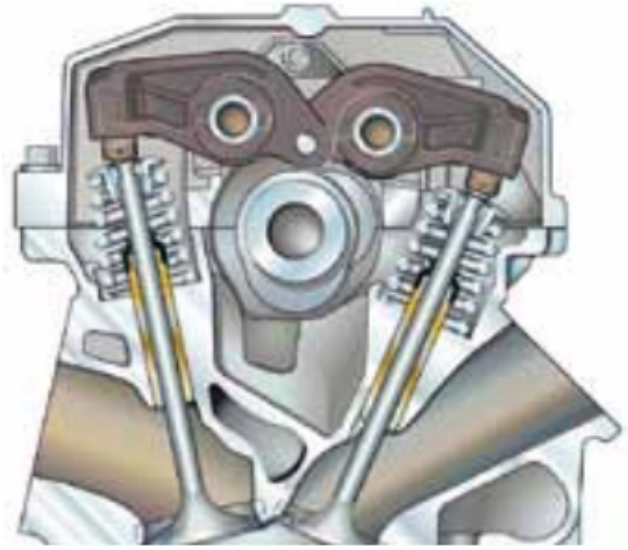

Figure 2.3.: Over Head Camshaft valve train system [3]

This system, presented in Figure 2.3, also called Single Over-Head Camshaft, is defined for having one camshaft over the cylinder whose lobes are responsible for acting both the intake and exhaust valves. It always require a rocker arm to transmit the impulse from the lobes to the valves.

Some of its advantages are the compactness and simplicity of assembly and calibration because there is only one camshaft to positioning relatively to the crankshaft. That means that the valves will always open in the correct time relatively to each other.

The major disadvantage is that the springs used needs to have a large stiffness, in order to provide the correct closing time of the valves, as so it has to beat the inertia of the valves and the respective rocker arm. Anyway, there is always a loss of power at high speeds because valve floating and bouncing effects are more probable to occur than in the DOHC system.

This is most used in small engines that don't require high regimes like road motorcycles or scooters.

2.1.2. Double Over-Head Camshaft (DOHC)

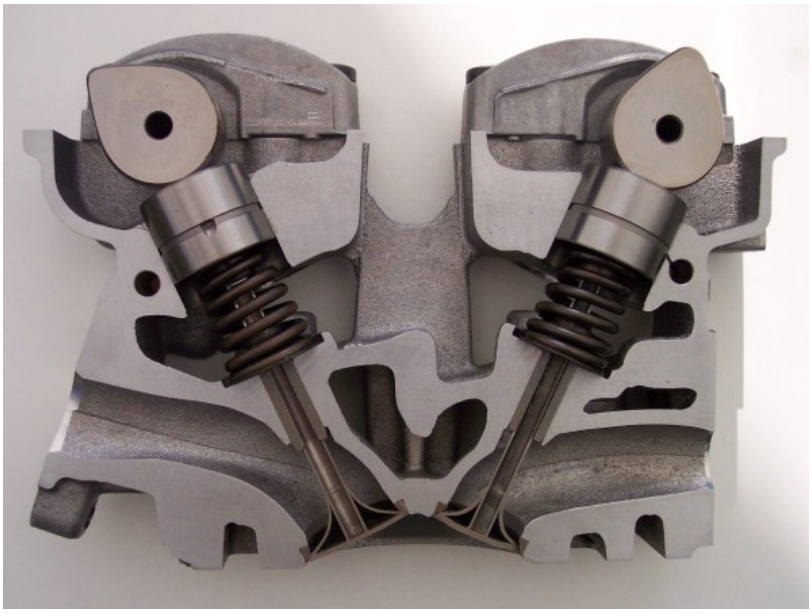

Figure 2.4.: Double Over Head Camshaft valve train system [3]

As the name says this type of valve train system is characterized by having 2 camshafts over the cylinder, one for the intake valves and one for the exhaust valves, as shown in Figure 2.4. Ergo, there are no rocker arms 'delaying' the movement of the valves.

The biggest advantage is the good response at high regime speeds, which are very important in enduro or cross markets, in which AJP Motos, S.A. competes.

On the other hand, a DOHC system tends to be less compact and heavier than the OHC, which can be an impediment for some smaller models. Also the calibration of the system is more complex because each camshaft is independent, as so, the groups of valves can move independently.

In the 250cc enduro or cross motorcyles the DOHC is used by some reference brands like Yamaha^{TM} or Suzuki^{TM} or Husqvarna^{TM} in its standard models.

2.1.3. Desmodromic

The Desmodromic Valve train is used by Ducati^{TM}. "The word 'Desmodromic' derives from two Greek words: '*desmos*' (controlled, linked) and '*dromos*' (stroke, course, track); in mechanics, it is used to refer to mechanisms which have a control for movement in one direction and another special control for movement in the opposite direction ('closure' or 'return')." [4] Over the last century there have been various Desmodromic valve train concepts. The first one documented was created by Arnott in 1910. In Figure 2.5 we can notice many similarities comparing to AJP's InnerCam system.

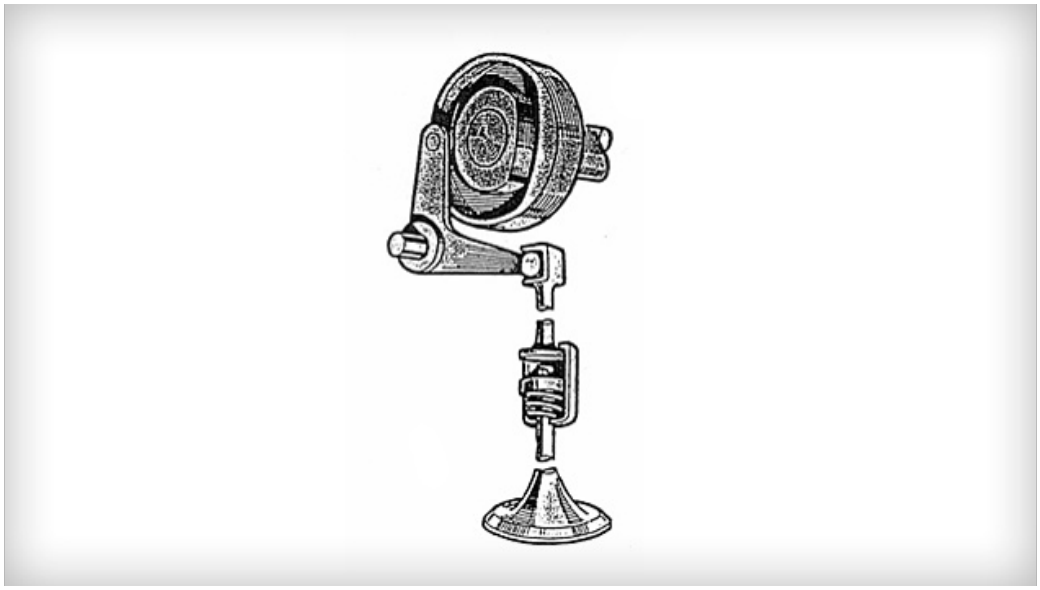

Figure 2.5.: Arnott's Desmodromic concept, 1910 [4]

"Today, 'Desmodromic' commonly refers to the typical valve control system of our motorcycles: it is currently used on all Ducati's manufactured Twin-cylinders and is an exclusive system. In practice, the opening stroke and closing stroke of exhaust and intake valves are controlled in this system, while normally, closure is obtained as a result of spring recovery." [4]. It consists of a single camshaft over the cylinder

with 2 rocker-arms per valve, where one is responsible to push it and the other to pull it back. The Ducati's Desmodromic^{TM}(Figure 2.6) is considered brand image in its motorcycles, due to its high performance and fast response.

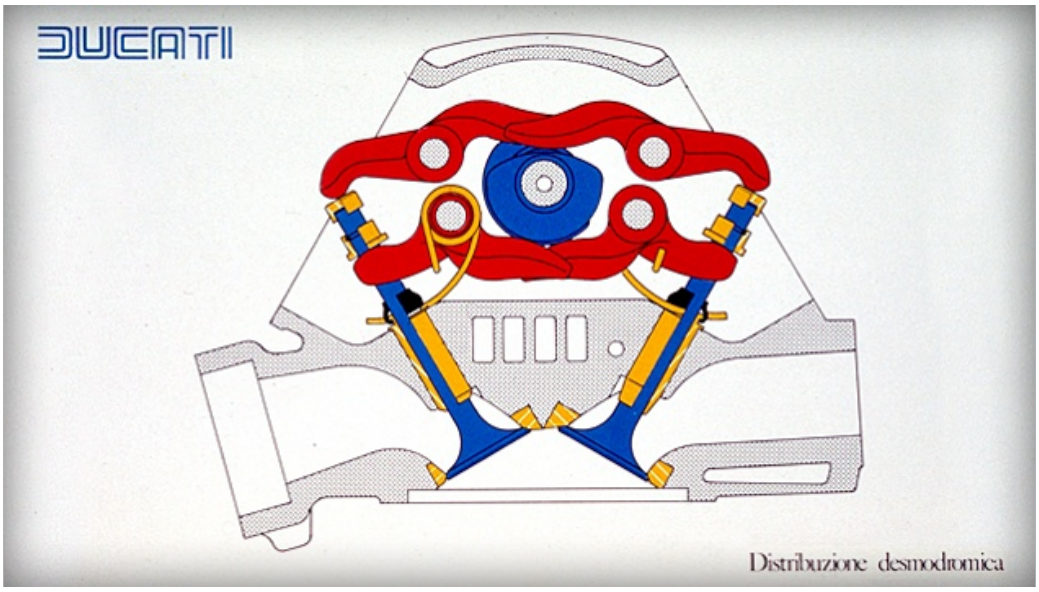

Figure 2.6.: Ducati's Desmodromic^{TM}valve train system [4]

2.1.4. Other Valve Train mechanisms

The **Unicam**^{TM} system is also a brand image, but for Honda^{TM}'s motorcycles. It has a single camshaft actuating the admission valves exactly like in a common DOHC system. At the same time that camshaft also actuates a rocker-arm, transmitting the impulse to the exhaust sub-system.

The **Over Head Valve** (OHV) system is composed by a camshaft engaged to the crankshaft and a push-rod transmitting the movement from the lobes to the corresponding rocker-arm, which in its turn actuates the valve(s). The OHV system is still used in North-America, also as a reason of tradition. We can find it in Harley-Davidson^{TM} models by the name of Twin-Cam (in 2-cylinder engines), for example.

Nevertheless, this solution is becoming obsolete because of the inefficiency of the combustion inside the chamber at medium/high regimes, due to the inertia forces of the push-rods and rocker-arms that cause delay in the valves lift. However it has as pros, the simplicity of assembly and reliability, because the distribution is transmitted through gears, instead of chains or geared belts.

Figure 2.7.: Scheme of the Honda's Unicam^{TM}system [5]

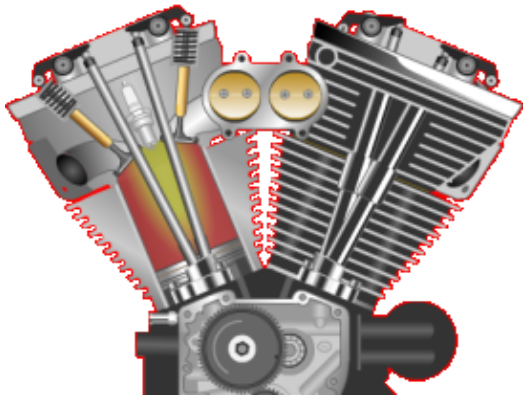

Figure 2.8.: View of a Harley-Davidson^{TM}Twin cam engine [6]

2.2. The AJP PR5^{TM}standard 250*cc* engine

The engine that equip the PR5 motorcycle is a 250*cc* produced by a Chinese company called Zongshen^{TM}. Its specifications are described in the Figure 2.9.

It is a water-cooled, 6-speed engine providing a consistent value of binary among a large range of regime. This is important in Endure motorcycles, because they usually work at low regime and requires high binary to keep it going through the obstacles and rocky ways.

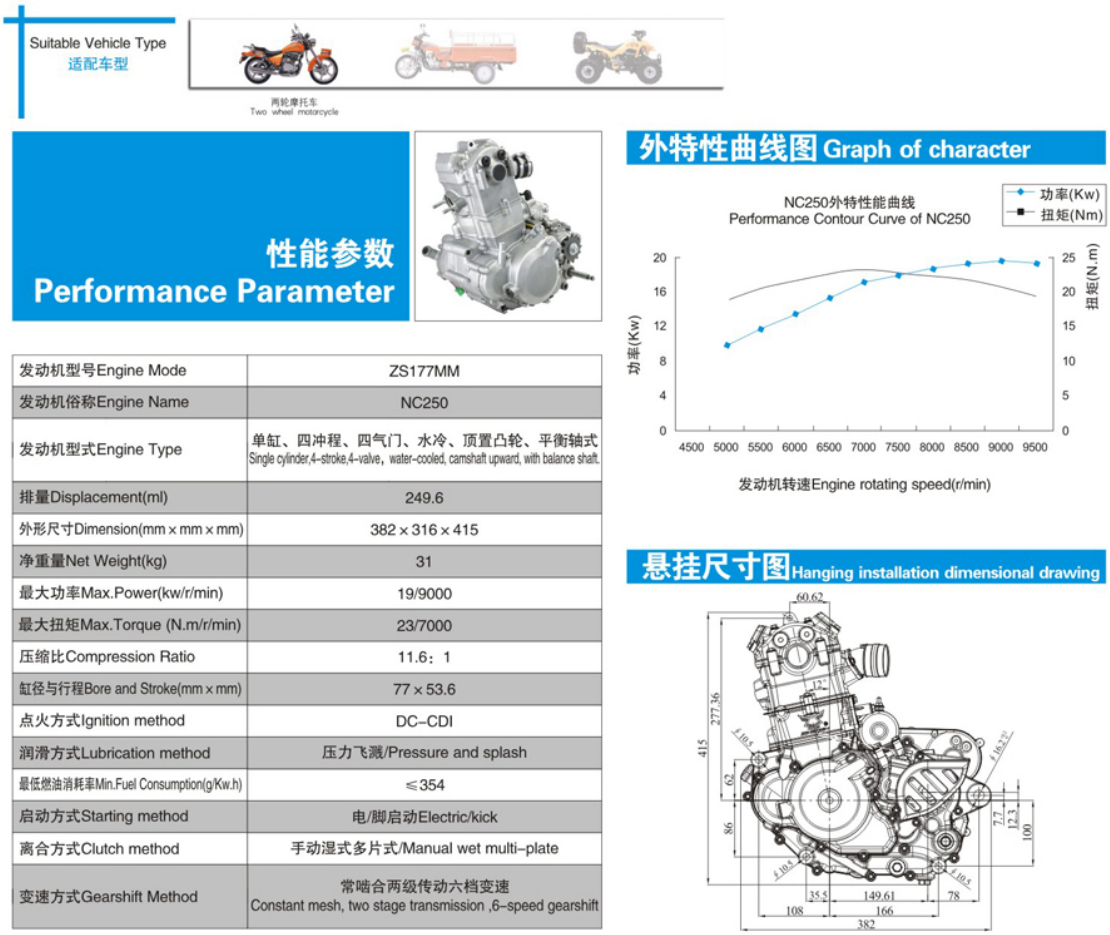

发动机型号Engine Mode	ZS177MM
发动机俗称Engine Name	NC250
发动机型式Engine Type	单缸、四冲程、四气门、水冷、顶置凸轮、平衡轴式 Single cylinder,4-stroke,4-valve, water-cooled, camshaft upward, with balance shaft.
排量Displacement(ml)	249.6
外形尺寸Dimension(mm × mm × mm)	382 × 316 × 415
净重量Net Weight(kg)	31
最大功率Max.Power(kw/r/min)	19/9000
最大扭矩Max.Torque (N.m/r/min)	23/7000
压缩比Compression Ratio	11.6：1
缸径与行程Bore and Stroke(mm × mm)	77 × 53.6
点火方式Ignition method	DC-CDI
润滑方式Lubrication method	压力飞溅/Pressure and splash
最低燃油消耗率Min.Fuel Consumption(g/Kw.h)	≤354
启动方式Starting method	电/脚启动Electric/kick
离合方式Clutch method	手动湿式多片式/Manual wet multi-plate
变速方式Gearshift Method	常啮合两级传动六档变速 Constant mesh, two stage transmission ,6-speed gearshift

Figure 2.9.: PR5^{TM}250cc engine - specifications [7]

2.2.1. $NC250$'s Cylinder Head

The Zongshen^{TM}'s engine uses a 4-valve OHC (Over Head Camshaft) valve train system. This concept consists of a single camshaft with two lobes, where each lobe touches a rocker-arm, which provides the onrush of a pair of valves, as shown in Figure 2.3.

Analysing the valves, we can notice that the intake valves have larger diameter that the exhaust ones. Actually, the power output of an engine is greatly affected by the amount of air it can draw in. Therefore, the size of the valves employed greatly affects the point at which peak power occurs. For instance, the larger the valves, the further up the regime range peak power occurs. So, usually, racing modified engines have larger seat valves than common ones, allowing the engine better 'breathing'.

Once the required intake valve size has been established, the general practice is to make the exhaust valve in a relation between .80 and .90 of the diameter. The reason why the exhaust valve does not need to be as large as the intake one is because the gases are forcibly expelled by the movement of the piston whereas the inlet has to draw in air, with the minimum drop in pressure, from a pressure source which is not very high to start with, unless the engine is super or turbocharged. [12]

This engine is mostly used in road motorcycles, therefore it is not prepared to reach high regime speeds. AJP^{TM} technicians tried to push the regime further by recalibrating the electronic central unit, but a problem emerged on the valve train system. What happened was that the valve's springs were too soft to overcome the inertia of the valves. For instance the rotational speed might also became closer to spring's natural frequency, causing a floating effect. As a result the valves didn't close completely. [11]

In order to explain the importance of the high regimes, let's introduce the definition for the volumetric efficiency (VE) as the ratio between normal atmospheric pressure and the pressure that exists within the cylinder when it has filled during admission stroke at the particular regime concerned. Assuming we have a perfect engine with maximum VE, it would have power directly proportional to the rotational speed, so that we would have infinite power at infinite regime. Instead, what happens is that the volumetric efficiency drops off as the rotation rises. For instance at peak power rotational speed, we can assume, VE is dropping as fast as regime increases. It is crucial, then, to keep our volumetric efficiency at high levels to take good profit from high regimes.

At the same time, if the valves don't close properly another effect is that the compression ratio also decreases, which also reduces the output power, as well as the thermal efficiency. For instance, if the intake or exhaust valve are not fully closed when the combustion starts, the air will escape from the chamber, so less amount of gas causes less pressure, considering the same control volume.

As a final result this 'valve float' behaviour on the valve train system causes a big drop in the output binary, and consequently in power as well, when we overcome the maximum power regime of the engine. [12]

In order to solve this problem, AJP Motos S.A. decided to redesign the valve train system in order to push the engine to higher rotational speeds, fulfilling the costumers demand for a more powerful, but yet small engine.

3. InnerCam™

3.1. The camshaft

The PR5™ motorcycle is the model equipped with the NC250 engine from Zongshen™ and the power it develops is low, comparing to the best-selling motorcycles in the market. It was thought that the power drop at high rotation speeds was due to valve floating effects in the valve train system. As so, AJP™ decided to develop a new concept of a valve train system, using only one camshaft, that could solve this problem by reducing the inertial forces during the lift movements.

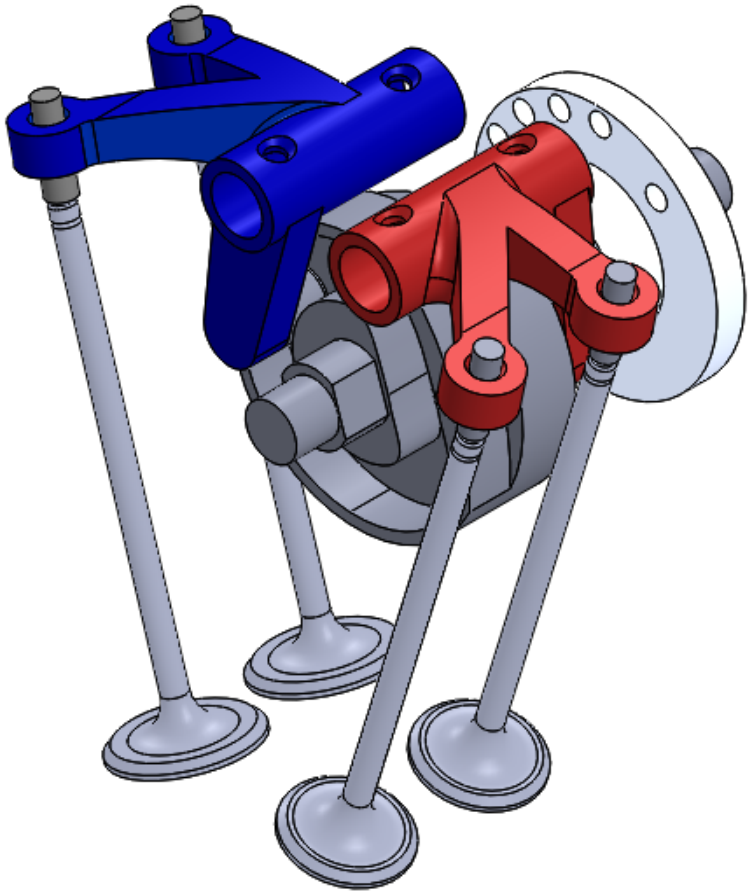

Figure 3.1.: Isometric view of the InnerCam™'s draw from SolidWorks™

The InnerCam^{TM} system is the solution developed by AJP Motos S.A. to push the performance and the efficiency to a top level. The difference between this and a OHC common valve train system is that the inertia of the rocker arms doesn't affect the return of the valves. In other words the movement of the rocker arms is fully dependent on the profile of the camshaft (once it moves along an exterior and interior cam), and consequently the spring only has to pull back the valve, requiring a lower spring stiffness. On the other hand, the spring also pushes the rocker arms to roll along the exterior surface of the cam due to its initial pre-load. This topic will be discussed later, because there are some issues in this contact, particularly the wear developed in just few hours of working, this being the main weakness of the system.

Comparing to a DOHC valve train system, the accuracy of the lift in the InnerCam^{TM} is expected to be about the same. However a DOHC system is larger and also heavier in a way that it could affect the manoeuvrability of the motorcycle. This is very important for AJP Motos S.A. because their brand image is precisely the good manoeuvrability of its motorcycles, achieved by a low centre of mass and light components.

Last year it was found that the power problem was a consequence of a deficit in the fuel injection system at high regimes. After changing the fuel pump and re-dimensioning of the admission canals as well as the valve's lift profile (for a better thermodynamic efficiency), it was possible to increase the power to values up to 35 horsepower (using the original Over Head Camshaft valve train system). This means that the engine being used has the potential to compete with other best selling motorcycles in the market. However as the wear problem of the InnerCam^{TM} is reduced and the engine performance increased, AJP Motos S.A. can have an 'important card to play in the market'.

What has been tried to find out in this study is the noise, vibration and harshness of this new valve train system, in order to understand where, kinematic and dynamically, we can reduce the wear of the InnerCam^{TM} by changing its inertia, stiffness or damping conditions.

3.2. Main components

3.2.1. The camshaft

As explained before, the InnerCam^{TM} system has the lift accuracy of a DOHC system, but the compactness of the OHC system. This is achieved by an innovative camshaft (Figure 3.2) with 2 surfaces commanding the movement of the rocker arms.

The more important surface is the inner one (considered the one with larger

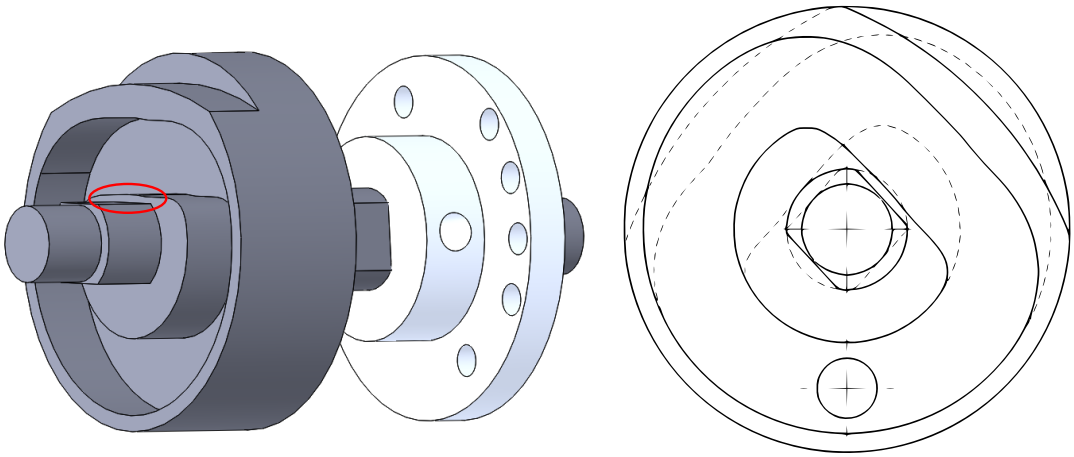

(a) Perspective view **(b)** Top view

Figure 3.2.: Camshaft's draw

diameter), because the springs of the valves force the rocker arms to follow it, due to the pre-load imposed. Although, because of the rolling friction between the surfaces, and mainly at high speeds, the rocker's roller will occasionally touch the outer profile too (considered the one with smaller diameter), particularly when the cam has to force the rocker arms to return to the default position (area marked in red, considering the clockwise rotation). At low speeds, the spring by itself can beat the inertia of the rocker arms.

This component is machined from a block of an alloy steel *34 CrNiMo 6*, provided by F. Ramada^{TM}, and submitted to a quenching thermal treatment. Its corresponding technical sheets can be consulted in the Appendix A.

In order to ensure the balancing of the camshaft to the centre of rotation (very important to avoid significant vibration responses) a hole in the camshaft was projected and an aluminium part was added (the one in white).

3.2.2. Rocker-arms

The rocker arms are fixed by a pin rod with centre in the point A, according to the Figure 3.3, in a way that it can only, and only, rotate along an axis that crosses A and is normal to the front view. Otherwise, it would also translate, because that axis is not a main axis of inertia (as will be seen later).

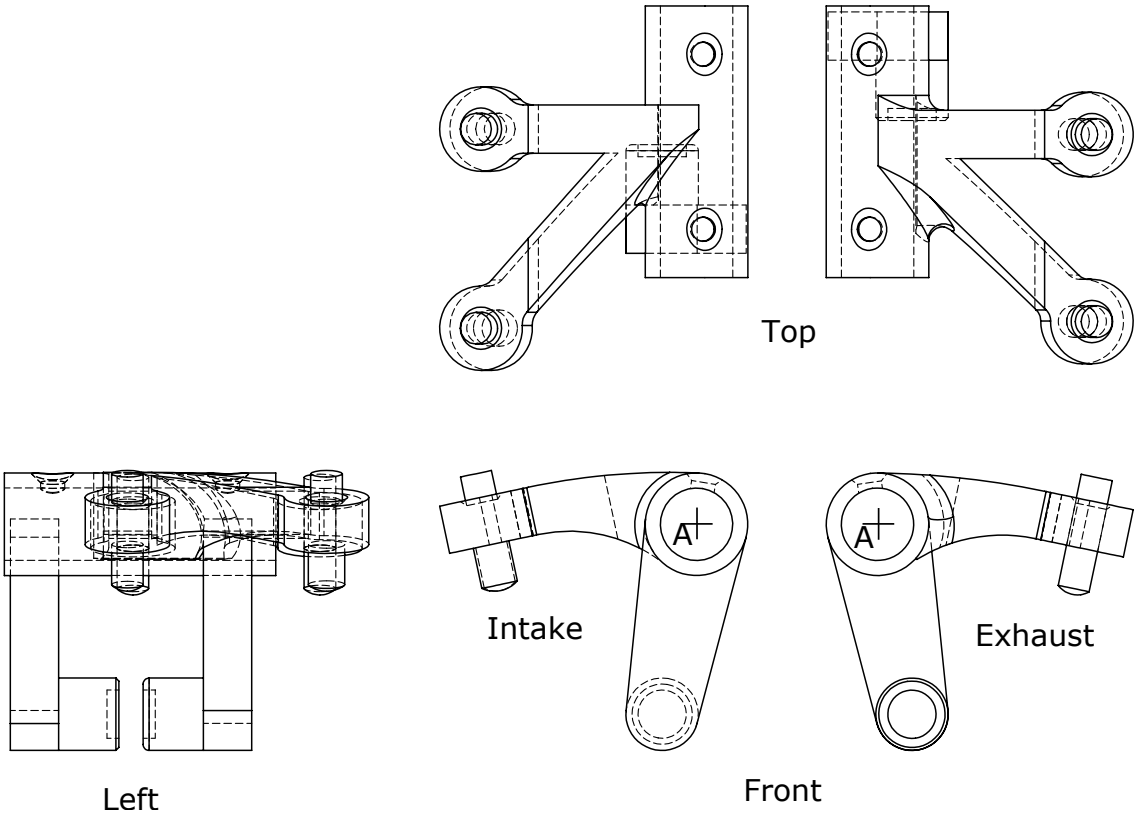

Figure 3.3.: Different views of the rocker arms in their relative positions

4. Kinematic Analysis

A kinematic analysis was already performed in previous works, besides some important steps were not achieved. The main goal of this current thesis is to study the vibration, noise and harshness of the InnerCam^{TM} system, therefore in this chapter it will be presented a kinematic study on the mechanism, developing the equations which describe the movement of all bodies, instant velocity, acceleration and the third derivative, called Jerk (variation in acceleration, which gives us an idea of impulse, or harshness of the mechanism).

As already performed in previous work, this kinematic analysis will be simplified to a 2D, OXY system, as there are no translational movements along the ZZ axis, but also because the only rotational axis are perpendicular to the mentioned plane. However, it is important to point out that there should be a special care for the dynamic equilibrium, because the rocker arms have no main inertia axis parallel to ZZ axis.

In Figure 4.1, we can take a look at the nomenclature used for the equations developed below. Notice that the soft red indicates the components belonging to the exhaust part and the soft blue to the ones belonging to the intake part (as we can see, the admission valve is larger).

Table 4.1.: Table of geometric distances and angles at stationary position

Parameter		units
a	32	mm
b	34	mm
$\beta_{0,exh}$	10	^{o}
$\beta_{0,adm}$	10	^{o}
$\phi_{0,exh}$	20	^{o}
$\phi_{0,adm}$	19	^{o}
ρ	17	^{o}

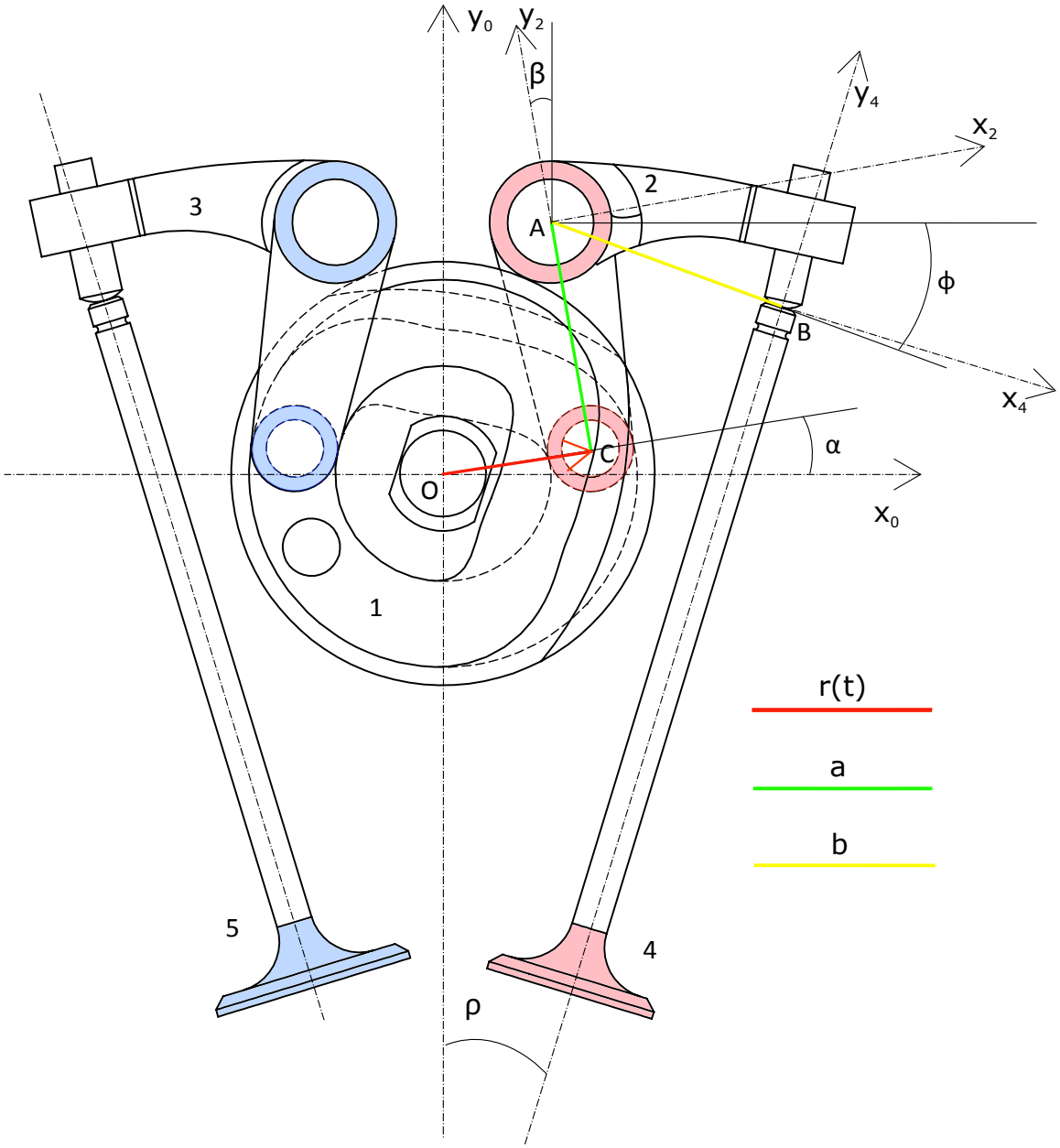

Figure 4.1.: 2D representation of the InnerCam^{TM}'s mechanism

4.1. Fourier approximation for lift curve

In previous works the lift of the valves had been defined by a frame function including a polynomial curve. Firstly, in [11], the full lift movement was assigned to only one polynomial 6th degree curve. But secondly, in [8], the lift movement was divided in two curves (opening and closing movement), making it a 4 frame polynomial function that revealed a discontinuity in the middle of the lift, but also in the beginning of the opening movement, as we see in Figure 4.2. This kind of analysis can only perform one cycle, as the approximation function is derived, in each frame separately and the discontinuity of the function is noticed in its derivatives.

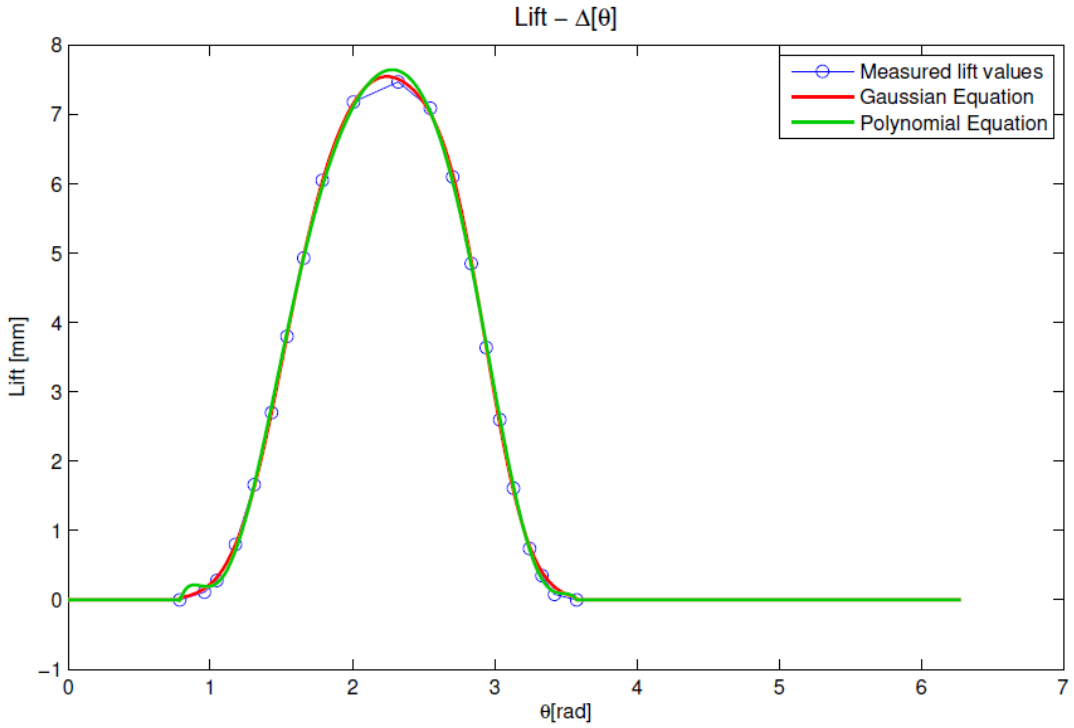

Figure 4.2.: Polynomial approximation curve [8]

To solve that problem a new approximation function is proposed, using a Fourier periodic function [13]. It has the advantage of being a continuous function in all domain. Therefore, it is possible to represent any number of cycles and manipulate the related variables the same way.

To perform it, the Matlab^{TM} Curve Fitting tool was used. For the exhaust valve lift, a 8^{th} degree Fourier approximation was applied, while for the admission valve lift, due to convergence problems, a 7^{th} degree approximation was preferred. The Fourier approximation function is presented in Equation 4.1, as well as its coefficients in Table 4.2 and the graphic, representing two full cycles of the Valve Train System in Figure 4.3.

$$f(t) = a_0 + \sum_{k=1}^{n} \left[a_k \cdot \cos\left(k \cdot w \cdot \theta\right) + b_k \cdot \sin\left(k \cdot w \cdot \theta\right) \right] \tag{4.1}$$

4.2. Importance of derivatives

In some literature (namely at [14]) it is possible to find out how the derivatives of displacement shall be interpreted. Notice that the shape of those derivatives will

Table 4.2.: Table of coefficients for Fourier series

	exhaust	admission
a_0	1.663	1.854
a_1	−1.801	−1.923
b_1	2.352	−2.651
a_2	−0.5166	−0.6903
b_2	−1.987	2.093
a_3	0.9201	0.9718
b_3	0.431	−0.2961
a_4	−0.234	−0.1248
b_4	0.06263	−0.1196
a_5	0.02973	−0.01894
b_5	0.14	−0.1801
a_6	−0.1384	−0.1441
b_6	−0.1202	0.1131
a_7	0.09954	0.07039
b_7	−0.0008081	0.02667
a_8	−0.02514	–
b_8	0.01082	–
w	0.9987	1
SSE	0.009841	0.006798
R-square	1	1
Adjusted R-square	1	1
RMSE	0.01221	0.01243

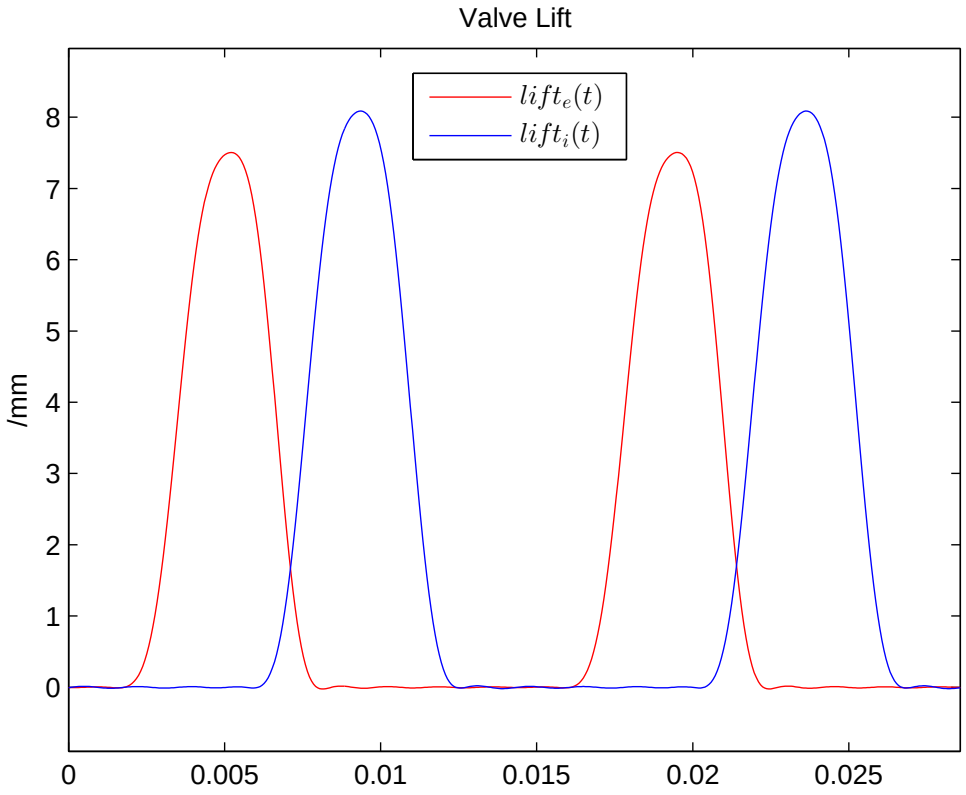

Figure 4.3.: Fourier lift approximation periodic functions along two full cycles

be influenced by the approximation method applied. For instance, in this case of the Fourier method it will appear an harmonic noise related to higher frequency harmonics (which, when derived, have a large increase in amplitude).

The first derivative of position, velocity "represents the slope of the displacement diagram at each angle θ. This derivative although it may now seem a practical value, is a measure of steepness of the displacement diagram." [14]. It is also related to the advantage of the cam system can give an idea of pressure angles.

The second derivative, acceleration, is compared to the radius of curvature of the cam, in an inverse relation. For instance, "as the acceleration becomes large, the radius of curvature becomes very small, the cam profile at that position becomes pointed, a highly unsatisfactory condition from the point of view of contact stresses between the cam and follower surfaces." [14]. This derivative also gives an idea of the shape of the interaction forces between bodies (calling the Newton's second law).

At last (usually the 4^{th} derivative is not considered in valve train system analysis), the third derivative, *jerk*, is the rate of change of the acceleration and, it is known that it should be controlled when choosing the detailed shape of the displacement diagram.

4.2.1. *Jerk*, the third derivative of position

Let's start by relating the jerk to Newton's second law. For instance, "if the net external force isn't constant, a system of constant mass will move with a jerk. That jerk is directly proportional to the time rate of change of the force and inversely proportional to the mass." [15]. As so, at each of the abrupt changes of acceleration, the *jerk* of the follower tends to be infinite.

Some applications of the information token from this derivative are, for instance, the design of roads and rail tracks or elevators, which require pattern levels of comfort (the bigger the jerk in a certain point, the bigger will be the variation in acceleration and the more the human body will notice it).

In a biological way, it is known that the human ear as a sense of jerk, which helps the body equilibrium, activating fast brain responses. It is the main cause of the adrenaline that human body frees, when experiencing brief periods of weightlessness or inversion, as for example in a roller coaster. These kinds of sensations generate intense mental activity, which is why people enjoy doing them. They also allows to keep people focused during possibly life ending moments, which is why the ability to sense jerk is vital to your health and well being. Jerk can be both frightening and exciting.

Jerk is also important to consider in manufacturing processes. In mechanical engineering, jerk is considered, in addition to velocity and acceleration, in the development of cam profiles because of tribological implications and the ability of the actuated body to follow the cam profile without chatter. Jerk must be often considered when the excitation of vibrations is a concern. A device that measures jerk is called a "jerkmeter". [16]

In this InnerCam^{TM} the *jerk* should give information about the shocks and impulses occurring during the cycle of the camshaft.

4.3. Kinematic relations for the exhaust sub-system

Looking back again to Figure 4.1, the kinematic relations will be established in the following equations.

4.3.1. Body 1 - Camshaft

$$\overrightarrow{\omega_{e,10}} = \begin{Bmatrix} 0 \\ 0 \\ \dot{\theta}_e \end{Bmatrix} \tag{4.2}$$

$$\overrightarrow{OC_e} = \begin{Bmatrix} r_e \cdot \cos\alpha_e \\ r_e \cdot \cos\alpha_e \\ 0 \end{Bmatrix} \tag{4.3}$$

$$\overrightarrow{v_{C_e,10}} = \dot{\overrightarrow{OC_e}} = \begin{Bmatrix} \dot{r_e} \cdot \cos\alpha_e - r_e \cdot \dot{\alpha_e} \cdot \sin\alpha_e \\ \dot{r_e} \cdot \sin\alpha_e + r_e \cdot \dot{\alpha_e} \cdot \cos\alpha_e \\ 0 \end{Bmatrix} \tag{4.4}$$

$$\overrightarrow{a_{C_e,10}} = \ddot{\overrightarrow{OC_e}} = \begin{Bmatrix} \ddot{r_e} \cdot \cos\alpha_e - 2\dot{r_e} \cdot \dot{\alpha_e} \cdot \sin\alpha_e - r_e \cdot \ddot{\alpha_e} \cdot \sin\alpha_e - r_e \cdot \dot{\alpha_e}^2 \cos\alpha_e \\ \ddot{r_e} \cdot \sin\alpha_e + 2\dot{r_e} \cdot \dot{\alpha_e} \cdot \cos\alpha_e + r_e \cdot \ddot{\alpha_e} \cdot \cos\alpha_e - r_e \cdot \dot{\alpha_e}^2 \sin\alpha_e \\ 0 \end{Bmatrix} \tag{4.5}$$

$$\overrightarrow{Jerk_{C_e,10}} = \dddot{\overrightarrow{OC_e}} = \begin{Bmatrix} \dddot{r_e} \cdot \cos\alpha_e - 3\ddot{r_e} \cdot \dot{\alpha_e} \sin\alpha_e - 3\dot{r_e} \cdot \ddot{\alpha_e} \cdot \sin\alpha_e - 3\dot{r_e} \cdot \dot{\alpha_e}^2 \cdot \cos\alpha_e \\ \dddot{r_e} \cdot \sin\alpha_e + 3\ddot{r_e} \cdot \dot{\alpha_e} \cos\alpha_e + 3\dot{r_e} \cdot \ddot{\alpha_e} \cdot \cos\alpha_e - 3\dot{r_e} \cdot \dot{\alpha_e}^2 \cdot \sin\alpha_e \\ 0 \end{Bmatrix} +$$

$$\begin{Bmatrix} r_e \cdot \dddot{\alpha_e} \cdot \sin\alpha_e - 3r_e \cdot \ddot{\alpha_e} \cdot \dot{\alpha_e} \cdot \cos\alpha_e - r_e \cdot \dddot{\alpha_e} \cdot \sin\alpha_e \\ -r_e \cdot \dddot{\alpha_e} \cdot \cos\alpha_e - 3r_e \cdot \ddot{\alpha_e} \cdot \dot{\alpha_e} \cdot \sin\alpha_e + r_e \cdot \dddot{\alpha_e} \cdot \cos\alpha_e \\ 0 \end{Bmatrix} \tag{4.6}$$

4.3.2. Body 2 - Exhaust Rocker-Arm

$$\overrightarrow{\omega_{e,20}} = \begin{Bmatrix} 0 \\ 0 \\ \dot{\beta}_e \end{Bmatrix} \tag{4.7}$$

Point C

$$\overrightarrow{AC_e} = \begin{Bmatrix} a \cdot \sin\beta_e \\ -a \cdot \cos\beta_e \\ 0 \end{Bmatrix} \tag{4.8}$$

$$\overrightarrow{v_{C_e,20}} = \dot{\overrightarrow{AC_e}} = \begin{Bmatrix} a \cdot \dot{\beta}_e \cdot \cos\beta_e \\ a \cdot \dot{\beta}_e \cdot \sin\beta_e \\ 0 \end{Bmatrix} \tag{4.9}$$

$$\overrightarrow{a_{C_e,20}} = \ddot{\overrightarrow{AC_e}} = \begin{Bmatrix} a \cdot \ddot{\beta}_e \cdot \cos\beta_e - a \cdot \dot{\beta}_e^{\,2} \cdot \sin\beta_e \\ a \cdot \ddot{\beta}_e \cdot \sin\beta_e + a \cdot \dot{\beta}_e^{\,2} \cdot \cos\beta_e \\ 0 \end{Bmatrix} \tag{4.10}$$

$$\overrightarrow{Jerk_{C_e,20}} = \dddot{\overrightarrow{AC_e}} = \begin{Bmatrix} a \cdot \dddot{\beta}_e \cdot \cos\beta_e - 3a \cdot \ddot{\beta}_e \cdot \dot{\beta}_e \cdot \sin\beta_e - a \cdot \dot{\beta}_e^{\,3} \cdot \cos\beta_e \\ a \cdot \dddot{\beta}_e \cdot \sin\beta_e + 3a \cdot \ddot{\beta}_e \cdot \dot{\beta}_e \cdot \cos\beta_e - a \cdot \dot{\beta}_e^{\,3} \cdot \sin\beta_e \\ 0 \end{Bmatrix} \tag{4.11}$$

Once defined the vector $\overrightarrow{OC_e}$ and $\overrightarrow{AC_e}$ we are now able to determine the values of two unknown time dependent variables: radius $r_e(t)$ and the angle $\alpha_e(t)$ between $\overrightarrow{OC_e}$ and the XX axis. Knowing that the points O and A are fixed in the main referential, as so, according to the Figure 4.4, and remembering Equations 4.3 and 4.8:

$$\overrightarrow{OC_e} = \overrightarrow{OA_e} + \overrightarrow{AC_e} \quad \Longrightarrow \quad \begin{Bmatrix} r_e \cdot \cos\alpha_e \\ r_e \cdot \cos\alpha_e \\ 0 \end{Bmatrix} = \begin{Bmatrix} 15 \\ -35 \\ 0 \end{Bmatrix} + \begin{Bmatrix} a \cdot \sin\beta_e \\ -a \cdot \cos\beta_e \\ 0 \end{Bmatrix} \tag{4.12}$$

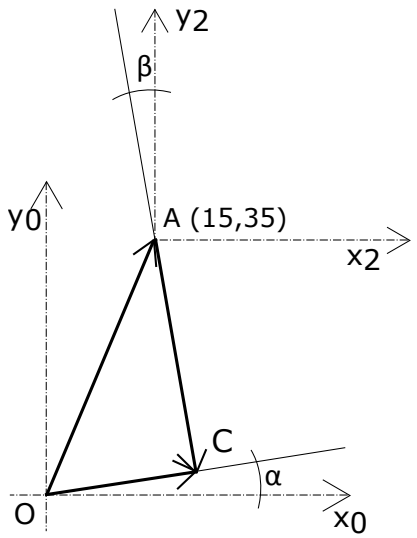

Figure 4.4.: Scheme of the sum of the vectors in the points O, A and C for the exhaust sub-system

$$\Longrightarrow \quad \begin{cases} \alpha_e &= \tan^{-1}\left(\dfrac{a\cdot\sin(\beta_e)+15}{a\cdot\cos(\beta_e)+35}\right) \\ r_e &= \dfrac{a\cdot\sin(\beta_e)+15}{\cos(\alpha_e)} \end{cases} \tag{4.13}$$

Point B

Being $\phi_e = \phi_{e,0} + \beta_e - \beta_{e,0}$:

$$\overrightarrow{AB_e} \begin{Bmatrix} b\cdot\cos\phi_e \\ -b\cdot\sin\phi_e \\ 0 \end{Bmatrix} \tag{4.14}$$

$$\overrightarrow{v_{B_e,20}} = \dot{\overrightarrow{AB_e}} = \begin{Bmatrix} -b\cdot\dot{\beta}_e\cdot\sin\phi_e \\ -b\cdot\dot{\beta}_e\cdot\cos\phi_e \\ 0 \end{Bmatrix} \tag{4.15}$$

$$\overrightarrow{a_{B_e,20}} = \ddot{\overrightarrow{AB_e}} = \begin{Bmatrix} -b\cdot\ddot{\beta}_e\cdot\sin\phi_e - b\cdot\dot{\beta}_e{}^2\cdot\cos\phi_e \\ -b\cdot\ddot{\beta}_e\cdot\cos\phi_e + b\cdot\dot{\beta}_e{}^2\cdot\sin\phi_e \\ 0 \end{Bmatrix} \tag{4.16}$$

$$\overrightarrow{Jerk_{B_e,20}} = \overrightarrow{\dddot{AB}_e} = \begin{Bmatrix} -b \cdot \dddot{\beta}_e \cdot \sin\phi_e - 3b \cdot \ddot{\beta}_e \cdot \dot{\beta}_e \cdot \cos\phi_e + b \cdot \dot{\beta}_e{}^3 \cdot \sin\phi_e \\ -b \cdot \dddot{\beta}_e \cdot \cos\phi_e + 3b \cdot \ddot{\beta}_e \cdot \dot{\beta}_e \cdot \sin\phi_e + b \cdot \dot{\beta}_e{}^3 \cdot \cos\phi_e \\ 0 \end{Bmatrix} \quad (4.17)$$

4.3.3. Body 4 - Exhaust Valve

$$\overrightarrow{v_{e,40}} = (\overrightarrow{\omega_{e,40}}; \overrightarrow{v_{G_e,40}}) \quad (4.18)$$

$$\overrightarrow{\omega_{e,40}} = \overrightarrow{0} \quad \wedge \quad \overrightarrow{v_{G_e,40}} = \overrightarrow{v_{B_e,40}} = \overrightarrow{v_{D_e,40}}* \quad (4.19)$$

*considering the rigid body translation movement

$$\overrightarrow{OB_{e,40}} = \begin{Bmatrix} b\left(\cos\phi_e \cdot \sin\rho + \sin\phi_e \cdot \cos\rho\right) \cdot \sin\phi_e \\ b\left(\cos\phi_e \cdot \sin\rho + \sin\phi_e \cdot \cos\rho\right) \cdot \cos\phi_e \\ 0 \end{Bmatrix} \quad (4.20)$$

$$Lift_e(t) = -b\left(\cos\phi_e \cdot \sin\rho - \sin\phi_e \cdot \cos\rho\right) \quad (4.21)$$

$$v_{e,slippering} = \left| b\left(\dot{\phi}_e \cdot \sin\phi_e \cdot \cos\rho + \dot{\phi}_e \cdot \cos\phi_e \cdot \sin\rho\right) \right| \quad (4.22)$$

4.4. Kinematic relations for the intake sub-system

4.4.1. Body 1 - Camshaft

$$\overrightarrow{\omega_{i,10}} = \begin{Bmatrix} 0 \\ 0 \\ \dot{\theta}_i \end{Bmatrix} \quad (4.23)$$

$$\overrightarrow{OC_i} = \begin{Bmatrix} -r_i \cdot \cos\alpha_i \\ r_i \cdot \cos\alpha_i \\ 0 \end{Bmatrix} \quad (4.24)$$

$$\overrightarrow{v_{C_i,10}} = \overrightarrow{\dot{OC}_i} = \begin{Bmatrix} -\dot{r_i} \cdot \cos\alpha_i + r_i \cdot \dot{\alpha_i} \cdot \sin\alpha_i \\ \dot{r_i} \cdot \sin\alpha_i + r_i \cdot \dot{\alpha_i} \cdot \cos\alpha_i \\ 0 \end{Bmatrix} \tag{4.25}$$

$$\overrightarrow{a_{C_i,10}} = \overrightarrow{\ddot{OC}_i} = \begin{Bmatrix} -\ddot{r_i} \cdot \cos\alpha_i + 2\dot{r_i} \cdot \dot{\alpha_i} \cdot \sin\alpha_i + r_i \cdot \ddot{\alpha_i} \cdot \sin\alpha_i + r_e \cdot {\dot{\alpha_i}}^2 \cos\alpha_i \\ \ddot{r_i} \cdot \sin\alpha_i + 2\dot{r_i} \cdot \dot{\alpha_i} \cdot \cos\alpha_i + r_i \cdot \ddot{\alpha_i} \cdot \cos\alpha_i - r_i \cdot {\dot{\alpha_i}}^2 \sin\alpha_e \\ 0 \end{Bmatrix} \tag{4.26}$$

$$\overrightarrow{Jerk_{C_i,10}} = \overrightarrow{\dddot{OC}_i} = \begin{Bmatrix} -\dddot{r_i} \cdot \cos\alpha_i + 3\ddot{r_i} \cdot \dot{\alpha_i} \sin\alpha_i + 3\dot{r_i} \cdot \ddot{\alpha_i} \cdot \sin\alpha_i + 3\dot{r_i} \cdot {\dot{\alpha_i}}^2 \cdot \cos\alpha_i \\ \dddot{r_i} \cdot \sin\alpha_i + 3\ddot{r_i} \cdot \dot{\alpha_i} \cos\alpha_i + 3\dot{r_i} \cdot \ddot{\alpha_i} \cdot \cos\alpha_i - 3\dot{r_i} \cdot {\dot{\alpha_i}}^2 \cdot \sin\alpha_i \\ 0 \end{Bmatrix} +$$

$$\begin{Bmatrix} -r_i \cdot \dddot{\alpha_i} \cdot \sin\alpha_i + 3r_i \cdot \ddot{\alpha_i} \cdot \dot{\alpha_i} \cdot \cos\alpha_i + r_i \cdot \dddot{\alpha_i} \cdot \sin\alpha_i \\ -r_i \cdot \dddot{\alpha_i} \cdot \cos\alpha_i - 3r_i \cdot \ddot{\alpha_i} \cdot \dot{\alpha_i} \cdot \sin\alpha_i + r_i \cdot \dddot{\alpha_i} \cdot \cos\alpha_i \\ 0 \end{Bmatrix} \tag{4.27}$$

4.4.2. Body 3 - Admission Rocker-Arm

$$\overrightarrow{\omega_{i,30}} = \begin{Bmatrix} 0 \\ 0 \\ \dot{\beta_i} \end{Bmatrix} \tag{4.28}$$

Point C

$$\overrightarrow{AC_i} = \begin{Bmatrix} -a \cdot \sin\beta_i \\ -a \cdot \cos\beta_i \\ 0 \end{Bmatrix} \tag{4.29}$$

$$\overrightarrow{v_{C_i,30}} = \overrightarrow{\dot{AC}_i} = \begin{Bmatrix} -a \cdot \dot{\beta_i} \cdot \cos\beta_i \\ a \cdot \dot{\beta_i} \cdot \sin\beta_i \\ 0 \end{Bmatrix} \tag{4.30}$$

$$\overrightarrow{a_{C_i,30}} = \overrightarrow{\ddot{AC}_i} = \begin{Bmatrix} -a \cdot \ddot{\beta}_i \cdot \cos\beta_i + a \cdot \dot{\beta}_i^{\,2} \cdot \sin\beta_i \\ a \cdot \ddot{\beta}_i \cdot \sin\beta_i + a \cdot \dot{\beta}_i^{\,2} \cdot \cos\beta_i \\ 0 \end{Bmatrix} \tag{4.31}$$

$$\overrightarrow{Jerk_{C_i,30}} = \overrightarrow{\dddot{AC}_i} = \begin{Bmatrix} -a \cdot \dddot{\beta}_i \cdot \cos\beta_i + 3a \cdot \ddot{\beta}_i \cdot \dot{\beta}_i \cdot \sin\beta_i + a \cdot \dot{\beta}_i^{\,3} \cdot \cos\beta_i \\ a \cdot \dddot{\beta}_i \cdot \sin\beta_i + 3a \cdot \ddot{\beta}_i \cdot \dot{\beta}_i \cdot \cos\beta_i - a \cdot \dot{\beta}_i^{\,3} \cdot \sin\beta_i \\ 0 \end{Bmatrix} \tag{4.32}$$

Once defined the vector $\overrightarrow{OC_i}$ and $\overrightarrow{AC_i}$ the same way we did for the exhaust sub-system we can determine the values of two unknown time dependent variables: radius $r_i(t)$, and the angle $\alpha_i(t)$ between $\overrightarrow{OC_i}$ and the XX axis. Knowing that the points O and A are fixed in the main referential, as so, according to the Figure 4.5, and remembering Equations 4.24 and 4.29:

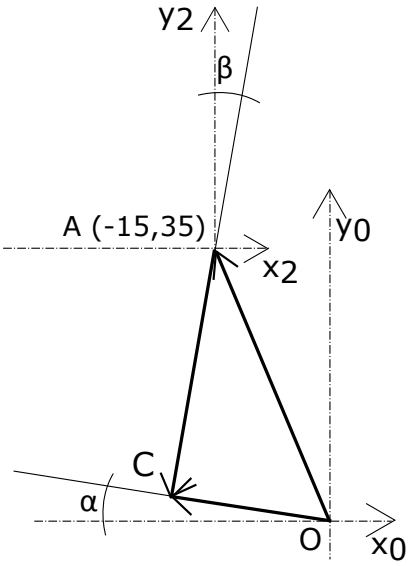

Figure 4.5.: Scheme of the sum of the vectors in the points O, A and C for the intake sub-system

$$\overrightarrow{OC_e} = \overrightarrow{OA_e} + \overrightarrow{AC_e} \quad \Longrightarrow \quad \begin{Bmatrix} -r_e \cdot \cos\alpha_e \\ r_e \cdot \cos\alpha_e \\ 0 \end{Bmatrix} = \begin{Bmatrix} -15 \\ -35 \\ 0 \end{Bmatrix} + \begin{Bmatrix} -a \cdot \sin\beta_e \\ -a \cdot \cos\beta_e \\ 0 \end{Bmatrix} \tag{4.33}$$

$$\Longrightarrow \quad \begin{cases} \alpha_e &= \tan^{-1}\left(\dfrac{a\cdot\sin(\beta_i)+15}{a\cdot\cos(\beta_i)+35}\right) \\ r_e &= \dfrac{a\cdot\sin(\beta_i)+15}{\cos(\alpha_i)} \end{cases} \tag{4.34}$$

Point B

Being $\phi_i = \phi_{i,0} + \beta_i - \beta_{i,0}$:

$$\overrightarrow{AB_i} = \begin{Bmatrix} -b\cdot\cos\phi_i \\ -b\cdot\sin\phi_i \\ 0 \end{Bmatrix} \tag{4.35}$$

$$\overrightarrow{v_{B_i,20}} = \dot{\overrightarrow{AB_i}} = \begin{Bmatrix} b\cdot\dot{\beta}_i\cdot\sin\phi_i \\ -b\cdot\dot{\beta}_i\cdot\cos\phi_i \\ 0 \end{Bmatrix} \tag{4.36}$$

$$\overrightarrow{a_{B_i,20}} = \ddot{\overrightarrow{AB_i}} = \begin{Bmatrix} b\cdot\ddot{\beta}_i\cdot\sin\phi_i + b\cdot\dot{\beta}_i^{\,2}\cdot\cos\phi_i \\ -b\cdot\ddot{\beta}_i\cdot\cos\phi_i + b\cdot\dot{\beta}_i^{\,2}\cdot\sin\phi_i \\ 0 \end{Bmatrix} \tag{4.37}$$

$$\overrightarrow{Jerk_{B_i,20}} = \dddot{\overrightarrow{AB_i}} = \begin{Bmatrix} b\cdot\dddot{\beta}_i\cdot\sin\phi_i + 3b\cdot\ddot{\beta}_i\cdot\dot{\beta}_i\cdot\cos\phi_i - b\cdot\dot{\beta}_i^{\,3}\cdot\sin\phi_i \\ -b\cdot\dddot{\beta}_i\cdot\cos\phi_i + 3b\cdot\ddot{\beta}_i\cdot\dot{\beta}_i\cdot\sin\phi_i + b\cdot\dot{\beta}_i^{\,3}\cdot\cos\phi_i \\ 0 \end{Bmatrix} \tag{4.38}$$

4.4.3. Body 5 - Admission Valves

$$\overrightarrow{v_{i,50}} = (\overrightarrow{\omega_{i,50}}; \overrightarrow{v_{G_{i,50}}}) \tag{4.39}$$

$$\overrightarrow{\omega_{i,50}} = \overrightarrow{0} \qquad \wedge \qquad \overrightarrow{v_{G_i,50}} = \overrightarrow{v_{B_i,50}} = \overrightarrow{v_{D_i,50}}* \tag{4.40}$$

*considering the rigid body translation movement

$$\overrightarrow{OB_{i,50}} = \begin{Bmatrix} b\left(\cos\phi_i \cdot \sin\rho + \sin\phi_i \cdot \cos\rho\right) \cdot \sin\phi_i \\ b\left(\cos\phi_i \cdot \sin\rho + \sin\phi_i \cdot \cos\rho\right) \cdot \cos\phi_i \\ 0 \end{Bmatrix} \tag{4.41}$$

$$Lift_i(t) = -b\left(\cos\phi_i \cdot \sin\rho - \sin\phi_i \cdot \cos\rho\right) \tag{4.42}$$

$$v_{i,slippering} = \left| b\left(\dot{\phi}_i \cdot \sin\phi_i \cdot \cos\rho + \dot{\phi}_i \cdot \cos\phi_i \cdot \sin\rho\right)\right| \tag{4.43}$$

4.5. Model results

The set of results produced had in consideration the position of each parameter considered in the previous equations. This parameters are followed by the corresponding derivatives, giving information about the velocity, acceleration and $Jerk$. Those evaluated results are, keeping in mind that each plot presents the results for both intake and exhaust sub-systems:

- Valve Lift
- Distance r (length of vector OC)
- Angle *alpha*
- Angle *beta*
- Point C
  - X component
  - Y component
- Point B
  - X component
  - Y component

In the figures presented it was considered a speed of 4200 rpm in the camshaft, corresponding to a 8400 rpm regime in the crankshaft. However, this set of results was repeated to other speeds (5100 and 12000 rpm engine regime), in order to identify the maximum values at each speed and verify the evolution of the parameters with the engine speed

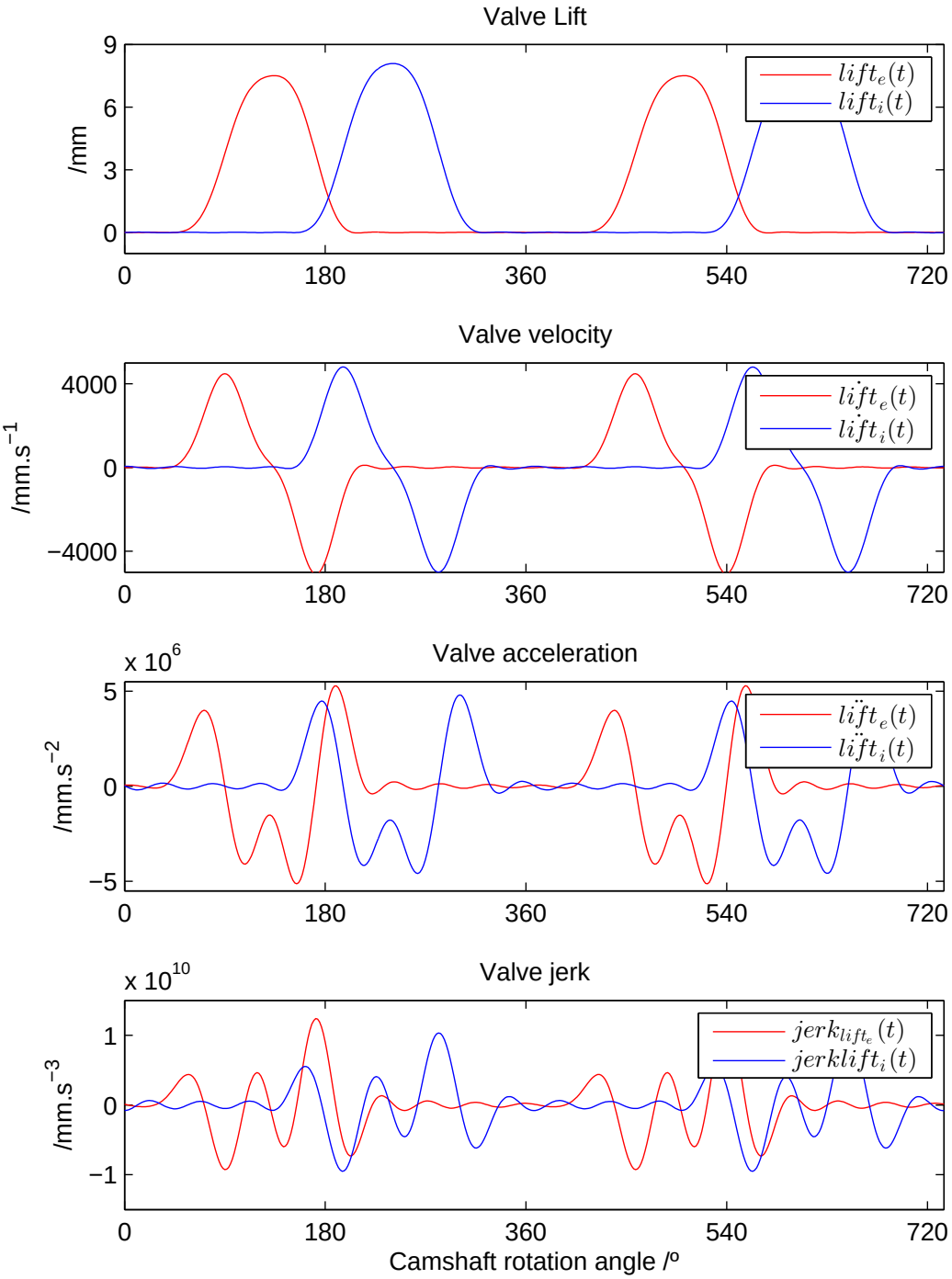

Figure 4.6.: $lift$, $\dot{lift}$, $\ddot{lift}$, $\dddot{lift}$ profiles at $4200rpm$ (in the camshaft)

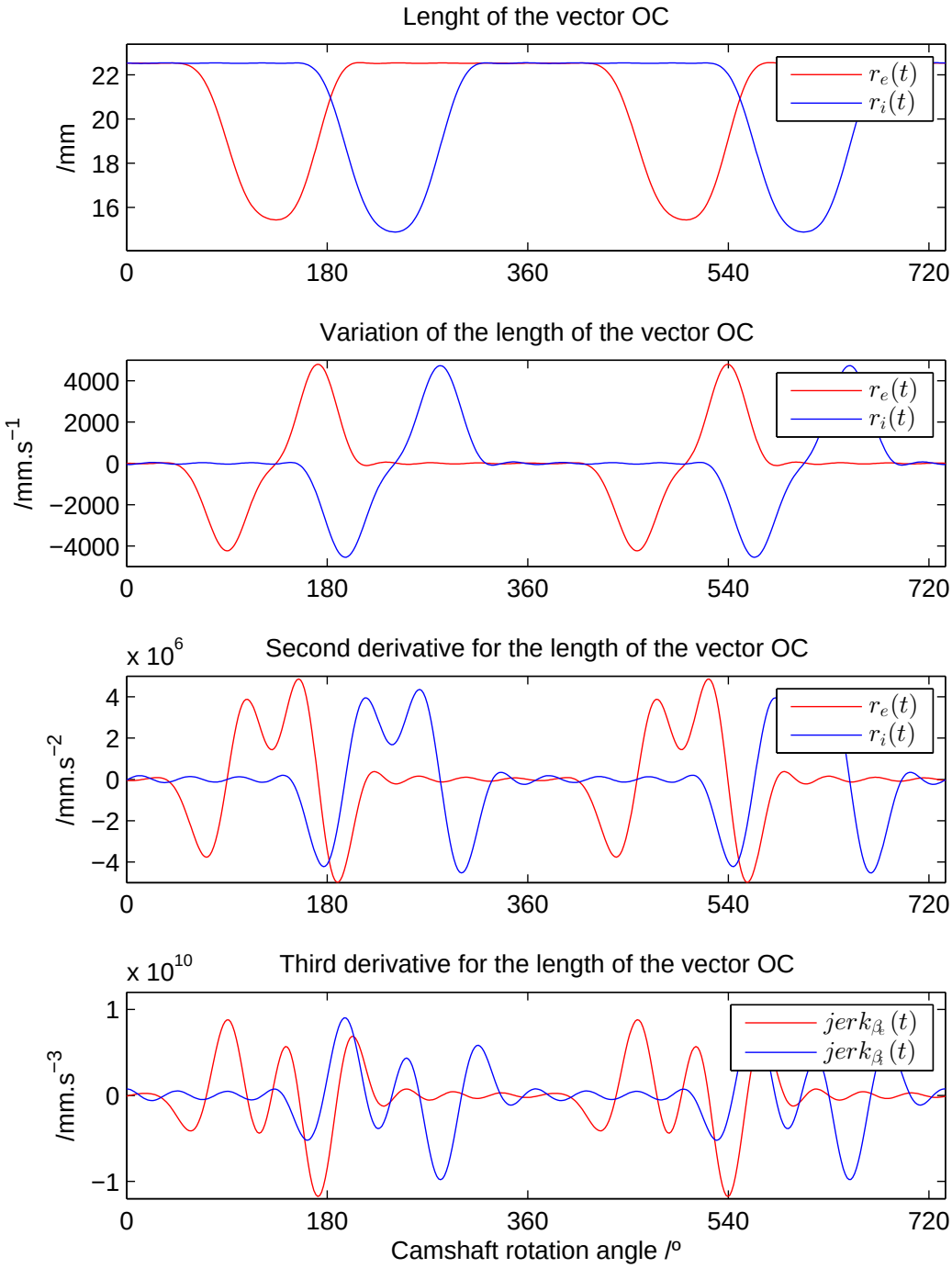

Figure 4.7.: r, $\dot{r}$, $\ddot{r}$, $\dddot{r}$ profiles at $4200rpm$ (in the camshaft)

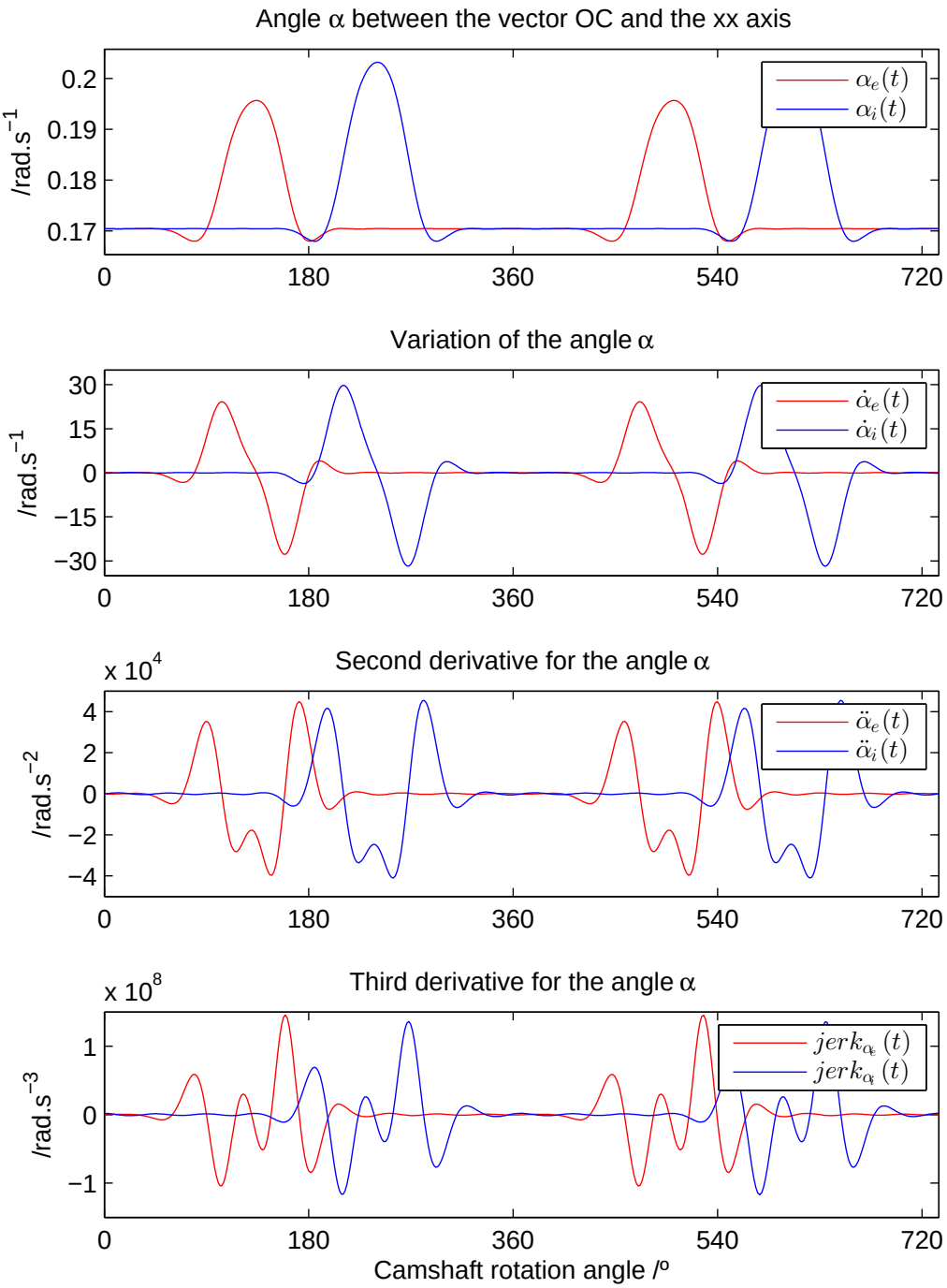

Figure 4.8.: α, $\dot{\alpha}$, $\ddot{\alpha}$, $\dddot{\alpha}$ profiles at $4200rpm$ (in the camshaft)

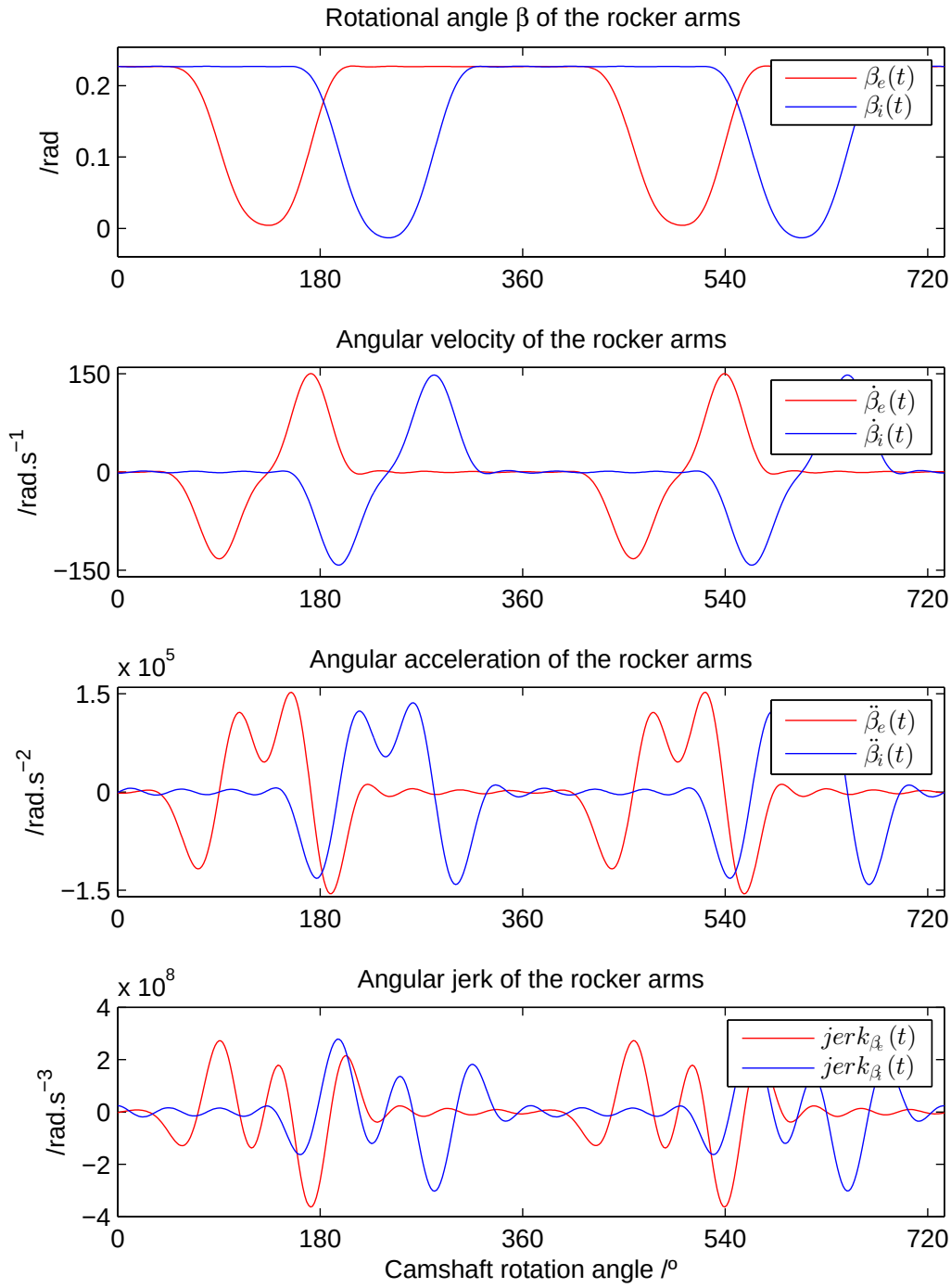

Figure 4.9.: β, $\dot{\beta}$, $\ddot{\beta}$, $\dddot{\beta}$ profiles at $4200rpm$ (in the camshaft)

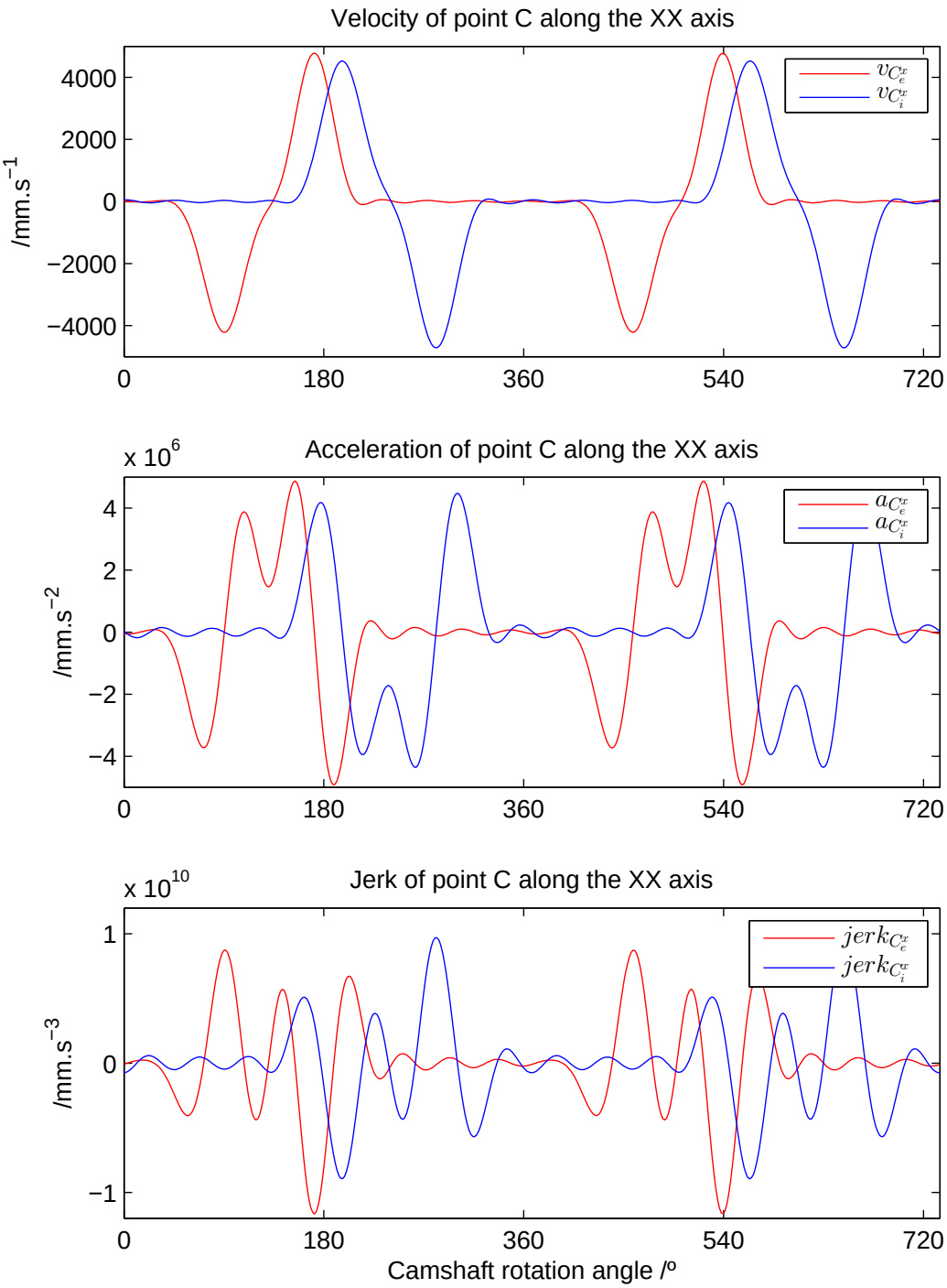

Figure 4.10.: Derivative profiles for the point C along XX axis at 4200rpm (in the camshaft)

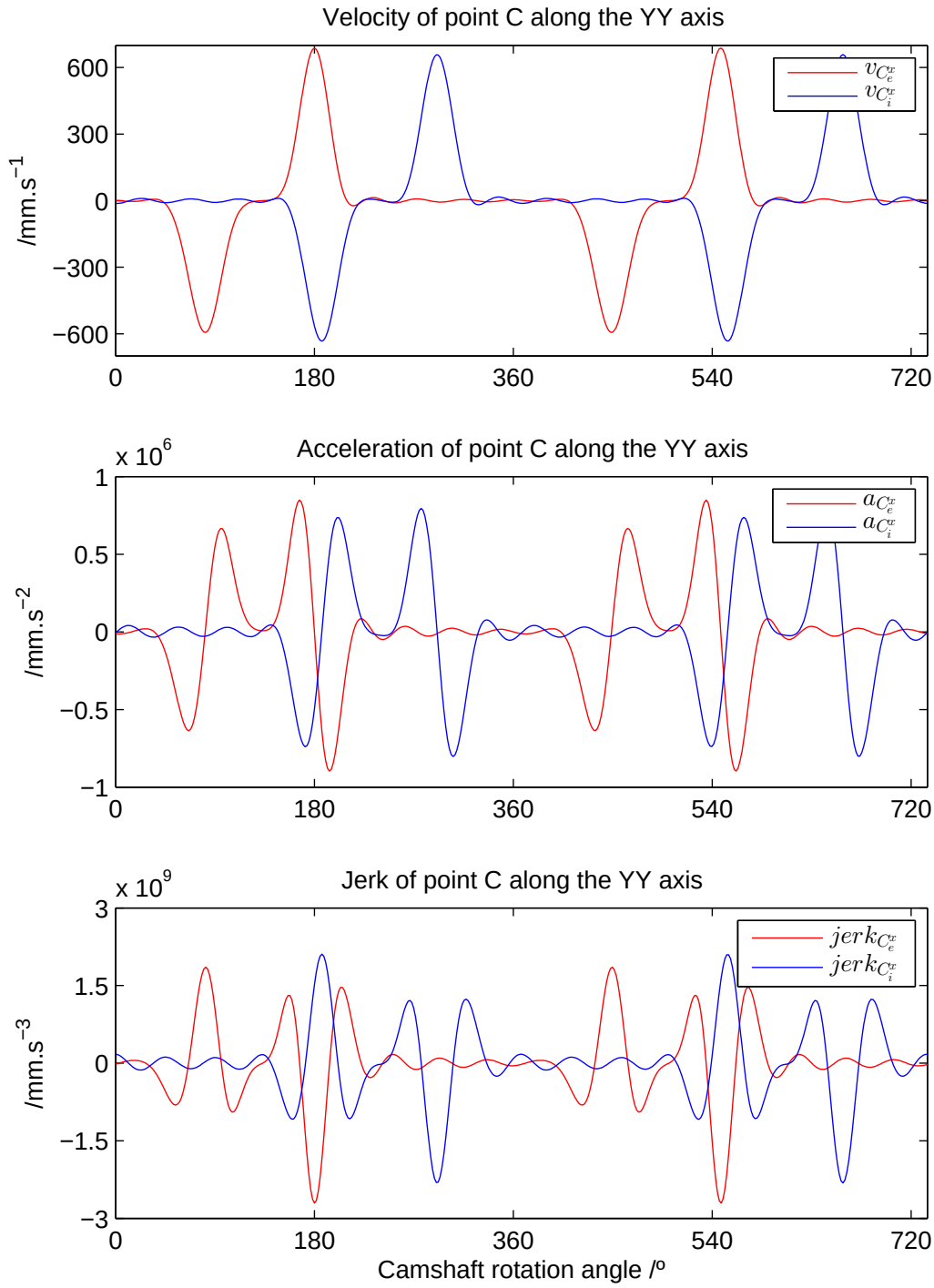

Figure 4.11.: Derivative profiles for the point C along XX axis at 4200rpm (in the camshaft)

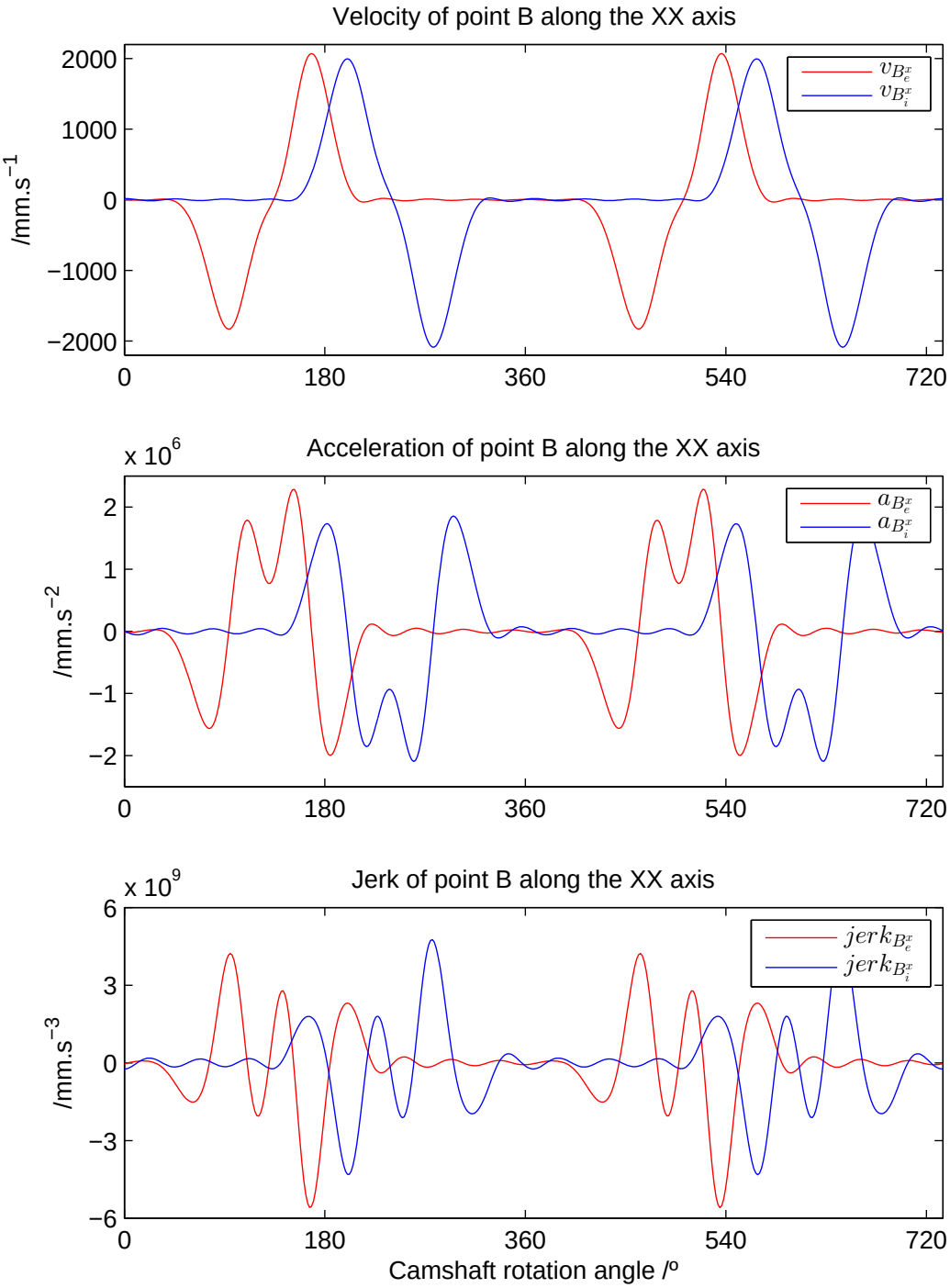

Figure 4.12.: Derivative profiles for the point B along XX axis at 4200rpm (in the camshaft)

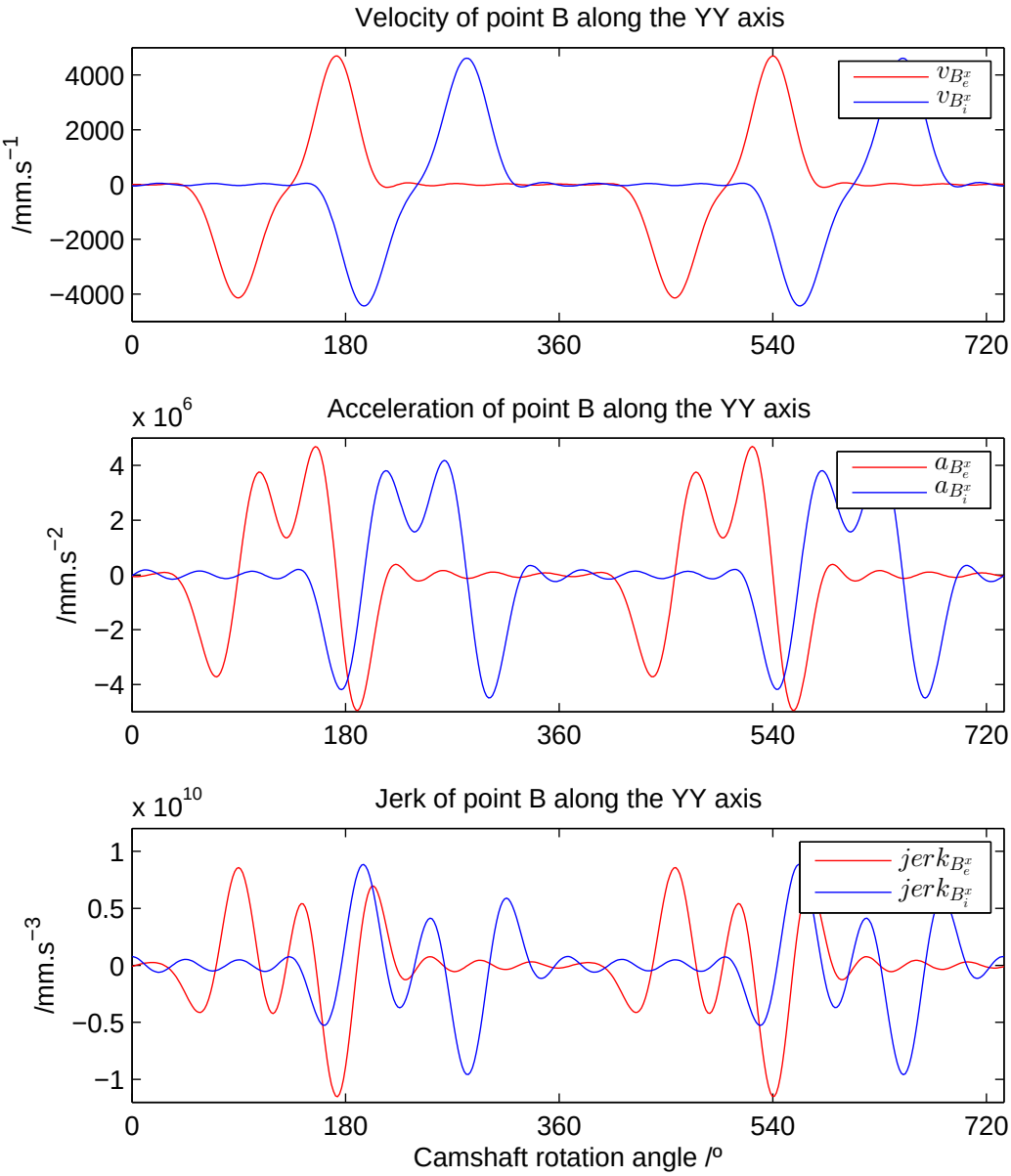

Figure 4.13.: Derivative profiles for the point B along XX axis at $4200rpm$ (in the camshaft)

4.6. Discussion of results

The set of results presented was repeated for other 2 different speeds (2550 and 6000 rpm). In order to compare those simulations, the maximum (absolute) values were obtained for each plot using MatLab^{TM} data cursor function, so that it would be possible to get an idea of the evolution of the kinematic behaviour with the increase of speed.

	5100 rpm		8400 rpm		12000 rpm		
	exhaust	intake	exhaust	intake	exhaust	intake	units
$\dot{lift}$	2721	2917	4482	4804	6403	6863	$mm.s^{-1}$
$\ddot{lift}$	1.945	1.771	5.276	4.805	10.77	9.805	$10^6\ mm.s^{-2}$
$\dddot{lift}$	2.773	2.311	12.39	10.33	36.12	30.11	$10^9\ mm.s^{-3}$

Table 4.3.: Maximum values for lift derivatives at different speeds

	5100 rpm		8400 rpm		12000 rpm		
	exhaust	intake	exhaust	intake	exhaust	intake	units
$\dot{\beta}$	91.27	90.02	150.3	148.3	214.7	211.8	$^o.s^{-1}$
$\ddot{\beta}$	-5.720	-5.217	-15.53	-14.15	-31.70	-28.89	$10^4\ ^o.s^{-2}$
$\dddot{\beta}$	-8.133	-6.766	-36.34	-30.23	-105.9	-88.13	$10^7\ ^o.s^{-3}$

Table 4.4.: Maximum values for β derivatives at different speeds

	5100 rpm		8400 rpm		12000 rpm		
	exhaust	intake	exhaust	intake	exhaust	intake	units
$\dot{r}$	2916	2875	4803	4736	6862	6765	$mm.s^{-1}$
$\ddot{r}$	1.945	1.771	5.276	4.805	10.77	9.805	$10^6\ mm.s^{-2}$
$\dddot{r}$	2.773	2.311	12.39	10.33	36.12	30.11	$10^9\ mm.s^{-3}$

Table 4.5.: Maximum values for length of vector OC, r, derivatives at different speeds

4.7. Comparison of results with previous work

Some differences can be identified between these results and the ones obtained in previous works, for example [8]. The Fourier approximation method revealed to be accurate in all time domain till the first derivative of position. In the acceleration

	5100 rpm		8400 rpm		12000 rpm		
	exhaust	intake	exhaust	intake	exhaust	intake	units
$\dot{\alpha}$	-16.85	-19.29	-27.75	-31.77	-39.65	-45.38	$^{o}.s^{-1}$
$\ddot{\alpha}$	-5.720	-5.217	-15.53	-14.15	-31.70	-28.89	$10^{4}\ ^{o}.s^{-2}$
$\dddot{\alpha}$	-8.133	-6.766	-36.34	-30.23	-105.9	-88.13	$10^{7}\ ^{o}.s^{-3}$

Table 4.6.: Maximum values for α derivatives at different speeds

	5100 rpm		8400 rpm		12000 rpm		
	exhaust	intake	exhaust	intake	exhaust	intake	units
$\overrightarrow{v^{x}_{C,20}}$	2901	2749	4778	4529	6862	6765	$mm.s^{-1}$
$\overrightarrow{a^{x}_{C,20}}$	-1.813	1.652	-4.918	4.481	-10.04	9.145	$10^{6}\ mm.s^{-2}$
$\overrightarrow{jerk^{x}_{C,20}}$	-2.610	2.173	9.711	-11.66	-34.00	28.31	$10^{9}\ mm.s^{-3}$

Table 4.7.: Maximum values for derivatives of movement in point C along XX axis at different speeds

	5100 rpm		8400 rpm		12000 rpm		
	exhaust	intake	exhaust	intake	exhaust	intake	units
$\overrightarrow{v^{y}_{C,20}}$	417.5	399.1	687.7	657.3	982.5	939	$mm.s^{-1}$
$\overrightarrow{a^{y}_{C,20}}$	-0.3304	-0.2959	-0.8964	-0.8027	-1.829	-1.638	$10^{6}\ mm.s^{-2}$
$\overrightarrow{jerk^{y}_{C,20}}$	-0.6056	-0.5165	2.706	-2.308	-7.889	6.729	$10^{9}\ mm.s^{-3}$

Table 4.8.: Maximum values for derivatives of movement in point C along YY axis at different speeds

	5100 rpm		8400 rpm		12000 rpm		
	exhaust	intake	exhaust	intake	exhaust	intake	units
$\overrightarrow{v^{x}_{B,20}}$	1257	-1266	2071	-2086	2959	-2979	$mm.s^{-1}$
$\overrightarrow{a^{x}_{B,20}}$	0.8413	-0.7714	2.282	-2.093	4.658	-4.271	$10^{6}\ mm.s^{-2}$
$\overrightarrow{jerk^{x}_{B,20}}$	-1.249	1.066	-5.580	4.762	-16.27	13.88	$10^{9}\ mm.s^{-3}$

Table 4.9.: Maximum values for derivatives of movement in point B along XX axis at different speeds

and *jerk* plots, the high frequency harmonics became more evident, at stationary positions. However, the curves present no discontinuities in all domain and it's now possible to plot more that one cycle in the same plot and get a better idea of periodicity.

	5100 rpm		8400 rpm		12000 rpm		
	exhaust	intake	exhaust	intake	exhaust	intake	units
$\overrightarrow{v^{y}_{B,20}}$	2849	2803	4696	4617	6703	6596	$mm.s^{-1}$
$\overrightarrow{a^{y}_{B,20}}$	-1.826	-1.656	-4.954	-4.491	-10.11	-9.166	$10^{6}\ mm.s^{-2}$
$\overrightarrow{jerk^{y}_{B,20}}$	-2.577	-2.142	-11.51	-9.570	-33.57	-27.90	$10^{9}\ mm.s^{-3}$

Table 4.10.: Maximum values for derivatives of movement in point B along YY axis at different speeds

In the exhaust sub-system results, it is possible to notice a difference in the 2^{nd} and 3^{rd} derivatives for an angle around 2 rad or, at this speed, $4200rpm$, for $t \approx 0.0045\ s$. The reason for that contrast maybe the polynomial approximation when derived.

Notice that the amplitude of the derivatives does not correspond, because in this work, the derivatives took into account a rotation speed of $4200rpm$, at the camshaft, while in [8] the derivatives were calculated in relation to the angle (in radians).

5. Dynamic Analysis

According to the kinematic results obtained in the previous chapter, a new dynamic model was developed. The differences between previous works is that the all mechanism was analysed as one. As so, the dynamic equilibrium of the first body (the camshaft) was calculated, considering the interactions between both the intake and exhaust rocker-arms. That way the InnerCam^{TM} will be treated as a single system, not separating the intake or exhaust sub-system.

5.1. Inertia properties

The inertia and mass properties of each element were determined using the software SolidWorks^{TM}'s functionalities. Those values can be consulted at Appendix B (take in consideration that the indicated axis may not correspond to the ones used in this calculations). The global and local coordinate systems used in this calculation were the ones represented in the Figure 4.1, which is recommended to be analysed again. The values presented here were obtained from the .STEP files provided by AJP Motos S.A. . The global mass of each body is presented in the table 5.1.

Table 5.1.: Mass properties of each body part

Body no.	Body name	mass /kg	Center of mass /mm
1	Camshaft	0.324	$(0.034, -0.0663, 0.141)$
2	Exhaust Rocker	0.127	$(10.725, -7.311, -22.115)$
3	Intake Rocker	0.127	$(-10.869, -7.333, 30.184)$
4	Exhaust Valve	0.024	$(0, -68.232, 0)$
5	Intake Valve	0.028	$(0, -71.643, 0)$

5.1.1. Body 1 - Camshaft

The inertia matrix presented bellow is taken at the origin referential and, for that reason, the main inertia moments, I_{xx} and I_{yy} are considerably large, because of the distance between the centre of mass and origin referential along ZZ axis.

$$[I_1] = \begin{bmatrix} 1527.596 & -0.293 & 1.378 \\ -0.293 & 1527.992 & -0.773 \\ 1.378 & -0.773 & 116.348 \end{bmatrix} \quad /kg \cdot mm^2 \tag{5.1}$$

$$\boxed{\tau_{G_1}^{QA}\left(\overrightarrow{\dot{Q}_1}; \overrightarrow{K_{G_1}}\right)} \tag{5.2}$$

$$\overrightarrow{\dot{Q}_1} = m_1 \cdot \overrightarrow{\ddot{OG}_1} = \begin{Bmatrix} 0 \\ 0 \\ 0 \end{Bmatrix} \tag{5.3}$$

$$\overrightarrow{K_{G_1}} = [I_1] \times \overrightarrow{\Omega_{10}} = \begin{Bmatrix} \overrightarrow{K_{G_1}^x} \\ \overrightarrow{K_{G_1}^y} \\ I_{zz,1} \cdot \ddot{\theta} \end{Bmatrix} \tag{5.4}$$

5.1.2. Body 2 - Exhaust Rocker-arm

The inertia matrix presented bellow is taken at the origin referential of the rocker-arm body-part, which corresponds to the centre of rotation.

$$[I_2] = \begin{bmatrix} 115.842 & -5.385 & 14.857 \\ -5.385 & 131.741 & -30.445 \\ 14.857 & -30.445 & 63.375 \end{bmatrix} \quad /kg \cdot mm^2 \tag{5.5}$$

$$\boxed{\tau_{A_e}^{QA}\left(\overrightarrow{\dot{Q}_2}; \overrightarrow{K_{A_e}}\right)} \tag{5.6}$$

$$\overrightarrow{\dot{Q}_2} = m_2 \cdot \overrightarrow{\ddot{AG}_2} = m_2 \cdot \left[\overrightarrow{\ddot{OA}_2} + \overrightarrow{\Omega_{20}} \times \overrightarrow{AG_2} + \overrightarrow{\omega_{20}} \times \left(\overrightarrow{\omega_{20}} \times \overrightarrow{G_2}\right)\right] \tag{5.7}$$

$$\overrightarrow{AG_2} = \begin{Bmatrix} \overline{AG_{2x}} \cdot \dot{\beta}_e \cdot \cos(\beta_e) + \overline{AG_{2y}} \cdot \dot{\beta}_e \cdot \sin(\beta_e) \\ \overline{AG_{2x}} \cdot \dot{\beta}_e \cdot \sin(\beta_e) - \overline{AG_{2y}} \cdot \dot{\beta}_e \cdot \cos(\beta_e) \\ 0 \end{Bmatrix} \tag{5.8}$$

$$\overrightarrow{K_{G_2}} = [I_2] \times \overrightarrow{\Omega_{20}} = \begin{Bmatrix} \overrightarrow{K^x_{G_2}} \\ \overrightarrow{K^y_{G_2}} \\ I_{zz,2} \cdot \ddot{\beta} \end{Bmatrix} \tag{5.9}$$

$$\overrightarrow{K_{A_e}} = \overrightarrow{K_{G_2}} + \overrightarrow{AG_2} \times \dot{\overrightarrow{Q_2}} \tag{5.10}$$

5.1.3. Body 3 - Intake Rocker-arm

The inertia matrix presented bellow is taken at the origin referential of the rocker-arm body-part, which corresponds to the centre of rotation.

$$[I_3] = \begin{bmatrix} 160.783 & -5.199 & 48.025 \\ -5.199 & 178.055 & -32.585 \\ 48.025 & -32.585 & 64.918 \end{bmatrix} \quad /kg \cdot mm^2 \tag{5.11}$$

$$\boxed{\tau^{QA}_{A_i}\left(\dot{\overrightarrow{Q_3}}; \overrightarrow{K_{A_i}}\right)} \tag{5.12}$$

$$\dot{\overrightarrow{Q_3}} = m_3 \cdot \ddot{\overrightarrow{AG_3}} = m_3 \cdot \left[\ddot{\overrightarrow{OA_3}} + \overrightarrow{\Omega_{30}} \times \overrightarrow{AG_3} + \overrightarrow{\omega_{30}} \times \left(\overrightarrow{\omega_{30}} \times \overrightarrow{AG_3}\right)\right] \tag{5.13}$$

$$\overrightarrow{AG_3} = \begin{Bmatrix} -\overline{AG_{3x}} \cdot \dot{\beta}_i \cdot \cos(\beta_i) - \overline{AG_{3y}} \cdot \dot{\beta}_i \cdot \sin(\beta_i) \\ \overline{AG_{3x}} \cdot \dot{\beta}_i \cdot \sin(\beta_i) - \overline{AG_{3y}} \cdot \dot{\beta}_i \cdot \cos(\beta_i) \\ 0 \end{Bmatrix} \tag{5.14}$$

$$\overrightarrow{K_{G_3}} = [I_3] \times \overrightarrow{\Omega_{30}} = \begin{Bmatrix} \overrightarrow{K^x_{G_3}} \\ \overrightarrow{K^y_{G_3}} \\ I_{zz,3} \cdot \ddot{\beta} \end{Bmatrix} \tag{5.15}$$

$$\overrightarrow{K_{A_i}} = \overrightarrow{K_{G_3}} + \overrightarrow{AG_3} \times \dot{\overrightarrow{Q_3}} \tag{5.16}$$

5.1.4. Body 4 - Exhaust Valves

The inertia matrix presented bellow is taken at the centre of mass of the valve, with directions of the local referential.

$$[I_4] = \begin{bmatrix} 26.174 & 0 & 0 \\ 0 & 0.631 & 0 \\ 0 & 0 & 26.174 \end{bmatrix} \quad /kg \cdot mm^2 \tag{5.17}$$

$$\boxed{\tau_{G_4}^{QA}\left(\dot{\overrightarrow{Q_4}}; \overrightarrow{K_{G_4}}\right)} \tag{5.18}$$

$$\dot{\overrightarrow{Q_4}} = m_4 \cdot \ddot{\overrightarrow{OG_4}} = \begin{Bmatrix} -li\ddot{f}t_e \cdot sin(\rho) \\ -li\ddot{f}t_e \cdot cos(\rho) \\ 0 \end{Bmatrix} \tag{5.19}$$

$$\overrightarrow{K_{G_4}} = [I_4] \times \overrightarrow{\Omega_{40}} = \overrightarrow{0} \tag{5.20}$$

5.1.5. Body 5 - Intake Valves

The inertia matrix presented bellow is taken at the centre of mass of the valve, with directions of the local referential.

$$[I_5] = \begin{bmatrix} 28.970 & 0 & 0 \\ 0 & 1.121 & 0 \\ 0 & 0 & 28.970 \end{bmatrix} \quad /kg \cdot mm^2 \tag{5.21}$$

$$\boxed{\tau_{G_5}^{QA}\left(\dot{\overrightarrow{Q_5}}; \overrightarrow{K_{G_5}}\right)} \tag{5.22}$$

$$\dot{\overrightarrow{Q_5}} = m_5 \cdot \ddot{\overrightarrow{OG_5}} = \begin{Bmatrix} li\ddot{f}t_i \cdot sin(\rho) \\ -li\ddot{f}t_i \cdot cos(\rho) \\ 0 \end{Bmatrix} \tag{5.23}$$

$$\overrightarrow{K_{G_5}} = [I_5] \times \overrightarrow{\Omega_{50}} = \overrightarrow{0} \tag{5.24}$$

5.2. Equations of equilibrium

Considering that all the bodies have the translation according to ZZ axis blocked by other exterior components, we can assume that the third component of the forces is not important in the dynamic equations of the system. For the same reason the rotation along the XX and YY will be considered null in this analysis.

Notwithstanding it is important to re-mention that the rocker arms have no main inertia axis along zz direction (see equations 5.5 and 5.11). As so, those bodies will tend to move against the camshaft in that direction. That phenomenon will also not be considered in this analysis, because there is no information about the way those bodies are fixed and how can they move through that direction. Some results will be plotted latter in a next chapter.

5.2.1. Body 1 - Camshaft

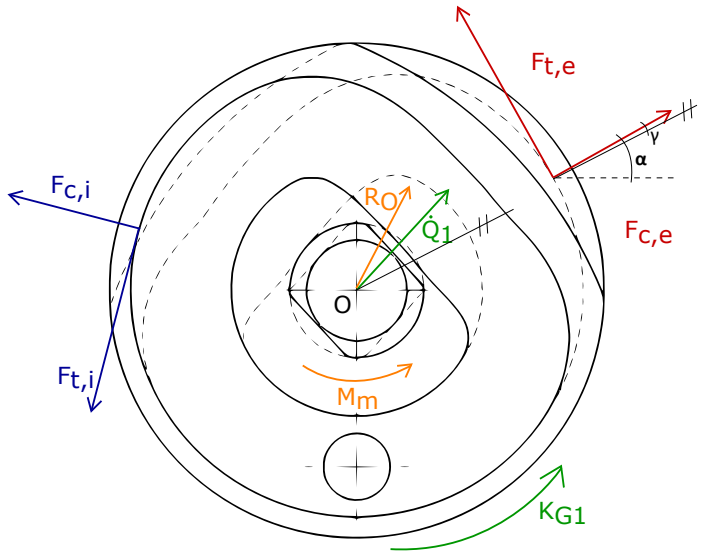

Figure 5.1.: Scheme for dynamic equilibrium on the Camshaft

$$\overrightarrow{R_O} + \overrightarrow{F_{c,e}} + \overrightarrow{F_{t,e}} + \overrightarrow{F_{c,i}} + \overrightarrow{F_{t,i}} + m_1 \cdot \overrightarrow{g} = \dot{\overrightarrow{Q_1}} \tag{5.25}$$

$$\overrightarrow{M_m} + \overrightarrow{OI_e} \times \left(\overrightarrow{F_{c,e}} + \overrightarrow{F_{t,e}}\right) + \overrightarrow{OI_i} \times \left(\overrightarrow{F_{c,i}} + \overrightarrow{F_{t,i}}\right) = \overrightarrow{K_{G_1}} \tag{5.26}$$

$$\overrightarrow{R_O} = \begin{Bmatrix} R_O^x \\ R_O^y \\ - \end{Bmatrix} \tag{5.27}$$

$$\overrightarrow{F_{c,e}} = F_{c,e} \cdot \begin{Bmatrix} cos(\alpha_e + \gamma_e) \\ sin(\alpha_e + \gamma_e) \\ - \end{Bmatrix}; \qquad \overrightarrow{F_{t,e}} = F_{c,e} \cdot \mu \cdot \begin{Bmatrix} -sin(\alpha_e + \gamma_e) \\ cos(\alpha_e + \gamma_e) \\ - \end{Bmatrix} \tag{5.28}$$

$$\overrightarrow{F_{c,e}} + \overrightarrow{F_{t,e}} = F_{c,e} \cdot \begin{Bmatrix} cos(\lambda_e) - \mu \cdot sin(\lambda_e) \\ sin(\lambda_e) + \mu \cdot cos(\lambda_e) \\ - \end{Bmatrix} \tag{5.29}$$

$$\overrightarrow{F_{c,i}} = F_{c,i} \cdot \begin{Bmatrix} -cos(\alpha_i + \gamma_i) \\ sin(\alpha_i + \gamma_i) \\ - \end{Bmatrix}; \qquad \overrightarrow{F_{t,i}} = F_{c,i} \cdot \mu \cdot \begin{Bmatrix} -sin(\alpha_i + \gamma_i) \\ -cos(\alpha_i + \gamma_i) \\ - \end{Bmatrix} \tag{5.30}$$

$$\overrightarrow{F_{c,i}} + \overrightarrow{F_{t,i}} = F_{c,i} \cdot \begin{Bmatrix} -cos(\lambda_i) - \mu \cdot sin(\lambda_i) \\ sin(\lambda_i) - \mu \cdot cos(\lambda_i) \\ - \end{Bmatrix} \tag{5.31}$$

$$\overrightarrow{g} = \begin{Bmatrix} 0 \\ -9.807 \\ 0 \end{Bmatrix} \tag{5.32}$$

$$\overrightarrow{OI_e} = \overrightarrow{OC_e} + \overrightarrow{CI_e} = r_e \cdot \begin{Bmatrix} cos(\alpha_e) \\ sin(\alpha_e) \\ - \end{Bmatrix} + s \cdot \begin{Bmatrix} cos(\lambda_e) \\ sin(\lambda_e) \\ - \end{Bmatrix} \tag{5.33}$$

$$\overrightarrow{OI_i} = \overrightarrow{OC_i} + \overrightarrow{CI_i} = r_i \cdot \begin{Bmatrix} -cos(\alpha_i) \\ sin(\alpha_i) \\ - \end{Bmatrix} + s \cdot \begin{Bmatrix} -cos(\lambda_i) \\ sin(\lambda_i) \\ - \end{Bmatrix} \tag{5.34}$$

5.2.2. Body 2 - Exhaust Rocker-arm

$$\overrightarrow{R_{A_e}} - \overrightarrow{F_{c,e}} - \overrightarrow{F_{t,e}} + \overrightarrow{F_{B,e}} + m_2 \cdot \overrightarrow{g} = \dot{\overrightarrow{Q_2}} \tag{5.35}$$

$$\overrightarrow{AB_e} \times \overrightarrow{F_{B,e}} - \overrightarrow{AI_e} \times \left(\overrightarrow{F_{c,e}} + \overrightarrow{F_{t,e}}\right) = \overrightarrow{K_{A_e}} \tag{5.36}$$

$$\overrightarrow{R_{A_e}} = \begin{Bmatrix} R^x_{A_e} \\ R^y_{A_e} \\ - \end{Bmatrix} \tag{5.37}$$

$$\overrightarrow{AI_e} = \overrightarrow{AC_e} + \overrightarrow{C_eI_e} = a \cdot \begin{Bmatrix} sin(\beta_e) \\ -cos(\beta_e) \\ - \end{Bmatrix} + s \cdot \begin{Bmatrix} cos(\lambda_e) \\ sin(\lambda_e) \\ - \end{Bmatrix} \tag{5.38}$$

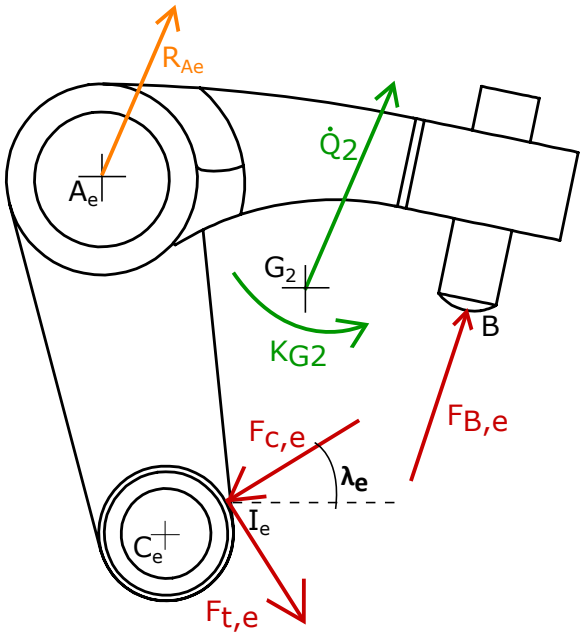

Figure 5.2.: Scheme for dynamic equilibrium on the exhaust rocker-arm

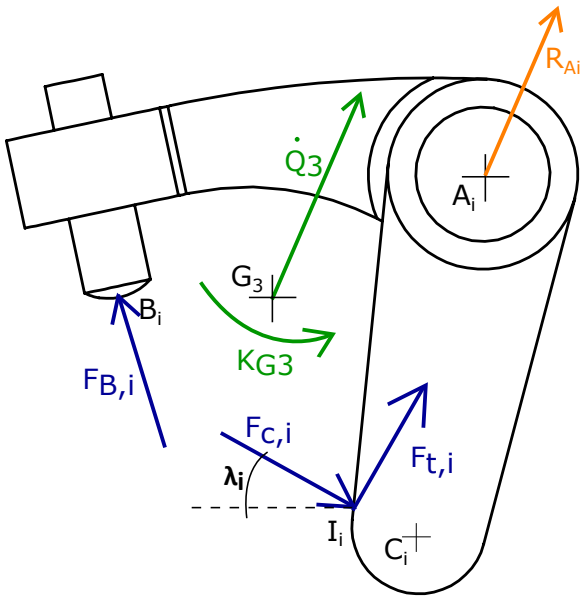

Figure 5.3.: Scheme for dynamic equilibrium on the intake rocker-arm

5.2.3. Body 3 - Intake Rocker-arm

$$\overrightarrow{R_{A_i}} - \overrightarrow{F_{c,i}} - \overrightarrow{F_{t,i}} + \overrightarrow{F_{B,i}} + m_3 \cdot \overrightarrow{g} = \dot{\overrightarrow{Q_3}} \tag{5.39}$$

$$\overrightarrow{AB_i} \times \overrightarrow{F_{B,i}} - \overrightarrow{AI_i} \times \left(\overrightarrow{F_{c,i}} + \overrightarrow{F_{t,i}}\right) = \overrightarrow{K_{A_i}} \tag{5.40}$$

$$\overrightarrow{R_{A_e}} = \begin{Bmatrix} R^x_{A_e} \\ R^y_{A_e} \\ - \end{Bmatrix} \tag{5.41}$$

$$\overrightarrow{AI_i} = \overrightarrow{AC_i} + \overrightarrow{C_iI_i} = a \cdot \begin{Bmatrix} -sin(\beta_i) \\ -cos(\beta_i) \\ - \end{Bmatrix} + s \cdot \begin{Bmatrix} cos(\lambda_i) \\ sin(\lambda_i) \\ - \end{Bmatrix} \tag{5.42}$$

5.2.4. Body 4 - Exhaust and Intake Valves

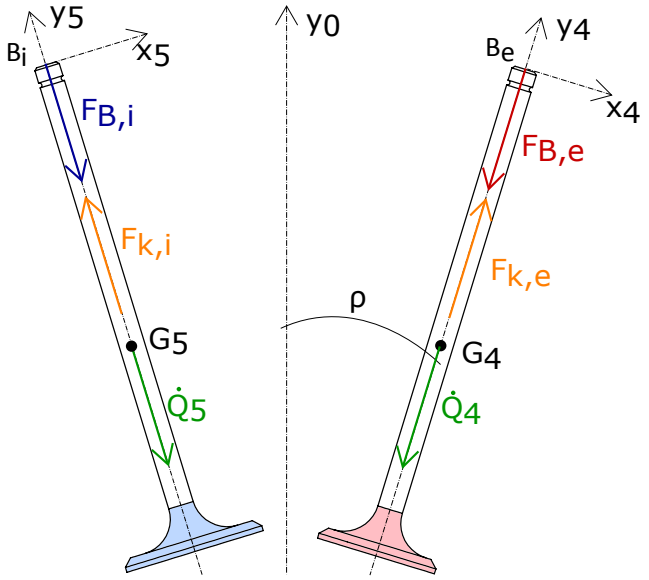

Figure 5.4.: Scheme for dynamic equilibrium on each valve

$$\|\mathbf{F_{B,e}}\| - 2 \cdot \|\mathbf{F_{k,e}}\| = 2 \cdot \|\dot{\mathbf{Q}}_\mathbf{4}\| \tag{5.43}$$

$$\|\mathbf{F_{B,i}}\| - 2 \cdot \|\mathbf{F_{k,i}}\| = 2 \cdot \|\dot{\mathbf{Q}}_\mathbf{5}\| \tag{5.44}$$

Notice that there are 2 exhaust valves and 2 admission valves and, for that reason, the spring forces and quantities of acceleration are multiplied by 2.

$$
\begin{cases}
R_O^x + F_{c,e}\left[\cos(\lambda_e) - \mu \cdot \sin(\lambda_e)\right] + F_{c,i}\left[-\cos(\lambda_i) - \mu \cdot \sin(\lambda_i)\right] = \dot{Q}_1^x \\
R_O^y + F_{c,e}\left[\sin(\lambda_e) + \mu \cdot \cos(\lambda_e)\right] + F_{c,i}\left[\sin(\lambda_i) - \mu \cdot \sin(\lambda_i)\right] - m_1 \cdot g = \dot{Q}_1^y \\
M_m + \overrightarrow{OI_2} \times (\overrightarrow{F_{c,e}} + \overrightarrow{F_{t,e}}) + \overrightarrow{OI_3} \times (\overrightarrow{F_{c,i}} + \overrightarrow{F_{t,i}}) = K_{G_1}^z \\
\hline
R_{A_e}^x - F_{c,e}\left[\cos(\lambda_e) - \mu \cdot \sin(\lambda_e)\right] + F_{b,e}\sin(\rho) = \dot{Q}_2^x \\
R_{A_e}^y - F_{c,e}\left[\sin(\lambda_e) + \mu \cdot \cos(\lambda_e)\right] + F_{b,e}\cos(\rho) - m_2 \cdot g = \dot{Q}_2^y \\
F_{b,e}\left(\overline{AB}_e^x \cdot \cos(\rho) - \overline{AB}_e^y \cdot \sin(\rho)\right) - \overrightarrow{AI_e} \times (\overrightarrow{F_{c,e}} + \overrightarrow{F_{t,e}}) - m_2 g\left(\overline{AG}_2^x \cdot \cos(\beta_e) + \overline{AG}_2^y \cdot \sin(\beta_e)\right) = K_{G_2}^z \\
\hline
R_{A_i}^x - F_{c,i}\left[-\cos(\lambda_i) - \mu \cdot \sin(\lambda_i)\right] - F_{b,e}\sin(\rho) = \dot{Q}_3^x \\
R_{A_i}^y - F_{c,i}\left[\sin(\lambda_i) - \mu \cdot \cos(\lambda_i)\right] + F_{b,e}\cos(\rho) - m_3 \cdot g = \dot{Q}_3^y \\
F_{b,i}\left(\overline{AB}_i^x \cdot cos(\rho) + \overline{AB}_i^y \cdot sin(\rho)\right) - \overrightarrow{AI_i} \times (\overrightarrow{F_{c,i}} + \overrightarrow{F_{t,i}}) + m_3 g\left(\overline{AG}_3^x \cdot cos(\beta_i) + \overline{AG}_3^y \cdot sin(\beta_i)\right) = K_{G_3}^z \\
\hline
F_{b,e} - 2\left(50.8 + 25.4 \cdot \|lift_e\|\right) = 2 \cdot \|\dot{Q}_4\| \\
F_{b,i} - 2\left(50.8 + 25.4 \cdot \|lift_i\|\right) = 2 \cdot \|\dot{Q}_5\| \\
\hline
R_O^x + R_{A_e}^x + R_{A_i}^x + F_{b,e}\sin(\rho) - F_{b,i}\sin(\rho) = \dot{Q}_2^x + \dot{Q}_3^x \\
R_O^y + R_{A_e}^y + R_{A_i}^y + F_{b,e}\cos(\rho) + F_{b,i}\cos(\rho) = \dot{Q}_2^y + \dot{Q}_3^y
\end{cases}
\tag{5.45}
$$

5.3. Results

The system of equations presented in the previous page is non-linear, with no symbolic solution. Due to problems of convergence it was not possible to solve it using MatLab^{TM} solvers, for instance. Nevertheless, some attempts were made in order to geometrically define the time dependent functions of the angles of contact between the camshaft and rocker-arms, without any success. That way the system of equations can be solved linearly, even dismissing the last 2 ones related a full system equilibrium.

As so, in order to obtain some appreciable results, a rough but sensible approximation was made:

$$\lambda \approx \alpha \tag{5.46}$$

With this consideration the system of equations becomes solvable. The results for the variables in analysis are presented in the following plots. Notice that there are some fictional oscillating forces, resulting from the Fourier approximation made in the definition of the lift curve.

At last, the coefficient of friction adopted was:

$$\mu = 0.15 \tag{5.47}$$

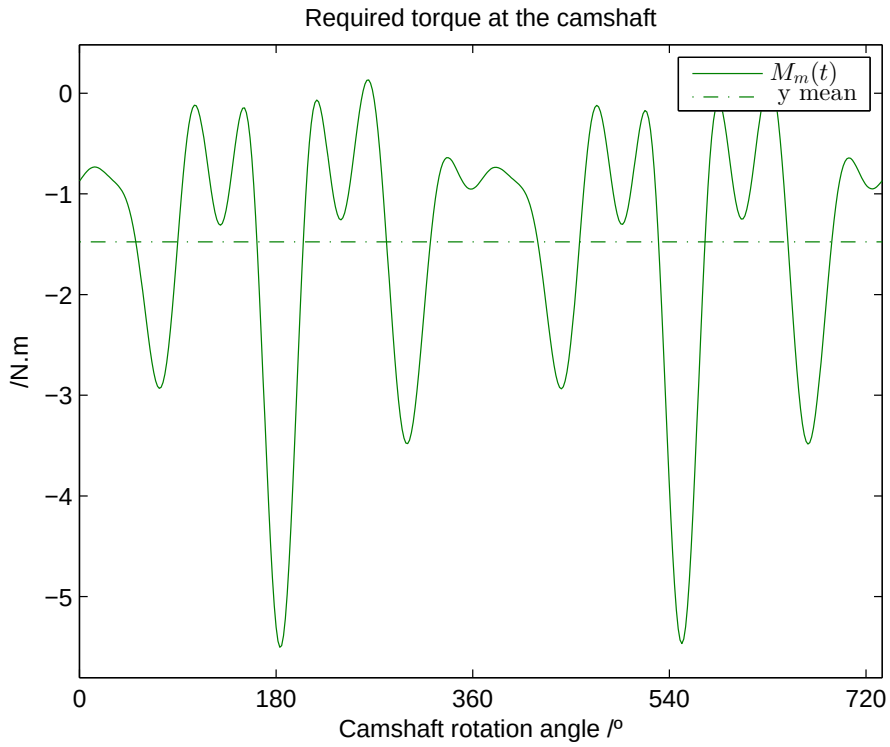

Figure 5.5.: Required torque to rotate the camshaft

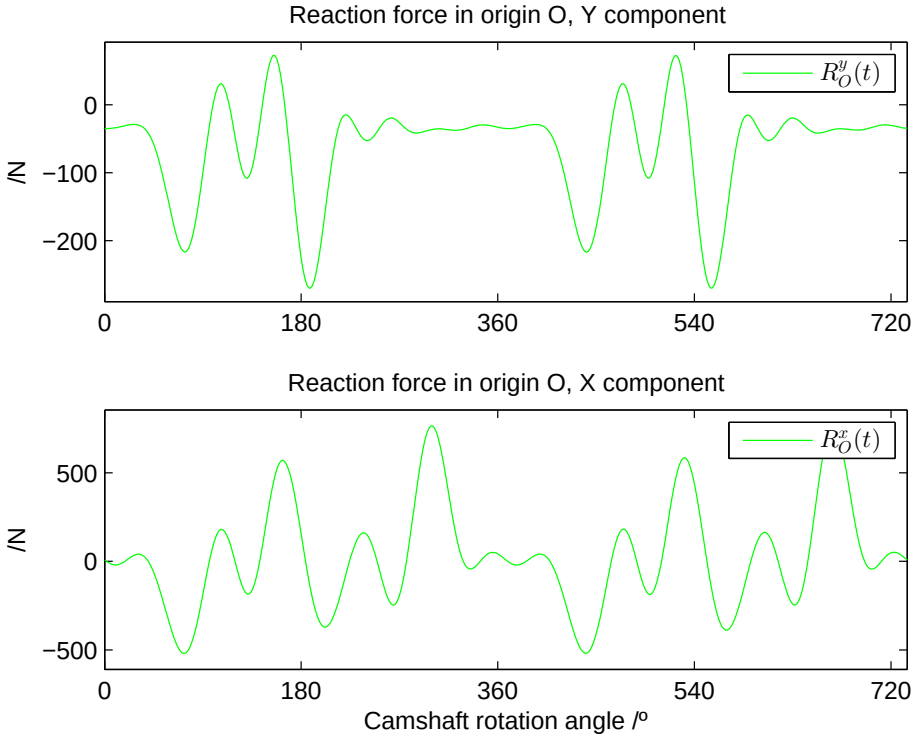

Figure 5.6.: Reaction forces at the origin referential applied to the camshaft

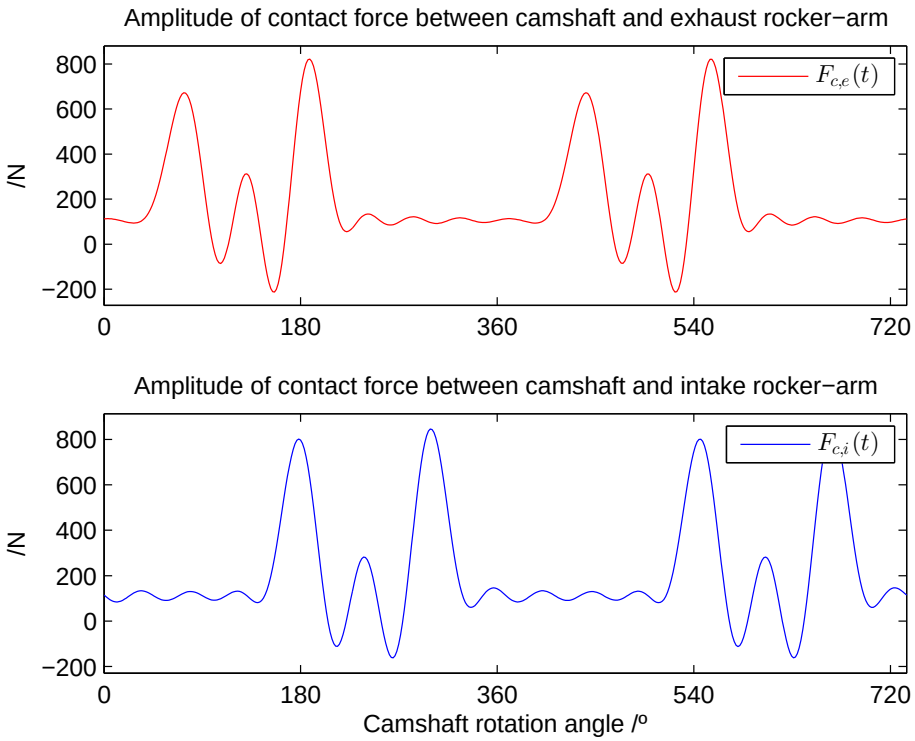

Figure 5.7.: Contact force between the camshaft and rocker-arms, normal component

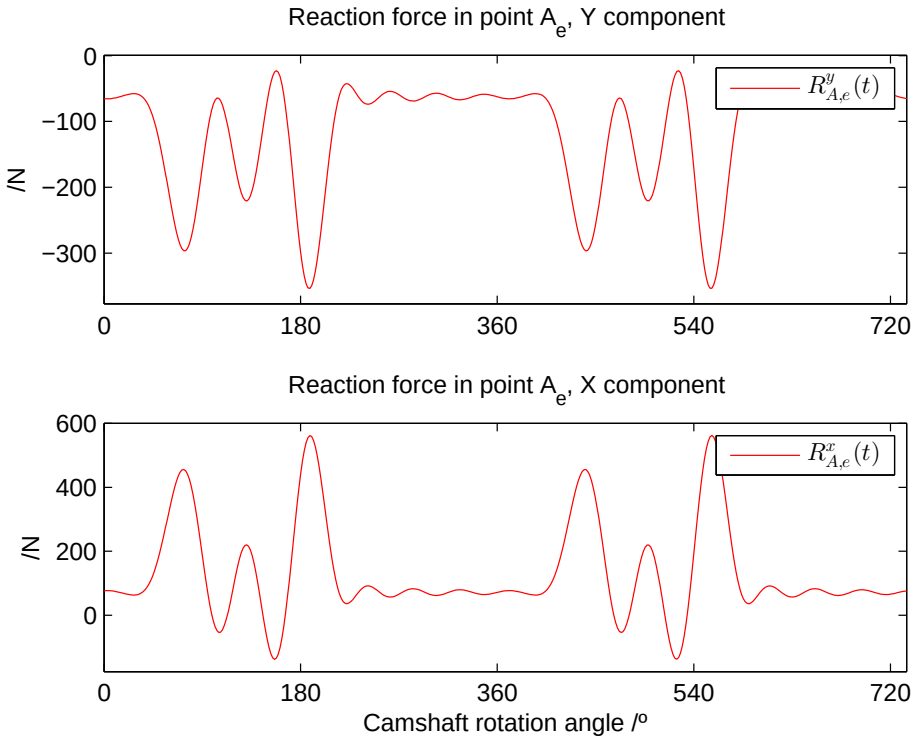

Figure 5.8.: Reaction forces at point A applied to the exhaust rocker-arm

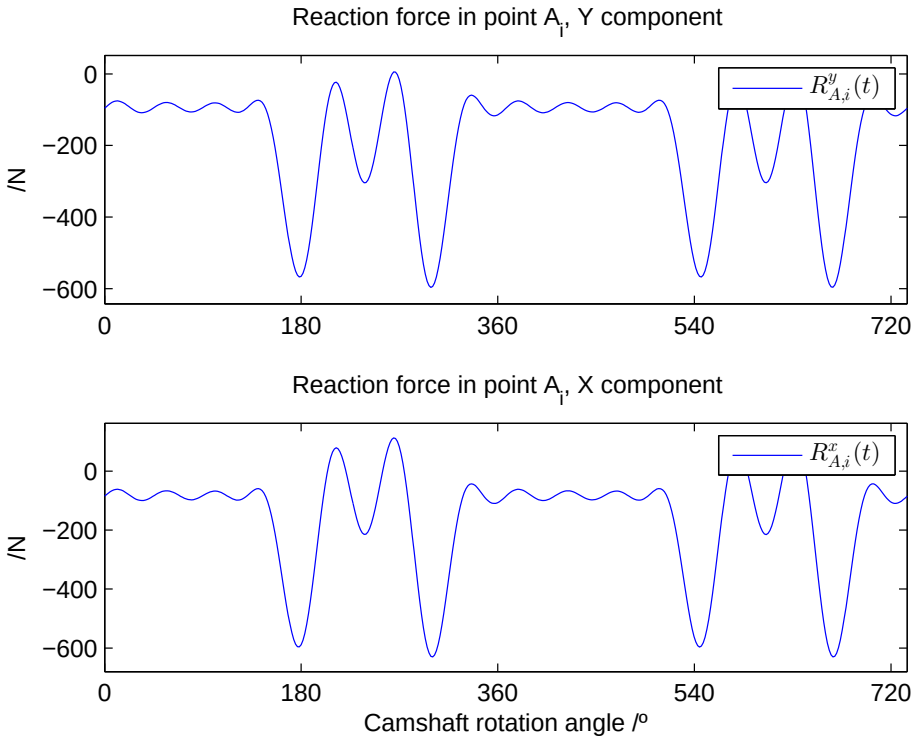

Figure 5.9.: Reaction forces at point A applied to the intake rocker-arm

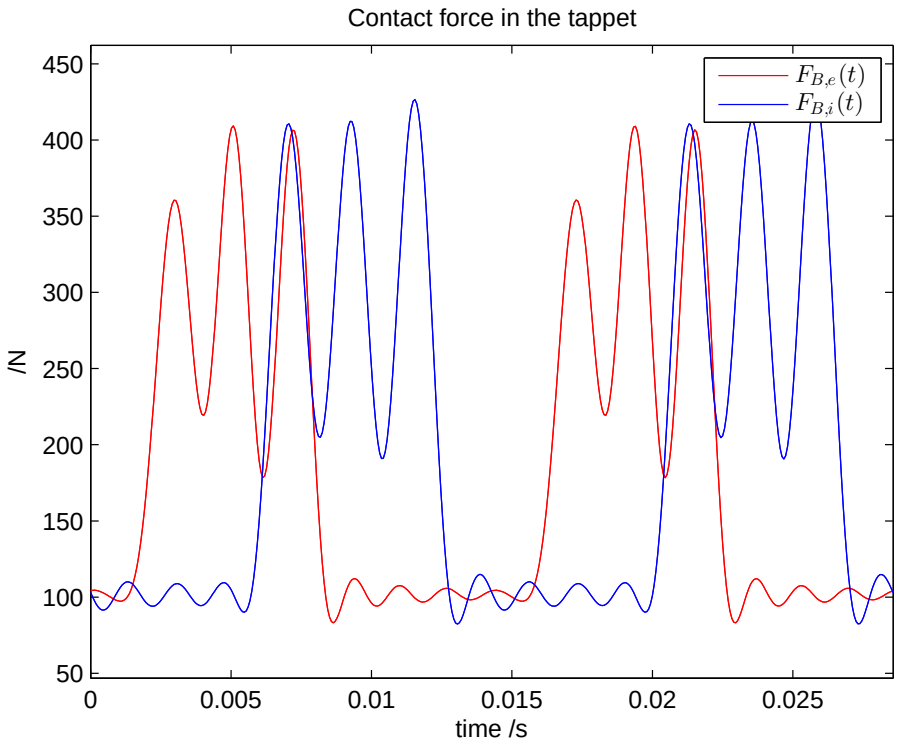

Figure 5.10.: Contact forces in the tappets, component in the direction of the valve

5.4. Interpretation of results

First of all, it is clear that the high frequency harmonics of the Fourier approximation are visible in every plots presented behind. For instance, when deriving a sinusoidal function against time, the frequency value will multiply the amplitude of the respective sinusoid function. As a consequence of this mathematical behaviour, there will appear some considerable fictional harmonic forces that don't exists in reality.

For this reason, and for what the plots show, the Fourier approximation may not be the most appropriate one to calculate the dynamic behaviour of the system.

5.4.1. Motor momentum required

According to the theory of cam dynamics, used in usual valve train systems (which requires a cam with lobes actuating a valve or a group of valves) explained in [14] (chapter 16), "the energy required to drive the follower in the forward direction is recovered when the follower returns. This recovery is accomplished by the springs energy storing", ignoring the presence of any dissipation forces.

This shall be the same way in the InnerCam^{TM}, as determined in previous works [8]. However, in the current study, in which it was made an approximation for the angle of contact λ, the motor momentum of the camshaft, considering no-friction condition ($\mu = 0$), is equal to zero in all time domain, as it is demonstrated bellow. Remembering Equation 5.26 and Figure 5.1:

$$\overrightarrow{M_m} = -\overrightarrow{OI_e} \times \left(\overrightarrow{F_{c,e}} + \overrightarrow{F_{t,e}}\right) - \overrightarrow{OI_i} \times \left(\overrightarrow{F_{c,i}} + \overrightarrow{F_{t,i}}\right) \tag{5.48}$$

Which can also be written as:

$$\begin{aligned}\overrightarrow{M_m} = &- \begin{Bmatrix} OC_e^x + s \cdot \cos(\lambda_e) \\ OC_e^y + s \cdot \sin(\lambda_e) \\ -- \end{Bmatrix} \times F_{c,e} \begin{Bmatrix} \cos(\lambda_e) - \mu \cdot \sin(\lambda_e) \\ \sin(\lambda_e) + \mu \cdot \cos(\lambda_e) \\ -- \end{Bmatrix} - \\ &- \begin{Bmatrix} OC_i^x - s \cdot \cos(\lambda_i) \\ OC_i^y + s \cdot \sin(\lambda_i) \\ -- \end{Bmatrix} \times F_{c,i} \begin{Bmatrix} -\cos(\lambda_i) - \mu \cdot \sin(\lambda_i) \\ \sin(\lambda_i) - \mu \cdot \cos(\lambda_i) \\ -- \end{Bmatrix}\end{aligned} \tag{5.49}$$

For instance, developing the vectorial product of the contact force between the camshaft and the exhaust rocker-arm, considering $\mu = 0$ and $\lambda_e = \alpha_e$, and equating it to *zero*:

$$(OC_e^x + s \cdot \cos(\lambda_e)) \cdot \sin(\lambda_e) - (OC_e^y + s \cdot \sin(\lambda_e)) \cdot \cos(\lambda_e) = 0 \tag{5.50}$$

$$\Leftrightarrow \tan(\lambda_e) = \frac{OC_e^y}{OC_e^x} \tag{5.51}$$

Which is always true for $\lambda_e \in \left[0;\ \frac{\pi}{2}\right]$.

The same way for the vectorial product of the contact force between the camshaft and the intake rocker-arm, considering $\mu = 0$ and $\lambda_i = \alpha_i$:

$$(OC_i^x - s \cdot \cos(\lambda_i)) \cdot \sin(\lambda_i) + \left(OC_i^y + s \cdot \sin(\lambda_i)\right) \cdot \cos(\lambda_i) = 0 \tag{5.52}$$

$$\Leftrightarrow \tan(\lambda_i) = -\frac{OC_i^y}{OC_i^x} \tag{5.53}$$

Which is also always true knowing that, despite λ_i being positive, it is located in the 2^{th} quadrant of the trigonometric circle.

Analysing the Figure 5.5, it is now known that the motor momentum, that is represented, only depends on the friction forces, and as so it is highly related to the coefficient of friction, μ. The average value obtained is equal to 1.477 $N.m$. Notice that this value is positive, because the direction of the displacement θ is negative (or clockwise), being the opposite direction of the representation of M_m in Figure 5.1.

It is also stated in literature that the required torque curve "consists of a double-frequency component, whose amplitude is a function of the cam velocity squared, superimposed on a single-frequency component whose amplitude is independent of velocity". In this case, there is a 4^{th}-frequency component which can be observed in the middle of the two positive peaks from exhaust and intake sub-system.

In order to prove the influence of the harmonics in previous results, another Fourier approximation function was determined in a 4^{th} degree. The resultant lift curves and motor momentum plots can be analysed in Figure 5.11. The average value is still near zero and shape of the plot curve is also similar, without the influence of high order harmonic frequency.

Notice that the maximum lift position is higher, despite its shape is correct. The average value for the required torque, 1.443 $N.m$, is almost the same, when comparing to the 8^{th} degree approximation.

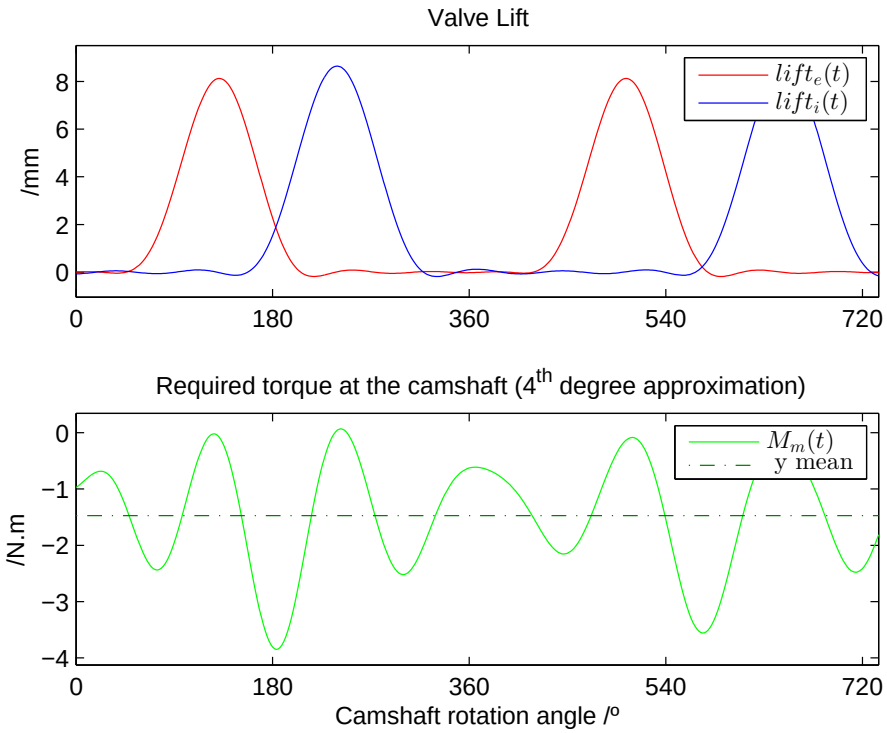

Figure 5.11.: Resultant lift and torque for a Fourier 4^{th} degree approximation function

5.4.2. Other results

When comparing exhaust related plots to the intake ones it is noticeable a small difference in the amplitude of high frequency harmonics, which is larger in the intake sub-system.

In Figure 5.7 it is observed that the shape of the curves is similar for both intake and exhaust rocker arms. At stationary position the values for the contact forces are related to the pre-load of the spring (balancing the momentum equation of the rocker-arms).

At the beginning and ending of the lift movement the amplitude is positive, but near maximum lift position, there is an area where this contact force is negative, which means that the rocker-arm will contact against the outer surface of the camshaft (the one with smaller diameter). This phenomenon means that the spring pre-load may not be enough to beat the inertia of the rocker arm. Although, an increasing of this pre-load also means that the average required torque will increase too.

In relation to Figures 5.8 and 5.9, they correspond to what is expected from the equilibrium diagrams and there are no remarkable phenomena to comment.

6. Vibration Analysis

In order to proceed to the MSC Adams modulation is required the development of some analytical dynamic models, in order to identify some natural frequencies and check up the behaviour of some body parts, namely the valves and rocker arms.

The first model in this chapter will be the most simple, but also maybe the most important that hasn't been analysed yet. Is the $1DoF$ system composed only by one valve and spring. With it I will be able to predict the speed for which the detachment from the rocker-arms occurs.

A second model with 3 DoFs, for exhaust and intake sub-system separately, includes the movement of the rocker-arm and valves in free regime in order to identify the natural frequency and modes of vibration.

Some modal analysis were already done in [11], using a FEA software ANSYS^{TM}, in which the body's natural frequencies of vibration where identified. Finally, this results will be compared to the ones obtained in the dynamic models.

6.1. Valve/Spring system

6.1.1. Exhaust valve

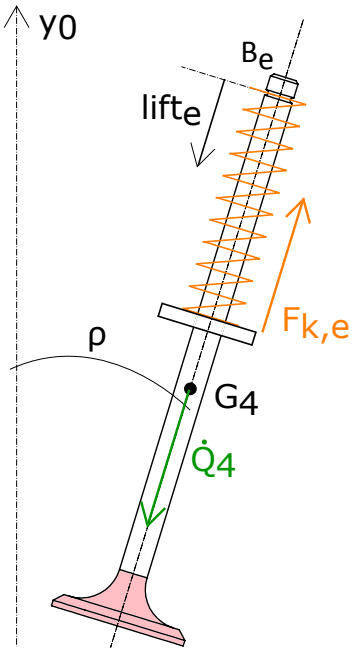

Figure 6.1.: Dynamic system for the exhaust valve movement

Equation of equilibrium, in a no load condition:

$$m_4 \cdot \ddot{lift}_e + c_{eq,e} \cdot \dot{lift}_e + k \cdot lift_e = 0 \tag{6.1}$$

Being,

$$\begin{cases} m_4 &= 0.024 & kg \\ \xi &= 0.05 & \\ c_{eq,e} &= 2.469 & N \cdot s \cdot m^{-1} \\ k &= 25400 & N \cdot m^{-1} \end{cases} \tag{6.2}$$

It's possible to determine the natural damped frequency of vibration:

$$\begin{cases} \omega_{n,4} &= 1028.8 & rad \cdot s^{-1} \\ \omega_{d,4} &= 1027.5 & rad \cdot s^{-1} \end{cases} \tag{6.3}$$

With these parameters it is possible to define the response of the lift in free regime, for a given initial condition of displacement, x_0, and velocity, $\dot{x}_0$:

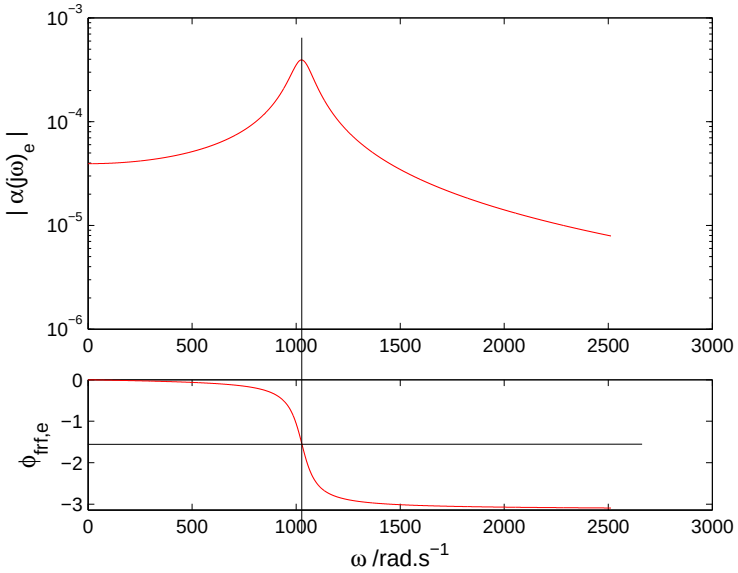

Figure 6.2.: FRF of type receptance for the exhaust valve system

$$x_e(t) = Amp \cdot e^{-\xi \cdot \omega_{n,e} \cdot t} \cdot \cos\left(w_{d,e}t - \Phi\right) \tag{6.4}$$

Building a parallelism with the lift of the valve, let's assume the initial conditions as:

$$\begin{cases} x_{0,e} = 0.00947\ m \\ \dot{x}_{0,e} = 0\ m \cdot s^{-1} \end{cases} \quad \Rightarrow \quad \begin{cases} Amp = x_{0,e} \\ \Phi = 0.0500\ rad \end{cases} \tag{6.5}$$

Using this free regime response to initial conditions, can be determined the time interval between the maximum lift position and the stationary position, $x_e(t) = 0.002$, can be determined. That way, it is possible to calculate at which speed is predicted the detachment between the valve and rocker-arm.

$$x_e(t) = 0.002\ mm \quad \Rightarrow \quad t = 0.001355\ s \tag{6.6}$$

To obtain the Frequency Response Function (FRF) in terms of amplitude and phase, we can use the following formulation. Being ω the frequency of solicitation:

$$\alpha(\omega)_e = \frac{1}{(k - w^2 \cdot m_e) - j\omega c_e} \tag{6.7}$$

6.1.2. Admission valve

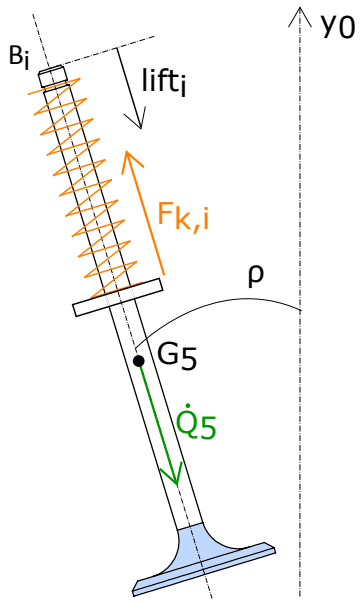

Figure 6.3.: Dynamic system for the intake valve movement

Equation of equilibrium, in a no load condition:

$$m_5 \cdot l\ddot{i}ft_i + c_{eq,i} \cdot l\dot{i}ft_i + k \cdot lift_i = 0 \tag{6.8}$$

Being,

$$\begin{cases} m_5 &= 0.028 & kg \\ \xi &= 0.05 & \\ c_{eq,i} &= 2.6668 & N \cdot s \cdot m^{-1} \\ k &= 25400 & N \cdot m^{-1} \end{cases} \tag{6.9}$$

It's possible to determine the natural damped frequency of vibration:

$$\begin{cases} \omega_{n,i} &= 952.4 & rad \cdot s^{-1} \\ \omega_{d,i} &= 951.2 & rad \cdot s^{-1} \end{cases} \tag{6.10}$$

With these parameters it is possible to define the response of the lift in free regime, for a given initial condition of displacement, x_0, and velocity, $\dot{x}_0$:

$$x_i(t) = Amp \cdot e^{-\xi \cdot \omega_{n,i} \cdot t} \cdot \cos\left(w_{d,i}t - \Phi\right) \tag{6.11}$$

Building a parallelism with the lift of the valve, let's assume the initial conditions as:

$$\begin{cases} x_{0,i} = 0.01003\ m \\ \dot{x}_{0,i} = 0\ m \cdot s^{-1} \end{cases} \Rightarrow \begin{cases} Amp = x_{0,i} \\ \Phi = 0.0500\ rad \end{cases} \tag{6.12}$$

Using this free regime response to initial conditions, the time interval between the maximum lift position and the stationary position, $x_i(t) = 0.002$, can be determined. That way, it is possible to calculate at which speed is predicted the detachment between the valve and rocker-arm.

$$x_i(t) = 0.002\ m \quad \Rightarrow \quad t = 0.001477\ s \tag{6.13}$$

To obtain the Frequency Response Function (FRF) in terms of amplitude and phase, we can use the following formulation. Being ω the frequency off solicitation:

$$\alpha(\omega)_i = \frac{1}{(k - w^2 \cdot m_i) - j\omega c_i} \tag{6.14}$$

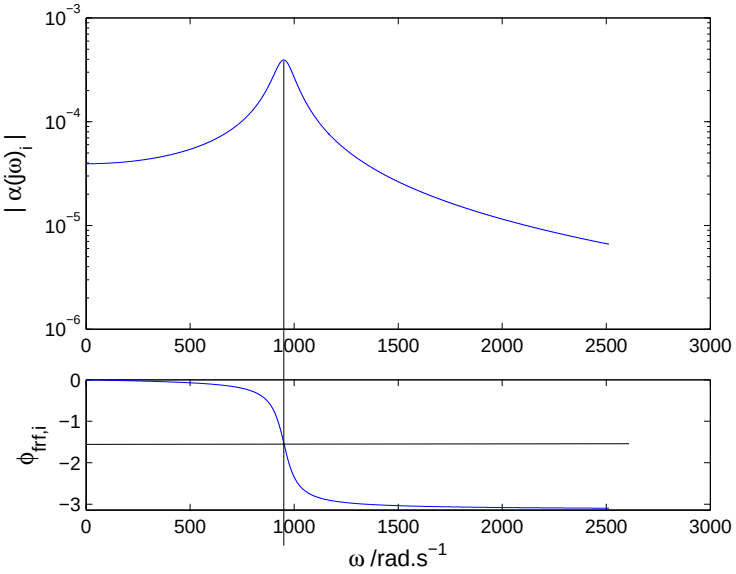

Figure 6.4.: FRF of type receptance for the intake valve system

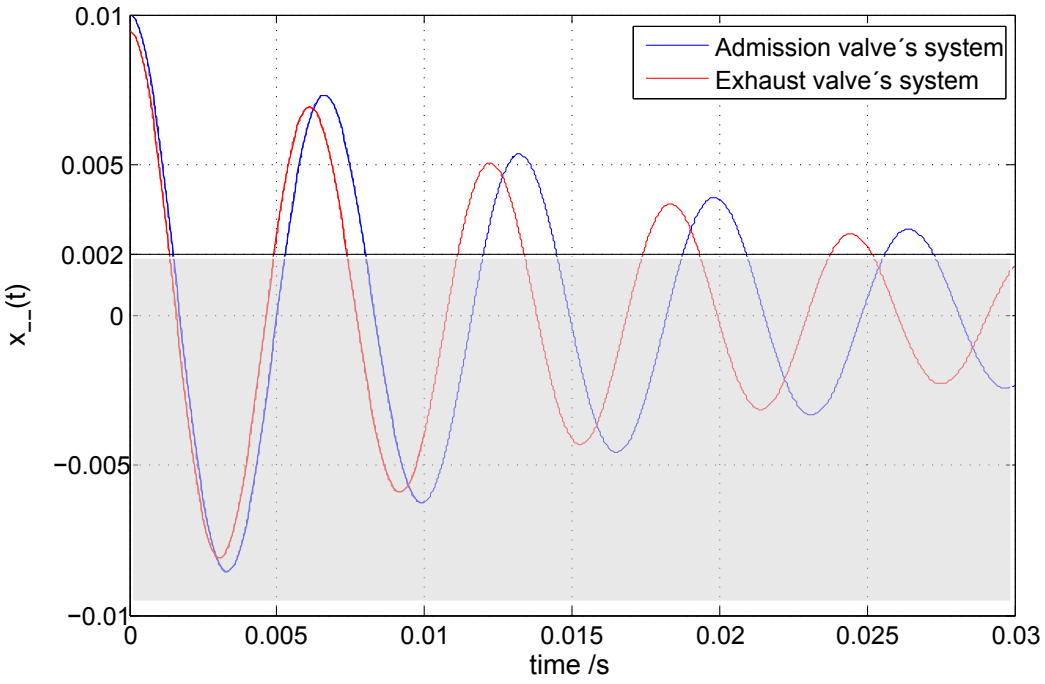

Figure 6.5.: Response of the 1 DoF valve's systems after a displacement solicitation equal to the maximum lift

6.2. Interpretation of Valve/spring system results

With the analytical model studied in the previous section, it is possible to determine the response of the valve's lift in a free regime condition. Extrapolating to the InnerCam^{TM} system, it is equivalent to the instants when a valve detaches its respective rocker-arm. Let's be the 'limit rotation speed', the on at which the detachment occurs.

Knowing that the time the rocker-arms take to return from maximum lift position to a stationary position corresponds to a given angle θ, on the camshaft, from the lift curve (Figure 4.3), equal to:

$$\begin{aligned} \theta_{liftback,e} &= 205 - 133 = 72^{o} \quad &= 1.2566\ rad \\ \theta_{liftback,i} &= 316 - 235 = 81^{o} \quad &= 1.4137\ rad \end{aligned} \tag{6.15}$$

A full rotation cycle of the valve train corresponds to $2\pi\ rad$. Therefore, that 'limit rotation speed' for the exhaust valves can be obtained by the following calculations:

$$T_{lim,e} = \frac{2 * pi}{1.2566\ rad} \times 0.001355\ s = 0.0068\ s \tag{6.16}$$

$$\omega_{lim,e} = 8856\ rpm \tag{6.17}$$

The same way, for the intake valves we obtain:

$$T_{lim,e} = \frac{2 * pi}{1.4137\ rad} \times 0.001477\ s = 0.0066\ s \tag{6.18}$$

$$\omega_{lim,i} = 9140\ rpm \tag{6.19}$$

Summing up, we conclude that the detachment of the valves (or floating effect), only occurs for engine speeds bigger than approximately 17700 rpm (considerably higher than the usable range of regimes).

6.2.1. Identification of resonance harmonic frequencies

Converting the values of the natural frequencies of those two systems, from $rad \cdot s^{-1}$ to Hz, we can compare them to the result plots obtained in the MSC Adams model.

$$\begin{cases} \omega_{d,e} = 163.53\ Hz \\ \omega_{d,i} = 151.40\ Hz \end{cases} \tag{6.20}$$

6.3. Exhaust sub-system, 3 DoF's

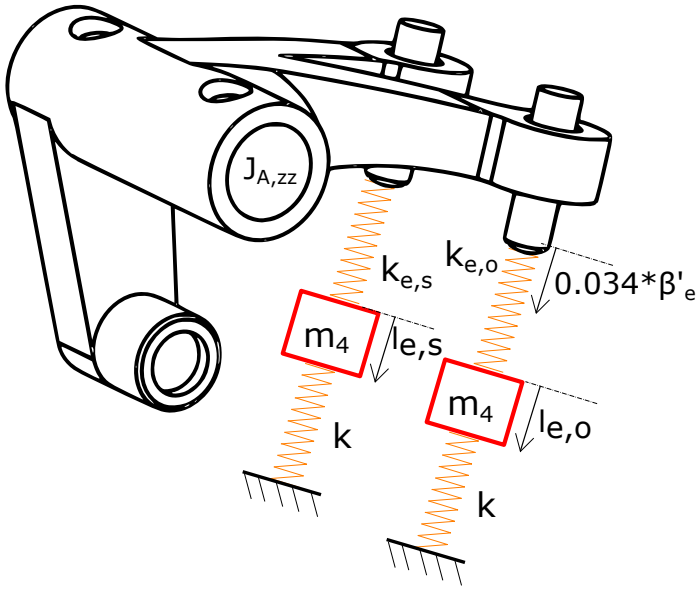

Figure 6.6.: Dynamic model for the exhaust sub-system, 3DoF's

This model is composed by three body parts. The stiffness properties of the springs are related to the valve's spring or to the flexibility of the exhaust rocker-arm. The contact rigidity was ignored, because it is dependent on penetration, geometry and consequently not well known. The 3 DoF's are:

- β'_e - the rotation angle of the exhaust rocker-arm, from stationary position;
- $l_{e,s}$ the displacement of the exhaust valve under the straight arm;
- $l_{e,o}$ the displacement of the exhaust valve under the oblique arm.

The stiffness properties of the springs, k, is already known - 25400 $N \cdot m^{-1}$. The other springs represent the flexibility of the rocker arm under bending solicitation. This property was calculated using FEA Analysis tool from SolidWorks^{TM}(a more specialized software could be used, however the limit of 1000 elements in its student versions available was not enough to reproduce the geometry) and the corresponding results can be consulted in Appendix C. Therefore, the values of $k_{e,s}$ and $k_{e,o}$ can be determined, by:

$$\frac{1}{k_{2,s,roller}} + \frac{1}{k_{2,s,pin}} = \frac{1}{k_{2,s}} \quad \Rightarrow \quad \frac{2.5 \cdot 10^{-5}}{1000} + \frac{6 \cdot 10^{-5}}{1000} = \frac{1}{k_{2,s}} \tag{6.21}$$

$$k_{2,s} = 1.1111 \cdot 10^{7} \quad N \cdot m^{-1} \tag{6.22}$$

$$\frac{1}{k_{2,o,roller}} + \frac{1}{k_{2,o,pin}} = \frac{1}{k_{2,o}} \quad \Rightarrow \quad \frac{2.5 \cdot 10^{-5}}{1000} + \frac{1.3 \cdot 10^{-4}}{1000} = \frac{1}{k_{2,o}} \tag{6.23}$$

$$k_{2,o} = 6.25 \cdot 10^{6} \quad N \cdot m^{-1} \tag{6.24}$$

6.3.1. Lagrangian dynamic equilibrium

The dynamic equilibrium equations for this system were determined using the Lagrangian method, from generalized coordinates, of kinetic total energy, potential energy variation of the system (in relation to equilibrium position) and work produced by non-conservative forces (like damping). In this case, the damping coefficient was considered to be low, comparing to the influence of the stiffness.

Being T, the kinetic energy and V, the potential energy:

$$T_2 = \frac{1}{2} J_{2,zz} \cdot \dot{\beta_e}^2 \tag{6.25}$$

$$V_2 = \frac{1}{2} m_2 \cdot g \cdot \left(\overrightarrow{AG_2}^y - \overline{AG_2}^y \right) \tag{6.26}$$

$$T_{4,s} = \frac{1}{2} m_4 \cdot \dot{l_{e,s}}^2 \tag{6.27}$$

$$V_{4,s} = \frac{1}{2} k_{2,s} \cdot \left(l_{e,s} - 0.034 \cdot \beta'_e \right)^2 + \frac{1}{2} k \cdot l_{e,s}^2 \tag{6.28}$$

$$T_{4,o} = \frac{1}{2} m_4 \cdot \dot{l_{e,o}}^2 \tag{6.29}$$

$$V_{4,o} = \frac{1}{2} k_{2,o} \cdot \left(l_{e,o} - 0.034 \cdot \beta'_e \right)^2 + \frac{1}{2} k \cdot l_{e,o}^2 \tag{6.30}$$

$$T = \frac{1}{2} \left[J_{2,zz} \cdot \dot{\beta_e}^2 + m_4 \cdot \left(\dot{l_{e,s}}^2 + \dot{l_{e,o}}^2 \right) \right] \tag{6.31}$$

$$V = \frac{1}{2} \left[k_{2,s} \cdot \left(l_{e,s} - 0.034 \cdot \beta'_e \right)^2 + k_{2,o} \cdot \left(l_{e,o} - 0.034 \cdot \beta'_e \right)^2 + k \cdot \left(l_{e,s}^2 + l_{e,o}^2 \right) \right] \tag{6.32}$$

It is known, from [13], that the Lagrange equations can be written as:

$$\frac{d}{dt} \left(\frac{\partial T}{\partial \dot{q}_n} \right) - \frac{\partial T}{\partial q_n} + \frac{\partial V}{\partial q_n} = F_n \tag{6.33}$$

The equilibrium equations, in free regime, can be written in the following matrix form:

$$\begin{bmatrix} J_{2,zz} & 0 & 0 \\ 0 & m_4 & 0 \\ 0 & 0 & m_4 \end{bmatrix} \begin{Bmatrix} \ddot{\beta}'_e \\ \ddot{l}_{e,s} \\ \ddot{l}_{e,o} \end{Bmatrix} + \begin{bmatrix} m_2 \cdot g \cdot \overline{AG_2}^y & -0.034^2 k_{2,s} & -0.034^2 k_{2,o} \\ -0.034^2 k_{2,s} & k_{2,s} + k & 0 \\ -0.034^2 k_{2,o} & 0 & k_{2,o} + k \end{bmatrix} \begin{Bmatrix} \beta'_e \\ l_{e,s} \\ l_{e,o} \end{Bmatrix} = \overrightarrow{0} \tag{6.34}$$

Eigenproblem

Let's assume that the solution for the system of homogeneous differential equations is of the type:

$$\begin{Bmatrix} \beta'_e \\ l_{e,s} \\ l_{e,o} \end{Bmatrix} = \begin{Bmatrix} u_1 \\ u_2 \\ u_3 \end{Bmatrix} \cos(\omega t - \Phi) \tag{6.35}$$

, where $\{u\}$ represents any eigenvector (which must be non-zero, in order to obtain the non-trivial solutions). Now, replacing 6.35 in the equilibrium equations 6.34, the eigenproblem is obtained:

$$\left[[k] - \omega^2 [m]\right] \{u\} = \{0\} \tag{6.36}$$

$$\left|\left[[k] - \omega^2 [m]\right]\right| = 0 \tag{6.37}$$

From the solution of this equation, the natural frequencies of vibration can be obtained:

$$\begin{cases} \omega_1 = & 0 & \\ \omega_2 = & 16170 & rad \cdot s^{-1} \\ \omega_3 = & 21540 & \end{cases} \quad \Rightarrow \quad \begin{cases} \omega_1 = & 0 & \\ \omega_2 = & 2573 & Hz \\ \omega_3 = & 3428 & \end{cases} \tag{6.38}$$

Notice that the first natural frequency is equal to 0, which represents a rigid body movement of all degrees of freedom.

Replacing this eigenvalues the Equation 6.36, one at each time, the eigenvectors are determined, through the set of Equations 6.39, which can be assembled in a matrix of eigenvectors.

$$\begin{cases} \dfrac{u_{2r}}{u_{1r}} = \dfrac{0.034^2 \cdot k_{2,s}}{k_{2,s} + k - \omega_r^2 \cdot m_4} \\ \dfrac{u_{3r}}{u_{1r}} = \dfrac{0.034^2 \cdot k_{2,o}}{k_{2,o} + k - \omega_r^2 \cdot m_4} \end{cases} \tag{6.39}$$

$$[u] = [u_1|u_2|u_3] = \begin{bmatrix} 1 & 1 & 1 \\ 0.0012 & 0.0026 & -2.2267 \\ 0.0012 & -4.4801 & -0.0014 \end{bmatrix} \tag{6.40}$$

This vectors can be normalized through the following expression:

$$\left\{\Phi\right\}_r = \frac{\left\{u\right\}_r}{\sqrt{\left\{u\right\}_r^T [M] \left\{u\right\}_r}} \tag{6.41}$$

$$\Rightarrow [\Phi] = [\Phi_1|\Phi_2|\Phi_3] = \begin{bmatrix} 125.5517 & 1.4407 & 2.8981 \\ 0.1448 & 0.0037 & -6.4533 \\ 0.1446 & -6.4545 & -0.0041 \end{bmatrix} \tag{6.42}$$

The same way as in the spring/valve systems, it is useful to determine the FRF of type receptance. In this case, as there are 3 DoF's, it will be represented the contribution of each harmonic, separately, because the FRF's are obtained by its sum:

$$\alpha_{jk}(\omega) = \sum_{r=1}^{3} \frac{\Phi_{jr}\Phi_{kr}}{(\omega_r^2 - \omega^2) + j2\xi_r\omega_r\omega} \tag{6.43}$$

,where the value of ξ_r will be considered equal to 0.02 (a common value for no damped dynamic systems), in order to obtain numerical consistence in the plots.

The FRF accelerance is obtained from the receptance by multiplying it for '$-\omega^2$'. This function is more interesting to analyse because it gives us an idea of the quantities of acceleration of the bodies.

For that reason, the accelerance responses are presented in the following Figures, while the receptance responses can be consulted in Appendix D.1

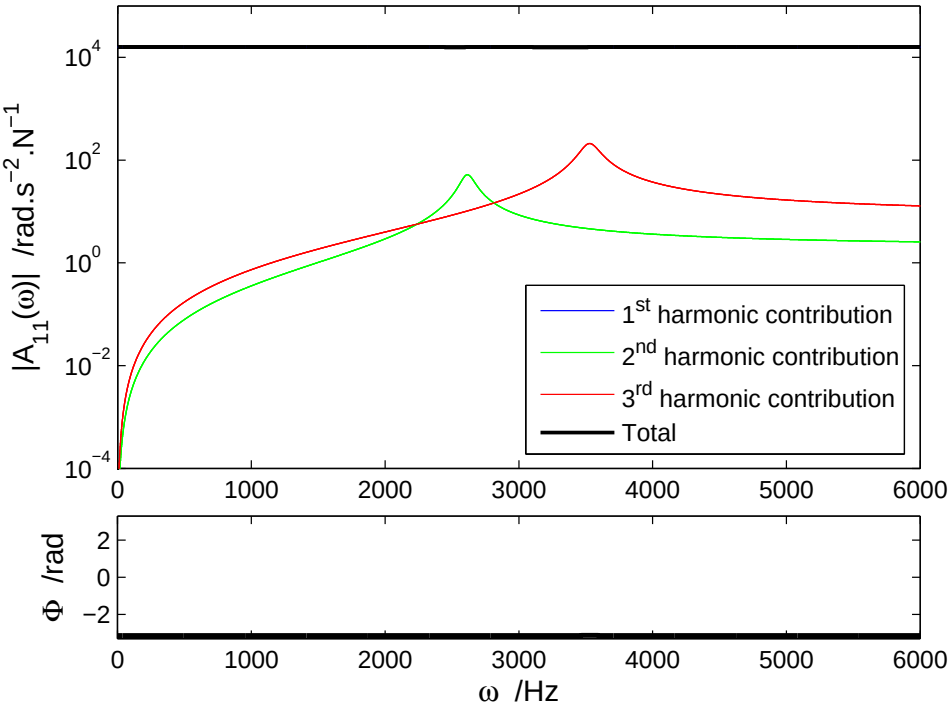

Figure 6.7.: FRF of type accelerance for direct solicitation in DoF β_e

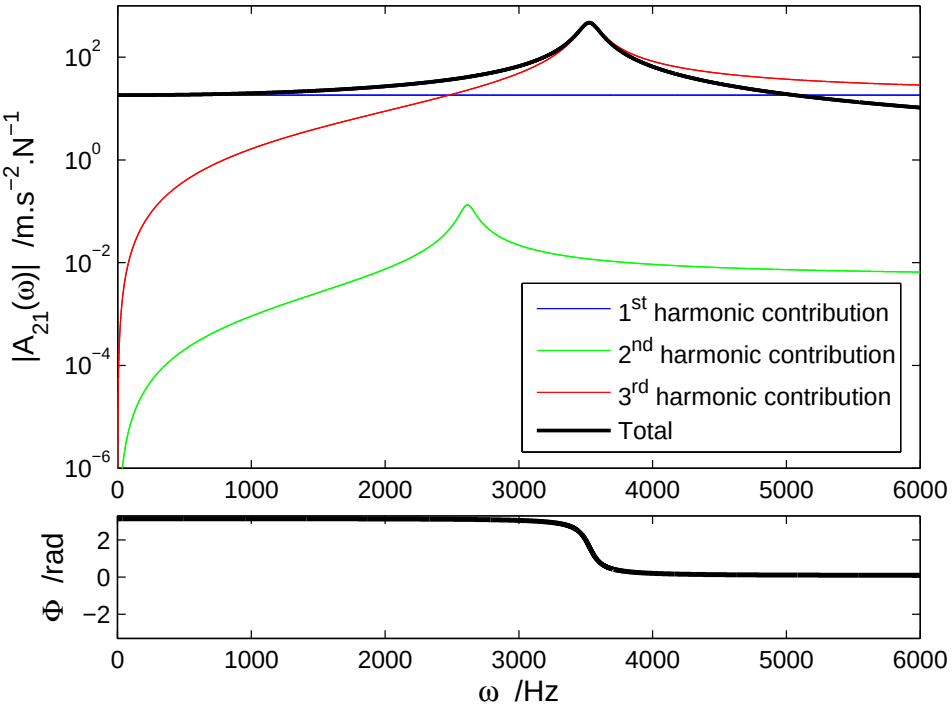

Figure 6.8.: FRF of type accelerance in DoF $l_{e,s}$ for crossed solicitation in DoF β_e

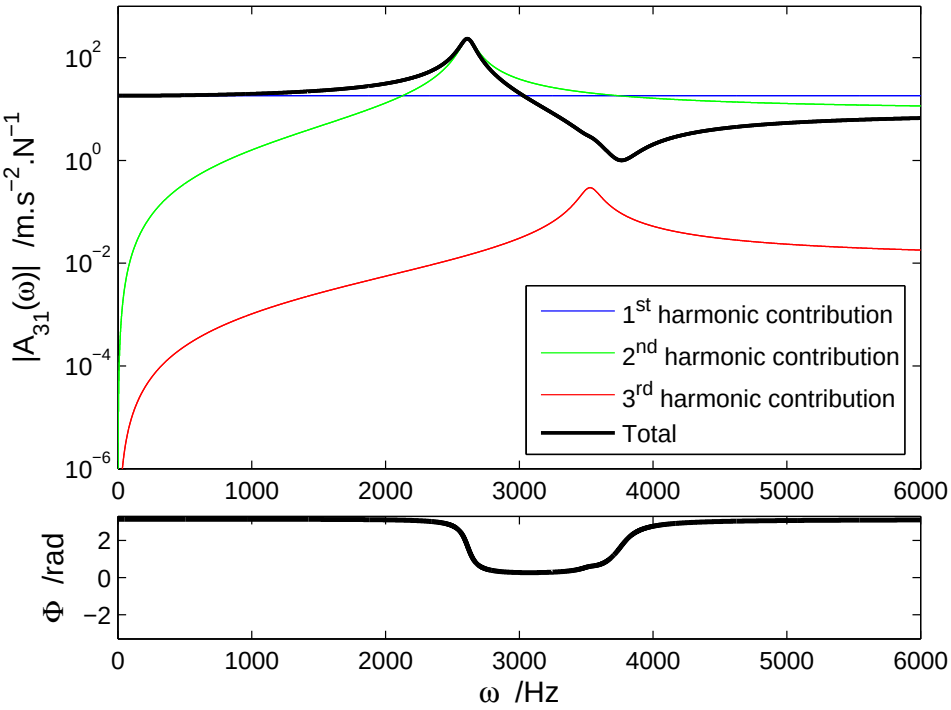

Figure 6.9.: FRF of type accelerance in DoF $l_{e,o}$ for crossed solicitation in DoF β_e

6.4. Intake sub-system, 3 DoF's

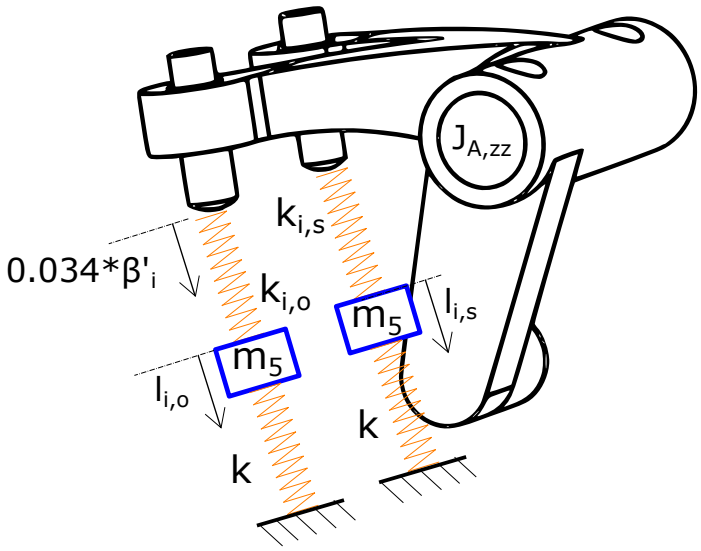

Figure 6.10.: Dynamic system for the intake sub-system, 3DoF's

This system is similar to the one presented before, but is associated to the intake sub-system. The 3 DoF's are:

- β_i' - the rotation angle of the intake rocker-arm, from stationary position;
- $l_{i,s}$ the displacement of the intake valve under the straight arm;
- $l_{i,o}$ the displacement of the intake valve under the oblique arm.

The flexibility of the rocker arm under bending solicitation was calculated using FEA Analysis tool from SolidWorks^{TM}.

$$\frac{1}{k_{3,s,roller}} + \frac{1}{k_{3,s,pin}} = \frac{1}{k_{3,s}} \quad \Rightarrow \quad \frac{2.5 \cdot 10^{-5}}{1000} + \frac{6 \cdot 10^{-5}}{1000} = \frac{1}{k_{3,s}} \tag{6.44}$$

$$k_{3,s} = 1.1765 \cdot 10^{7} \ \ N \cdot m^{-1} \tag{6.45}$$

$$\frac{1}{k_{3,o,roller}} + \frac{1}{k_{3,o,pin}} = \frac{1}{k_{3,o}} \quad \Rightarrow \quad \frac{2.5 \cdot 10^{-5}}{1000} + \frac{1.6 \cdot 10^{-4}}{1000} = \frac{1}{k_{3,o}} \tag{6.46}$$

$$k_{3,o} = 5.4054 \cdot 10^{6} \ \ N \cdot m^{-1} \tag{6.47}$$

6.4.1. Lagrangian dynamic equilibrium

The energy equations for this system are similar to the exhaust one. The final Lagrange equilibrium equations, in free regime, can be written in the following matrix form:

$$\begin{bmatrix} J_{3,zz} & 0 & 0 \\ 0 & m_5 & 0 \\ 0 & 0 & m_5 \end{bmatrix} \begin{Bmatrix} \ddot{\beta}'_i \\ \ddot{l}_{i,s} \\ \ddot{l}_{i,o} \end{Bmatrix} + \begin{bmatrix} m_4 \cdot g \cdot \overline{AG_3}^y & -0.034^2 k_{3,s} & -0.034^2 k_{3,o} \\ -0.034^2 k_{3,s} & k_{3,s} + k & 0 \\ -0.034^2 k_{3,o} & 0 & k_{3,o} + k \end{bmatrix} \begin{Bmatrix} \beta'_i \\ l_{i,s} \\ l_{i,o} \end{Bmatrix} = \overrightarrow{0} \tag{6.48}$$

Eigenproblem

The same way it was done for the exhaust sub-system, using the condition:

$$\left[[k] - \omega^2 [m]\right] \{u\} = \{0\} \tag{6.49}$$

, we obtain the natural frequencies of the system.

$$\begin{cases} \omega_1 = & 0 & \\ \omega_2 = & 13930 & rad \cdot s^{-1} \\ \omega_3 = & 20530 & \end{cases} \Rightarrow \begin{cases} \omega_1 = & 0 & \\ \omega_2 = & 2217 & Hz \\ \omega_3 = & 3267 & \end{cases} \tag{6.50}$$

As in the exhaust sub-system, the first natural frequency is equal to 0, which represents a rigid body movement of all degrees of freedom.

The matrix of Eigenvectors is

$$[u] = [u_1|u_2|u_3] = \begin{bmatrix} 1 & 1 & 1 \\ 0.0012 & 0.0021 & -1.1973 \\ 0.0012 & -2.5486 & -0.0010 \end{bmatrix} \tag{6.51}$$

The normalized vectors are:

$$\Rightarrow [\Phi] = [\Phi_1|\Phi_2|\Phi_3] = \begin{bmatrix} 124.0421 & 2.3445 & 4.9875 \\ 0.1431 & 0.0050 & -5.9713 \\ 0.1427 & -5.9751 & -0.0049 \end{bmatrix} \tag{6.52}$$

The FRF accelerance functions for this system are presented in the following graphics and the receptance in Appendix D.2

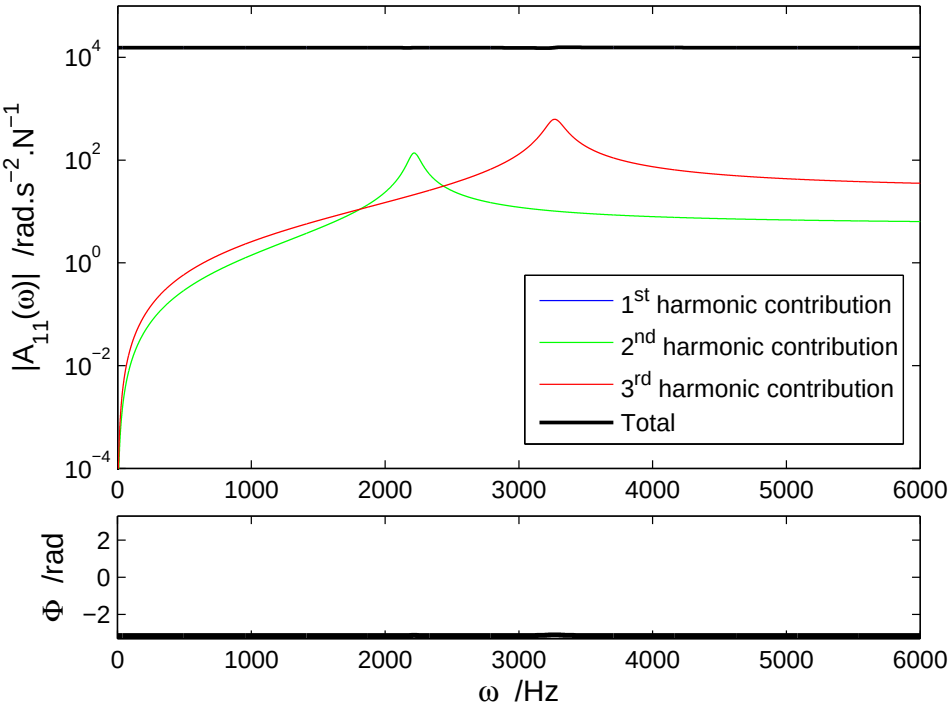

Figure 6.11.: FRF of type accelerance for direct solicitation in DoF β_i

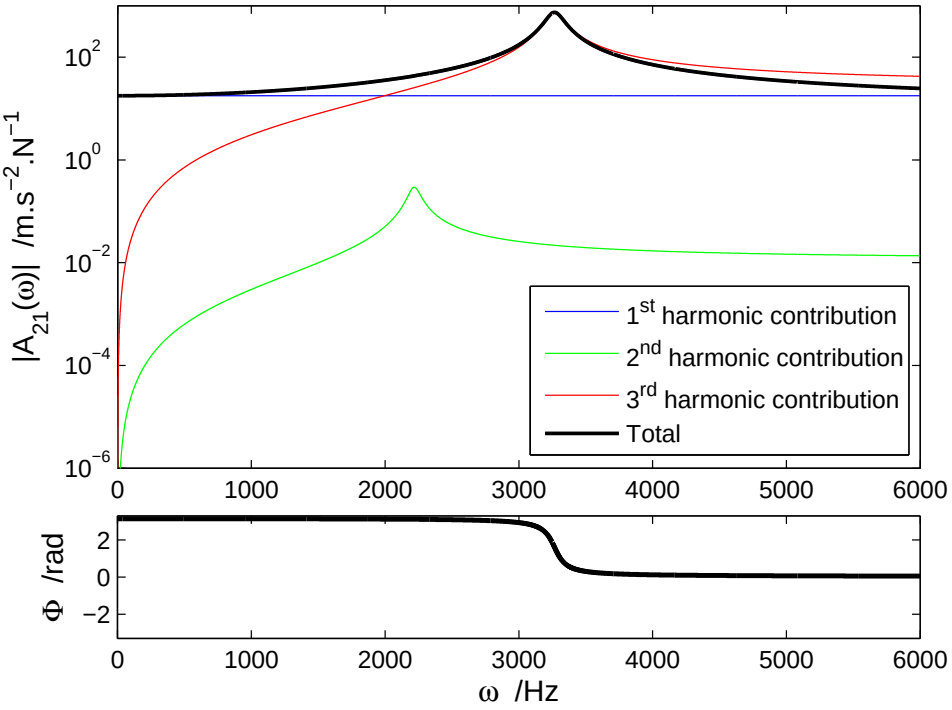

Figure 6.12.: FRF of type accelerance in DoF $l_{e,s}$ for crossed solicitation in DoF β_i

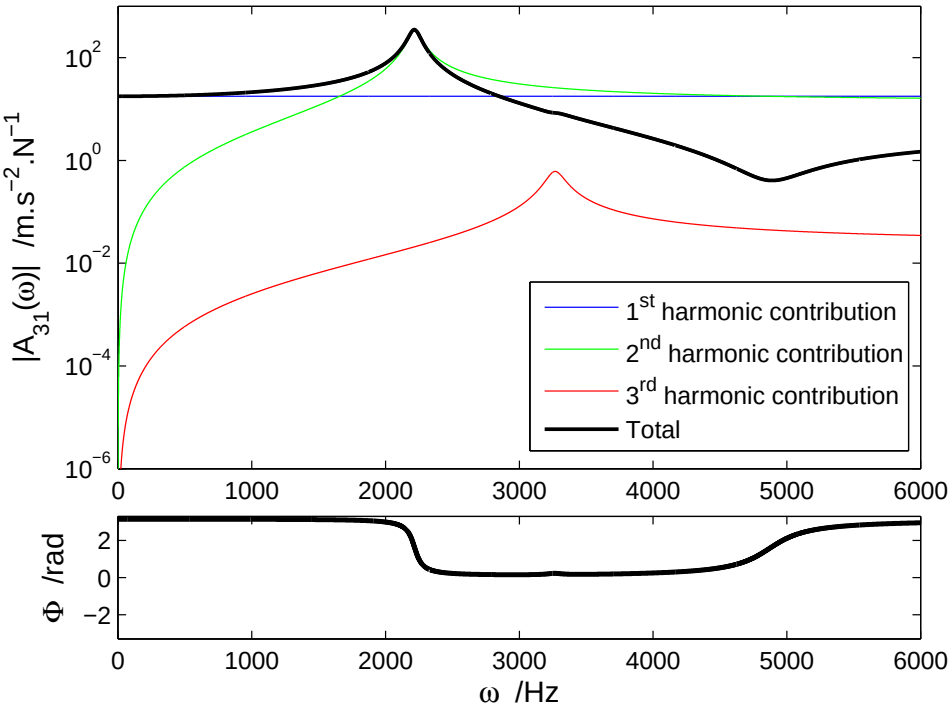

Figure 6.13.: FRF of type accelerance in DoF $l_{e,o}$ for crossed solicitation in DoF β_i

6.5. Body parts modal analysis

In previous work, Thesis [11], a modal analysis was performed for 3 body parts: camshaft and rocker-arms. A set of first natural frequencies of vibration were identified for each one in order to compare them with the regime of the engine. Those results are gathered in the following tables.

Mode	Frequency /Hz	Engine speed /rpm
1	0.0	0.0
2	3856.3	462756
3	4640.0	556800

Table 6.1.: Exhaust rocker-arm natural frequencies [11]

Mode	Frequency /Hz	Engine speed /rpm
1	0.0	0.0
2	3297.5	395700
3	4457.3	534876

Table 6.2.: Intake rocker-arm natural frequencies [11]

Mode	Frequency /Hz	Engine speed /rpm
1	0.0	0.0
2	3376.0	405120
3	3544.9	425388

Table 6.3.: Camshaft natural frequencies [11]

It was concluded that the natural frequencies of vibration were too high to cause any impact. However, notice that the frequency of solicitation (variation of β, for instance) is considerably higher than the engine speed, corresponding to a ratio of $\frac{\pi}{1.2566}$ for the exhaust sub-system and $\frac{\pi}{1.4137}$, as determined in Section 6.2.

For instance, at $8400rpm$ (engine's crankshaft speed), the frequency of solicitation will be: $21000.6rpm$ and $18666.9rpm$ (analogously to the reasoning explained in 6.2), for exhaust and intake system, respectively.

7. Modelling the InnerCam™ in MSC Adams™

The software Adams™, from MSC, is widely used in Multibody Dynamic analysis. It is considered one of the most important tools for automotive and aerospace industries to evaluate and measure the complex interactions between disciplines including motion, structures, vibration, actuation and control to better optimize product designs for performance, safety, and comfort. Some interesting study examples in valve train systems can be seen in References [17] and [18].

It was purposed the use of this software to accurately measure the system in study, in order to understand correctly the dynamic behaviour of all the parts at different speeds, including a vibration analysis of the system response to different solicitations. This software also provides results for a numerical analysis of the contact and friction problem, producing enough data to determine the dynamic solution for the contact problem between the camshaft and the rocker arms.

In this chapter I will explain the modelling of the InnerCam™'s system in the Student Version of MSC Adams™ software, which can be downloaded from the MSC's website after authorized registration. This step took a long time to be ready and, due to lack of time available for learning and testing the software's capabilities, there were made some considerations in order to make progress with the work and produce results.

The default units system selected was the one named as MMKS (Milimiter, Kilogram, Newton, Second, Degree, Hertz) and the earth gravity vector oriented according to Y axis direction.

7.1. Considerations

The bodies have no stiffness properties, because that would require a finite element mesh assigned to them, but unfortunately there was only a student version available, which has many limitations working with flexible bodies (for instance, the limit of

1000 elements in a meshed body). Therefore, Adams/Flex tool cannot perform a mesh assignment to the majority of the parts in this problem.

In this modelling analysis rigid bodies were used, which means that MSC Adams interprets it in a way which there are interference between the bodies (they have no physic boundaries). Therefore, some contact forces must be computed independently and characterized with stiffness and damping parameters.

The use of rigid bodies have another implication in vibration analysis. Basically, it will not be possible to identify the real natural frequencies or shapes of vibration, because the only flexibility degrees of freedom in the system are associated with contact and spring force's stiffness.

Another simplification adopted is located in the coupling between the rocker-arms and the camshaft. In InnerCam^{TM} prototype there is a roller providing the contact between the rocker-arms follower and the camshaft profile, which is responsible for the reduction of friction. In MSC Adams^{TM}, the model built doesn't include this roller. Therefore, the contact between the rocker arms and the camshaft occurs in pure sliding condition, and consequently no friction forces were characterized in this contact.

Further in this chapter it will be introduced the spring forces that were applied between the valves and the fixed body. Accurately the springs should be introduced in the model as a part with mass and stiffness properties, because the inertia of the valve plays an important role in the dynamic behaviour of the system. Nevertheless this version/package of MSC Adams^{TM} does not include a toolbox to introduce springs (or even designing a spring, I wouldn't be able to mesh it), instead there is an alternative to apply a spring force, according to a certain direction, between two points of different parts. Anyway, since the material of the spring is Titanium, its specific mass is low, therefore it is not so important, comparing to the rocker-arms.

7.2. Geometry Construction

A .STEP file was provided by AJP Motos with the assembly of the InnerCam™ mechanism within 7 parts, to know:

- Camshaft
- Admission rocker-arm
- Exhaust rocker-arm
- 2 Admission valves
- 2 Exhaust valves

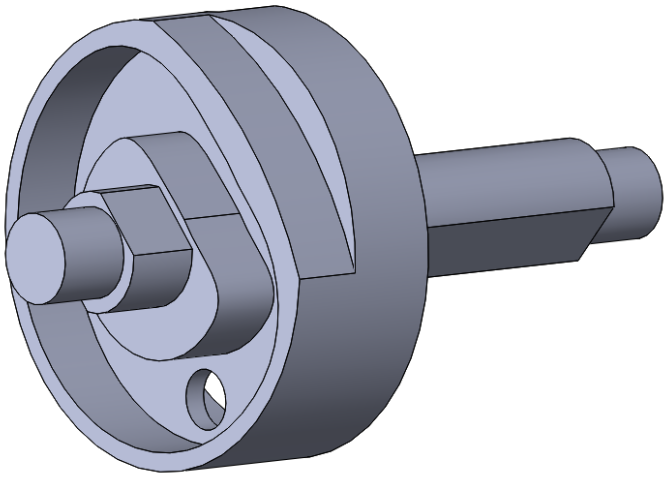

Figure 7.1.: InnerCam's Camshaft (SolidWorks™ view)

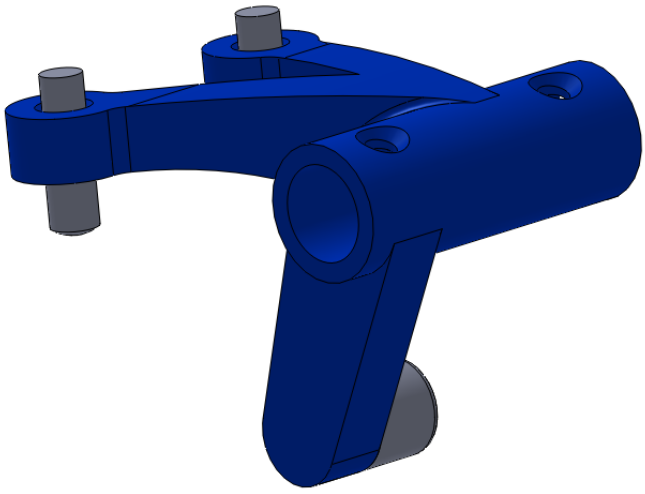

Figure 7.2.: InnerCam's Admission Rocker-arm (SolidWorks™ view)

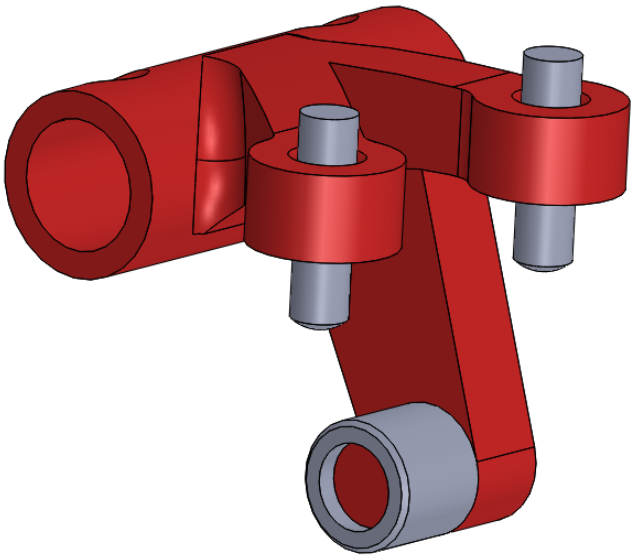

Figure 7.3.: InnerCam's Exhaust Rocker-arm (SolidWorks^{TM} view)

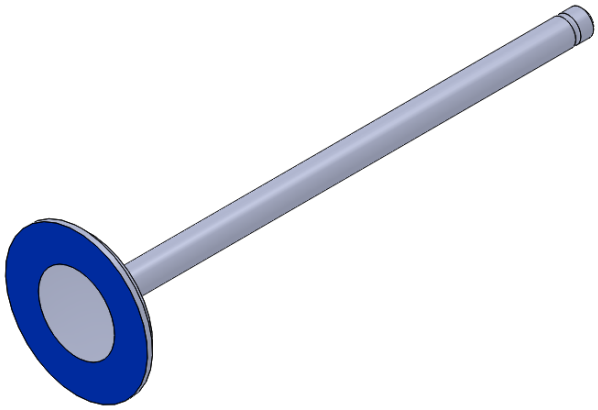

Figure 7.4.: InnerCam's Admission Valve (SolidWorks^{TM} view)

This file was imported to SolidWorks^{TM} as an assembly of the mechanism, from which each individual part was recognized geometrically into features. Mass properties were also identified and can be consulted in the Appendix B.

In order to build the dynamic model in MSC Adams^{TM}, two more parts were designed to add the system, namely a washer and a fixed body (which pretends to be a body in which the valves will be coupled through a bushing and the springs fixed).

After all the parts have been kinematically assembled in SolidWorks^{TM} and every position and angles defined, each one of the parts was exported to Parasolid format (.x_t). This choice is justified because: "Adams can use Parasolid to determine geometrical aspects of the 3D contacts that occur during simulations. It is an exact boundary-representation geometric modeler, which means that objects have

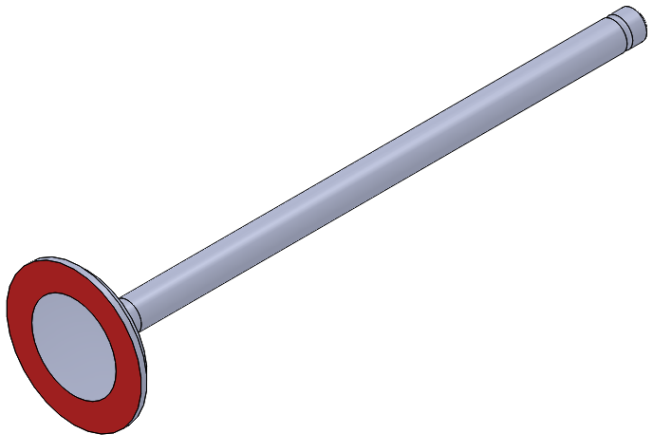

Figure 7.5.: InnerCam's Exhaust Valve (SolidWorks^{TM} view)

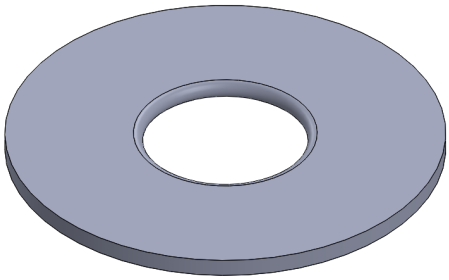

Figure 7.6.: InnerCam's spring washer (Solidworks^{TM} view)

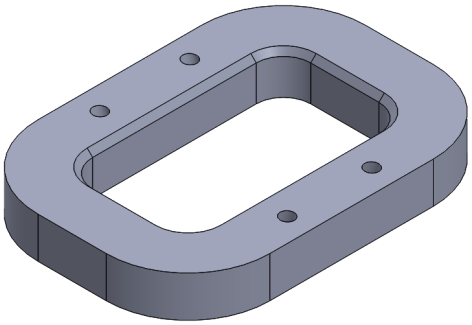

Figure 7.7.: InnerCam's fixed body (Solidworks^{TM} view)

exact surfaces. Curved surfaces are truly curved and do not consist of polygons. Because surfaces are not divided in smaller parts, their representation is as accurate as possible. The simulation times are relatively high when using Parasolid." [9]

Having this in mind, each part was imported to MSC Adams^{TM}, separately, and its local coordinate referential was moved (in relation to the Global one assigned to the Ground part, by software's definition) and rotated according to its equilibrium position. Important to refer that each valve was assigned with its corresponding washer in a separate part (therefore, 4 different parts with 2 bodies each). The full list off parts is as follows.

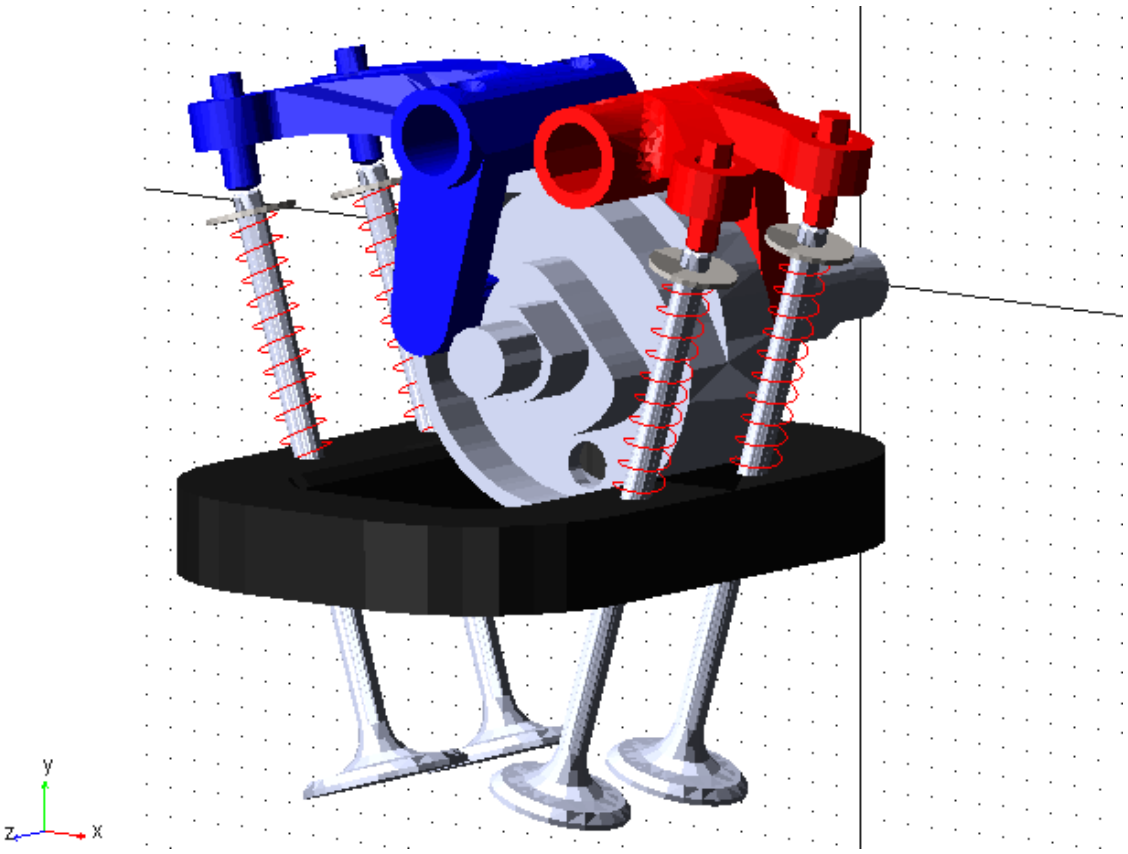

Figure 7.8.: Innercam's assembly model in MSC Adams^{TM}

Table 7.1.: List of parts in Innercam's MSC Adams™ model

Name	bodies	position /mm	orientation /°	Comments
Camshaft	1	$(0;0;0)$	$(0;90;0)$	
Fixed_body	1	$(0;-34;87.5)$	$(0;0;0)$	
Ground	none	-	-	Global referential
Rocker_adm	1	$(-15;35;50)$	$(80.5;0;0)$	
Rocker_exh	1	$(15;35;95)$	$(98.5;180;0)$	
Valve_adm_o	2	$(-47;24;103.5)$	$(107;0;0)$	Admission Valve under the oblique arm
Valve_adm_s	2	$(-47;24;70.5)$	$(107;0;0)$	Admission Valve under the straight arm
Valve_exh_o	2	$(47;24;102.5)$	$(73;0;0)$	
Valve_exh_s	2	$(47;24;71.5)$	$(73;0;0)$	

7.3. Boundary conditions

The kinematic relations in this software can be applied as joints, primitives or constrains. However, by the lack of learning time, it was only possible to correctly use joints in this model. This is a way to define the degrees of freedom (DoF) each part can move through (in relation to the global coordinate system or other part's local coordinate system).

The DoFs defined by this joints are rigid, which means that the model cannot move or vibrate in other directions, but the one allowed by indicated vector.

There were used 2 different types of joints:

- **Revolute** - this constraint allows the part to only rotate according to 1 chosen direction, that way, the part only has one degree of freedom;
- **Cylindrical** - this constraint allows the part to move in two degrees of freedom according to the same direction, in other words, the body can translate or rotate along the same, and only the same, defined common axis.

Table 7.2.: List of joints in InnerCam™'s MSC Adams™ model

Name	Type of Joint	Moving Part	Reference	DoF's	Description
Fixed_joint	revolute	*Fixed_body*	*Ground*	0	
Cam_rot	revolute	*Camshaft*	*Ground*	1	rotation according to OZ axis
Arm_adm_rot	revolute	*Rocker_adm*	*Ground*	1	rotation according to OZ parallel axis, point $(-15, 35, --)$
Arm_exh_rot	revolute	*Rocker_exh*	*Ground*	1	rotation according to OZ parallel axis, point $(15, 35, --)$
Cil_adm_o	cylindrical	*Valve_adm_o*	*Fixed_body*	2	rotation and translation according to the defined axis, point $(-47, 24, 103.5)$, orientation $(17, 90, 0)$
Cil_adm_s	cylindrical	*Valve_adm_s*	*Fixed_body*	2	rotation and translation according to the defined axis, point $(-47, 24, 70.5)$, orientation $(17, 90, 0)$
Cil_exh_o	cylindrical	*Valve_exh_o*	*Fixed_body*	2	rotation and translation according to the defined axis, point $(-47, 24, 102.5)$, orientation $(163, 90, 180)$
Cil_exh_s	cylindrical	*Valve_exh_s*	*Fixed_body*	2	rotation and translation according to the defined axis, point $(-47, 24, 71.5)$, orientation $(163, 90, 180)$

7.4. Contact Forces

Since rigid bodies are being used in this modelling, the coupling between the camshaft and the rocker-arms or the tappet contact between the rocker arms and the valves has to be defined by contact forces. These forces parameters, like contact stiffness, damping, penetration depth, or friction, had to be determined using Hertz contact theory.

There are two available contact force calculation methods: impact or restitution. In the impact method, if a contact between two bodies is defined, then a contact force will emerge as the geometry of the two bodies begin to overlap (or penetrate). Considering the following variables:

- Contact normal force, N_C or F_k
- Contact stiffness, K_C
- Penetration depth, g or d
- Penetration distance, q
- Maximum penetration distance, δ_max
- Maximum damping coefficient, c_max
- Force exponent, e_f

That way, the Contact Normal Forces are calculated according to:

$$\underbrace{N_C}_{\text{Contact Normal Force}} = \underbrace{K_C \cdot g^{e_f}}_{\text{Stiffness contribution}} + \underbrace{step(g, 0, 0, \delta_{max}, c_{max}) \cdot \frac{dg}{dt}}_{\text{Damping contribution}} \tag{7.1}$$

The value identified as e_f is called Force Exponent and it is recommended to be more than 1, so that the slope of the spring force is continuous even when passing from the non-contact domain to the contact domain. According to the reference [9], this value can be equal to 2.2 for hard metals (which is the case of hardened steel used).

On the other hand, using the restitution method, a coefficient of restitution ϵ is defined (where 1 corresponds to perfectly elastic collision and 0 perfectly inelastic). Also a 'penalty' p is required, which has damping units (force under velocity), but is not associated with a material property, it should be a big value that will not sacrifice numerical robustness instead.

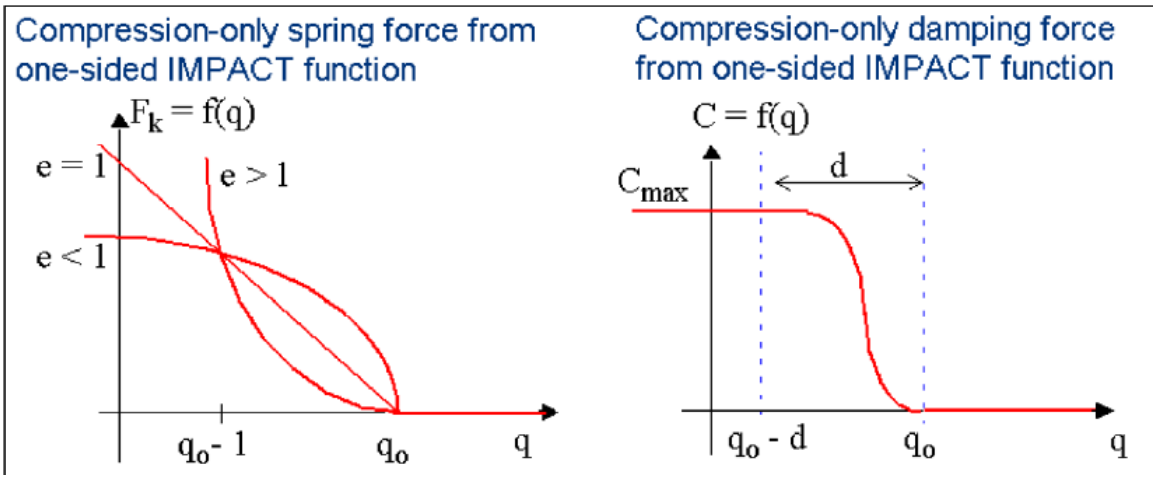

Figure 7.9.: Graphs of the two force parameters of the IMPACT function

$$N_C = p \cdot \epsilon \cdot \frac{dg}{dt} \tag{7.2}$$

Summing up, the restitution method suffers less from numerical damping and may be more appropriate when energy loss is a key parameter. However, the impact method is more robust and considerably less sensitive to error tolerances. Considering this, the impact method was chosen for this study because it allows the use of Hertz Contact Theory for determine the parameters required.

In order to accurately obtain the stiffness coefficient and penetration in the contact the idea was to use an iterative method, once that stiffness would depend on the contact force which has a static and a dynamic component. That way, the static solution was used to perform the first step of the iteration and the resultant Normal Contact Forces obtained performing a simulation in MSC Adams^{TM} at the speed of $5000rpm$. Both solutions are time dependent, because the contact radius of the camshaft is not constant. The contact model used is described bellow.

For the damping coefficient, as indicated by Adams/solver Help, it was selected a value corresponding to 1% of the respective stiffness. Looking back at Figure 7.9, on the graphic at the right, the maximum damping coefficient, C_{max}, is associated to a penetration depth, d. Then, for a penetration value smaller that d the damping tends to *zero*, and for a value bigger than d, the damping tends to C_{max}.

This contact constraint also provides a tool to define the friction conditions. There is only one predefined calculation method, to know: Coulomb's friction. This require 4 parameters to be fully characterized:

- Static coefficient, μ_s
- Dynamic coefficient, μ_d

- Stiction transition velocity, v_s
- Friction transition velocity, v_d

Recording the Coulomb's friction theory, this parameters are defined according to the curve in Figure 7.10.

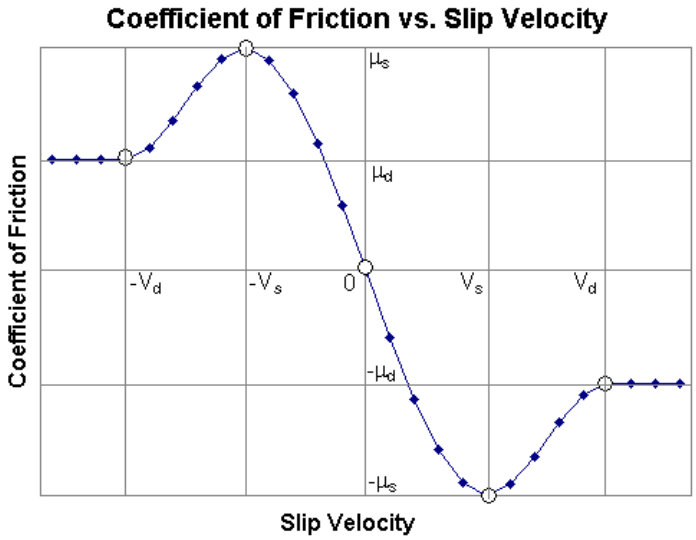

Figure 7.10.: Coulomb's friction MSC's curve - Coefficient of Friction vs Velocity [9]

7.4.1. Contact between Camshaft and Rocker Arms

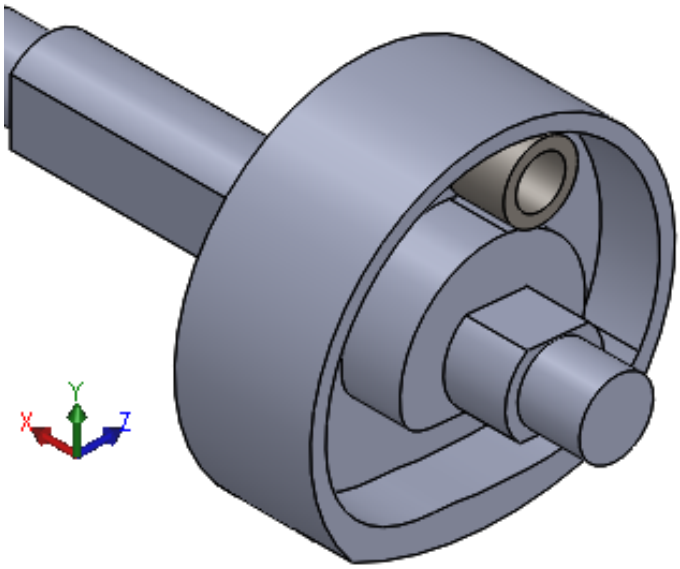

Figure 7.11.: Diagram representing the bodies in contact (Solidworks^{TM} view)

In order to determine the parameters of this contact force, it is considered that

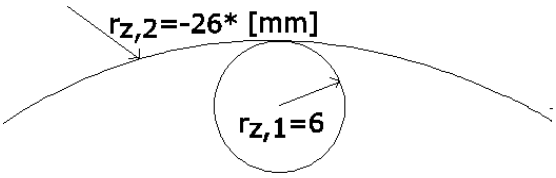

Figure 7.12.: Representation of the cam's contact in Oyz plane

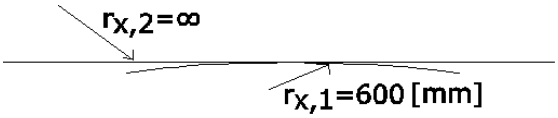

Figure 7.13.: Representation of the cam's contact in Oxy plane

the roller has a big contact radius, non infinite, in Oyz plane (10 times bigger than in Oxy plane (according to the Figure 7.11). This way it is possible to determine a penetration depth and thereafter obtain the stiffness of the contact, according to [19]. We can check the geometry of the contact in Figures 7.12 and 7.13.

Noticing that the radius of the camshaft surface is not constant, therefore the stiffness of contact will depend on the angle θ of the camshaft every instant. For the first step of iteration, an average stiffness value was determined using the static solution for the problem, i.e. considering the load applied by the spring.

$$\frac{1}{R_{z,eq}} = \frac{1}{2}\left(\frac{1}{R_{z,1}} + \frac{1}{R_{z,2}}\right) \Rightarrow R_{z,eq} = 15,6 * \ mm \tag{7.3}$$

Note: the symbol $*$ means that this value depends on the radius of the cam profile which is not constant.

$$\frac{1}{R_{x,eq}} = \frac{1}{2}\left(\frac{1}{R_{x,1}} + \frac{1}{R_{x,2}}\right) \Rightarrow R_{x,eq} = 1200 \ mm \tag{7.4}$$

Being,

$$A_H = \frac{1}{R_{x,eq}} \qquad \wedge \qquad B_H = \frac{1}{R_{z,eq}} \tag{7.5}$$

then,

$$\frac{A_H}{B_H} \simeq 77* \qquad \Rightarrow \begin{cases} k = 0.064* \\ C_a = 0.313* \\ C_\delta = 0.398* \end{cases} \tag{7.6}$$

Equivalent Young modulus:

$$\frac{1}{E_{eq}} = 2\frac{1-\nu^2}{E} = 2\frac{1-0.29^2}{210000} \Leftrightarrow E_{eq} = 114641\ MPa \tag{7.7}$$

As explained earlier, the first iteration considers the static solution, so the normal force depends on the stiffness of the spring. Being so,

$$F_N = 50.8 + \frac{34}{32} \cdot 25.4 \cdot Lift \tag{7.8}$$

$$a = C_a \left[\frac{F_N}{(A_H + B_H) \cdot E_{eq}}\right]^{\frac{1}{3}} \tag{7.9}$$

$$\delta = C_\delta \frac{F_N}{\pi \cdot a_H \cdot E_{eq}} \tag{7.10}$$

By definition, the stiffness of the contact is a result of the contact force F_N against the penetration depth δ. Therefore,

$$k_C = \frac{F_N}{\delta} \tag{7.11}$$

The average values were determined in order to produce a first iteration on the software MSC Adams^{TM}:

$$\begin{aligned} \overline{k_{C,adm}} &\simeq 6.55e4 \quad N \cdot mm^{-1} \\ \overline{k_{C,adm}} &\simeq 5.48e4 \quad N \cdot mm^{-1} \end{aligned} \tag{7.12}$$

Because in this model there is no rollers in the contact between the rocker arms and the Camshaft, a friction coefficient wasn't considered, as the relative movement is full slip.

7.4.2. Contact in Tappet joints

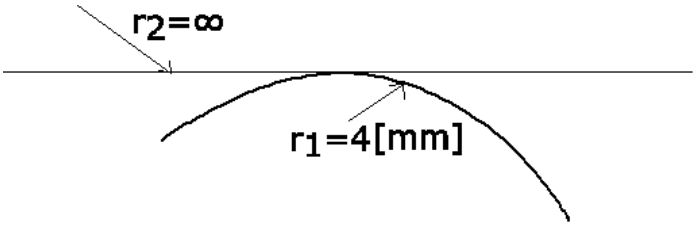

Figure 7.14.: Representation of the tappet's contact in a plane perpendicular to YY axis

For the first step of iteration, an average stiffness value was determined using the static solution for the problem, i.e. considering the load applied by the spring.

$$\frac{1}{R_{z,eq}} = \frac{1}{2}\left(\frac{1}{R_{z,1}} + \frac{1}{R_{z,2}}\right) \Rightarrow R_{z,eq} = 8\ mm \tag{7.13}$$

$$\frac{1}{R_{x,eq}} = \frac{1}{2}\left(\frac{1}{R_{x,1}} + \frac{1}{R_{x,2}}\right) \Rightarrow R_{x,eq} = 8\ mm \tag{7.14}$$

Being,

$$A_H = \frac{1}{R_{x,eq}} \qquad \wedge \qquad B_H = \frac{1}{R_{z,eq}} \tag{7.15}$$

then,

$$\frac{A_H}{B_H} = 1 \qquad \Rightarrow \begin{cases} k = 1 \\ C_a = 0.909 \\ C_\delta = 2.356 \end{cases} \tag{7.16}$$

Equivalent Young modulus:

$$\frac{1}{E_{eq}} = 2\frac{1-\nu^2}{E} = 2\frac{1-0.29^2}{210000} \Leftrightarrow E_{eq} = 114641/MPa \tag{7.17}$$

$$F_N = 50.8 + 25.4 \cdot Lift \tag{7.18}$$

The average values were determined in order to produce a first iteration on the software MSC Adams^{TM}:

$$\begin{aligned} \overline{k_{C,adm}} &\simeq 1.90e4 \quad N \cdot mm^{-1} \\ \overline{k_{C,adm}} &\simeq 1.86e4 \quad N \cdot mm^{-1} \end{aligned} \tag{7.19}$$

Using the Coulomb friction's model from the MSC's software, the following values were considered for all 4 tappet contacts (which occur in pure sliding condition), according to [9]:

$$\begin{cases} \mu_s = 0.16 \\ \mu_d = 0.15 \\ v_s = 0.1 \ /m \cdot s^{-1} \\ v_d = 10 \ /m \cdot s^{-1} \end{cases} \tag{7.20}$$

7.4.3. Tappet clearances

Another useful tool from this software is the ability to interpret the clearances in the dynamic analysis. This characteristic of contact between bodies is crucial in the well functioning of a system, when it is subjected to considerable variations of temperature or sources of vibration.

The values for this clearances were given by AJP Motos S.A. and are equal to 0.05 mm for the exhaust valves, and 0.08 mm for the admission valves.

7.5. Spring forces

For each valve a spring force was applied. In MSC Adams^{TM}, a spring force is defined by 2 specific points, each one belonging to a different body. That way, it is possible to indicate the direction and points of application of the force.

The parameters that characterize this type of force are:

- Stiffness - 25.4 $N \cdot mm^{-1}$
- Damping - 0.254 $N \cdot s \cdot mm^{-1}$ (first model)
- Pre-load - 50.8 N
- Length at preload (Default)

The damping coefficient was defined using the same logic as before, 1% of the stiffness, since the real damping coefficient of the bushing contact in the InnerCam^{TM} was not known. No calculation had been done before in the vibrational damping properties of the system, as so, this value was set to have a previous idea of the results.

Notice that the spring pre-load, in this model, is only transmitted to the tappet contact. However, in the real model, the valve seat plays an important role in the interactions between bodies and a part of that spring force is also transmitted to the valve seat. Actually, according to [20], [21] and [22], there are big impacts occurring when the valve is unseating and seating, but specially when seating. That phenomenon is then one of the main sources of vibration. It is known that this interaction is very sensitive to contact parameters and geometries. By that reason that improvement was left to a future work, with more information available about the valve seating.

7.6. MSC Adams^{TM} results - model validation

In order to validate the model described in this Chapter, some simulations were made during the process of model formulation, in order to properly characterize the system and correct errors. At last, it was found that the final simulations ended up by having some non-proportional numerical noise.

The amount of noise is influenced by the number of iterations (the simulation was performed with $2,000,000$ iterations per second, and took $4h\ 03m\ 27s$ of calculation time) and also depend on the clearances applied in the tappet contacts (as analysed in [23]). Nevertheless, it is possible to apply a 'low pass' filter, in order to

obtain a more smooth curve.

Since the main goal of this chapter is to validate the model, the simulation was performed for a speed of 4200 rpm at the camshaft, during two full cycles in the engine. It is expected that these results will be more accurate, but also more floating than the analytical ones, due to the presence of clearances, parameters of contact (including stiffness and damping) and a more accurate measure of asymmetric inertia parameters on the bodies.

To be considered is also the fact that in the analytical dynamic calculations the position of the valves was introduced as granted (i.e. there is no possibility of valve floating or bounce effect). In this Adams^{TM} simulations this is not so, therefore the real contact forces in the tappet can be determined and its detachment can be observed, or not.

7.6.1. Lift response at $4200rpm$ (camshaft)

In Figures 7.15, 7.16 and 7.17 we can clearly identify the detachment of valves from rocker-arms. That phenomenon happens because the frequency of the rocker-arm's movement is larger than the natural damped frequency of the valve/spring system. As so, we observe a time length of around 0.006 s for the exhaust valve/spring system of free movement and 0.008 s for the admission one. In order to understand better that phenomenon the next chapter it will be studied the vibrational response of this system in the frequency spectrum of the engine.

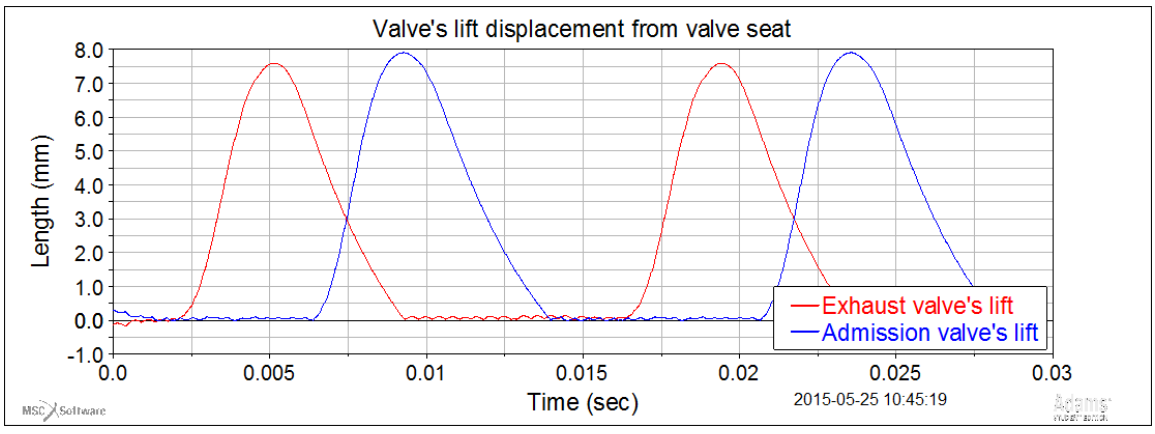

Figure 7.15.: [Adams_1] Valve's Lift displacement from valve seat

The other plot results can be observed at Appendix E.1.

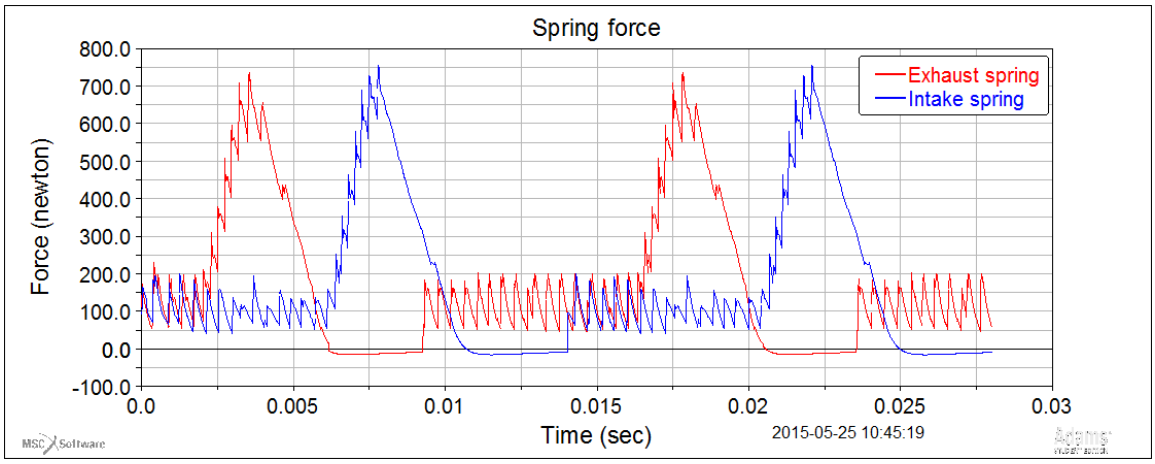

Figure 7.16.: [Adams_1] Force actuated by springs in exhaust and admission valves

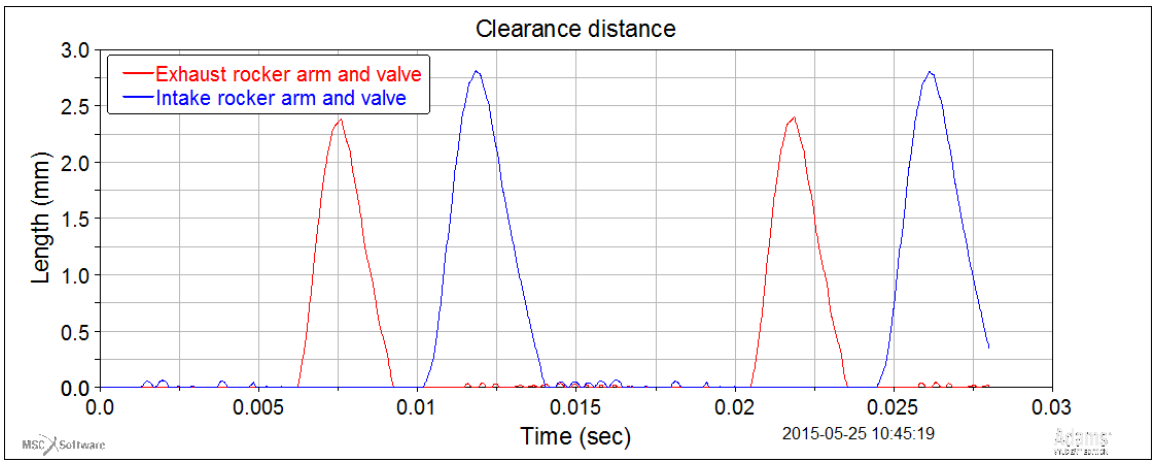

Figure 7.17.: [Adams_1] Distance between valves and rocker arms

7.7. Main modifications to the model

The parameters that were found to cause conflict in the resulting plots were the damping in the contact and spring forces for being too high. As seen in Chapter 7, it is recommended in the software's manual to use a value of 1% of the stiffness parameter. Although, in other references, as [9], the conclusions point to the fact that some experienced users admit that the maximum damping coefficient should be smaller. As so, a new ratio of 0.01% of the stiffness parameter is indicated as promising.

A new model was run at the same speed and same conditions as the previous one, but only changing the damping coefficients from a ratio of 1% to a ratio of 0.01%. Although, this model's results, which can be consulted in Appendix E.2, showed up to be inconclusive, mainly in FFT plots.

For that reason, a new ratio of 0.1% was selected.

7.7.1. Damping in spring forces

This parameter was determined according to the results obtained for the 1 DoF valve/spring dynamic model.

In that models, the damping values were determined considering a equivalent coefficient of damping equal to 5%. Those values can be taken from Equations 6.2 and 6.9.

$$\begin{cases} \xi & = & 0.05 & \\ c_{eq,e} & = & 2.469 & N \cdot s \cdot m^{-1} \\ c_{eq,i} & = & 2.6668 & N \cdot s \cdot m^{-1} \\ k & = & 25400 & N \cdot m^{-1} \end{cases} \tag{7.21}$$

8. MSC Adams - Refined Model

After some conclusions comparing the results of the first model produced in MSC Adams in Chapter 7 with the ones obtained for the analytical solutions in Chapters 5 and 6, incompatibilities were found. Therefore, some improvements were applied to the initial properties in the Adams model.

In this model, three different test were made at three different speeds (5100 8400 12000 rpm at the crankshaft), in order to understand if the harmonic frequencies obtained from the FFT's are around the same values independently of the speed and build some conclusions with that.

These simulations were run with the same number of iterations. Some noise were identified in the resultant plots. In the next chapter it is explained the way those plots were filtered using MSC Adams^{TM}Post/Processor tools.

8.1. Filtering of results

It shall be clear that the noise identified did only happen for acceleration and force results, particularly related to the contact between bodies. MSC Adams^{TM} has integrated 2 kinds of filter functions: Transfer functions and Butterworth filters (which was developed by The MathWorks^{TM}, Inc. and creates a cutoff frequency filter). The software also provides two methods for Fast Fourier Transform (FFT):

- **Analog filtering -** transfer the time signal into frequency domain through FFT, multiply the resulting function by the filter function and perform an inverse FFT;
- **Digital filtering -** operates directly on the time signal. The filtered signal at a certain time step is a linear combination of previous input and output signals, with the discrete transfer function defining the coefficients.

According to the MSC Adams Post/Processor manual, the digital low pass Butterworth filter was chosen, once we wanted to cutoff the isolated outliers which can be seen as very high frequency values. This filter is characterized by 2 parameters, to know:

- **Order -** as explained in Figure 8.1, the ploted results will benefit from a high order filter, because we want to fully eliminate the outliers;
- **Scaled cut-off frequency -** This frequency is dependent on data frequency, as so to choose the more appropriate one, firstly, it was selected a very small value, and after all, picked the smallest value which ensured numerical stability.

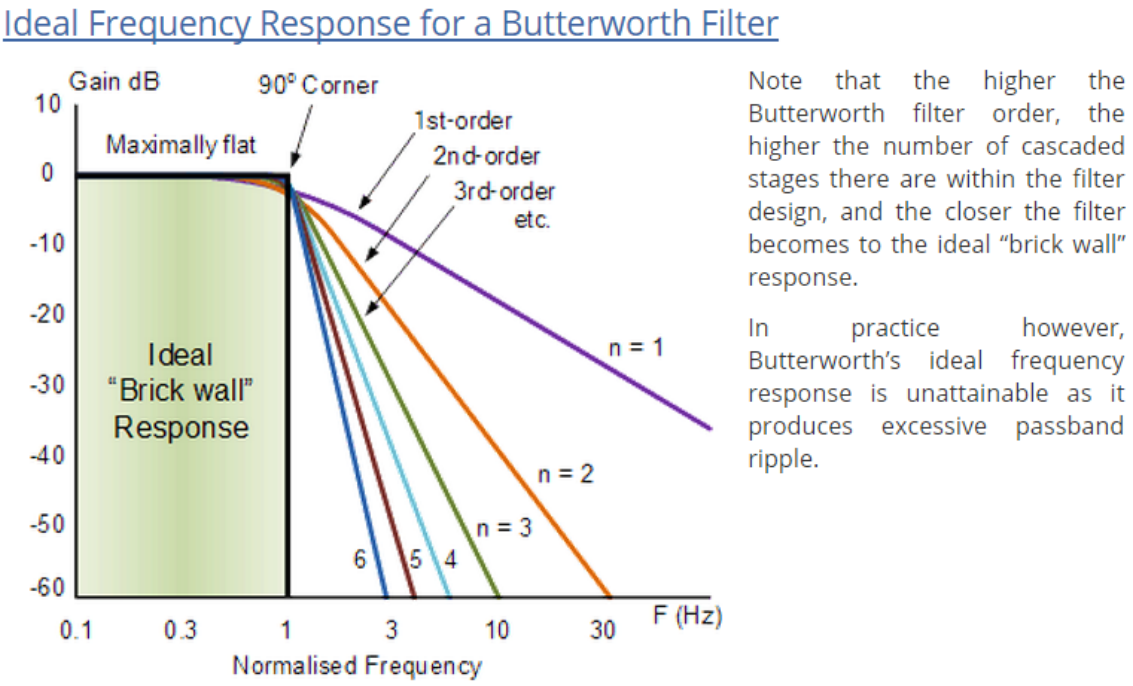

Figure 8.1.: Influence of the Butterworth order in a filtering process [10]

After some trials, three different filters were selected and compared, so that it could be reached to a final choice. The process resulted by analysing the plot results in two different scales: a global one (in full time domain, Figure 8.2) and another zoomed (6*times* in a random, representative interval from time domain, Figure 8.3). All the filters were applied with a phase angle set to zero, so that the peaks and the valleys of the waves match in time with the original plot.

Comparing the filters it was decided to use the 6^{th} order one with scaled frequency cutoff of 5×10^{-3} (represented in green in the plots). The 8^{th} order filter tends not to absorb some outliers, revealing to be too influenced by them. On the other hand, the 5^{th} order filter is not sensitive enough to represent correctly the zero values and the amplitude of the peaks.

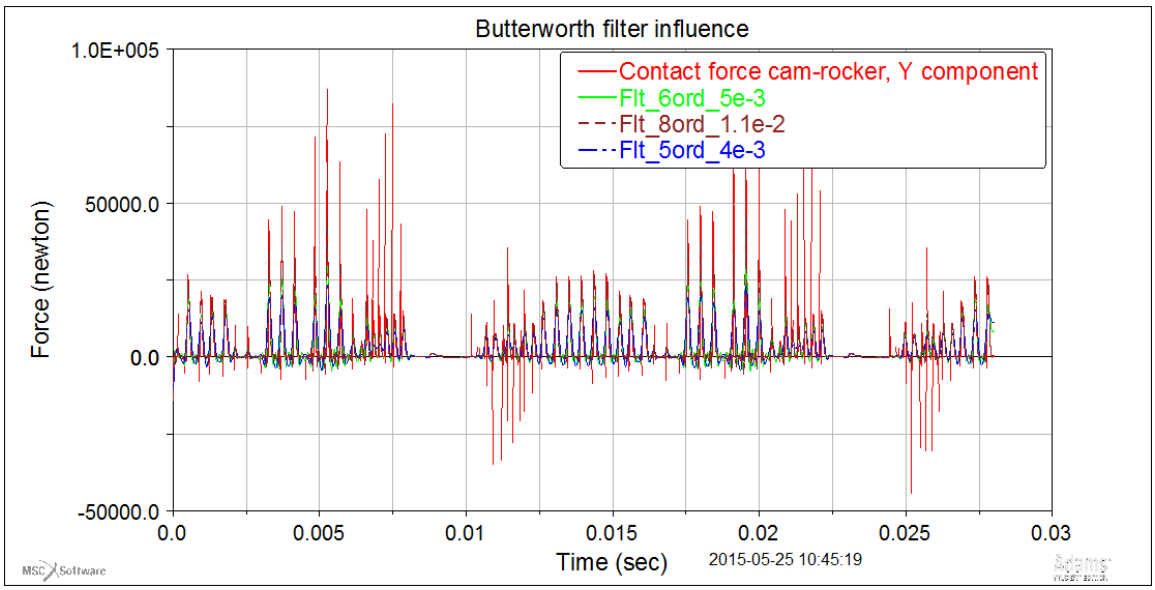

Figure 8.2.: Different results from 3 filters of various orders (full time domain)

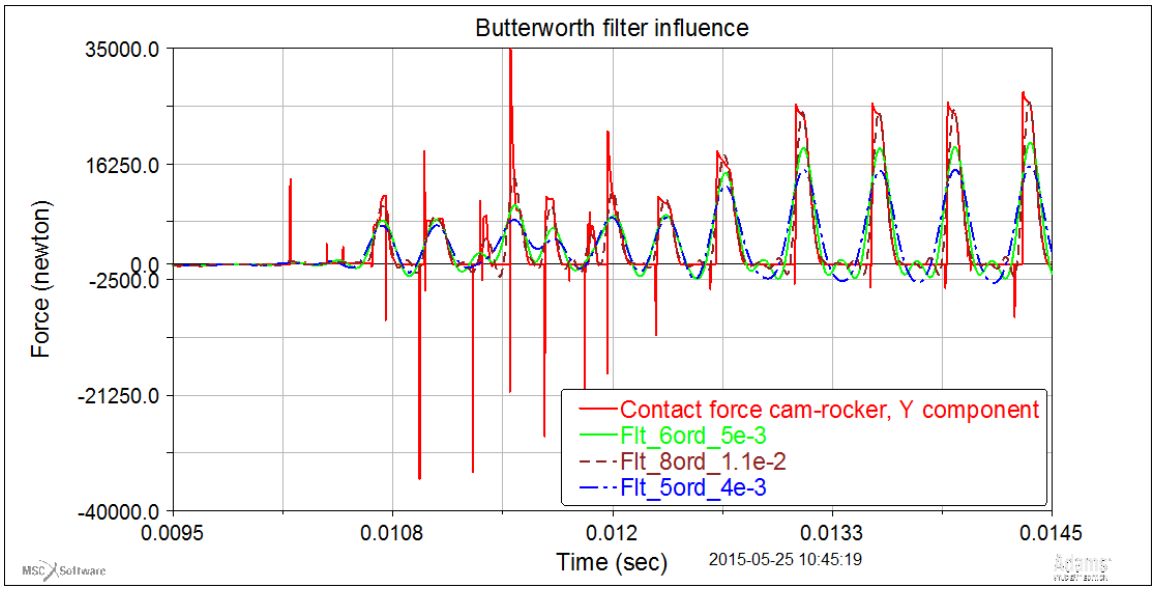

Figure 8.3.: Different results from 3 filters of various orders (zoomed in)

8.2. Improved model results

The following plots in this chapter represents the *FFT* transformations for the results being presented. The solutions obtained are time dependent and are represented in time domain. However, due to its shapes, it would be convenient to get a representation in frequency domain, in order to identify the most important harmonics of response.

The FFT allows us to make that transformation from time domain to frequency domain, and MSC Adams Post/Processor has a tool to perform it easily.

In this section, follows the resultant plots for some variables in time domain and the respective frequency domain on the right.

8.2.1. Regime: 5100 rpm

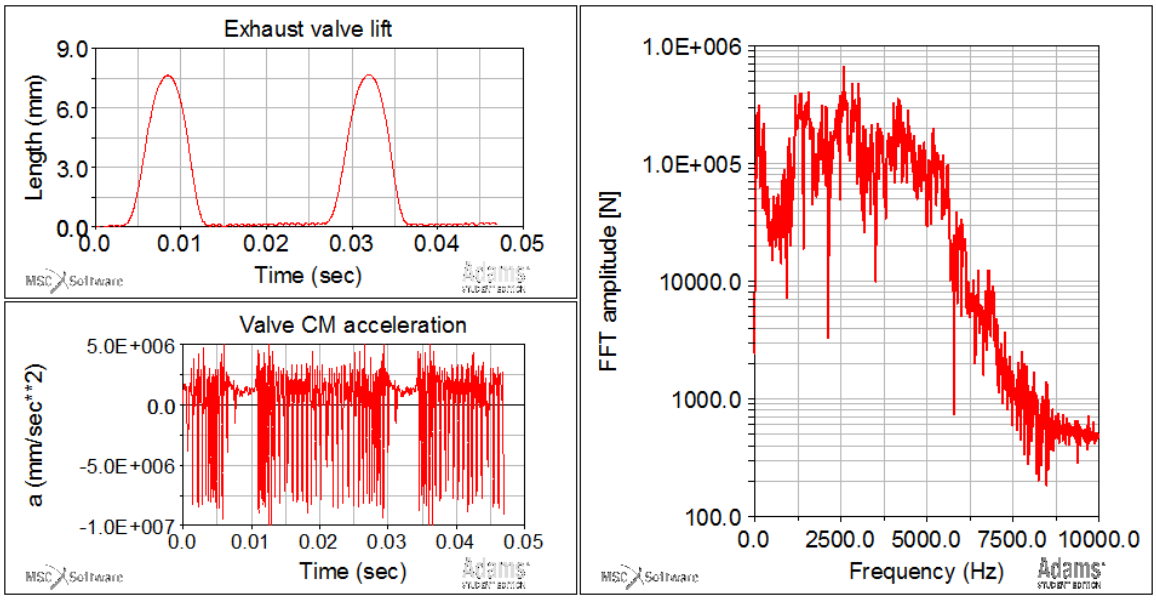

Figure 8.4.: [Adams_01_rpm51] Exhaust valve's lift, acceleration in the centre of mass (filtered) and corresponding FFT

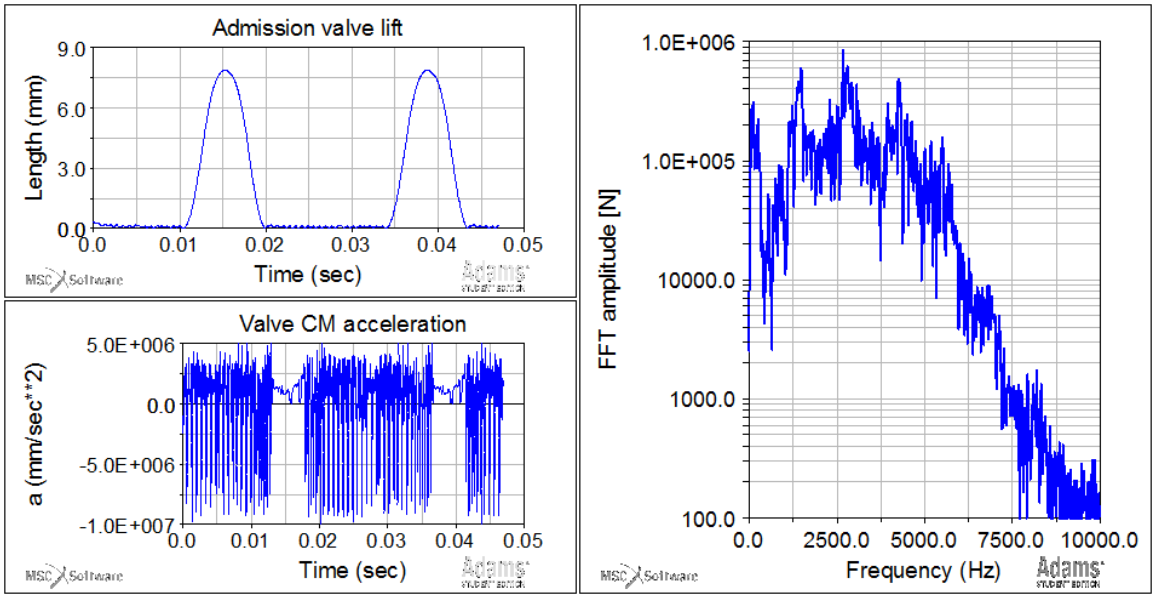

Figure 8.5.: [Adams_01_rpm51] Admission valve's lift, acceleration in the centre of mass (filtered) and corresponding FFT

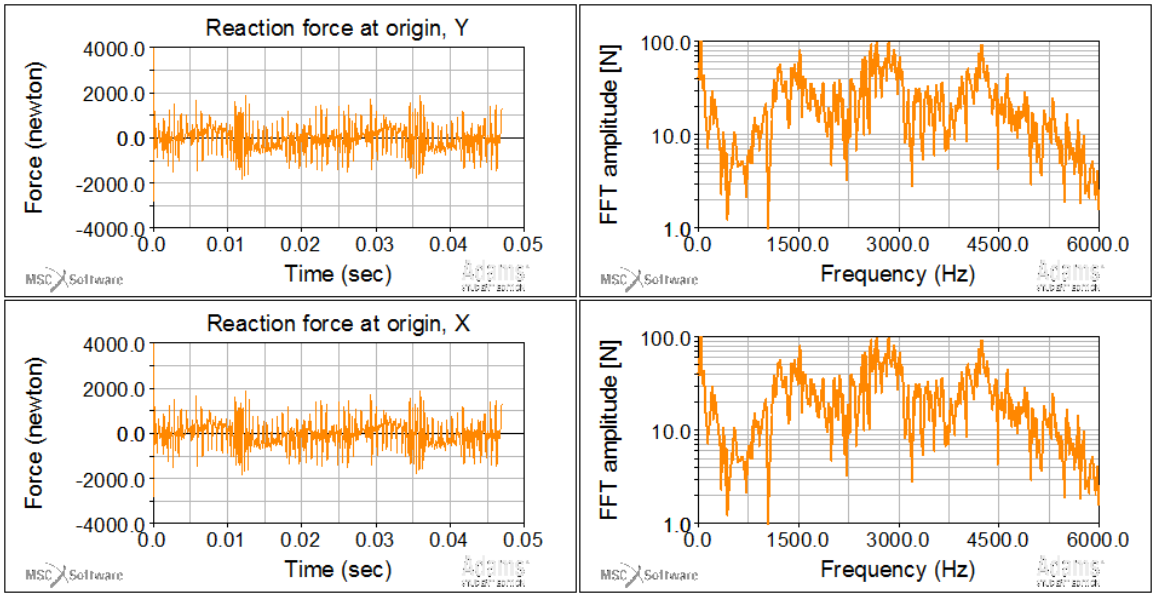

Figure 8.6.: [Adams_01_rpm51] Reaction forces at origin point in the camshaft (filtered), with FFT plot

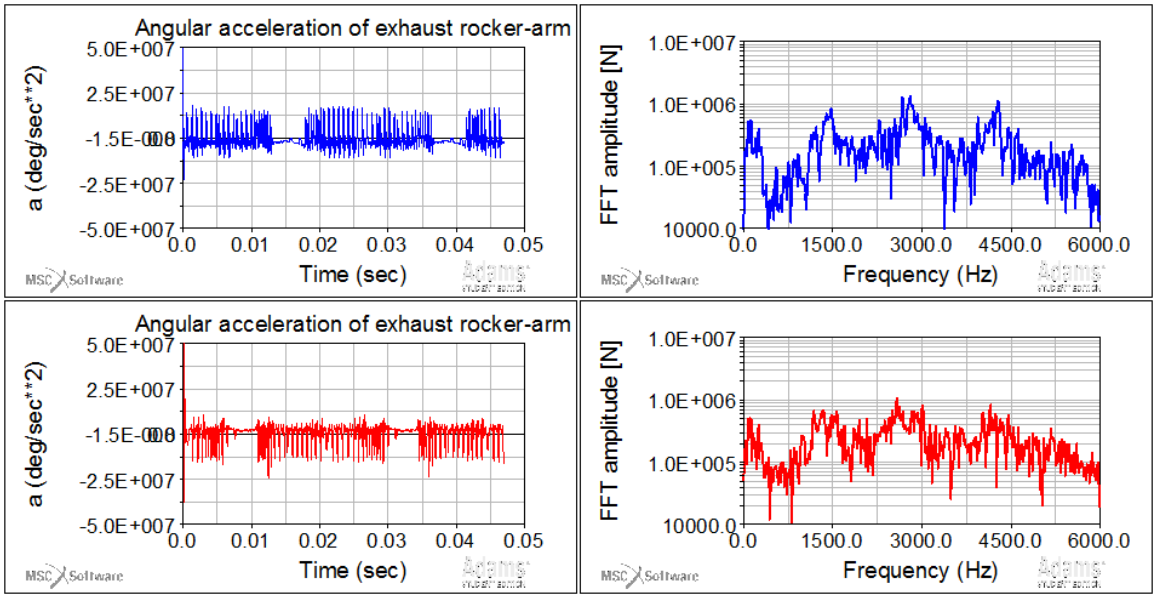

Figure 8.7.: [Adams_01_rpm51] Angular acceleration of the rocker arms (filtered), with FFT plot

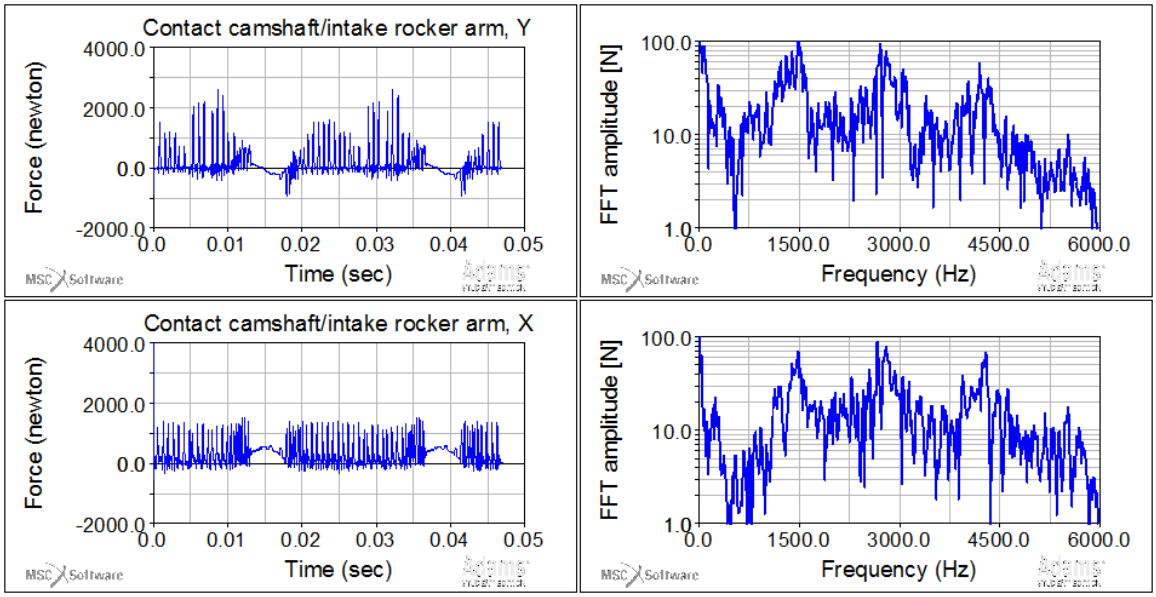

Figure 8.8.: [Adams_01_rpm51] Contact forces between the camshaft and intake rocker-arm (filtered), with FFT plot

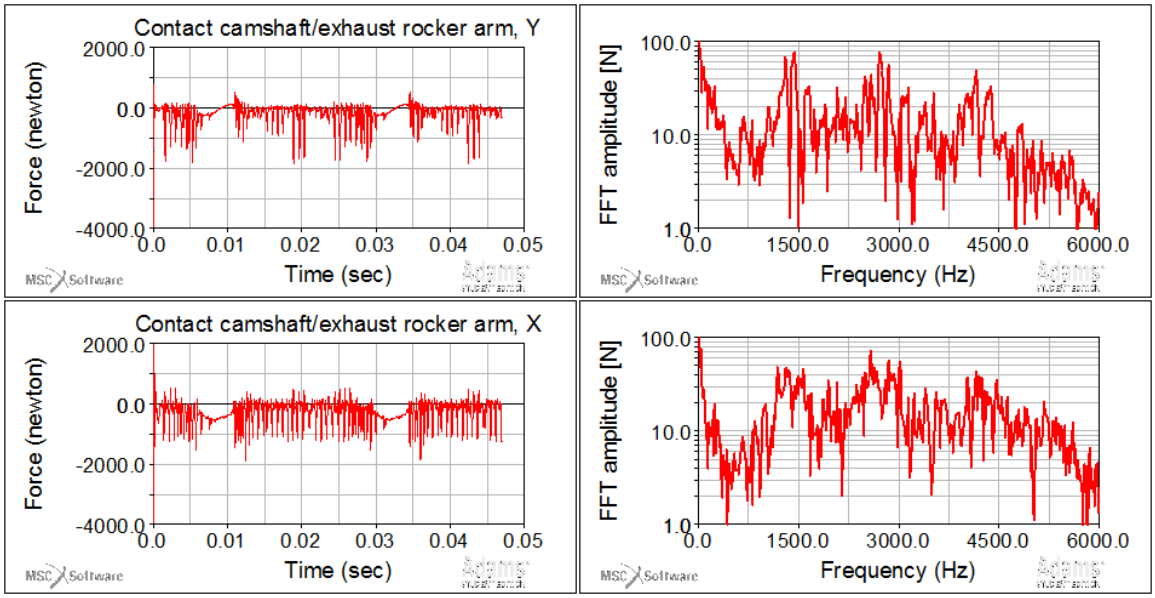

Figure 8.9.: [Adams_01_rpm51] Contact forces between the camshaft and exhaust rocker-arm (filtered), with FFT plot

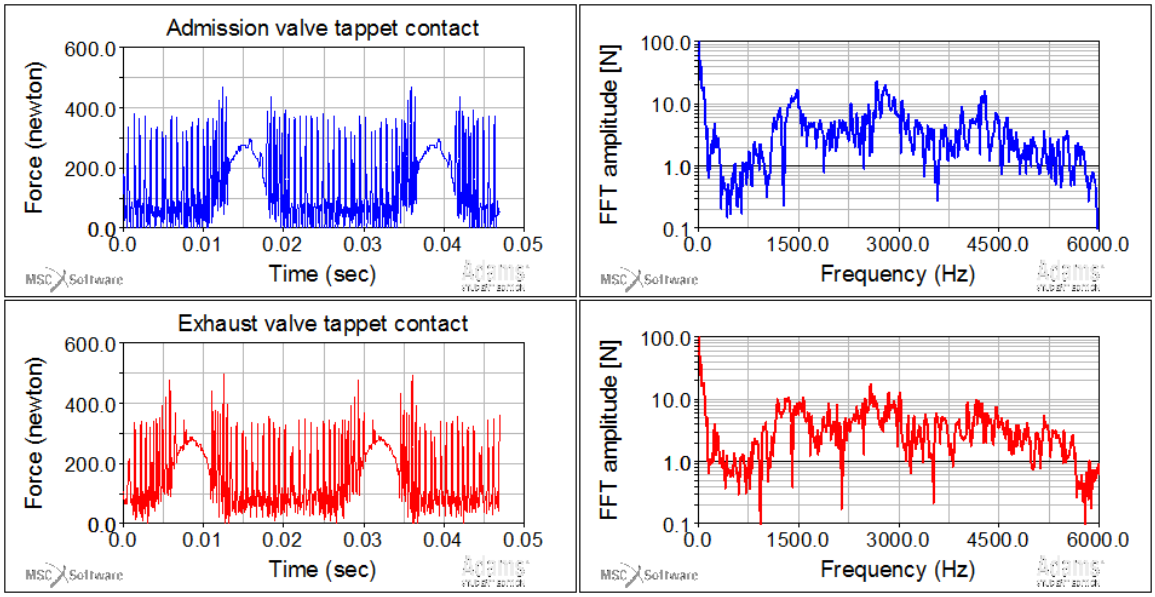

Figure 8.10.: [Adams_01_rpm51] Contact forces in the tappets (filtered), with FFT plot

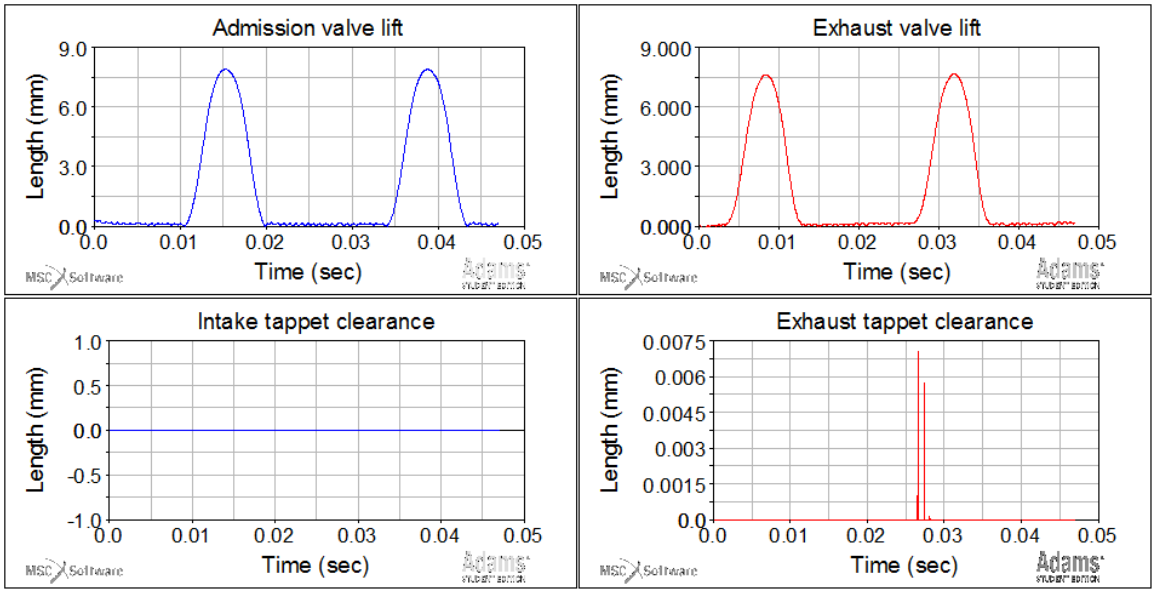

Figure 8.11.: [Adams_01_rpm51] Clearance distance in the tappet contacts

8.2.2. Regime: 8400 rpm

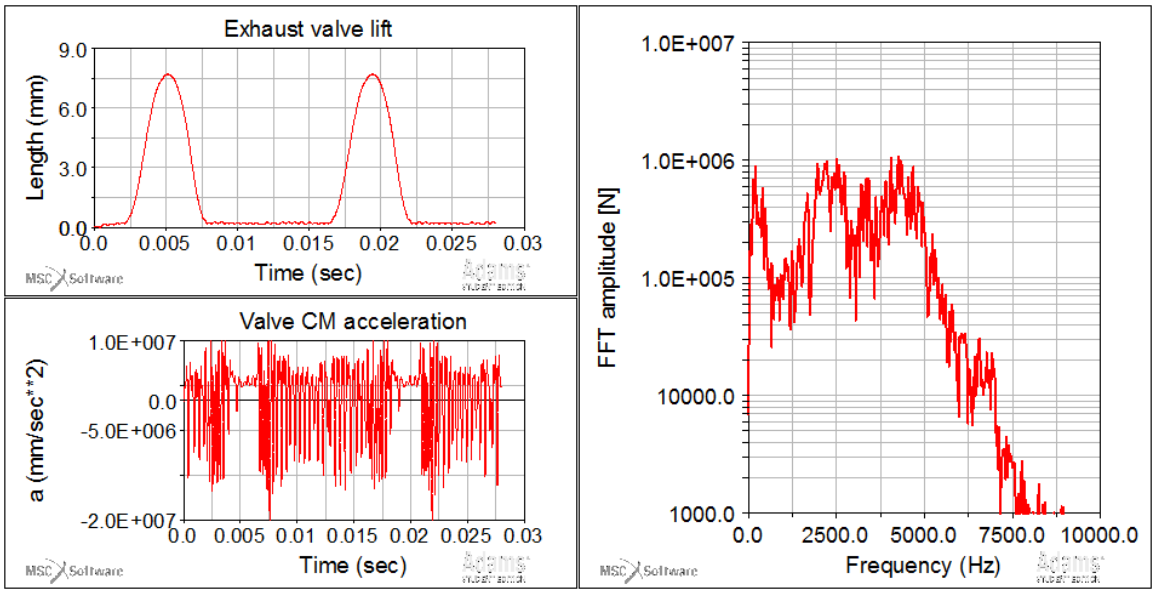

Figure 8.12.: [Adams_01] Exhaust valve's lift, acceleration in the centre of mass (filtered) and corresponding FFT

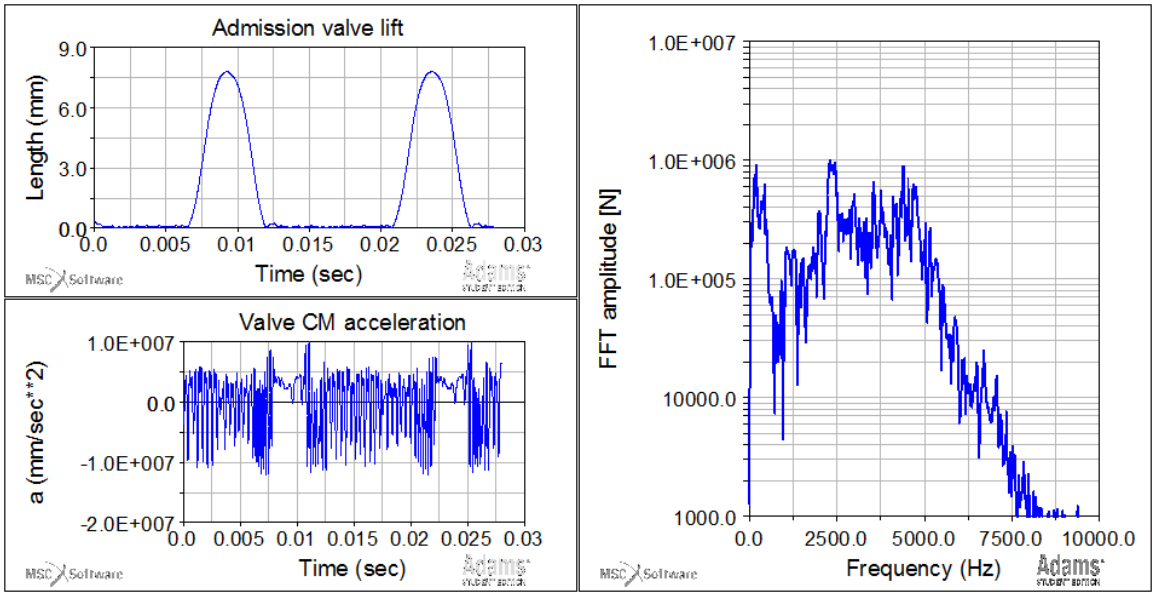

Figure 8.13.: [Adams_01] Admission valve's lift, acceleration in the centre of mass (filtered) and corresponding FFT

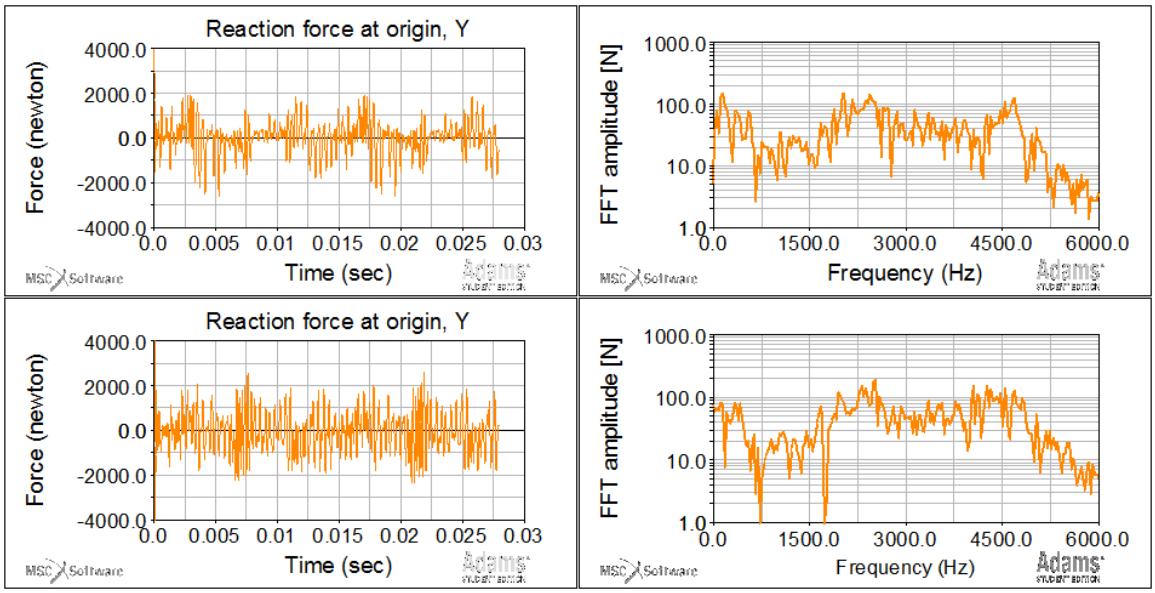

Figure 8.14.: [Adams_01] Reaction forces at origin point in the camshaft (filtered), with FFT plot

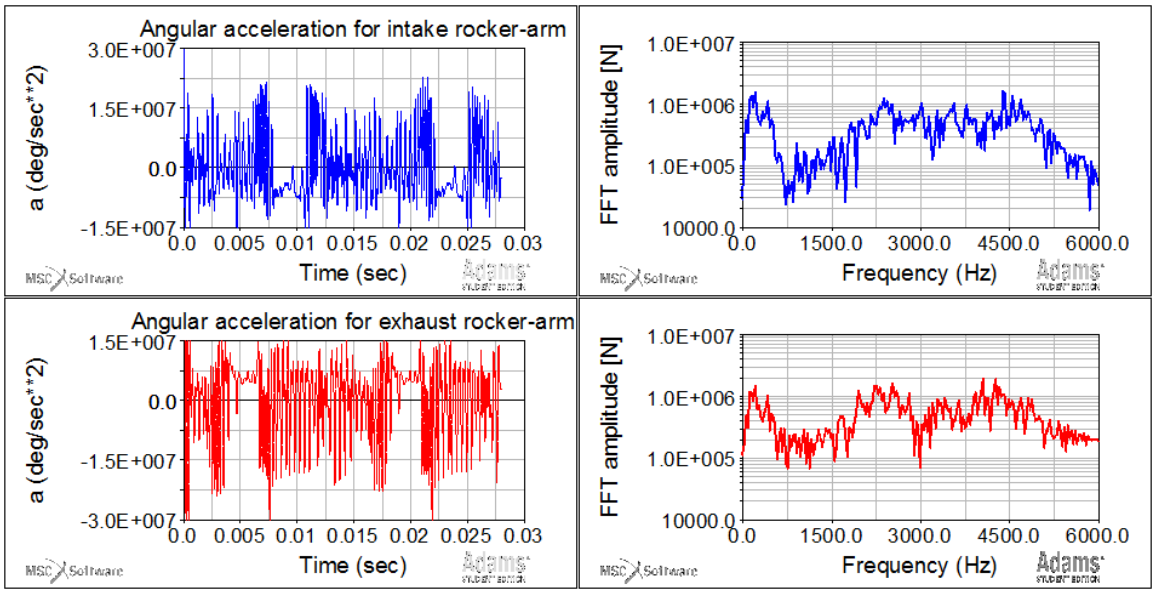

Figure 8.15.: [Adams_01] Angular acceleration of the rocker arms (filtered), with FFT plot

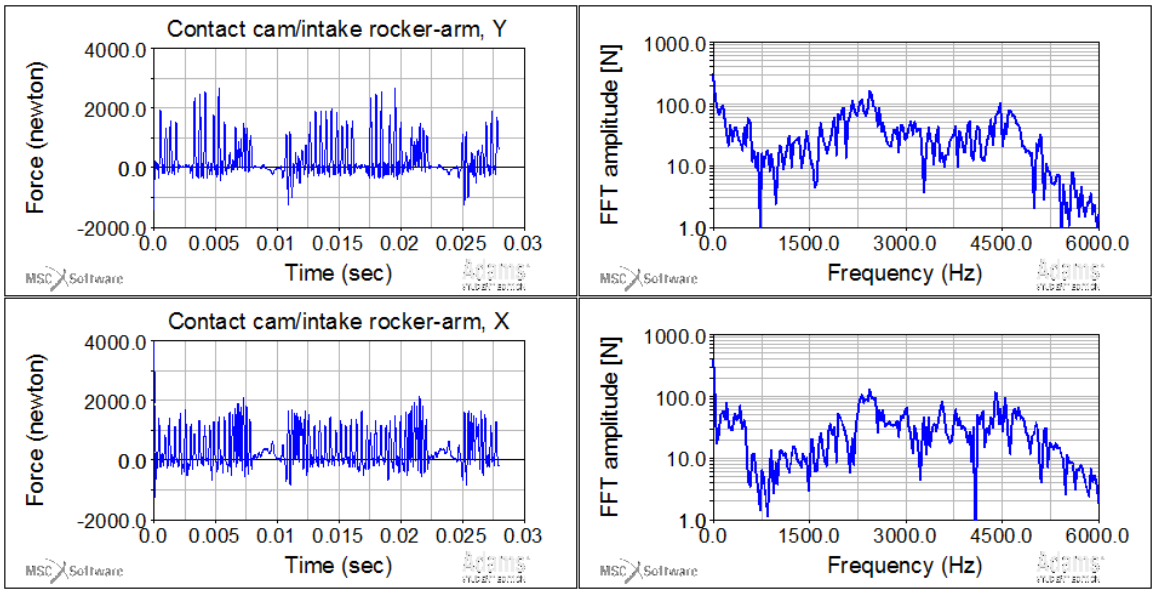

Figure 8.16.: [Adams_01] Contact forces between the camshaft and intake rocker-arm (filtered), with FFT plot

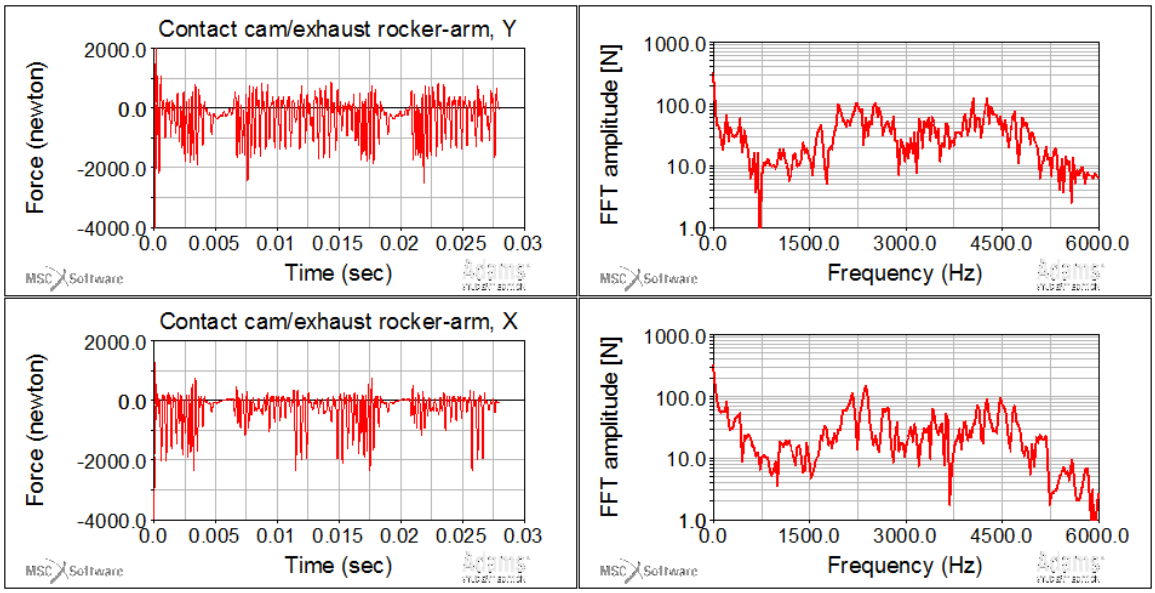

Figure 8.17.: [Adams_01] Contact forces between the camshaft and exhaust rocker-arm (filtered), with FFT plot

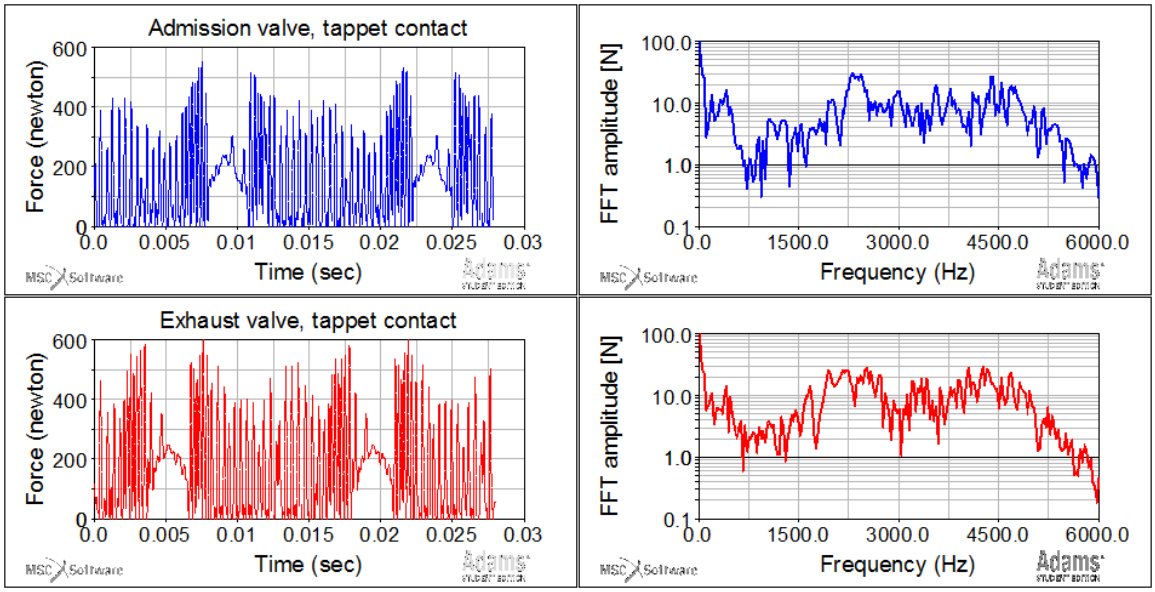

Figure 8.18.: [Adams_01] Contact forces in the tappets (filtered), with FFT plot

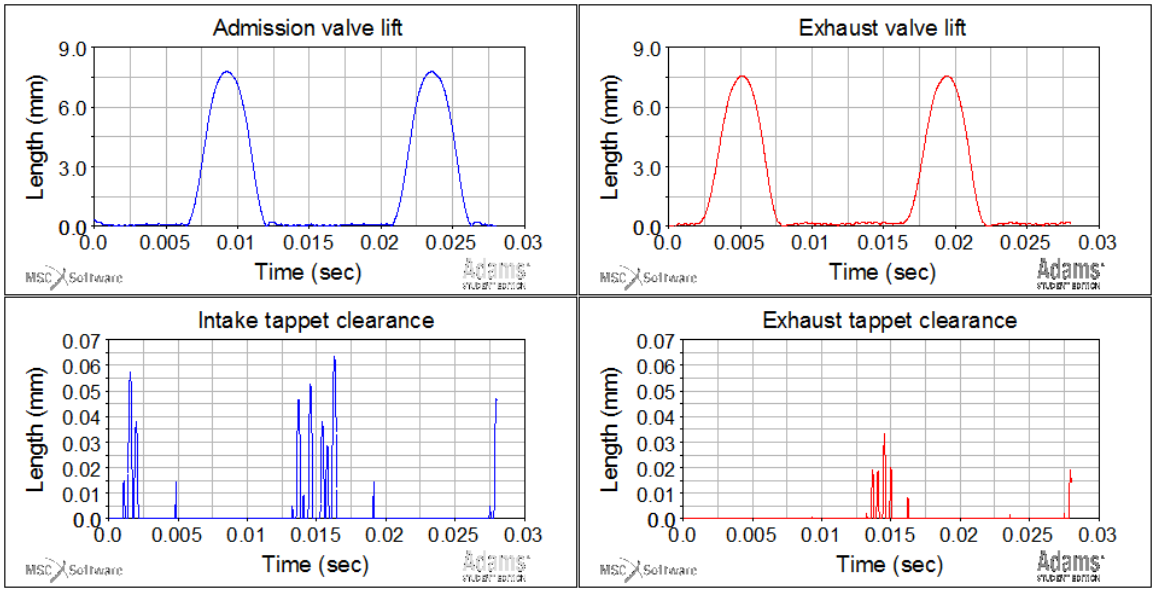

Figure 8.19.: [Adams_01] Clearance distance in the tappet contacts

8.2.3. Regime: 12000 rpm

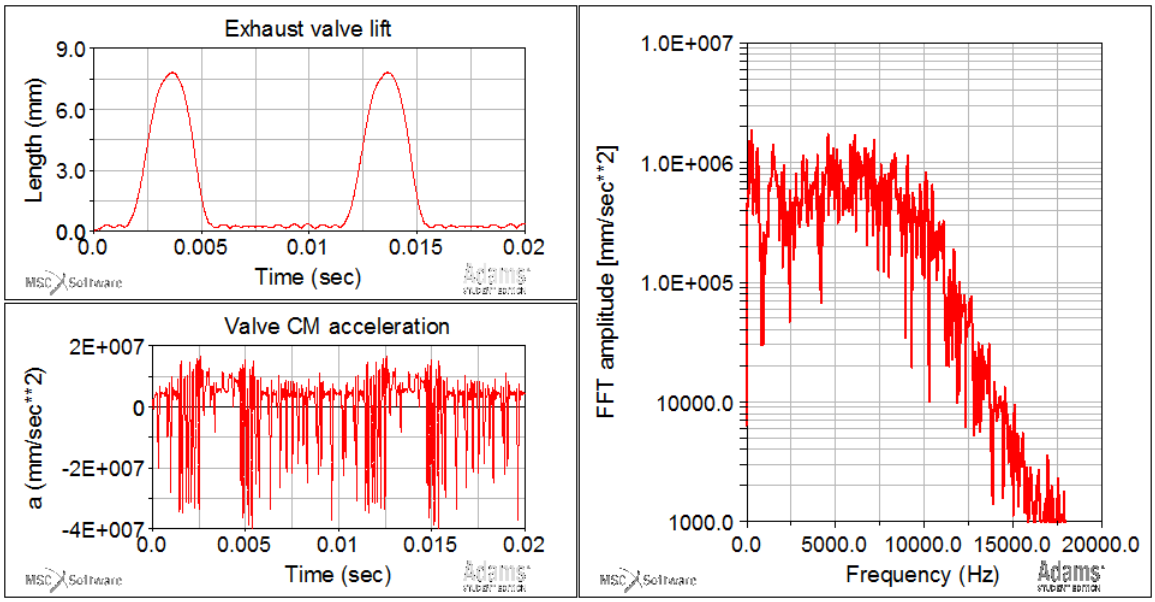

Figure 8.20.: [Adams_01_rpm120] Exhaust valve's lift, acceleration in the centre of mass (filtered) and corresponding FFT

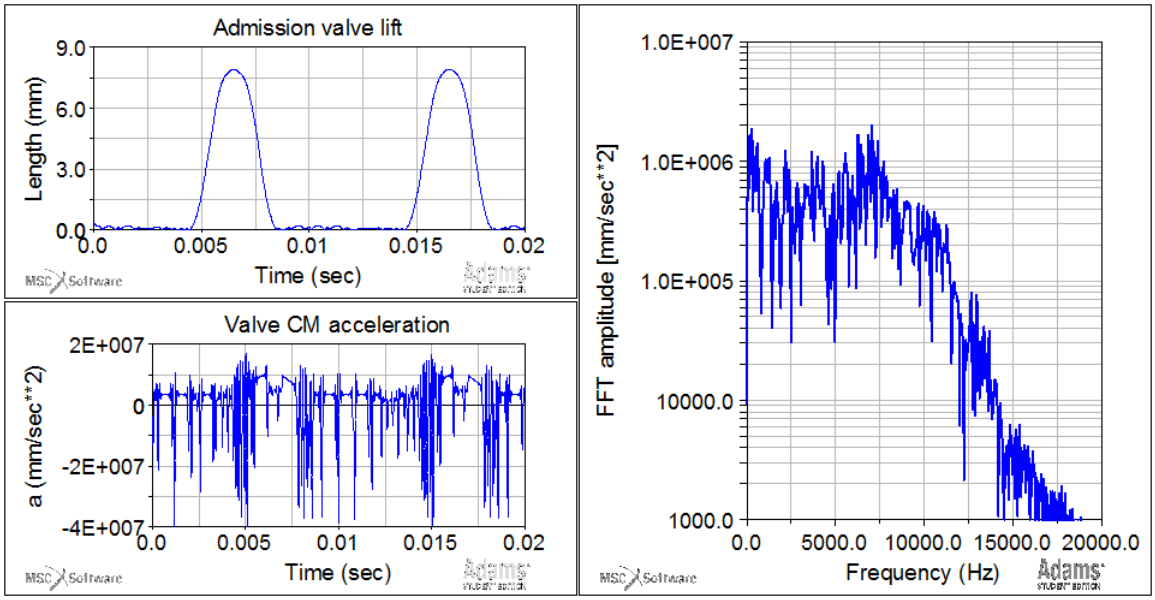

Figure 8.21.: [Adams_01_rpm120] Admission valve's lift, acceleration in the centre of mass (filtered) and corresponding FFT

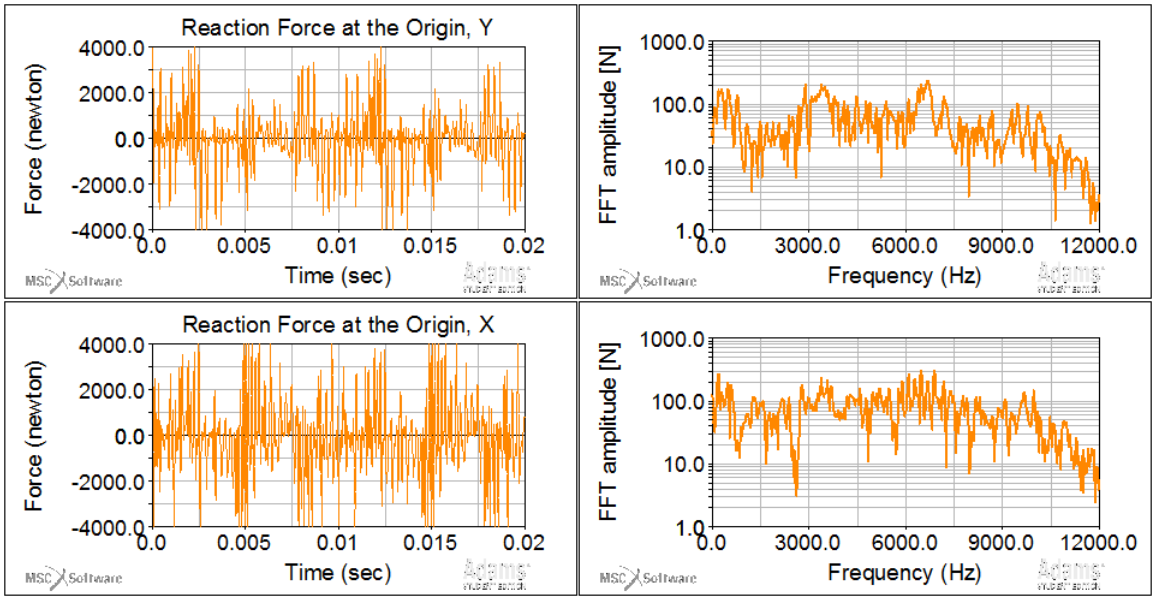

Figure 8.22.: [Adams_01_rpm120] Reaction forces at origin point in the camshaft (filtered), with FFT plot

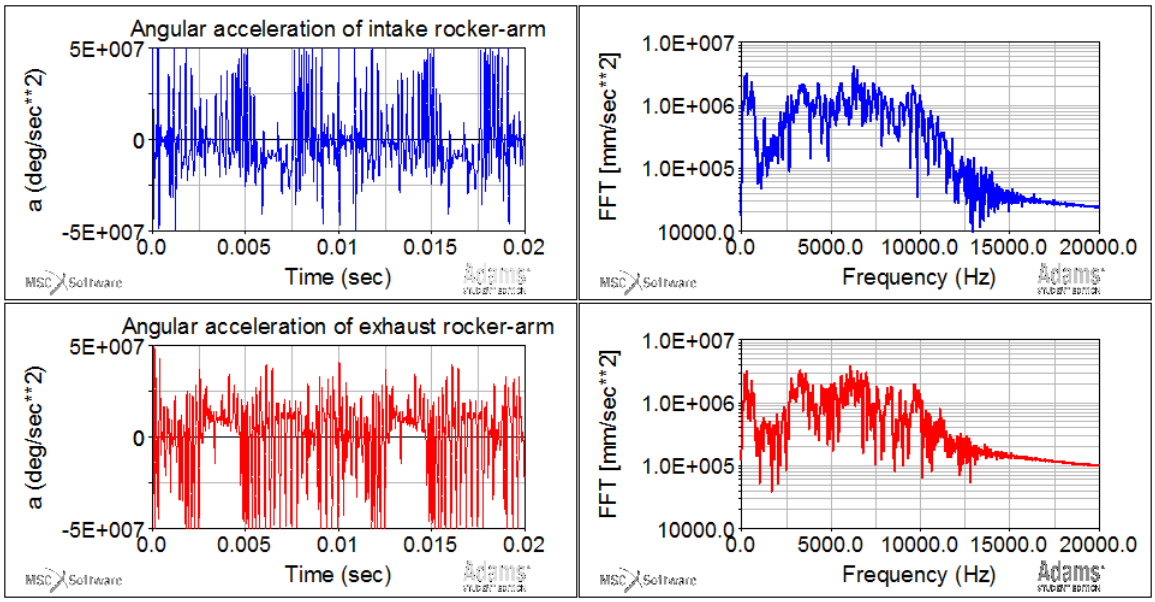

Figure 8.23.: [Adams_01_rpm120] Angular acceleration of the rocker arms (filtered), with FFT plot

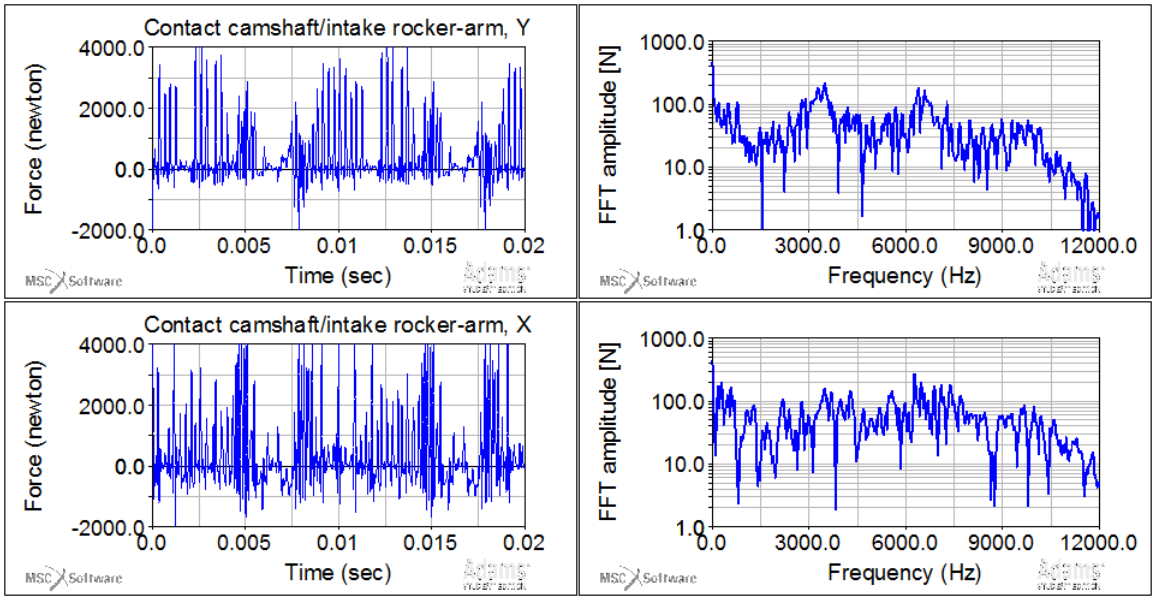

Figure 8.24.: [Adams_01_rpm120] Contact forces between the camshaft and intake rocker-arm (filtered), with FFT plot

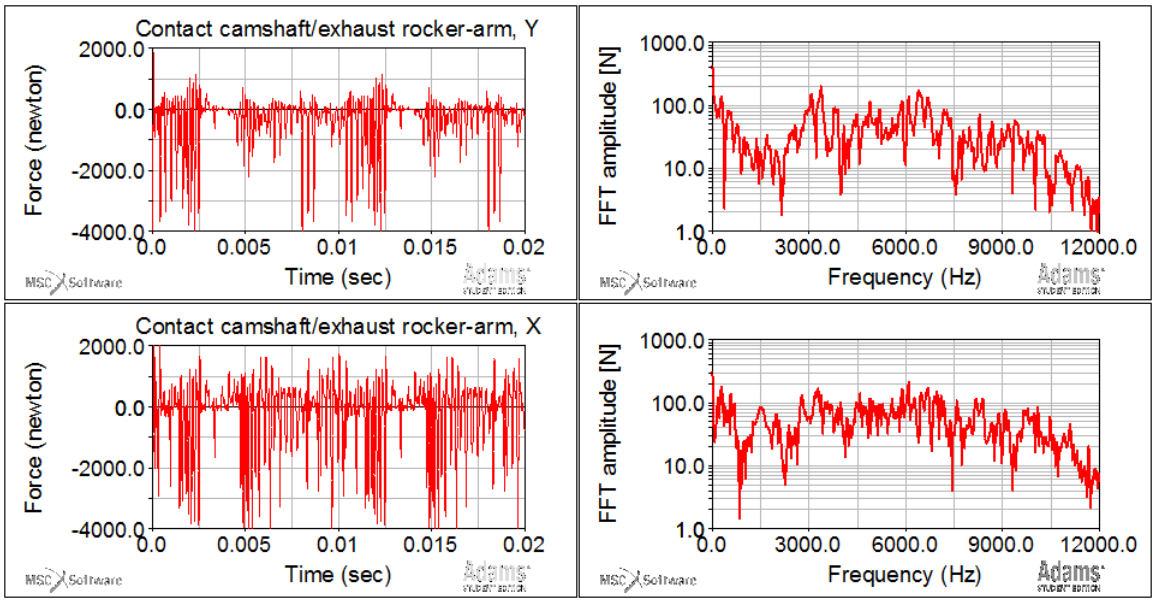

Figure 8.25.: [Adams_01_rpm120] Contact forces between the camshaft and exhaust rocker-arm (filtered), with FFT plot

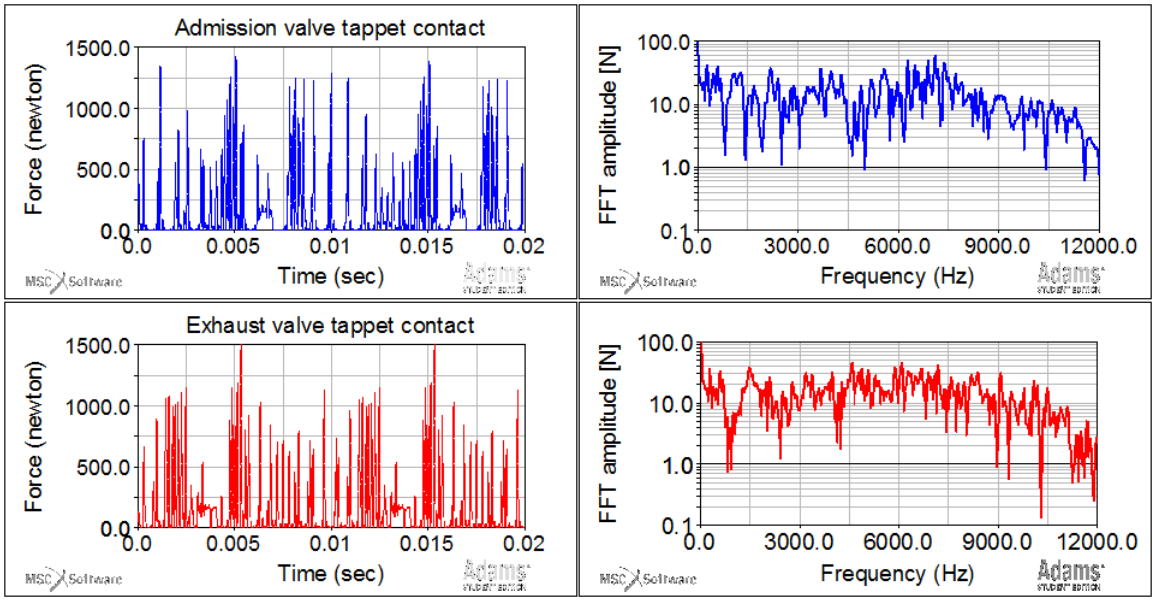

Figure 8.26.: [Adams_01_rpm120] Contact forces in the tappets (filtered), with FFT plot

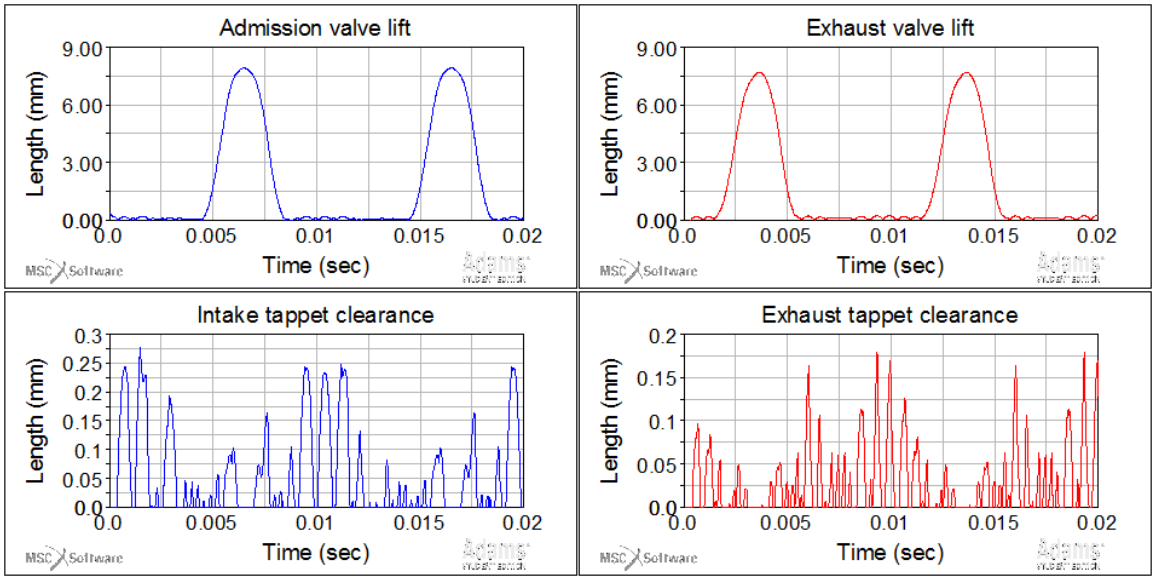

Figure 8.27.: [Adams_01_rpm120] Clearance distance in the tappet contacts

8.3. Discussion of results

8.3.1. Results related to the lift of the valves

Let's start to analyse the position of the valves during the 2 cycles by comparing the exhaust and admission lift profile with the clearance distances, in order to identify some bouncing effects.

At the lower speed of 5100 rpm, see Figures 8.4, 8.5 and 8.11, there are no significant events to report.

At 8400 rpm, see Figures 8.12, 8.13 and 8.19, it is possible to identify some minor effects in the exhaust valves immediately before the unseating movement. Whereas in the admission valves we can observe a more common phenomenon after the seating of the valves.

At the higher regime, 12000 rpm, see Figures 8.20, 8.21 and 8.27, the amplitude of the bouncing is noticeable in the lift profiles, reaching values around 0.2 to 0.3 mm. In the intake valves the bouncing effect happens during a bigger portion of the cycle than at lower speeds, as expected. In the exhaust valves, the bouncing occurs before and after the lift movement.

There is another possible cause for this phenomena, visible in clearance plots, in addition to the contact impulses and body accelerations. The body geometries were imported to MSC Adams^{TM} in Parasolid format which is characterized by having perfect surface continuity conditions. Although it was also said that the InnerCam^{TM} draw was received in .STEP format and interpreted by SolidWorks^{TM}. It is left opened the possibility of imperfections in the geometry surfaces and curves, due to format conversions, that may cause noise in the calculations.

In concern to the harmonic frequencies in the FFT plots, obtained from the acceleration in the centre of mass of the valves, it's possible to identify 3 or 4 bands from the frequency spectrum with bigger amplitudes at low/medium regimes. At 12000 rpm the number of important harmonics is higher, which may occur because other DoF's may be solicited.

Comparing the FFT results, in intake spectra the resonance frequencies usually appear as a single higher value, while in exhaust spectra the resonance frequencies appear in a band of multiple values. Those frequency band's values were identified zooming the plots using Adams Post/Processor tool, and can be consulted in the following tables.

This results leads to a conclusion that in this model, the resonance frequency values increase with the regime speed. It is also clear that at 12000 rpm there are

Engine speed: 5100rpm

Harmonic no	Intake freq. (Hz)	Exhaust freq. (Hz)
1	80 – 300	80 – 300
2	1480	1200; 1400; 1950
3	2680	2600; 2850; 3000
4	4280	4000 – 4250

Table 8.1.: Valve CM acceleration - resonance frequencies at 5100 rpm regime

Engine speed: 8400rpm

Harmonic no	Intake freq. (Hz)	Exhaust freq. (Hz)
1	200	200
2	2200 – 2500	2000; 2220; 2520
3	4350 – 4900	4050; 4260; 4700

Table 8.2.: Valve CM acceleration - resonance frequencies at 8400 rpm regime

Engine speed: 12000rpm

Harmonic no	Intake freq. (Hz)	Exhaust freq (Hz)
1	300 – 600	300 – 600
2	1500	1300
3	—	2200
4	4600	3700 – 4300
5	—	5200
6	6100	6300
7	7200	7100

Table 8.3.: Valve CM acceleration - resonance frequencies at 12000 rpm regime

more quantity of excited harmonics.

8.3.2. Analysis of other results

Contact forces between camshaft and rocker-arms

Engine speed: 5100rpm

Harmonic no	Intake freq. (Hz)	Exhaust freq. (Hz)
1	0	0
2	1500	1300; 1500
3	2720	2720
4	4210	4160

Table 8.4.: Contact force between camshaft and rocker arms (Y component) - resonance frequencies at 5100 rpm regime

Engine speed: 8400rpm

Harmonic no	Intake freq. (Hz)	Exhaust freq. (Hz)
1	0	0
2	2440	1900; 2200; 2500
3	4450	4050; 4280

Table 8.5.: Contact force between camshaft and rocker arms (Y component) - resonance frequencies at 8400 rpm regime

Engine speed: 12000rpm

Harmonic no	Intake freq. (Hz)	Exhaust freq (Hz)
1	0	0
2	$300 - 800$	1300
3	$3300 - 3500$	$3070 - 4420$
4	$6350 - 6600$	$6100 - 6700$

Table 8.6.: Contact force between camshaft and rocker arms (Y component) - resonance frequencies at 12000 rpm regime

Engine speed: 5100rpm

Harmonic no	Intake freq. (Hz)	Exhaust freq. (Hz)
1	0	0
2	1500	1180; 1300; 1560
3	2660 – 2820	2600; 2850; 3000
4	4290	4040; 4160; 4480

Table 8.7.: Contact force between camshaft and rocker arms (X component) - resonance frequencies at 5100 rpm regime

Engine speed: 8400rpm

Harmonic no	Intake freq. (Hz)	Exhaust freq. (Hz)
1	0	0
2	2250 – 2530	2160; 400
3	4380; 4550	4260; 4490

Table 8.8.: Contact force between camshaft and rocker arms (X component) - resonance frequencies at 8400 rpm regime

Engine speed: 12000rpm

Harmonic no	Intake freq. (Hz)	Exhaust freq (Hz)
1	0	0
2	300 – 600	1300
3	3500 – 4300	3270
4	5500 – 5600	5580
5	6300 – 7350	6050

Table 8.9.: Contact force between camshaft and rocker arms (X component) - resonance frequencies at 12000 rpm regime

Contact forces in the tappets

Engine speed: 5100rpm

Harmonic no	Intake freq. (Hz)	Exhaust freq. (Hz)
1	0	0
2	1480	$1190 - 1570$
3	2670; 2800	2560
4	4210	$4000 - 4250$

Table 8.10.: Contact force in the tappets - resonance frequencies at 5100 rpm regime

Engine speed: 8400rpm

Harmonic no	Intake freq. (Hz)	Exhaust freq. (Hz)
1	0	0
2	430	430
3	$2280 - 2420$	1900; 2500
4	4400	4050; 4250

Table 8.11.: Contact force in the tappets - resonance frequencies at 8400 rpm regime

Engine speed: 12000rpm

Harmonic no	Intake freq. (Hz)	Exhaust freq (Hz)
1	0	0
2	$300 - 600$	$300 - 600$
3	$1060 - 1300$	1500
4	2200	—
5	$3680 - 4300$	$3200 - 4000$
6	5550	4600
7	$6250 - 7050$	6100

Table 8.12.: Contact force in the tappets - resonance frequencies at 12000 rpm regime

Angular acceleration of the rocker arms

Engine speed: 5100rpm

Harmonic no	Intake freq. (Hz)	Exhaust freq. (Hz)
1	80 – 260	80 – 260
2	1480	1200; 1350; 1560
3	2680	2600; 3020
4	4300	4160

Table 8.13.: Angular acceleration of the rocker-arms - resonance frequencies at 5100 rpm regime

Engine speed: 8400rpm

Harmonic no	Intake freq. (Hz)	Exhaust freq. (Hz)
1	120 – 420	120 – 420
2	2320 – 2530	1950; 2250; 2520
3	4400; 4556; 4700	4060; 4270

Table 8.14.: Angular acceleration of the rocker-arms - resonance frequencies at 8400 rpm regime

Engine speed: 12000rpm

Harmonic no	Intake freq. (Hz)	Exhaust freq (Hz)
1	190 – 600	190 – 600
2	3300 – 3500	3200 – 3600
3	55000 – 5600	—
4	6280 – 6500	6100
5	9600	9200

Table 8.15.: Angular acceleration of the rocker-arms - resonance frequencies at 12000 rpm regime

8.3.3. Interpretation of results

Generally, comparing the results from the different speeds, its evident that at any speed there are no considerable detachment events occurring in the lift of the valves. The amplitude of the accelerations and forces increase with the speed of the camshaft.

In relation to harmonics, we can highlight some results and comparisons:

- In plots related to contact forces, there is always a harmonic at *zero* Hz, which in this case is not related to rigid body movement (because the speed is not zero), but maybe associated with the pre-load of the springs;
- In acceleration FFTs, there is allways a first harmonic related to rigid body movement and the quantity of acceleration of the bodies, which analytical results can be found in previous chapters;
- It is possible to find harmonics around the same values in every plots. For instance, at 2550 rpm in the camshaft, for the intake sub-system the harmonic frequencies are around 1500 Hz, 2700 Hz and 4250Hz;
- For the exhaust sub-system, at 2550 rpm in the camshaft, the harmonic frequencies appear within an interval with average values around 1400 Hz, 2700 Hz and 4160 Hz;
- At 4200 rpm in the camshaft, for the intake sub-system the harmonic frequencies are around 2400 Hz and 4400 Hz;
- For the exhaust sub-system, at 4200 rpm in the camshaft, the harmonic frequencies appear within an interval with average values around 2250 Hz and 4250 Hz;
- At the highest speed of 6000 rpm in the camshaft, some common values for the intake sub-system are 3500 Hz or 6500 Hz, while in exhaust sub-system we find 1300 Hz, 6100 Hz and the interval between 3200 and 3700 Hz.

The vibration of any DoF depends on two parameters: stiffness and mass. The equivalent mass is always definite positive and depends on the mass of the bodies. On the other hand, the equivalent stiffness is definite semi-positive and, in this model, only depends on the contact forces properties. That way, different contacts will lead to different harmonic responses.

The most important harmonic frequencies in FFT plots for each parameters, tend to have higher values as regime increase (in other words, the peaks move to the right). This can be explained because the contact forces are defined with a Force Exponent, e, equal to 2.2, which means that the stiffness of contact is not constant, depending on the penetration at each instant.

Looking at the quality of the plot's data, namely to the FFT ones, they are more unclear for the last simulation at 6000 rpm at the camshaft. It's possible to identify more harmonic frequencies being excited, namely at speeds near to 10000 Hz (for that reason the domain of the plots had to be necessary bigger than for the other speeds).

8.4. Camshaft's MSC Adams analysis

Contact forces in ZZ direction

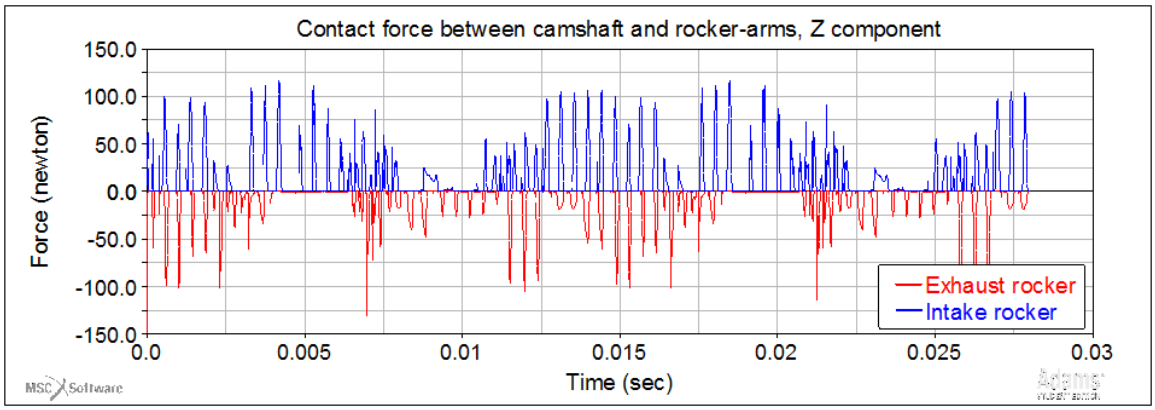

Figure 8.28.: [Adams_01] Contact forces between the camshaft and rocker arms, along the Z direction (no filter)

In Figures 8.6, 8.14 and 8.22 we could see the forces applied to the camshaft in the contacts within the rocker arms along the axis perpendicular to rotation direction. Till now I've only analysed results excluding any force effects along zz direction, as mentioned in Chapter 5.

Using the potentialities of MSC Adams^{TM}, it was possible to check if the asymmetry of the rocker arms has importance in the resultant forces of contact in the camshaft. The conclusions can be taken, analysing Figure 8.28.

8.4.1. Camshaft's misalignment influence

In order to understand the importance of the displacement between the centre of rotation and centre of mass of the camshaft, an analysis was ran only with this component rotating at the same speed of 4200rpm. The resultant forces at the center of rotation were obtained.

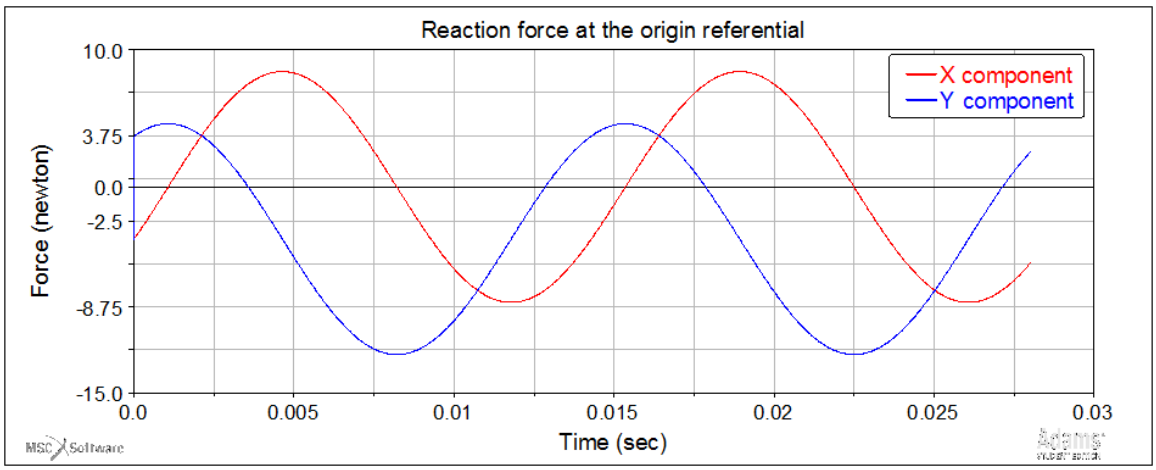

Figure 8.29.: Reaction force at the centre of rotation for the camshaft isolated system

It is possible to conclude that the camshaft shall be enough equilibrated, because the amplitude of the forces resulting from the centre of mass displacement are not so important when compared to the amplitude of the other forces like contacts or springs, and so on. Although, a future analysis should be done considering the flexibility of this body part.

9. Conclusions and future work

9.1. Conclusions

The results obtained with the different analytical models developed during this work lead to the following conclusions:

- The new analytical kinematic model reinforced the results obtained in previous work and the Fourier approximation for the lift curve showed good behaviour till first derivative, in the opposite to acceleration and jerk plots that were affected fictitious harmonics;
- In the dynamic analysis, it was found that the results were considerably affected by high frequency harmonics from the Fourier approximation, meaning that the polynomial approximations made before have better results in this calculations;
- The pre-load of the springs are not enough to avoid the 'negative contact force' between the rocker arms and the camshaft (in other words, to avoid the rocker-arms bouncing between inner and outer camshaft surfaces);
- because of the large diameter of the cam inner profile the average value for the required torque in the camshaft is considerably high (around 1.45 $N.m$);
- The vibration analysis to the valve-spring system showed that the InnerCam^{TM} is ready to work till 17700 rpm regime keeping the original designed lift for the valves, and guaranteeing good thermodynamic conditions to the combustion cycle;
- The natural frequencies of vibration for the intake and exhaust sub-system were identified in the range of 2217 to 3428 Hz;
- The most important harmonic identified by FRF was the *zero* one, corresponding to the rigid body movement.

Also during this thesis there are presented the results obtained with the MSC Adams^{TM} software, considering different properties in the model, and different speeds. In order to help some future works, I present also some conclusions in concern to future analysis with this software:

- First off all, some limitations in the student version didn't let me to introduce correctly some important properties to the model, like flexibility or influence of other components that were not part of the given draw;

- The values of damping coefficients should be studied in the real prototype (namely in bushings), because it is proved that this parameter highly affects the behaviour of the model;

- The rigidity of the body-parts used in the model didn't allow me to compare the results to the analytical vibration models in what concern for example to natural frequencies of vibration;

- The contact forces introduced to the model, as a way to define geometrical interference between bodies, may not be very accurate because some parameters are chosen from experience and common sense, and others depend on the variable geometry of contact (instead, if the components can be transformed to flexible bodies, this parameters are calculated automatically).

In concern to the results obtained from the simulations in MSC Adams^{TM}, with the defined model, at different speeds, we can present the following assumptions:

- The lift movement of the valves occurs properly, as it was expected from analytical vibrational valve/spring system;

- There are important harmonics being excited in frequencies much higher than the rotation speed of the camshaft;

- The contact forces in the camshaft are very impulsive and showed that in specific points of the cycle the contact occurs against the outer surface of the camshaft, suggesting that there is high frequency vibration harmonics acting in this contact, which may lead to wear problems;

- The non axis-symmetry of the rocker arms may cause inconvenient contact interactions between rocker-arms and camshaft, justifying the wear shapes that appeared in the tested camshaft in previous works;

- The frequency of the harmonics identified by FFTs should have origin in contact stiffness (which is not constant) and, maybe for that reason, are variable with the speed.

9.2. Future work

In order to produce accurate and correct conclusions, some changes should be made to the model in software MSC Adams^{TM}, and that model should be validated by instrumenting a prototype of the InnerCam^{TM}. The suggestions I leave for the computer model are:

- A professional license of MSC Adams should be used, in order to create flexible parts of some components of the InnerCam^{TM}, namely to camshaft, rocker arms, and valves;
- A more complete and detailed draw of the InnerCam^{TM} is needed, including more body parts as bushings, valve seats, camshaft's supporting rollers and rocker-arm's supporting pins;
- It is important to take some precautions when converting formats between different software to guarantee the continuity of the surfaces (the PARASOLID format is recomented).

In what concerns to the instrumentation of the prototype I also leave some suggestions:

- The purpose of this test would be to correctly validate the system, so the InnerCam^{TM}'s camshaft can be actuated by an electric engine;
- One important measurement would be the acceleration of the valves (which is easy to instrument);
- Those measured results could be directly compared to the computer model ones.

At last, taking in consideration the application of the InnerCam^{TM} system, which is a 250cc 4-stroke engine to run a motorcycle, and since it was found that an important weakness of the engine was the petrol pump, it would be interesting to study the dynamic behaviour of the original *OHC* valve train system to find out what is its limit regime (whose information and models about similar systems can be easily find in literature). With that study AJP Motos S.A. would be able to make an informed decision about the interest of applying considerable resources in developing a concept that may not be so significant to the performance of the PR5^{TM} model.

Bibliography

[1] C. F. A. Afonso, Termodinâmica para Engenharia, 1st Edition, Vol. Chapter 10, FEUP, 2012.

[2] C. M. Coutinho Tavares de Pinho, Apontamentos de Sistemas Térmicos (2014).

[3] A. a. Schaeffler, Valve train components: Technology, failure diagnosis.

[4] Ducati, History of desmodromic timing, (2015-05-22).
URL http://ducati.com/history/editorials/history_of_desmodromic_timing/index.do

[5] Unicam valve train, (01-06-2015).
URL http://www.scigacz.pl/zdjecia/gallery/test_motocykli/Honda_Crosstourer_potencjal_perfekcja_luz/Unicam-valve-train.jpg.html

[6] Harley engine history update, (01-06-2015).
URL https://nwhog.wordpress.com/2009/05/08/harley-engine-history-update/

[7] Z. Power, Motorcycle product engines - nc250, (07/04/2015).
URL http://www.zse.cc/productsdetail.aspx?ProductsCateId=43&ProductsID=386&CateID=43

[8] J. A. Nogueira, Dynamic Behavior of a Valve Train System, Master Thesis, Faculdade de Engenharia da Universidade do Porto (July, 2014).

[9] J. Giesbers, Contact Mechanics in MSC Adams, University of Twentee (July, 2012).

[10] Butterworth filter design, (26-05-2015).
URL http://www.electronics-tutorials.ws/filter/filter_8.html

[11] C. Ferreira, Dynamic and tribological analysis of a cam / rocker arm / valve mechanism, used in a four stroke engine, controlling valves opening and closing, Master Thesis, Faculdade de Engenharia da Universidade do Porto (July, 2013).

[12] D. Vizard, Theory and Practice of Cylinder Head Modifications, Speed and Sports Publications Ltd., Acorn House, Victoria Road, London, W.3., 1971.

[13] J. Dias Rodrigues, Apontamentos de Vibrações de Sistemas Mecânicos, Faculdade de Engenharia da Universidade do Porto (2014).

[14] J. E. Shigley, J. J. Uicker, Theory of Machines and Mechanisms, McGraw-Hill, 1980.

[15] T. R. Sandin, The jerk, American Society of Physics Teachers (1990), Tom R. Sandin, The jerk, American Society of Physics Teachers (1990).

[16] S. Gragert, What is the term used for the third derivative of position?, (13/06/2015).
URL `http://math.ucr.edu/home/baez/physics/General/jerk.html`

[17] Y. Zhang, R. Li, L. Xiao, J. Yang, Study on dynamic simulation of cam mechanism based on pro/e and adams (2012).

[18] V. A. Rainer Luhrig, Calculation of effects of free inertial forces and torques of the valve train to the engine vibration of a w12 from volkswagen (2001).

[19] J. H. O. Seabra, Mecânica do Contacto Hertziano, Faculdade de Engenharia da Universidade do Porto, 2nd Edition (2003).

[20] J. Guo, W. Zhang, D. Zou, Investigation of dynamic characteristics of a valve train system (2011).

[21] J. Guo, W. Zhang, X. Zhang, Y. Cao, Dynamic and exciting analysis with modal characteristics for valve train using a flexible model (2014).

[22] A. Raviola, M. Troncossi, G. Dalpiaz, A. Carlini, Elastodynamic analysis of the desmodromic valve train of a racing motorbike engine by mmeans of a combined lumped/finite element method (2006).

[23] Z. Zhang, L. Xu, P. Flores, H. M. Lankarani, A kriging model for dynamics of mechanical systems with revolute joint clearances (2014) vol. 9 (031013-1).

A. Alloy steel $34CrNiMo6$

A.1. Technical sheet

RAMADA
F. RAMADA, AÇOS E INDÚSTRIAS, S.A.

FICHA TÉCNICA DO AÇO

Marca: FR3

Cor: Laranja

Designação: Aço de construção Ligado

Cópia Não Controlada

1 ⇒ QUALIDADE E NORMAS EQUIVALENTES

Num. Do Material	EURONORM	AISI	DIN	AFNOR
1.6582	34 CrNiMo 6	4337	34 CrNiMo 6	35NCD6

2 ⇒ ESTADO DE FORNECIMENTO:

Temperado e Revenido

3 ⇒ CARACTERÍSTICAS MECÂNICAS:

	Rm (MPa)	Rp0,2 (MPa)	% A (l_0=5d_0)
Máximo	1400	-	-
Mínimo	700	490	9

4 ⇒ COMPOSIÇÃO QUÍMICA

Elemento Químico (%)	C	Si	Mn	Cr	Mo	Ni	P	S
Máximo	0,38	0,40	0,80	1,70	0,30	1,70	0,035	0,035
Mínimo	0,30	-	0,50	1,30	0,15	1,30	-	-

5 ⇒ CERTIFICADOS AÇOS (segundo a norma EN 10204:2004)

2.1- Certificado de conformidade	⊙
2.2- Relatório de ensaio	⊙
3.1- Certificado de inspecção (+)	⊙

(+) Em casos especiais quando previamente acordado

Elaborado por: Paulo Duarte | Aprovado Por: José Oliveira | Revisão: 07 | Data de emissão: 17-12-2008

D1008-0

A.2. Thermal treatment applied

RAMADA
F. RAMADA, AÇOS E INDÚSTRIAS, S.A.

FICHA TÉCNICA DO AÇO

Marca: FR3

Cor: Laranja

Designação: Aço de construção Ligado

Cópia Não Controlada

1 ⇒ QUALIDADE E NORMAS EQUIVALENTES

Num. Do Material	EURONORM	AISI	DIN	AFNOR
1.6582	34 CrNiMo 6	4337	34 CrNiMo 6	35NCD6

2 ⇒ ESTADO DE FORNECIMENTO:

Temperado e Revenido

3 ⇒ CARACTERÍSTICAS MECÂNICAS:

	Rm (MPa)	Rp0,2 (MPa)	% A (l_0=5d_0)
Máximo	1400	-	-
Mínimo	700	490	9

4 ⇒ COMPOSIÇÃO QUÍMICA

Elemento Químico (%)	C	Si	Mn	Cr	Mo	Ni	P	S
Máximo	0,38	0,40	0,80	1,70	0,30	1,70	0,035	0,035
Mínimo	0,30	-	0,50	1,30	0,15	1,30	-	-

5 ⇒ CERTIFICADOS AÇOS (segundo a norma EN 10204:2004)

2.1- Certificado de conformidade	⊙
2.2- Relatório de ensaio	⊙
3.1- Certificado de inspecção (+)	⊙

(+) Em casos especiais quando previamente acordado

Elaborado por: Paulo Duarte | Aprovado Por: José Oliveira | Revisão: 07 | Data de emissão: 17-12-2008

D1008-0

B. Mass Properties, SolidWorks™

B.1. Body 1 - Camshaft

Mass properties of Camshaft_new
Configuration: Default
Coordinate system: -- default --

Mass = 0.387 kilograms
Volume = 64716.671 cubic millimeters
Surface area = 26666.526 square millimeters

Center of mass: (millimeters)
X = 0.104
Y = 56.948
Z = 0.004

Principal axes of inertia and principal moments of inertia: (kilograms * square millimeters)
Taken at the center of mass.

Ix = (-0.006, 1.000, -0.006)	Px = 116.334
Iy = (-0.880, -0.002, 0.476)	Py = 273.068
Iz = (0.476, 0.008, 0.880)	Pz = 273.781

Moments of inertia: (kilograms * square millimeters)
Taken at the center of mass and aligned with the output coordinate system.

Lxx = 273.224	Lxy = -0.904	Lxz = -0.294
Lyx = -0.904	Lyy = 116.344	Lyz = -0.868
Lzx = -0.294	Lzy = -0.868	Lzz = 273.615

Moments of inertia: (kilograms * square millimeters)
Taken at the output coordinate system.

Ixx = 1527.596	Ixy = 1.378	Ixz = -0.293
Iyx = 1.378	Iyy = 116.348	Iyz = -0.773
Izx = -0.293	Izy = -0.773	Izz = 1527.992

Figure B.1.: Inertia and mass properties of the camshaft

B.2. Body 2 - Exhaust rocker-arm

Mass properties of Exhaust_rocker
Configuration: Default
Coordinate system: -- default --

Mass = 0.127 kilograms
Volume = 16279.379 cubic millimeters
Surface area = 9636.892 square millimeters

Center of mass: (millimeters)
X = -7.311
Y = 10.725
Z = 22.115

Principal axes of inertia and principal moments of inertia: (kilograms * square millimeters)
Taken at the center of mass.

Ix = (-0.335, -0.588, 0.736)	Px = 25.263
Iy = (0.728, -0.658, -0.194)	Py = 56.516
Iz = (0.598, 0.470, 0.649)	Pz = 62.189

Moments of inertia: (kilograms * square millimeters)
Taken at the center of mass and aligned with the output coordinate system.

Lxx = 55.032	Lxy = 4.571	Lxz = -9.915
Lyx = 4.571	Lyy = 46.951	Lyz = -15.259
Lzx = -9.915	Lzy = -15.259	Lzz = 41.984

Moments of inertia: (kilograms * square millimeters)
Taken at the output coordinate system.

Ixx = 131.741	Ixy = -5.385	Ixz = -30.445
Iyx = -5.385	Iyy = 115.842	Iyz = 14.857
Izx = -30.445	Izy = 14.857	Izz = 63.375

Figure B.2.: Inertia and mass properties of the exhaust rocker-arm

B.3. Body 3 - Intake rocker-arm

Mass properties of Intake_rocker
Configuration: Default
Coordinate system: -- default --

Mass = 0.127 kilograms
Volume = 16337.947 cubic millimeters
Surface area = 9188.967 square millimeters

Center of mass: (millimeters)
X = -7.333
Y = 10.869
Z = 30.184

Principal axes of inertia and principal moments of inertia: (kilograms * square millimeters)
Taken at the center of mass.

Ix = (0.159, 0.860, 0.485)	Px = 33.409
Iy = (-0.693, -0.252, 0.675)	Py = 40.838
Iz = (0.703, -0.443, 0.556)	Pz = 53.496

Moments of inertia: (kilograms * square millimeters)
Taken at the center of mass and aligned with the output coordinate system.

Lxx = 46.902	Lxy = 4.958	Lxz = -4.378
Lyx = 4.958	Lyy = 37.829	Lyz = 6.220
Lzx = -4.378	Lzy = 6.220	Lzz = 43.011

Moments of inertia: (kilograms * square millimeters)
Taken at the output coordinate system.

Ixx = 178.055	Ixy = -5.199	Ixz = -32.585
Iyx = -5.199	Iyy = 160.783	Iyz = 48.025
Izx = -32.585	Izy = 48.025	Izz = 64.918

Figure B.3.: Inertia and mass properties of the intake rocker-arm

B.4. Body 4 - Exhaust Valve

Mass properties of Exhaust_valve
Configuration: Default
Coordinate system: -- default --

Mass = 0.024 kilograms
Volume = 3136.218 cubic millimeters
Surface area = 2534.265 square millimeters

Center of mass: (millimeters)
X = -68.232
Y = 0.000
Z = 0.000

Principal axes of inertia and principal moments of inertia: (kilograms * square millimeters)
Taken at the center of mass.

Ix = (1.000, 0.000, 0.000)	Px = 0.631
Iy = (0.000, 0.000, -1.000)	Py = 26.174
Iz = (0.000, 1.000, 0.000)	Pz = 26.174

Moments of inertia: (kilograms * square millimeters)
Taken at the center of mass and aligned with the output coordinate system.

Lxx = 0.631	Lxy = 0.000	Lxz = 0.000
Lyx = 0.000	Lyy = 26.174	Lyz = 0.000
Lzx = 0.000	Lzy = 0.000	Lzz = 26.174

Moments of inertia: (kilograms * square millimeters)
Taken at the output coordinate system.

Ixx = 0.631	Ixy = 0.000	Ixz = 0.000
Iyx = 0.000	Iyy = 140.062	Iyz = 0.000
Izx = 0.000	Izy = 0.000	Izz = 140.062

Figure B.4.: Inertia and mass properties of the exhaust valve

B.5. Body 5 - Admission Valve

Mass properties of Admission_valve
Configuration: Default
Coordinate system: -- default --

Mass = 0.028 kilograms
Volume = 3530.488 cubic millimeters
Surface area = 2881.365 square millimeters

Center of mass: (millimeters)
X = -71.643
Y = 0.000
Z = 0.000

Principal axes of inertia and principal moments of inertia: (kilograms * square millimeters)
Taken at the center of mass.

Ix = (1.000, 0.000, 0.000)	Px = 1.121
Iy = (0.000, 0.000, -1.000)	Py = 28.970
Iz = (0.000, 1.000, 0.000)	Pz = 28.970

Moments of inertia: (kilograms * square millimeters)
Taken at the center of mass and aligned with the output coordinate system.

Lxx = 1.121	Lxy = 0.000	Lxz = 0.000
Lyx = 0.000	Lyy = 28.970	Lyz = 0.000
Lzx = 0.000	Lzy = 0.000	Lzz = 28.970

Moments of inertia: (kilograms * square millimeters)
Taken at the output coordinate system.

Ixx = 1.121	Ixy = 0.000	Ixz = 0.000
Iyx = 0.000	Iyy = 170.314	Iyz = 0.000
Izx = 0.000	Izy = 0.000	Izz = 170.314

Figure B.5.: Inertia and mass properties of the admission valve

C. FEA Analysis, exported from SolidWorks™

C.1. Body 2 - Exhaust rocker-arm

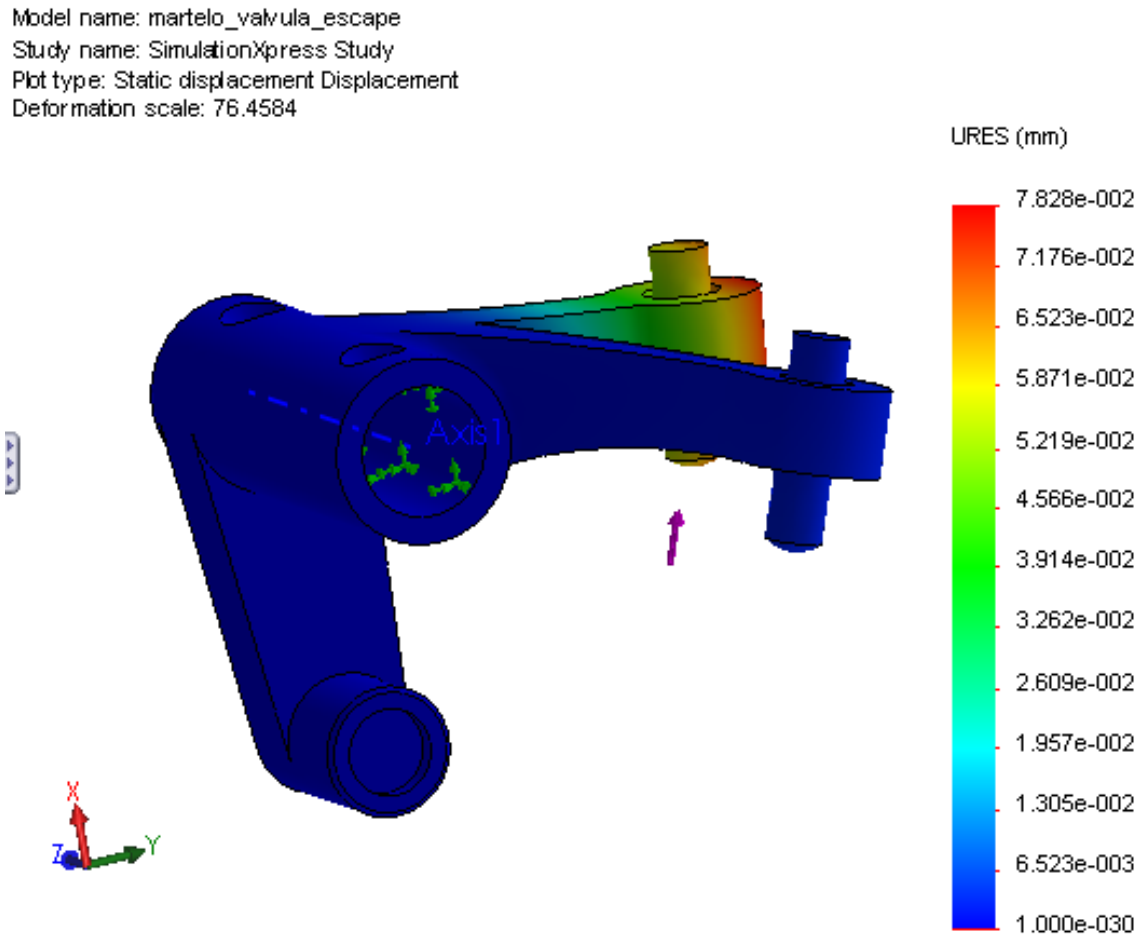

Figure C.1.: Displacement of the pins in relation to rotation center. The applied force has an amplitude of 1000 $/N$

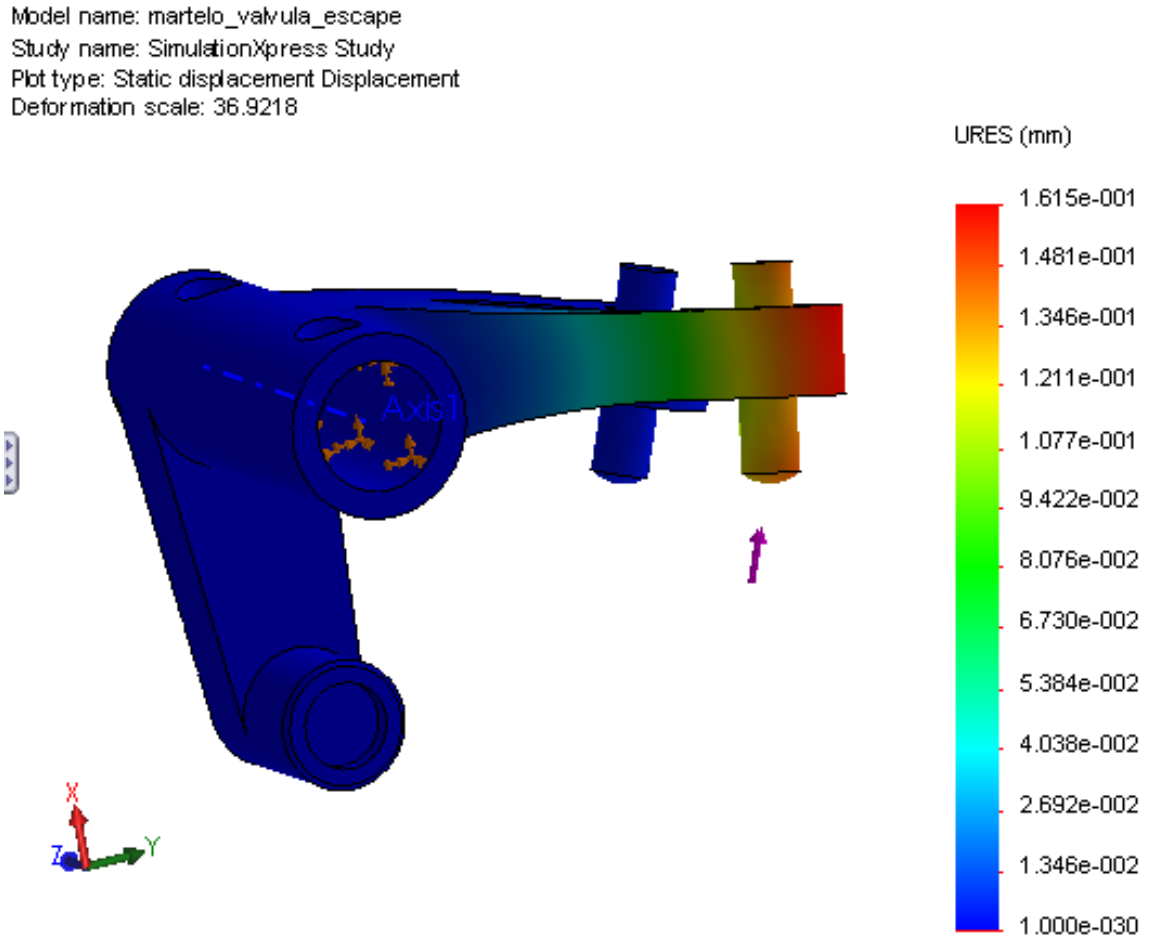

Figure C.2.: Displacement of the pins in relation to rotation center. The applied force has an amplitude of 1000 $/N$

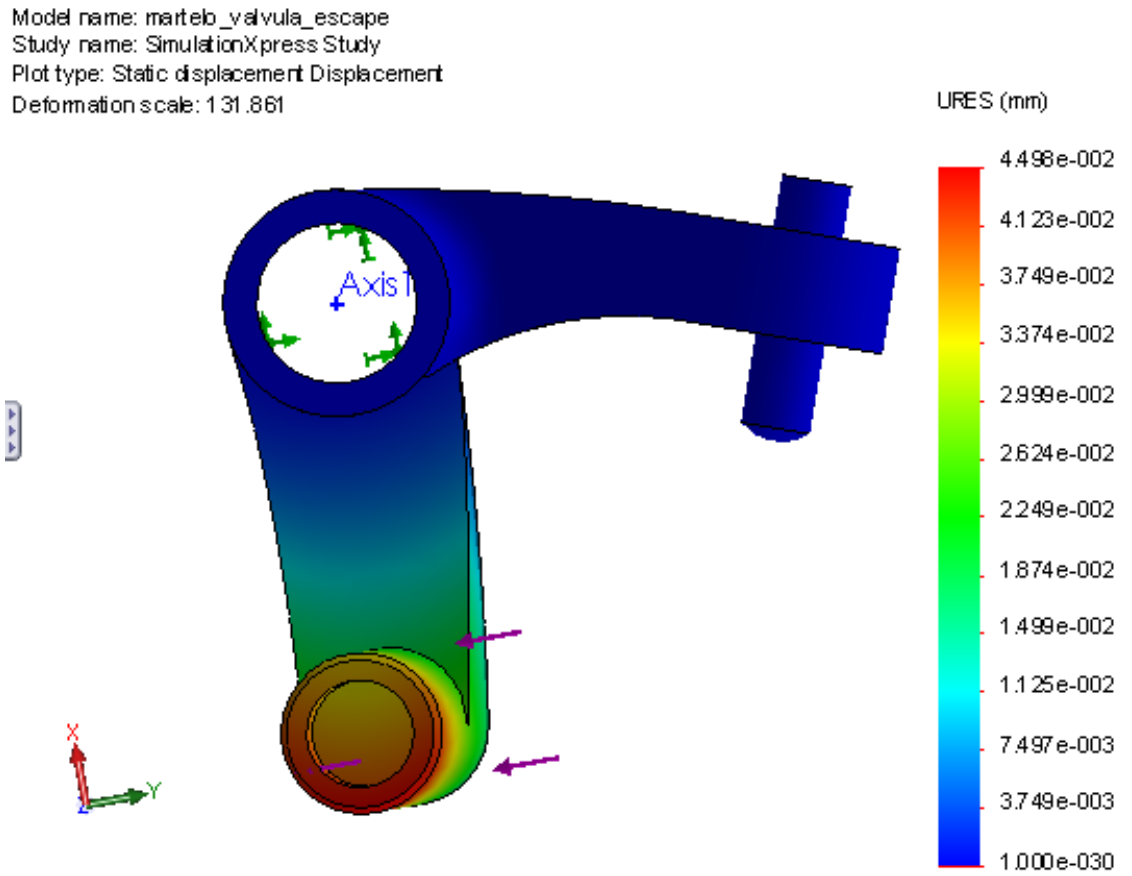

Figure C.3.: Displacement of the pins in relation to rotation center. The applied force has a total amplitude of 1000 $/N$

C.2. Body 3 - Intake rocker-arm

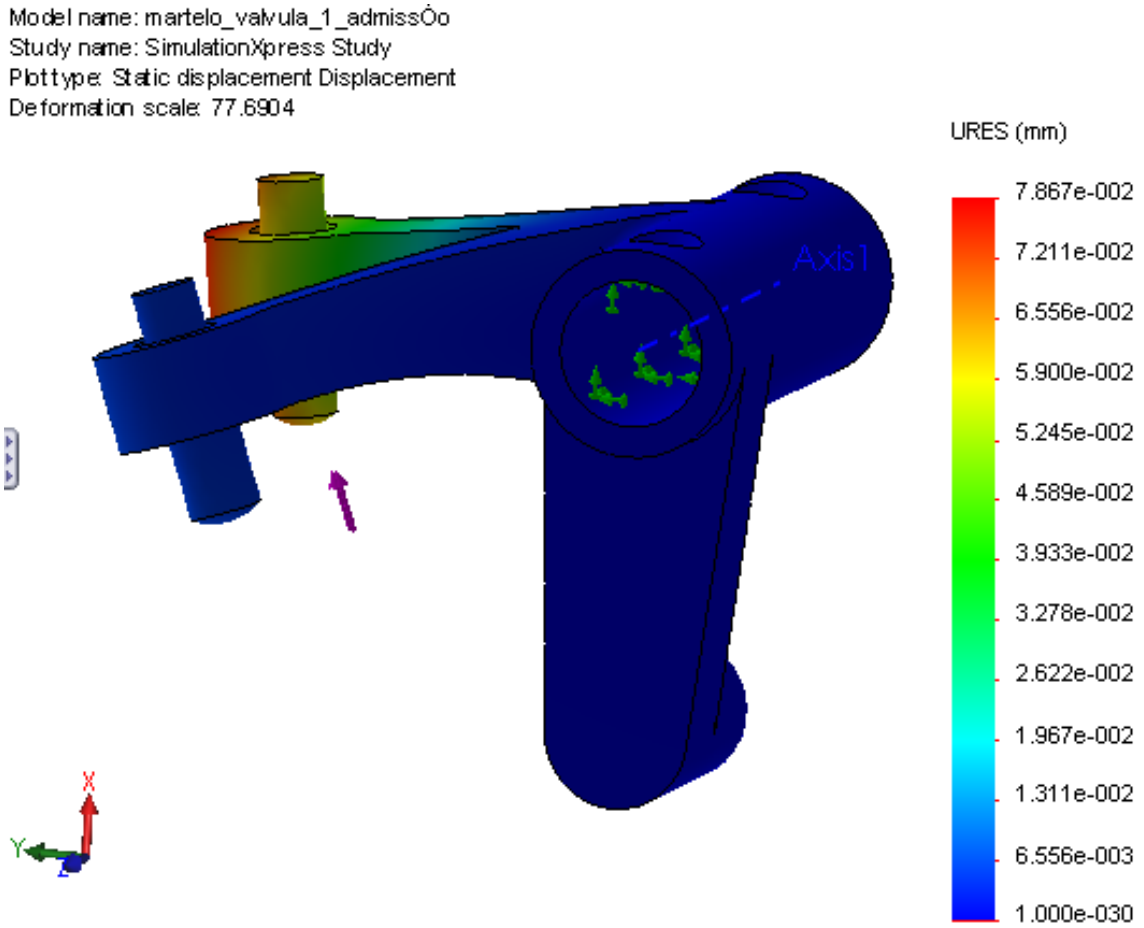

Figure C.4.: Displacement of the pins in relation to rotation center. The applied force has an amplitude of 1000 $/N$

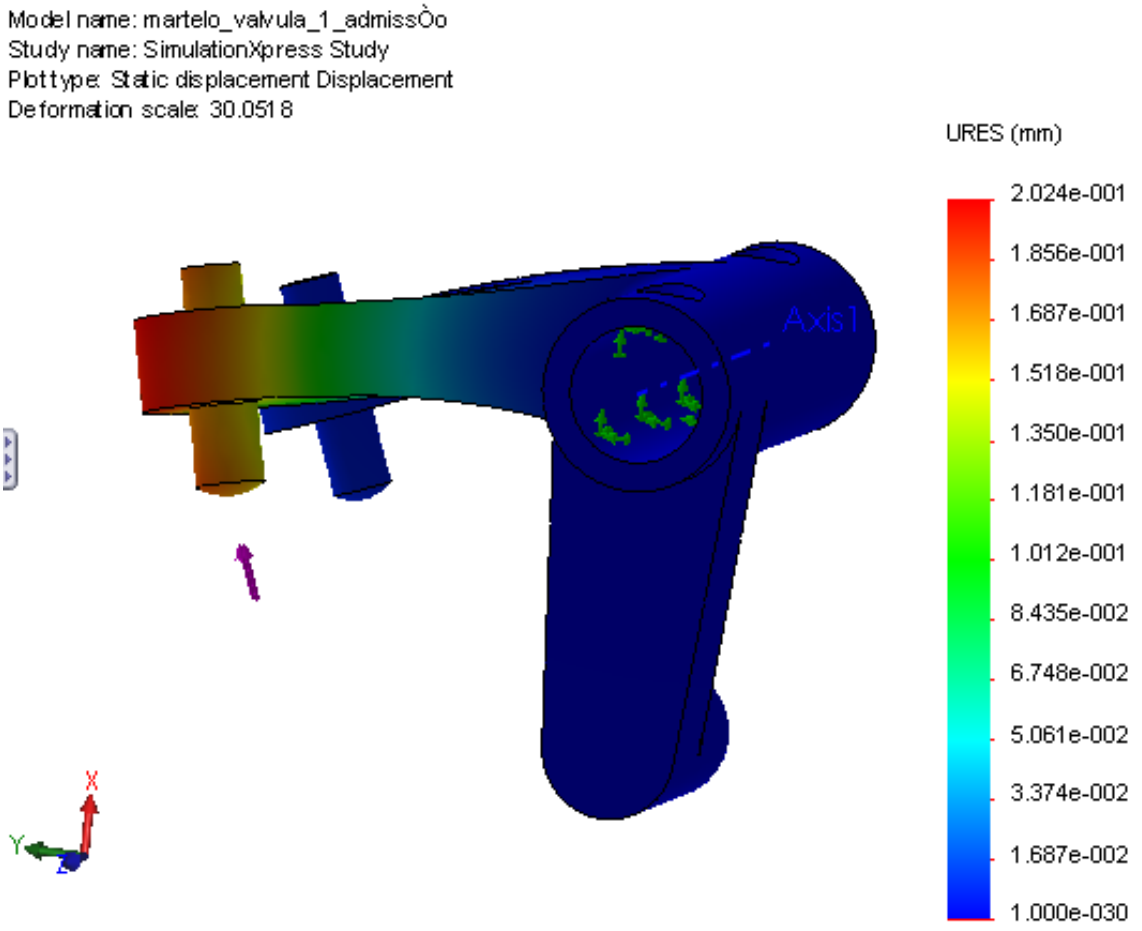

Figure C.5.: Displacement of the pins in relation to rotation center. The applied force has an amplitude of 1000 $/N$

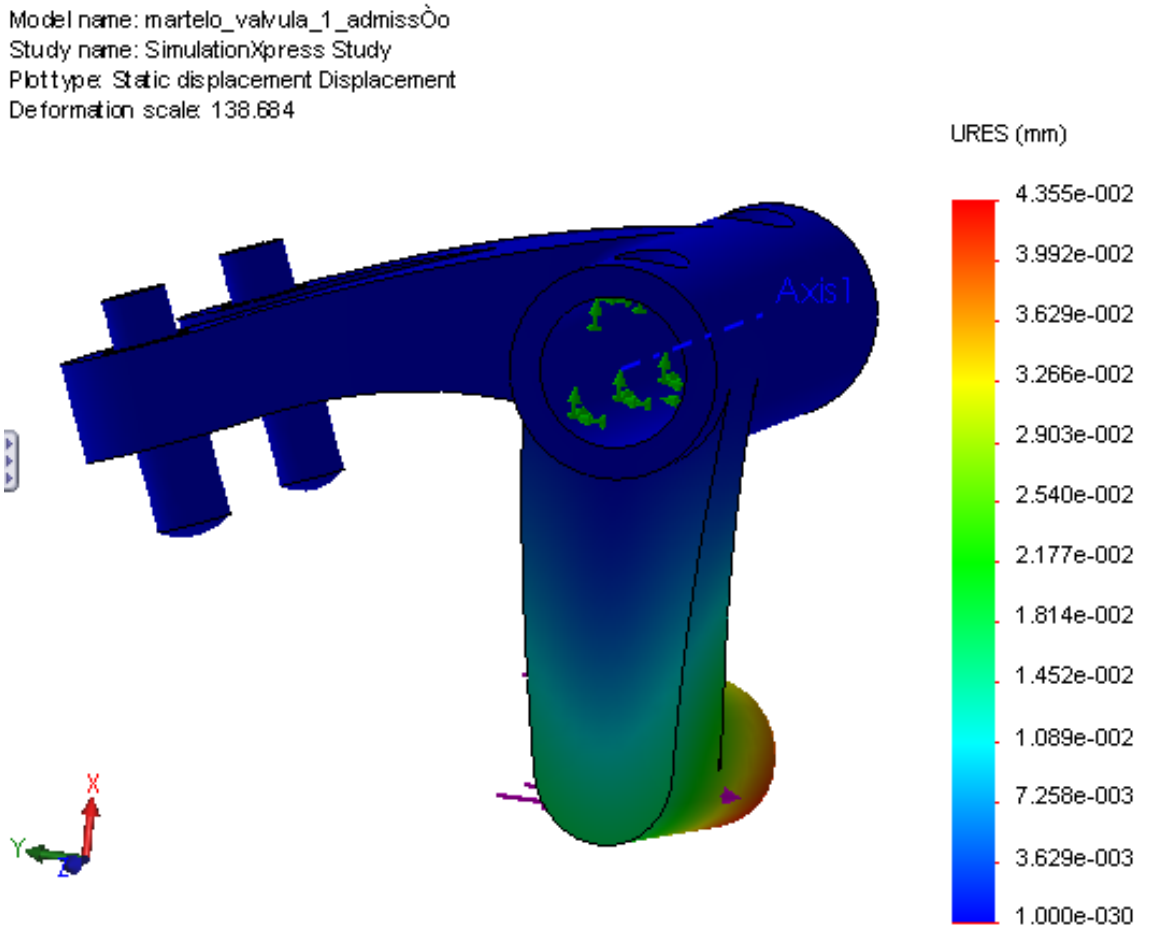

Figure C.6.: Displacement of the pins in relation to rotation center. The applied force has a total amplitude of 1000 $/N$

D. Vibration analysis results for the 3 DoF's model

D.1. Exhaust sub-system

D.1.1. FRF's of the type receptance

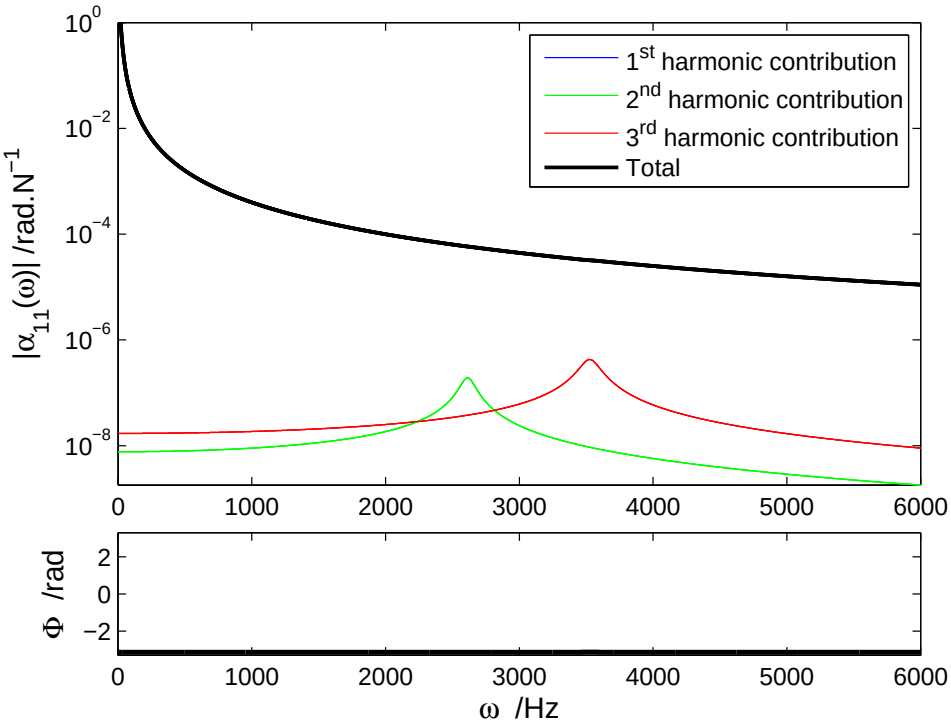

Figure D.1.: FRF of type receptance for direct solicitation in DoF β_e

D.1.2. FRF's without the contribution of rigid body harmonic

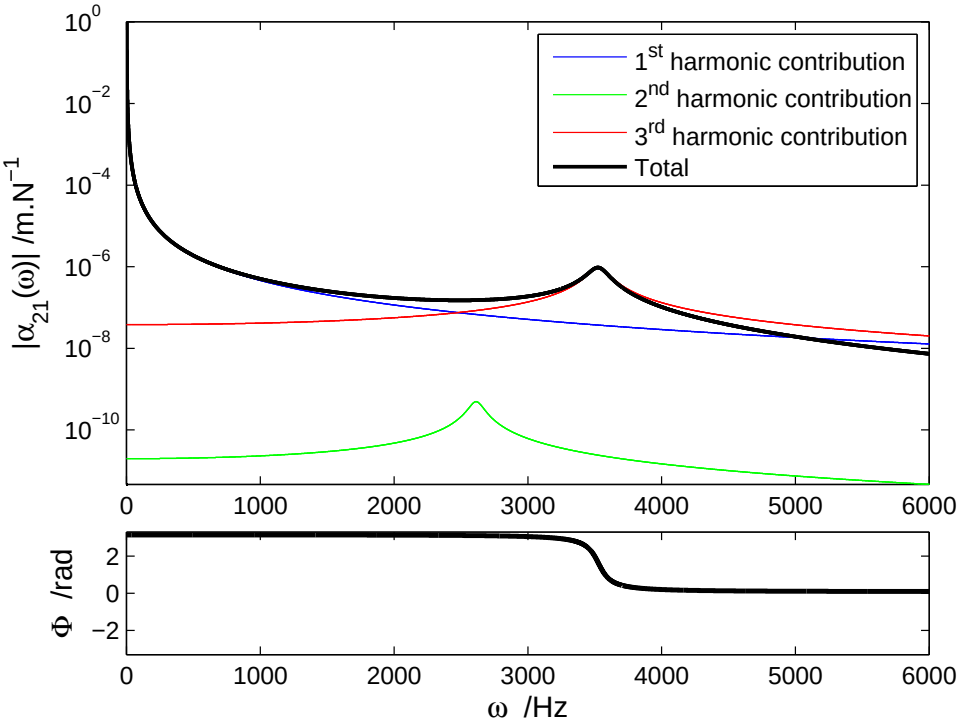

Figure D.2.: FRF of type receptance in DoF $l_{e,s}$ for crossed solicitation in DoF β_e

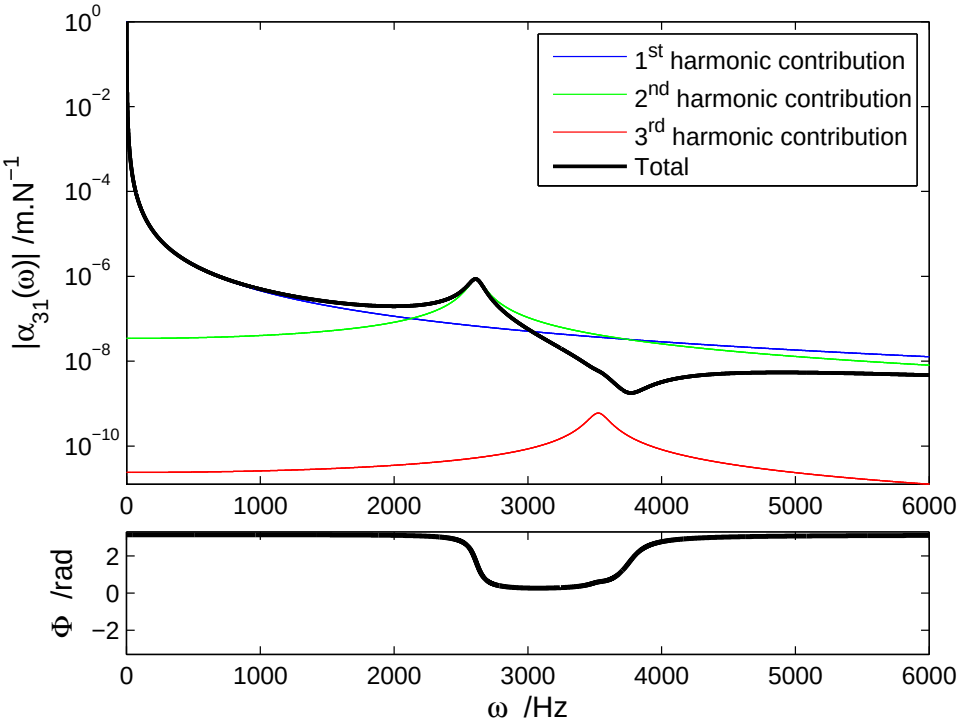

Figure D.3.: FRF of type receptance in DoF $l_{e,o}$ for crossed solicitation in DoF β_e

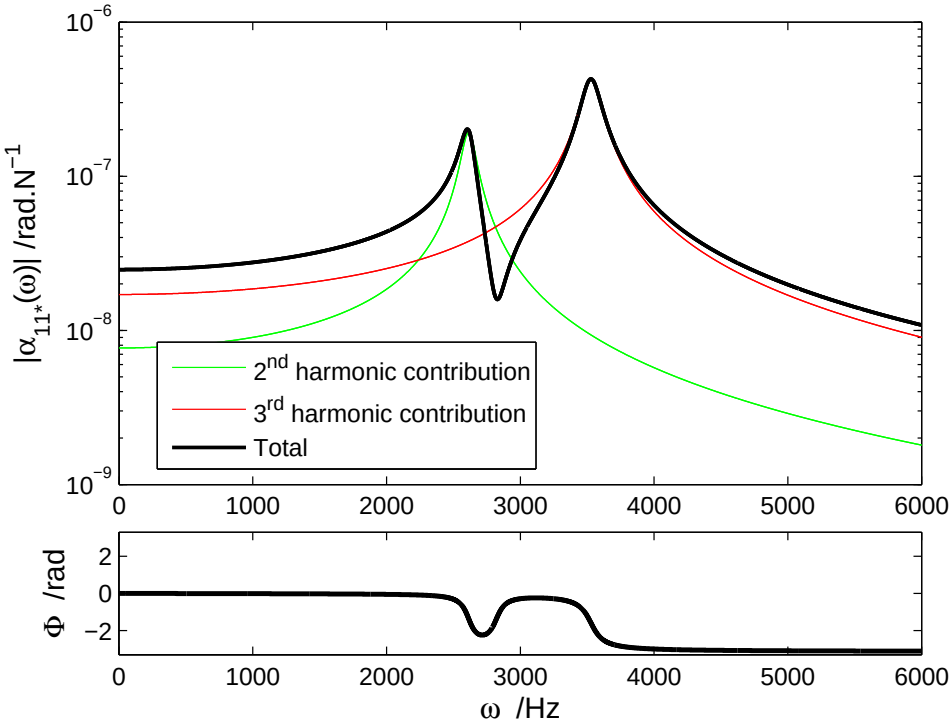

Figure D.4.: FRF of type receptance for direct solicitation in DoF β_e, without first mode

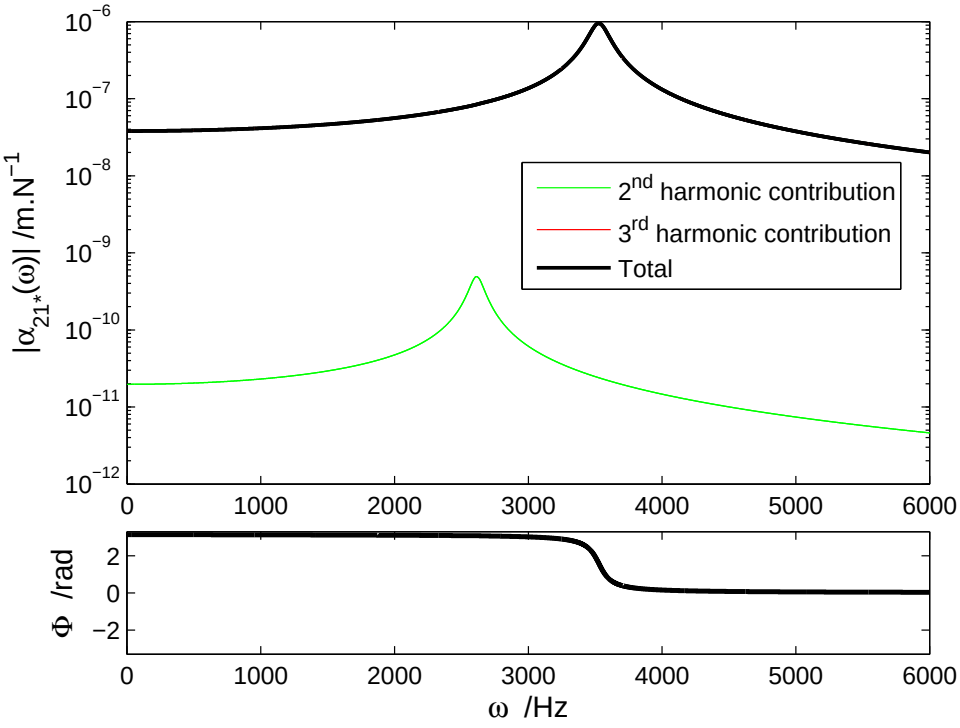

Figure D.5.: FRF of type receptance in DoF $l_{e,s}$ for crossed solicitation in DoF β_e, without first mode

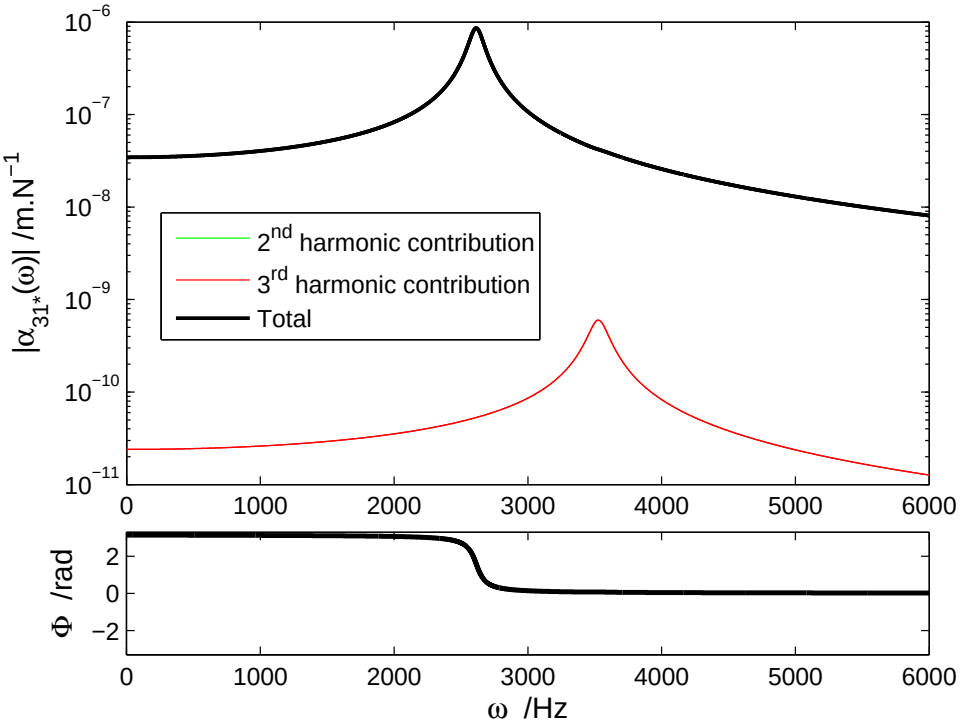

Figure D.6.: FRF of type receptance in DoF $l_{e,o}$ for crossed solicitation in DoF β_e, without first mode

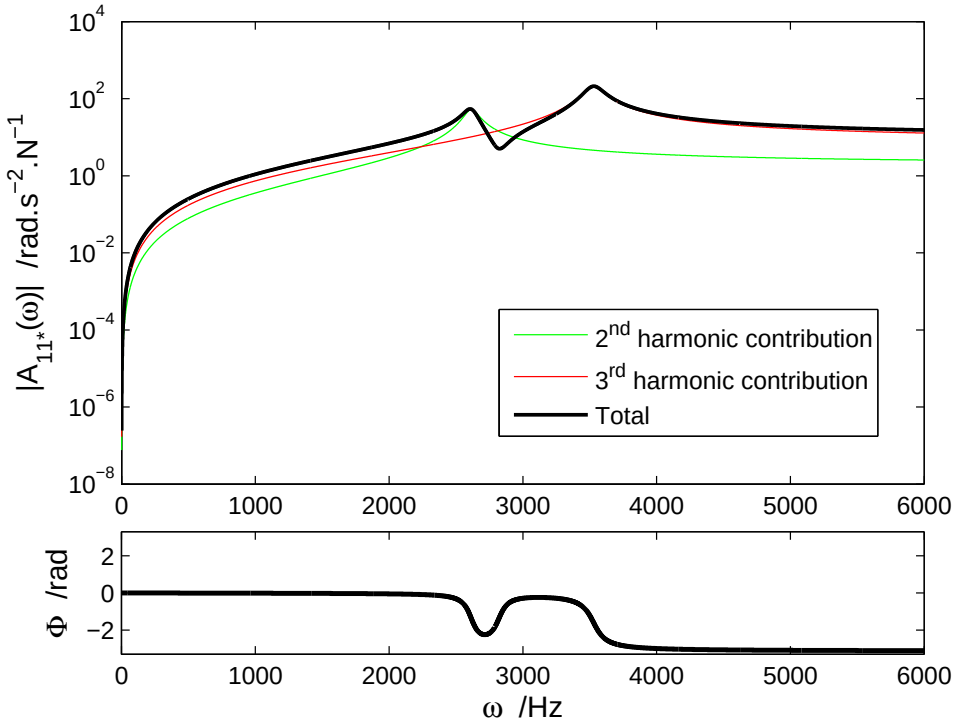

Figure D.7.: FRF of type accelerance for direct solicitation in DoF β_e, without first mode

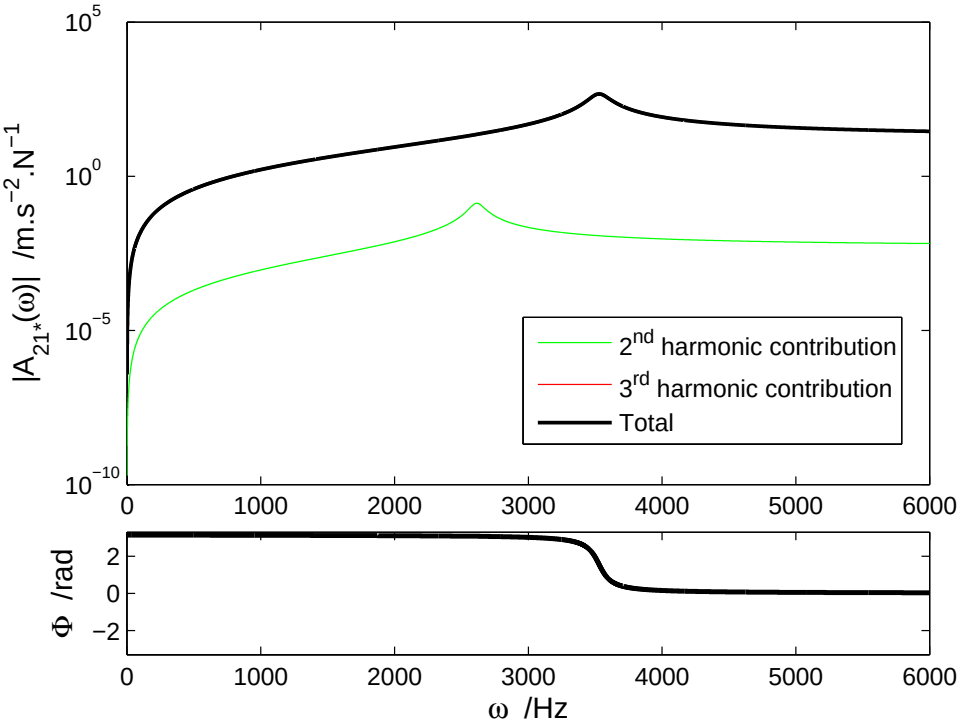

Figure D.8.: FRF of type accelerance in DoF $l_{e,s}$ for crossed solicitation in DoF β_e, without first mode

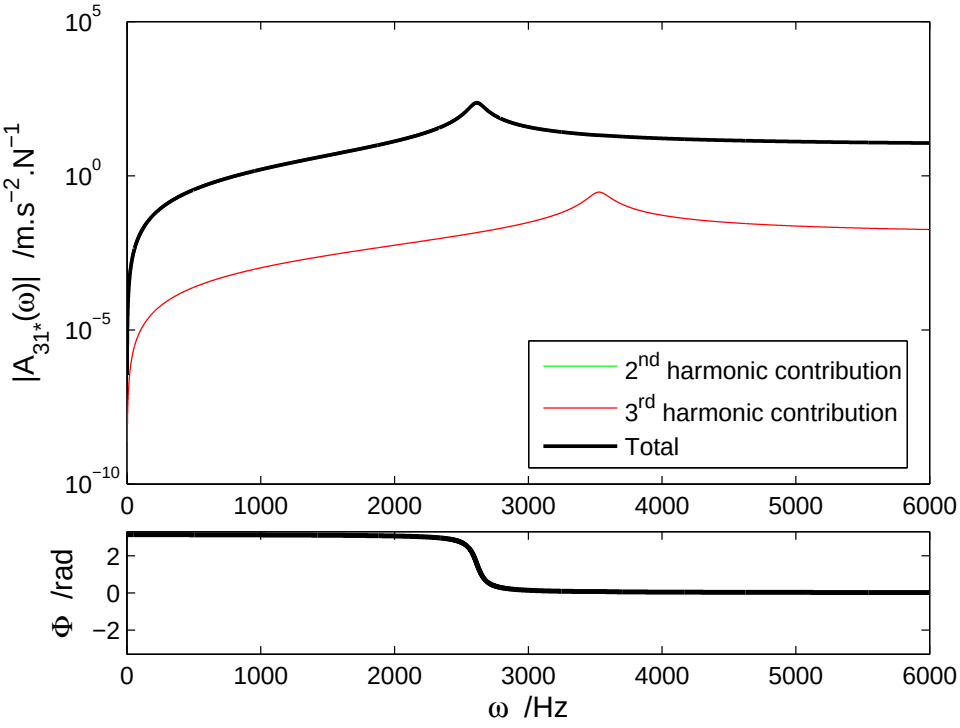

Figure D.9.: FRF of type accelerance in DoF $l_{e,o}$ for crossed solicitation in DoF β_e, without first mode

D.2. Intake sub-system

D.2.1. FRF's of the type receptance

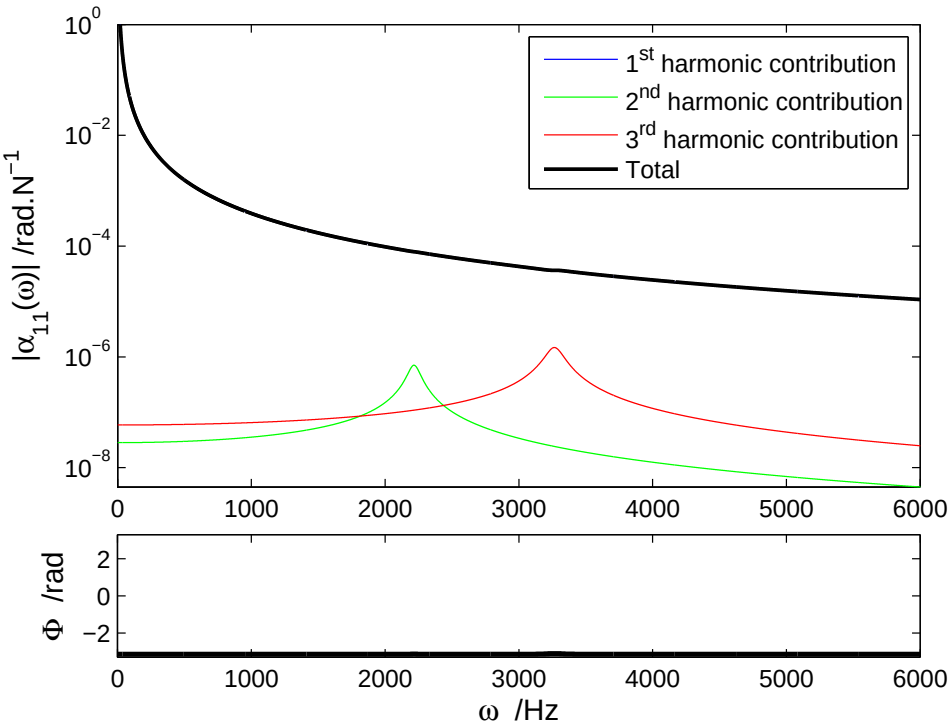

Figure D.10.: FRF of type receptance for direct solicitation in DoF β_i

D.2.2. FRF's without the contribution of rigid body harmonic

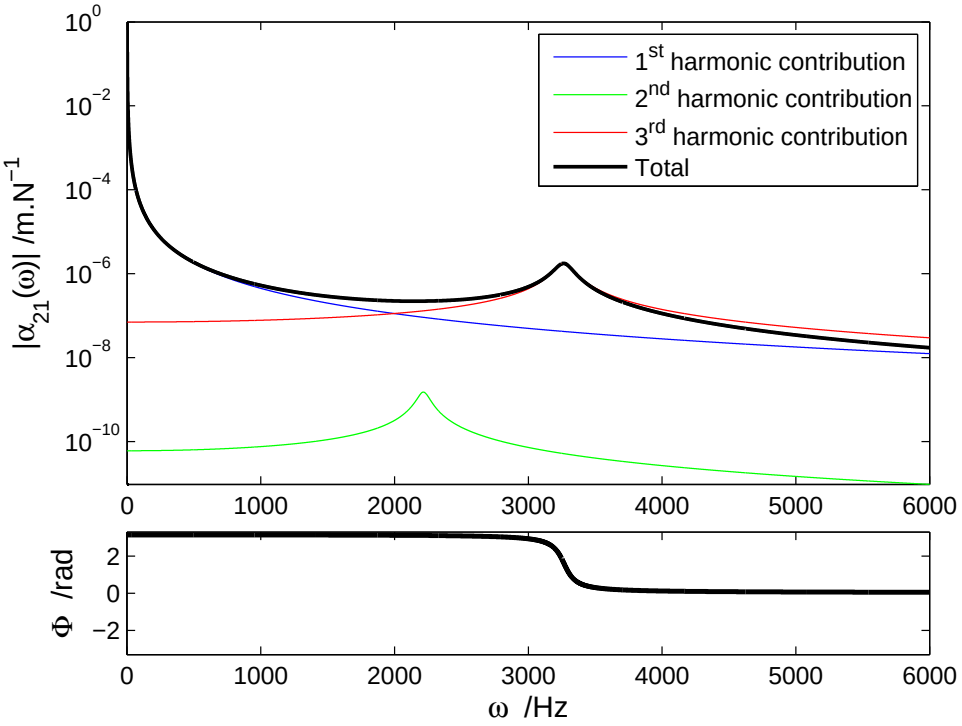

Figure D.11.: FRF of type receptance in DoF $l_{i,s}$ for crossed solicitation in DoF β_i

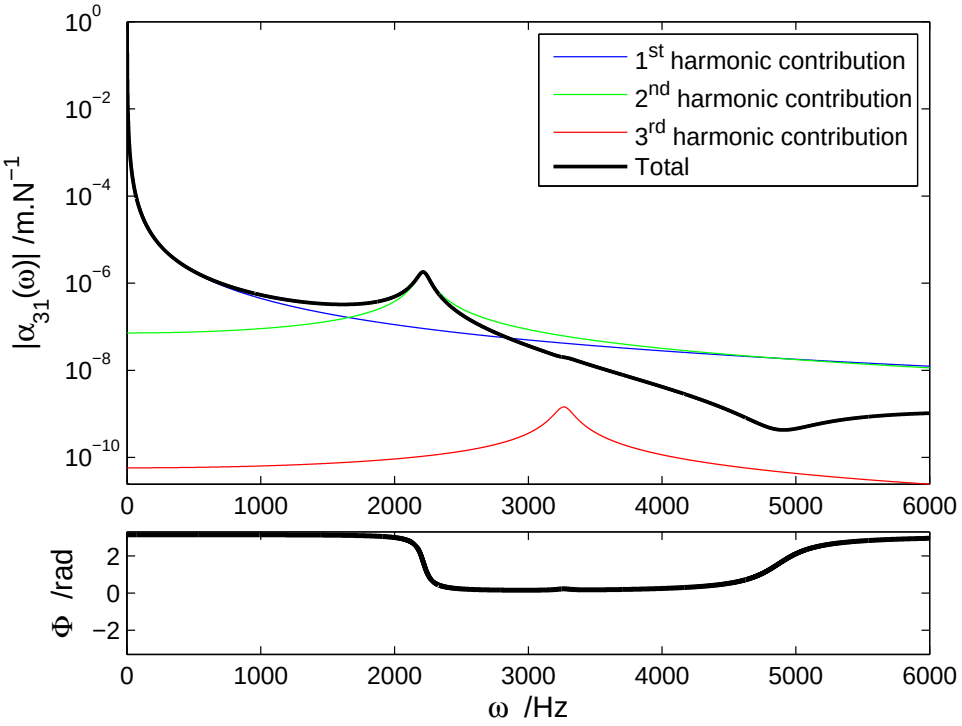

Figure D.12.: FRF of type receptance in DoF $l_{i,o}$ for crossed solicitation in DoF β_i

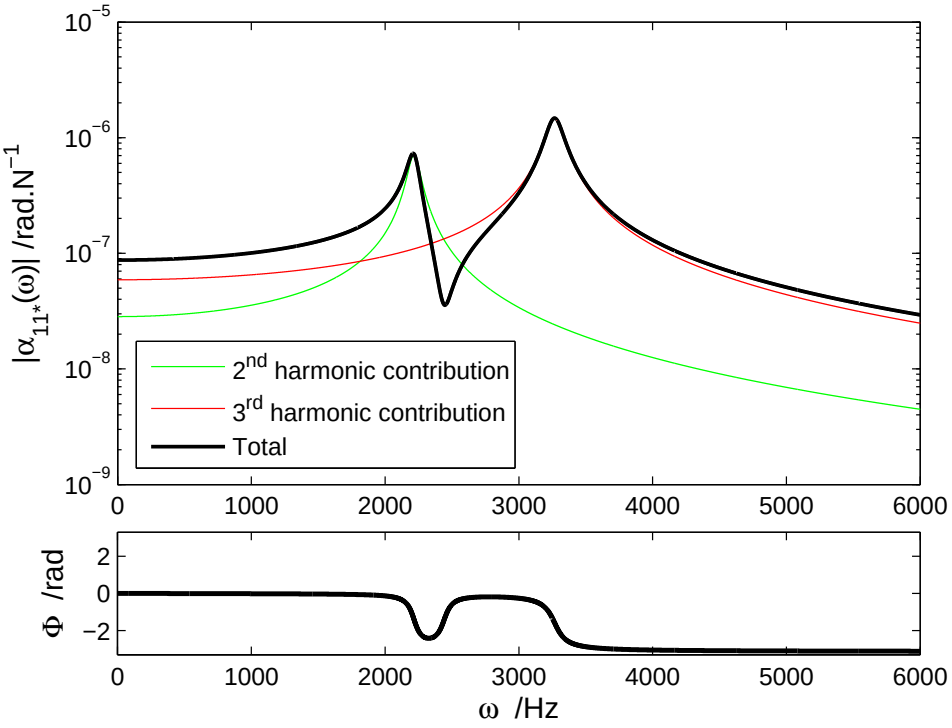

Figure D.13.: FRF of type receptance for direct solicitation in DoF β_i, without first mode

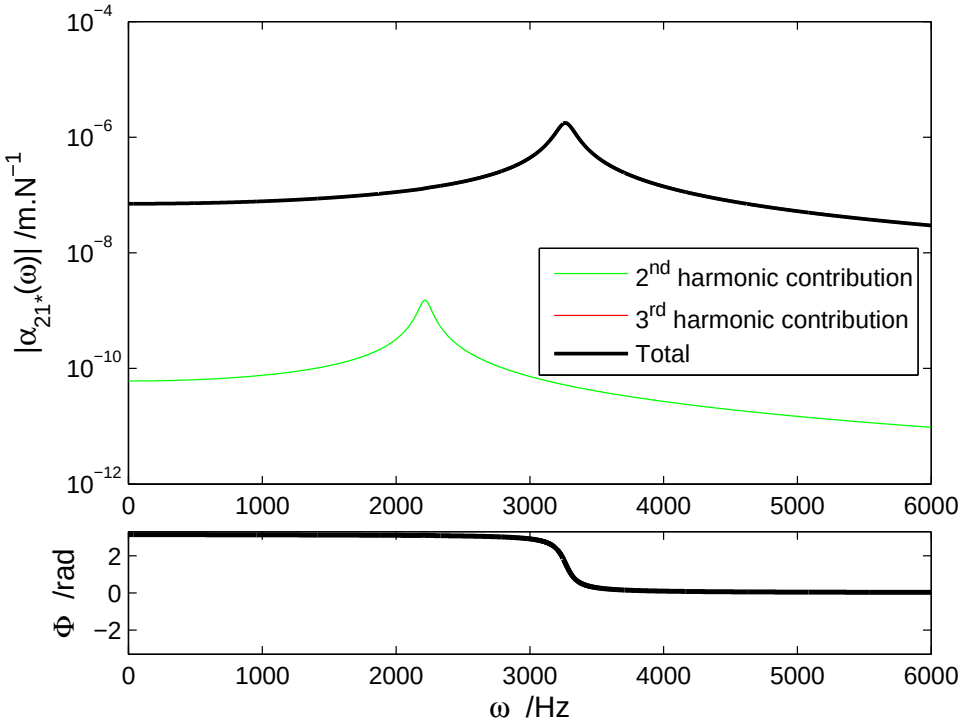

Figure D.14.: FRF of type receptance in DoF $l_{i,s}$ for crossed solicitation in DoF β_i, without first mode

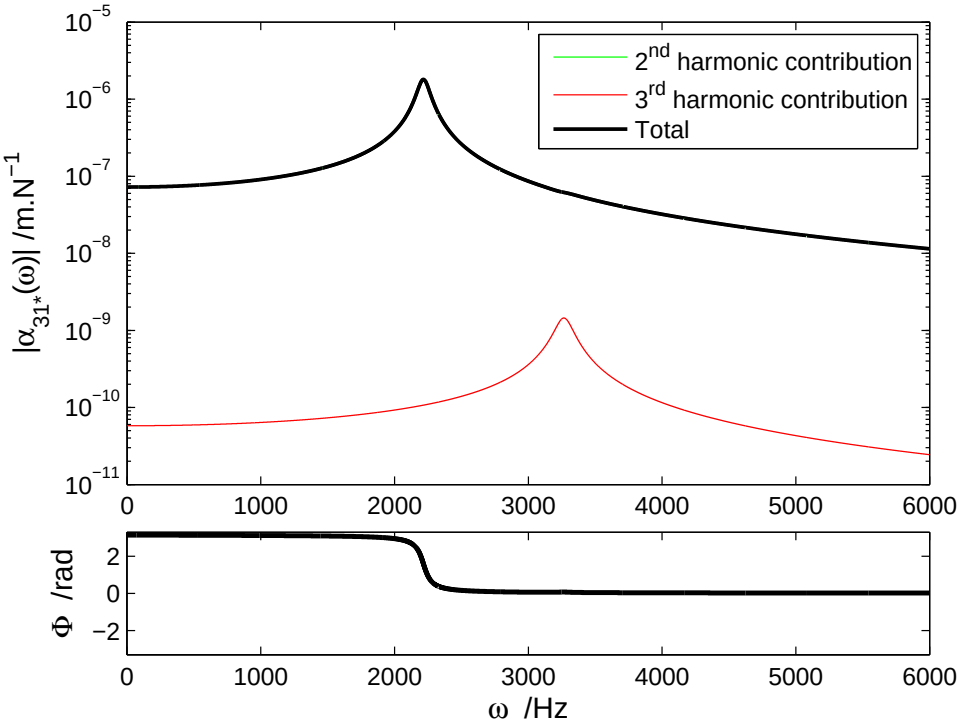

Figure D.15.: FRF of type receptance in DoF $l_{i,o}$ for crossed solicitation in DoF β_i, without first mode

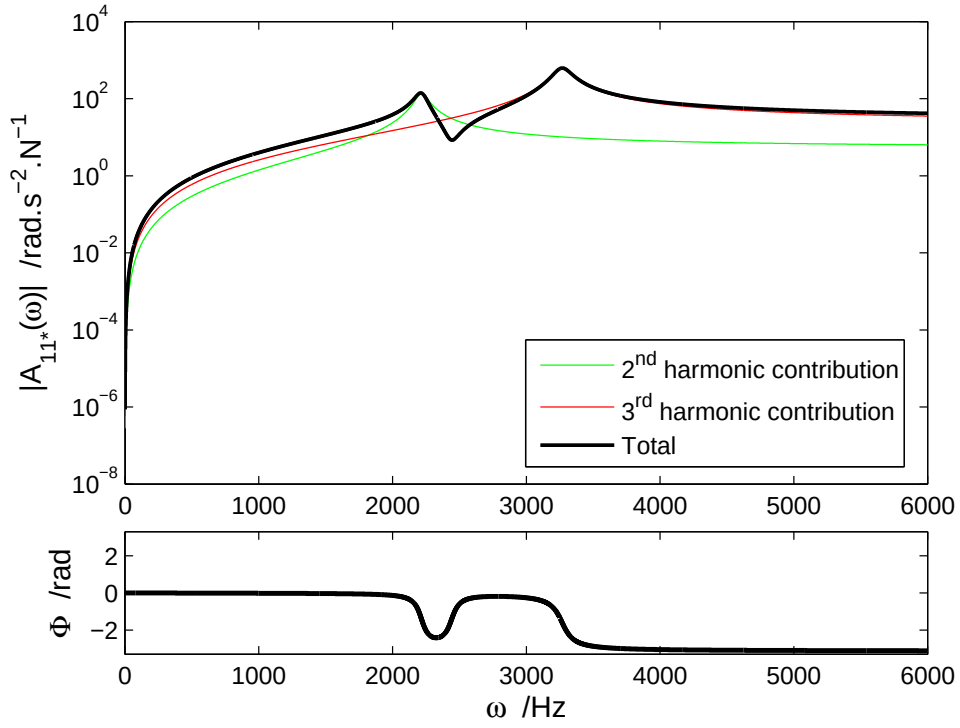

Figure D.16.: FRF of type accelerance for direct solicitation in DoF β_i, without first mode

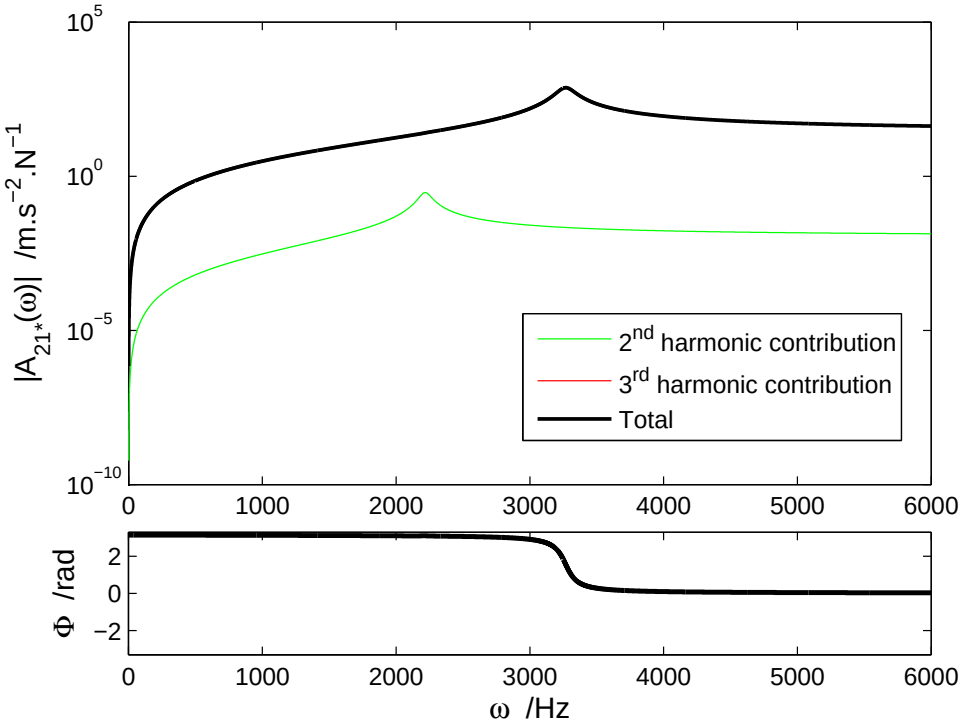

Figure D.17.: FRF of type accelerance in DoF $l_{i,s}$ for crossed solicitation in DoF β_i, without first mode

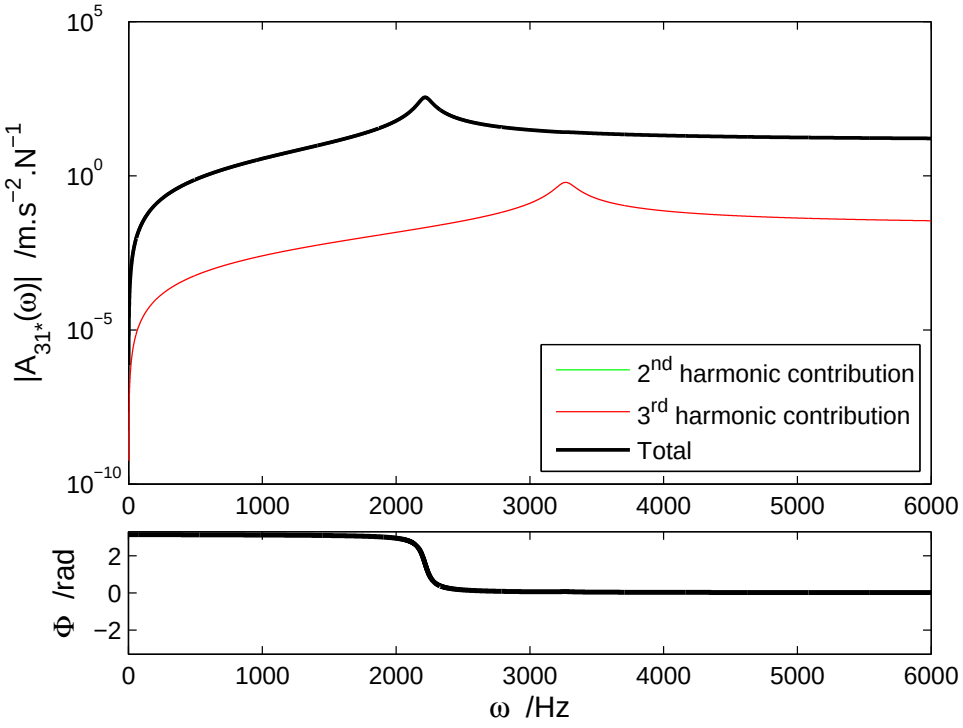

Figure D.18.: FRF of type accelerance in DoF $l_{i,o}$ for crossed solicitation in DoF β_i, without first mode

E. MSC Adams™ results

E.1. Model with damping ratio of 0.1, at 4200 rpm

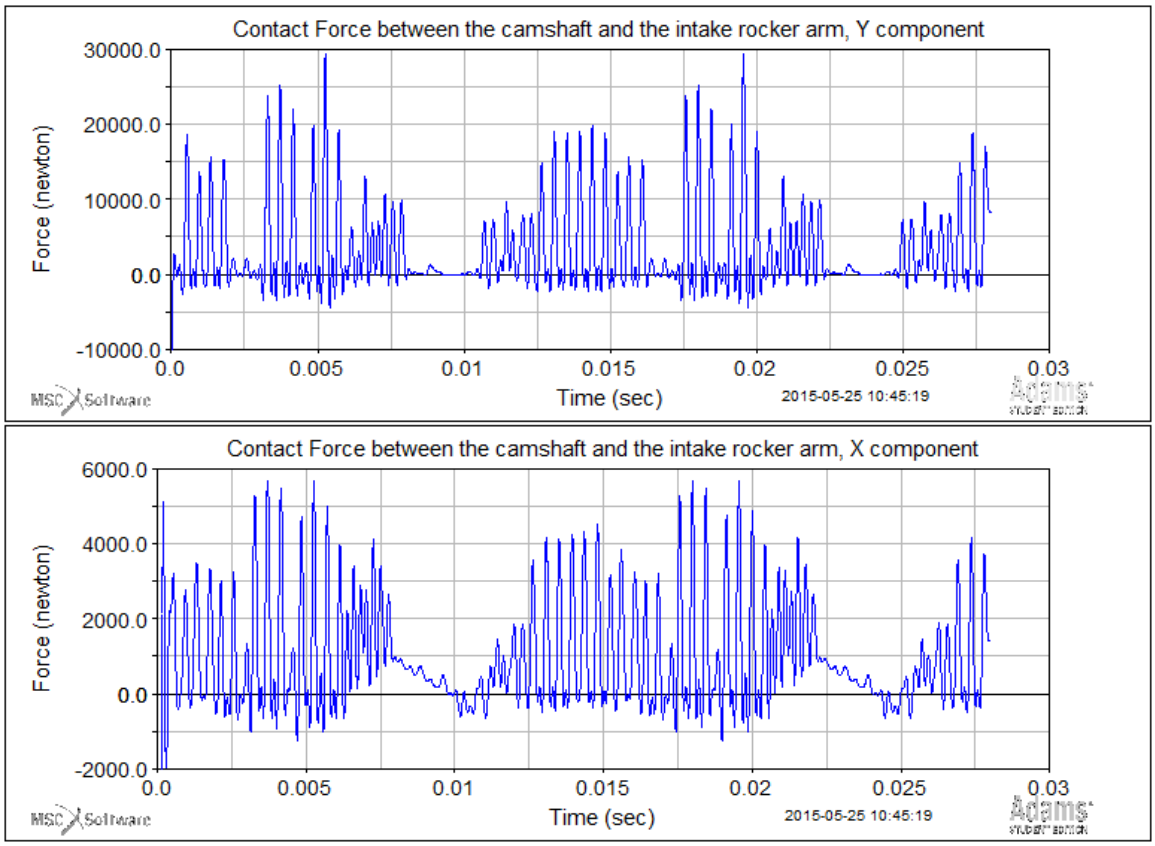

Figure E.1.: [Adams_1] Contact forces between the camshaft and the intake rocker-arm (filtered)

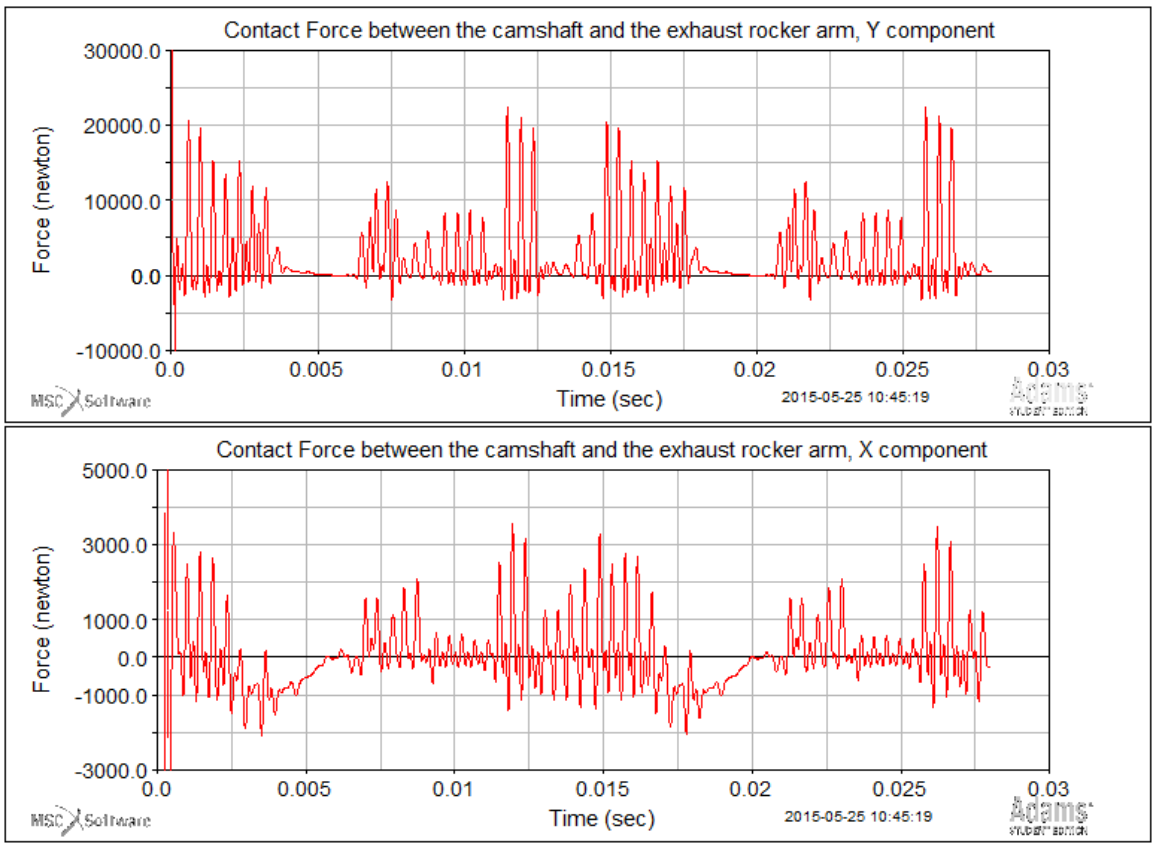

Figure E.2.: [Adams_1] Contact forces between the camshaft and the exhaust rocker-arm (filtered)

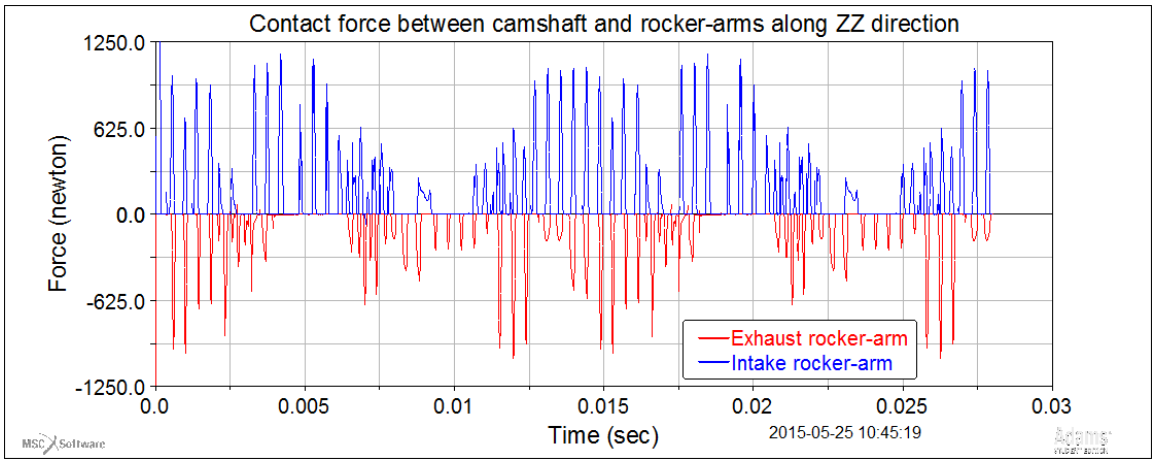

Figure E.3.: [Adams_1] Contact forces between the camshaft and rocker arms, along the Z direction (no filter)

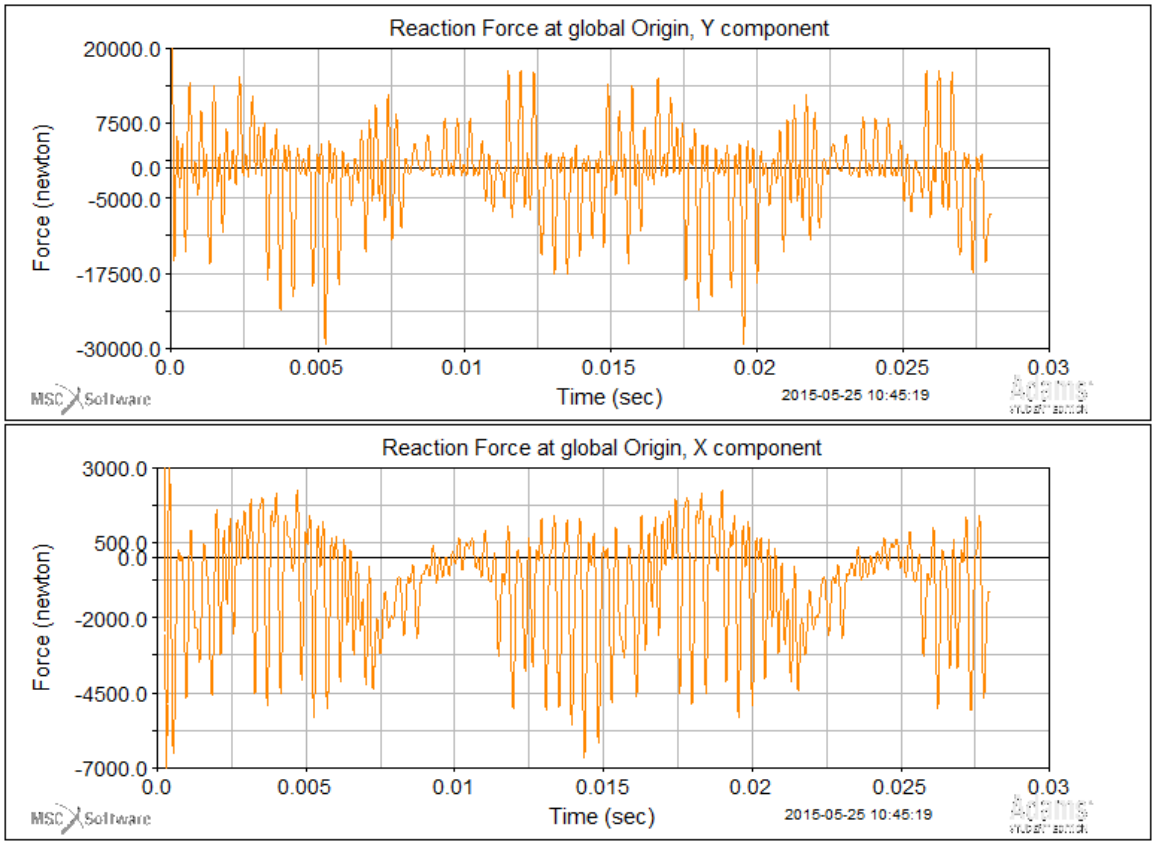

Figure E.4.: [Adams_1] Reaction forces in the Origin of the referential (filtered)

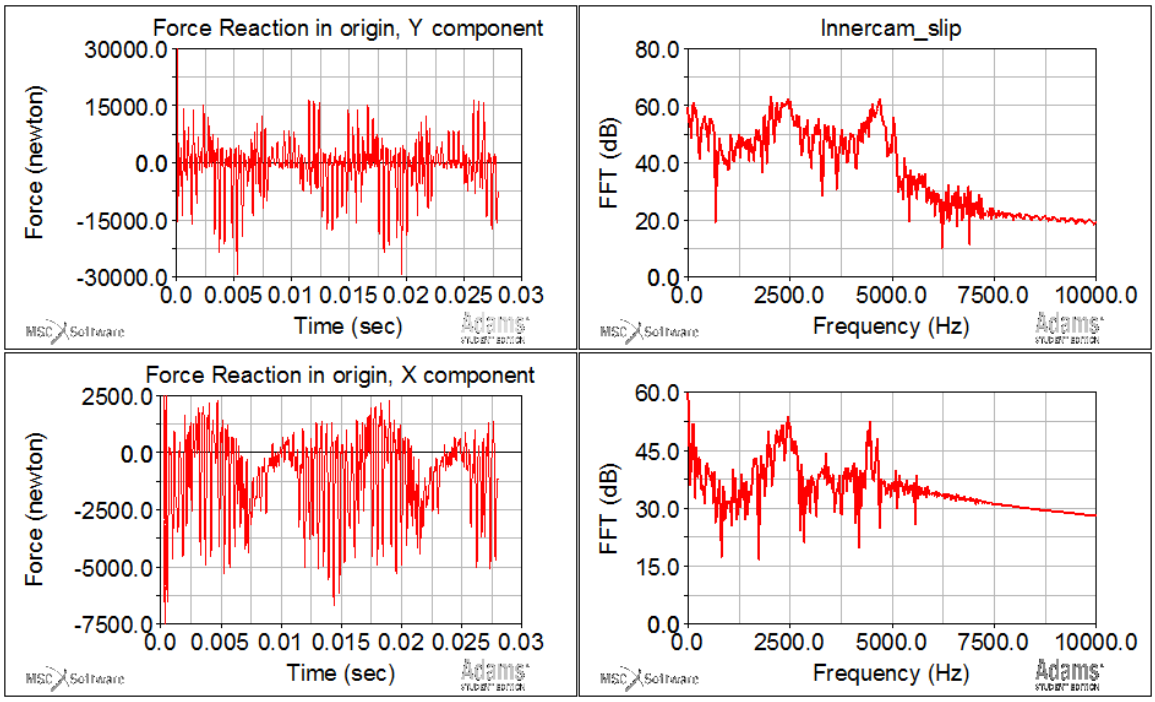

Figure E.5.: [Adams_1] FFT Transformation for Reaction force in the origin

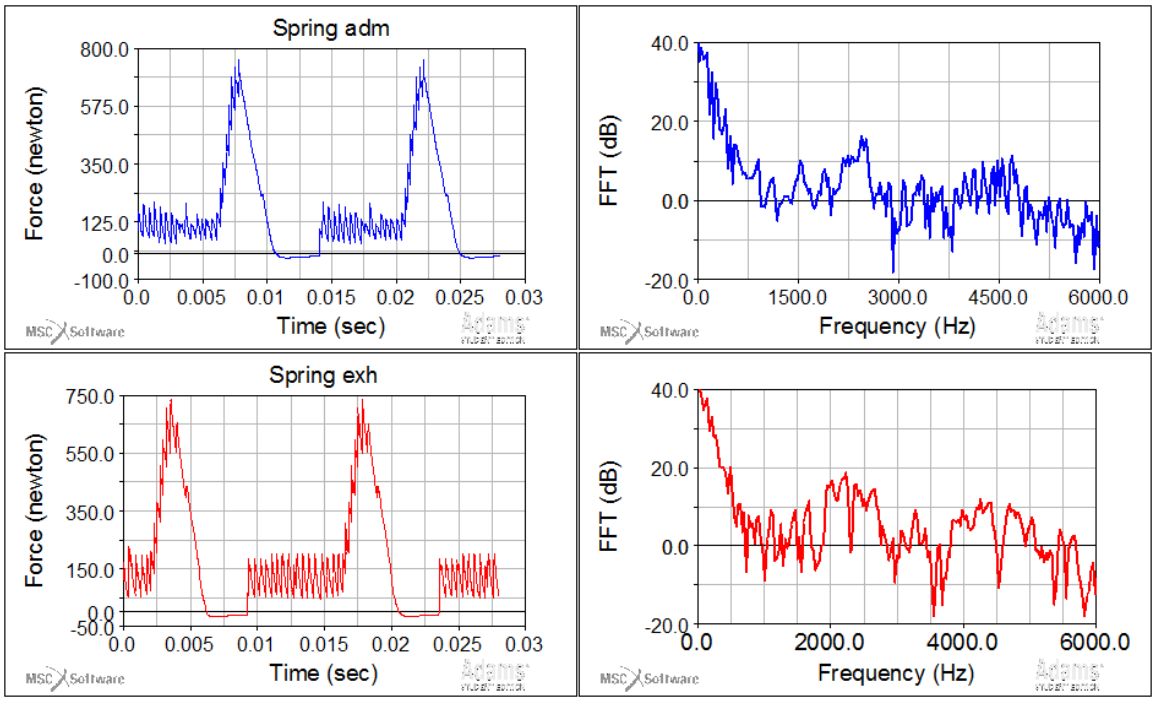

Figure E.6.: [Adams_1] FFT Transformation applied to the spring forces

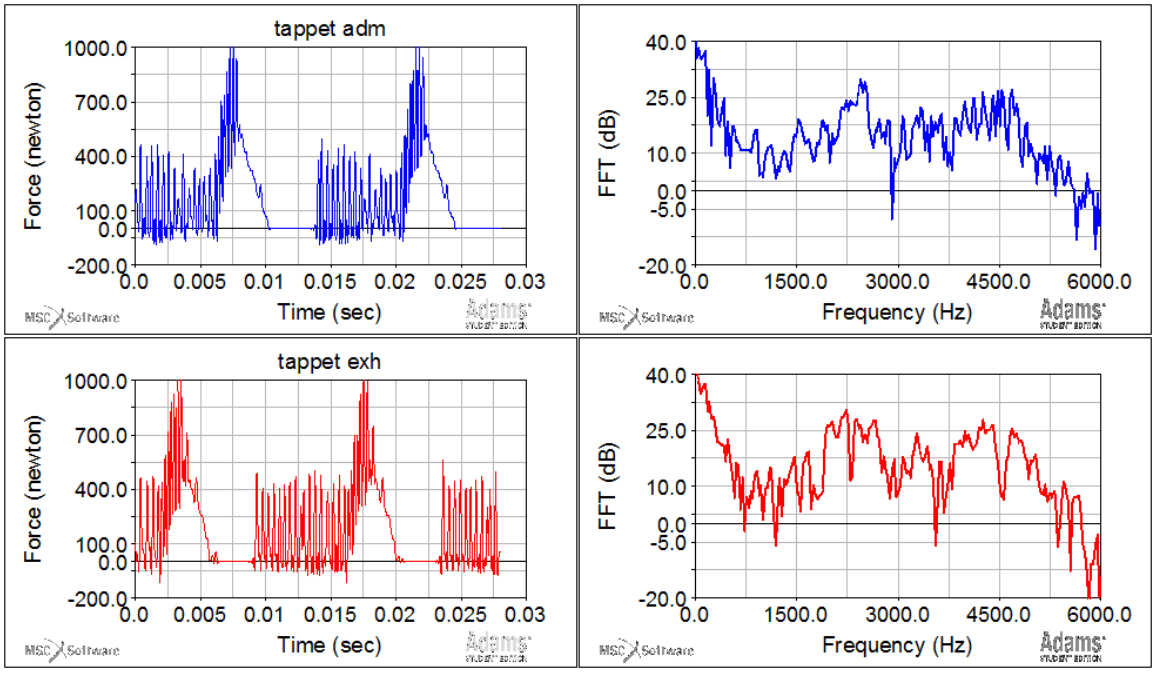

Figure E.7.: [Adams_1] FFT Transformation applied to the tappet's contact forces

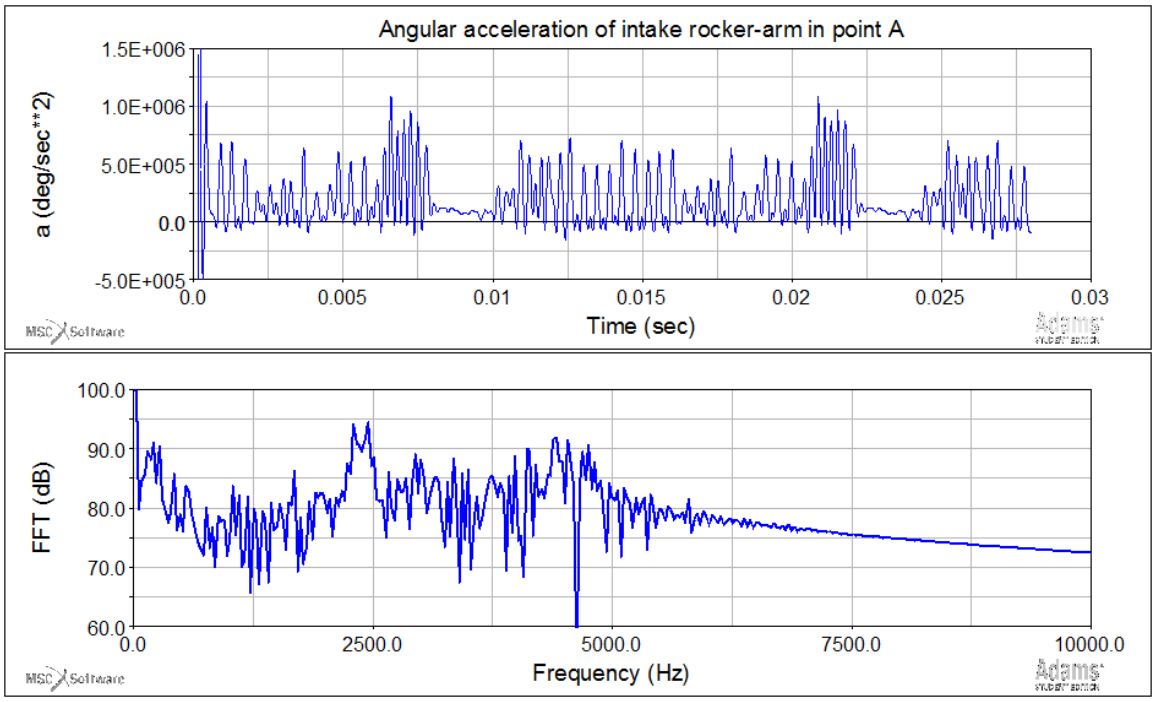

Figure E.8.: [Adams_1] FFT Transformation for the angular acceleration of intake rocker-arm

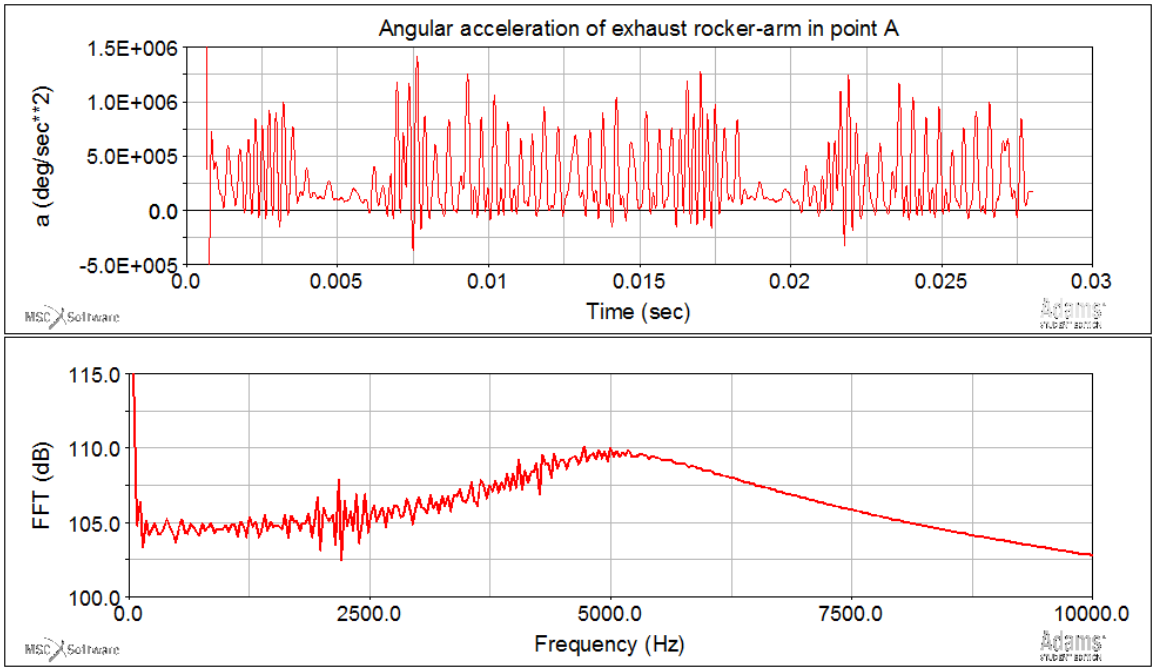

Figure E.9.: [Adams_1] FFT Transformation for the angular acceleration of exhaust rocker-arm

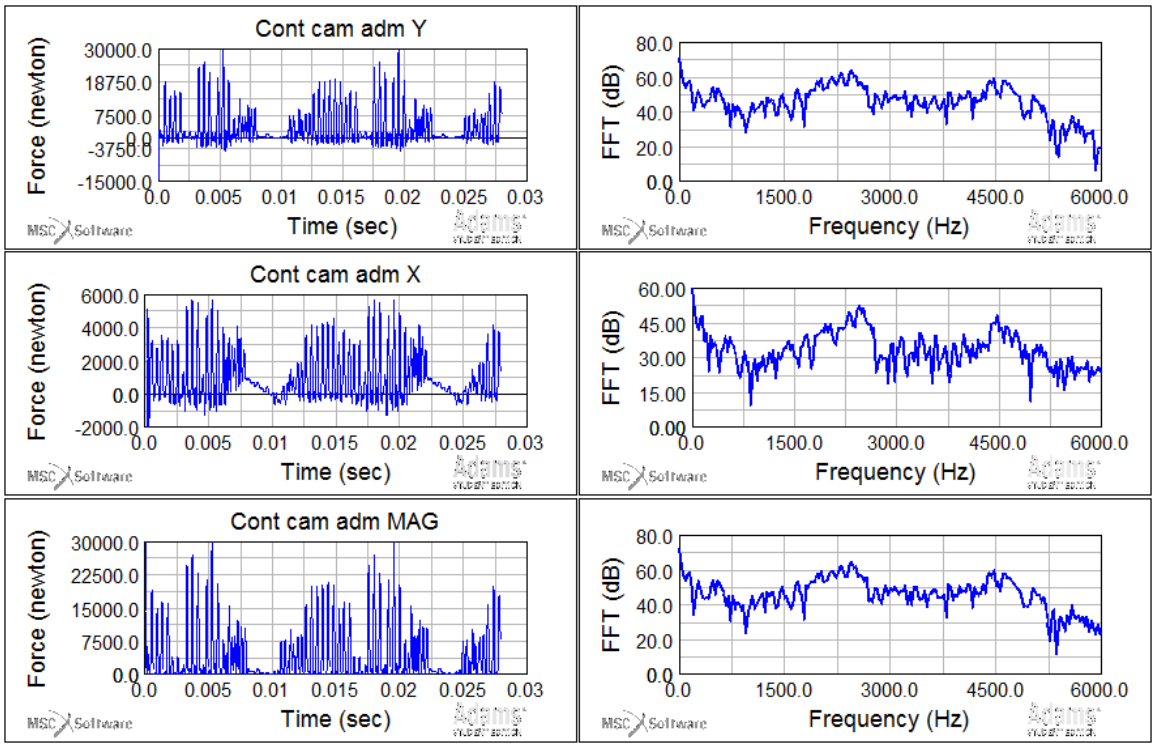

Figure E.10.: [Adams_1] FFT Transformation for the contact force between the camshaft and intake rocker-arm

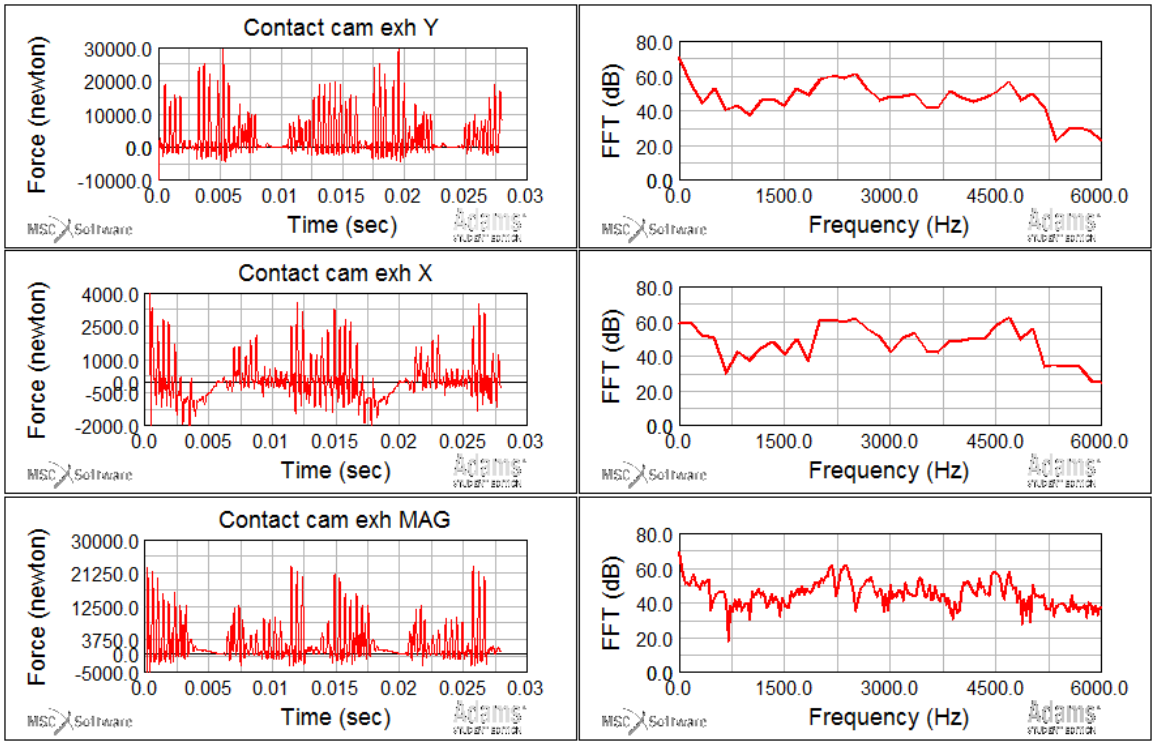

Figure E.11.: [Adams_1] FFT Transformation for the contact force between the camshaft and exhaust rocker-arm

E.2. Model with damping ratio of 0.001, at 4200 rpm

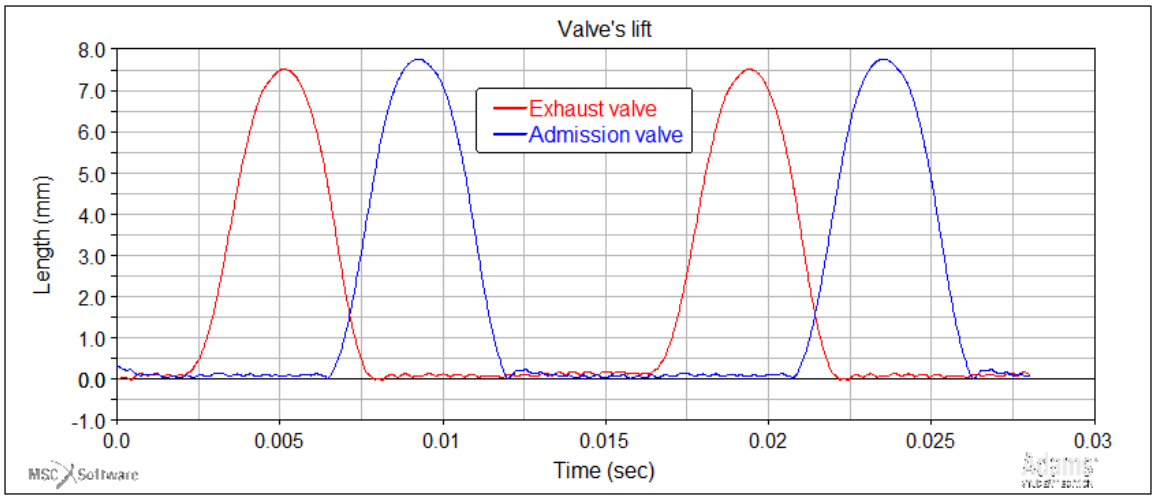

Figure E.12.: [Adams_001] Valve's lift

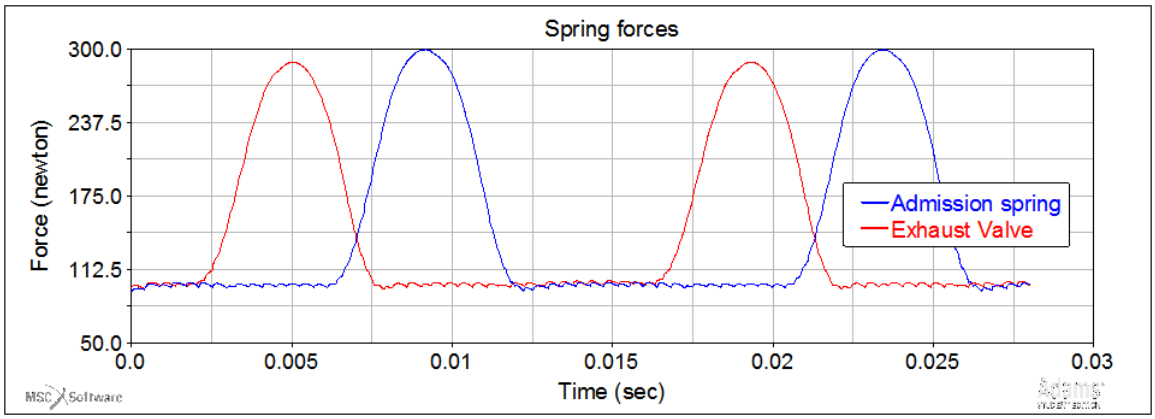

Figure E.13.: [Adams_001] Spring force

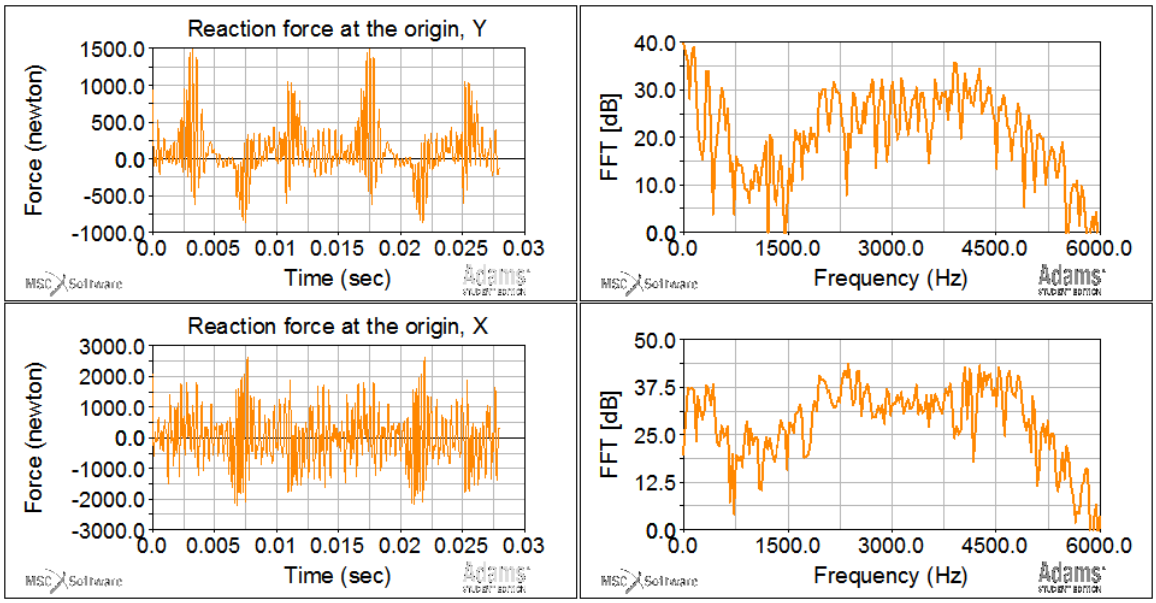

Figure E.14.: [Adams_001] Reaction forces at origin point in the camshaft (filtered), with FFT plot

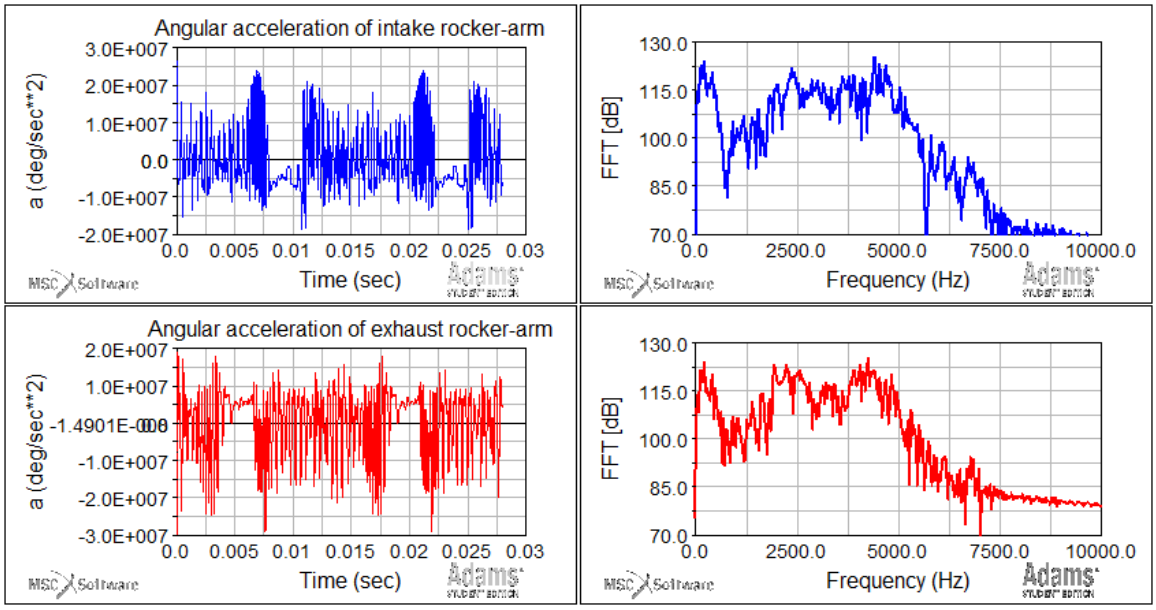

Figure E.15.: [Adams_001] Angular acceleration of the rocker arms (filtered), with FFT plot

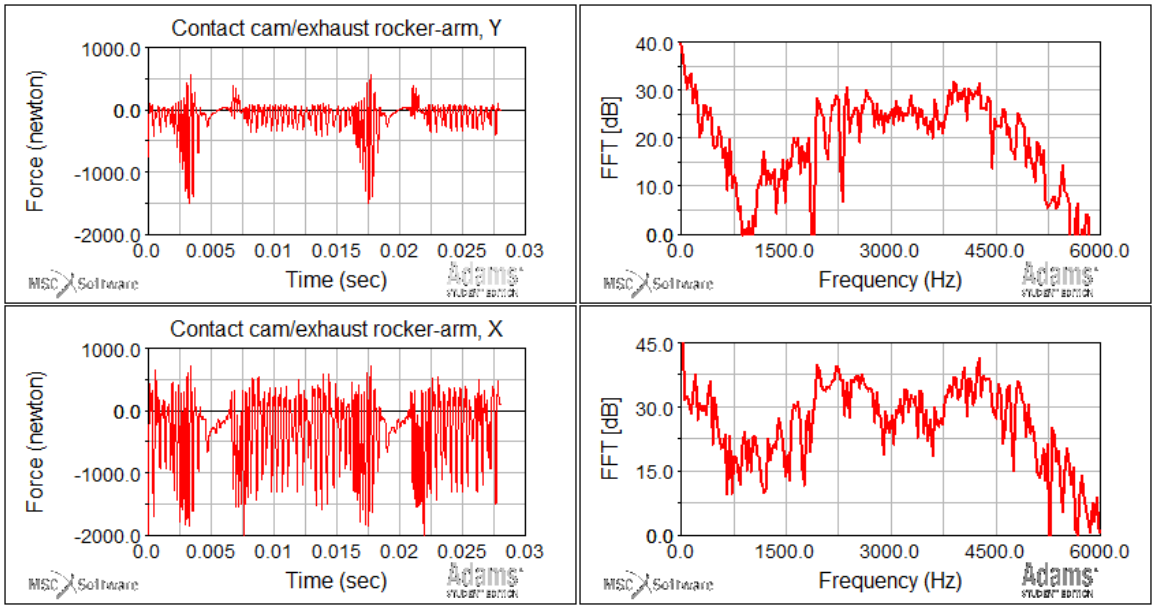

Figure E.16.: [Adams_001] Contact forces between the camshaft and exhaust rocker-arm (filtered), with FFT plot

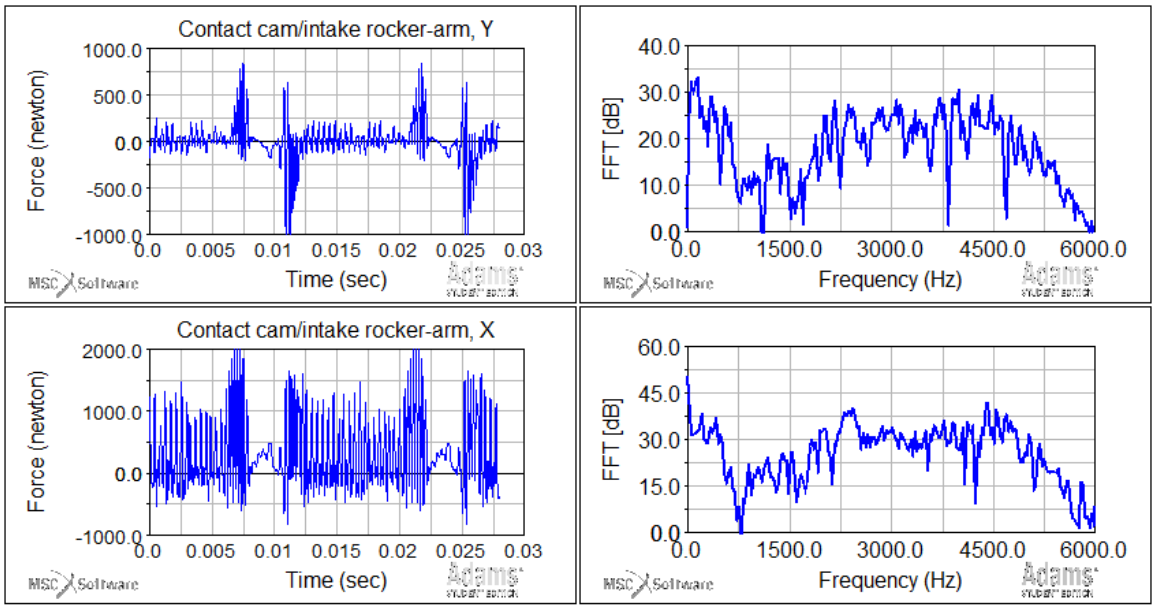

Figure E.17.: [Adams_001] Contact forces between the camshaft and intake rocker-arm (filtered), with FFT plot

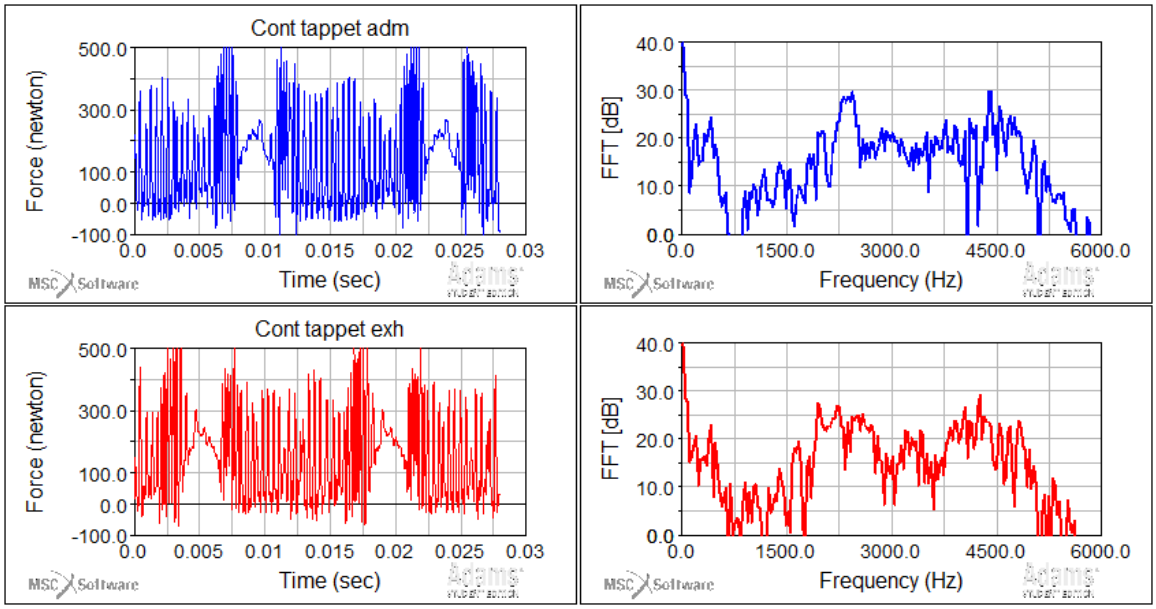

Figure E.18.: [Adams_001] Contact forces in the tappets (filtered), with FFT plot

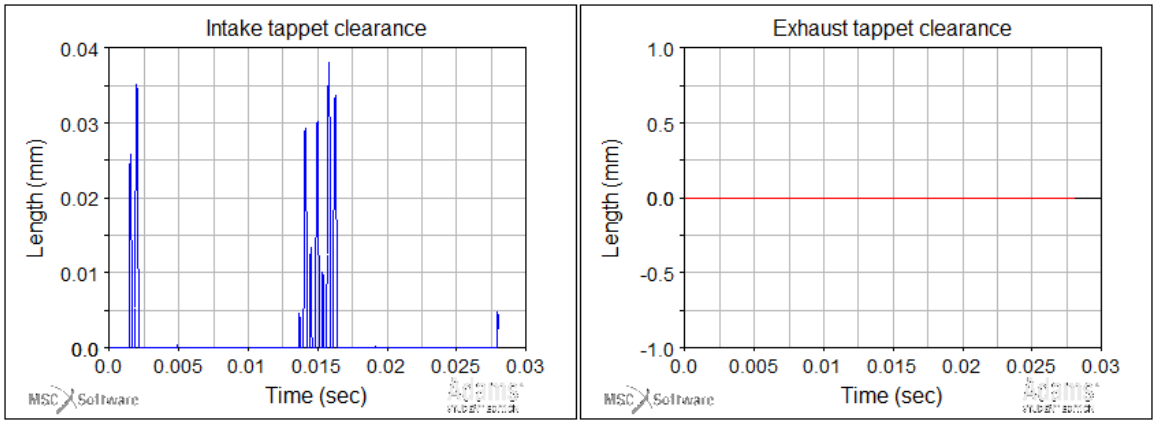

Figure E.19.: [Adams_001] Clearance distance in the tappet contacts